Using moment tracking to improve macroparticles in particle-in-cell codes

Alexander John Warwick, MPhys

Physics Department

Lancaster University

This thesis is submitted for the degree of

Doctor of Philosophy

October, 2024

Using moment tracking to improve macroparticles in particle-in-cell codes

Alexander John Warwick, MPhys.

Physics Department, Lancaster University

A thesis submitted for the degree of *Doctor of Philosophy*. October, 2024.

Abstract

Particle-in-cell codes usually represent large groups of particles as a single macroparticle. These codes are computationally efficient but lose information about the internal structure of the macroparticle. To improve the accuracy of these codes, this thesis presents a method in which, as well as tracking the macroparticle, the moments of the macroparticle are also tracked.

One representation of moments uses integrals. In this representation of moments, the moment tracking equations are known, but the coordinate transformations for moments where the space and time coordinates are mixed cannot be calculated. These coordinate transformations are important in astrophysical plasma, where there is no preferred coordinate system. An alternative representation of moments uses Schwartz distributions. By using the language of Schwartz distributions, the equations to track the moments, and perform coordinate transformations of moments are calculated. The moment tracking and coordinate transformation equations are tested by modelling the motion of uncharged particles in a circular orbit around a black hole. Numerical testing shows that the error in tracking moments is small, and scales quadratically.

Two different methods to find the current distribution from a set of moments are presented. The first reconstructs the original distribution function used to find the moments, and derives the current distribution from the reconstructed distribution

function. The second method uses the language of Schwartz distributions to directly calculate the current from the set of moments. The current distribution construction equations are tested for a variety of distribution functions, and show that using the language of Schwartz distributions introduces errors, but is computationally faster. The error in moment tracking, coordinate transformations, and in finding the current can be improved by including higher order moments.

The considerations needed to create a full particle-in-cell code, and how this code can be evaluated, are discussed.

Acknowledgements

Firstly, I would like to express my gratitude to my supervisor Jonathan Gratus, for introducing me to the world of differential geometry, and for his knowledge and enthusiasm inspiring me throughout my PhD.

I would like to thank my office colleague Finlay, for many useful and insightful discussions about reconstructing functions from moments.

I would like to thank my parents, for their support throughout my life, and reading the draft of my thesis.

Lastly, I would like to thank Lydia, who has patiently listened to me complain about every time my code failed to run, and kept me sane throughout my PhD.

Declaration

I declare that the work presented in this thesis is, to the best of my knowledge and belief, original and my own work. The material has not been submitted, either in whole or in part, for a degree at this, or any other university. This thesis does not exceed the maximum permitted word length of 80,000 words including appendices and footnotes, but excluding the bibliography. A rough estimate of the word count is: 28,000

Alexander John Warwick

Publications

One publication, shown below, has been developed whilst generating this thesis, from which large portions of this published work is used within chapters 2, 3, 4, 5, and 8:

A. Warwick and J. Gratus. *Plasma Phys. Control. Fusion*, 66(1):015014, Dec. 2023

Contents

List of Tables

List of Figures

Chapter 1

Introduction

1.1 The numerical modelling of plasmas

A plasma is the de-localisation of electrons from their nuclei, causing the motion of particles within a medium to be dominated by electromagnetic fields [2]. Despite plasma being observed for millennia, in the form of lightning and fire, it was not created in the laboratory until 1879 by Crookes [3]. Even after this laboratory observation, it took until 1928 for Langmuir to make the first theoretical description of a plasma [4]. Since then, plasma has become increasingly important within modern physics, being used for nuclear fusion [5, 6], high gradient acceleration in particle accelerators [7, 8, 9], and observed in space physics [10, 11, 12, 13] and extreme astrophysical environments [10, 14]. Plasma has also become ubiquitous within modern society, appearing in plasma televisions, fluorescent lightbulbs, and used in arc welding for metalwork, amongst others [15, 16]. There are many new areas where plasma is being used to innovate within existing fields, including medical applications [17, 18], creating carbon-neutral jet fuels [19], and purifying wastewater [20]. Because of the vast variety of applications plasma has within modern physics and society, it is important to accurately understand how plasma behaves, and to be able to model this behaviour numerically.

An important property of a plasma is the ability to shield individual particles from charges far away in the plasma. If a single ion is added to the plasma, the nearby electrons are attracted to it, and the nearby ions are repelled from it. This means an electron far away from the newly added ion will not see any additional electromagnetic force [21]. This phenomena is called 'Debye shielding'. The sphere around an ion, beyond which the charge is shielded, is the 'Debye sphere' of a plasma. The number of electrons within the Debye sphere shows how dominant collisions are within a plasma. The larger the number of electrons within the Debye sphere, the less importance collisions have within the plasma, and the more importance there is on collective effects [2].

In many plasmas there are too many particles to model every particle at once. Instead, some approximation of the motion within the plasma must be made. There are a variety of different approximations that are used, which are each valid for specific scenarios. The simplest method to model a plasma is to use *magnetohydrodynamics*. In this case either the entire plasma is treated as a single charged fluid, or each species (e.g. the electrons or the ions) is a separate charged fluid. These charged fluids are solved alongside Maxwell's equations to model the plasma. This is the computationally fastest model, and is used for modelling magnetic confinement fusion [22], and in some models of solar plasma [23], amongst others. Magnetohydrodynamics gives large scale behaviour of a plasma, but fails to model important properties within the plasma, such as wave breaking (part of the plasma travelling faster than another area, and overtaking it) [24, 25], or Landau damping (the damping of space charge effects as particles travelling at different speeds to the bulk plasma are accelerated or decelerated to match the bulk flow of the plasma) [2].

A more accurate, but computationally intensive method to model plasma is to use *kinetic* models. There are two choices when developing a kinetic model. If the plasma

being modelled can be approximated as collisionless, then the Vlasov equation describes the system [26]. The situations in which collisions need to be considered within a plasma include establishing thermodynamic equilibrium within a plasma, or in the collisions required for nuclear fusion [27]. If the plasma needs to include collisions, then the Fokker-Planck equation is used to describe the motion of the particles [2, 27]. Both of these methods suffer from being incredibly computationally intensive, as they require solving a seven-dimensional partial differential equation (time, three spatial coordinates, and three velocity coordinates). This computational intensity has restricted solving the Vlasov equation directly to a (1+1)D (one spatial dimension and one velocity dimension) problem, and it has only become possible in the last 20 years to simulate a basic (3+3)D Vlasov model [10, 28].

Rather than solving the full (3+3)D Vlasov equation, another option is to use a *particle-in-cell* (PIC) code. These treat the plasma as a collection of particles, which are updated in six-dimensional position and velocity phase space. It is too computationally intensive to model the behaviour of every particle within the plasma. PIC codes solve this issue by grouping large numbers of particles into a single *macroparticle*. Macroparticles make these codes computationally feasible, at the expense of losing information about the fine structure within the plasma.

Whilst PIC codes are predominantly used for modelling plasma, they can also be used for modelling electrons travelling through a particle accelerator. This is particularly useful for cases where the non-linear effects, such as space charge, and complicated magnetic fields within the accelerator need to be modelled [29, 30]. They can also be used in the modelling of a klystron, used to generate high intensity radio frequency (RF) waves used for accelerating particles [31, 32].

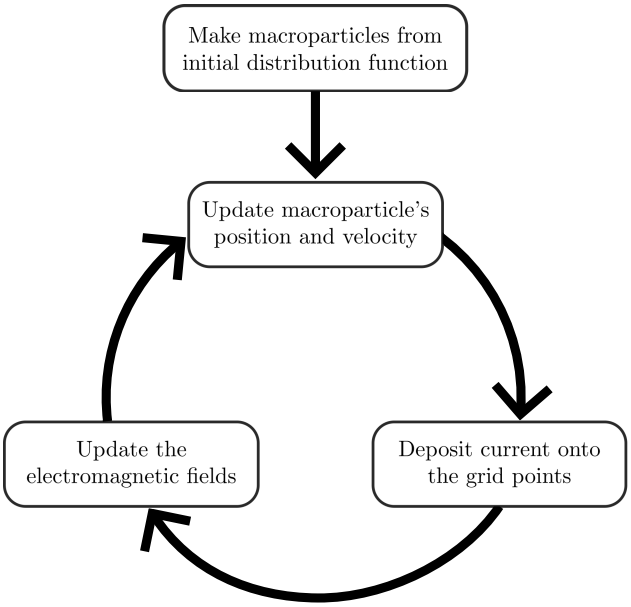

Figure 1.1: *The algorithm for a standard particle-in-cell code.*

The original algorithm for the PIC code was pioneered by Dawson [33]. A standard PIC code consists of three parts: update the macroparticle's positions and velocities, deposit the current to a discretised grid, and solve Maxwell's equations on this discretised grid (figure 1.1). Modern PIC codes contain extra features, with some codes being able to work in arbitrary curvilinear coordinates [34], conserve energy to within machine precision (in certain circumstances) [35], simulate quantum electrodynamic effects [36, 37], and model collisions [38, 39, 40]. Despite this, all PIC codes suffer from the same fundamental issue: there is no information about the structure within a macroparticle.

1.2 Using moments to improve macroparticles

In most PIC codes, accuracy is improved by increasing the number of macroparticles. By contrast, this thesis presents a different method, in which a macroparticle represents the moments of a group of particles [41, 42, 43, 44, 45] (figure 1.2). Such a model may be more efficient in cases where a large number of particles can be accurately modelled by a small number of macroparticles and their moments, and

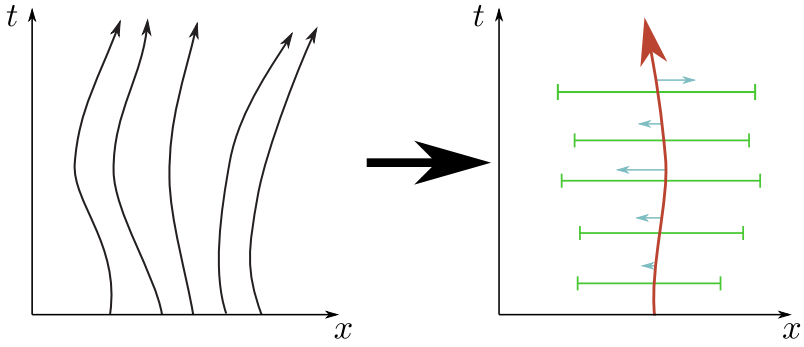

Figure 1.2: *Tracking several individual particles compared to a macroparticle with moments. The five particles (the black lines) in the left diagram are replaced by a single macroparticle (the orange line) in the right diagram. By tracking the moments, quantities such as the difference between the centre of charge of the five particles and the position of the macroparticle (the first order moment, represented by the horizontal blue arrows), and the variance in position of the particles (the second order moment, represented by the green error bars) can be tracked.*

the electromagnetic field does not vary much across the extent of the macroparticle. Additionally, when the dominating interactive force can be calculated from the Liénard-Wiechert potential, the electromagnetic fields can be calculated directly from the moments of the macroparticle [46].

There are several existing methods for tracking moments: the code MERLIN implements a transition matrix approach for particle accelerators [44] and a continuous model has been developed through a Hamiltonian approach [45]. Moment tracking can also be done continuously by differentiating the definition of a moment and using the Vlasov equation [43, 47]. In the literature of plasma physics, the concept of moment tracking is often used when discussing magnetohydrodynamics [10, 48, 49]. Moments in the context of magnetohydrodynamics are constructed by integrating over velocity space only and can be interpreted as physical quantities such as temperature and pressure, and shall be referred to as *plasma moments*. In this work, moments shall be constructed by integrating over both velocity and

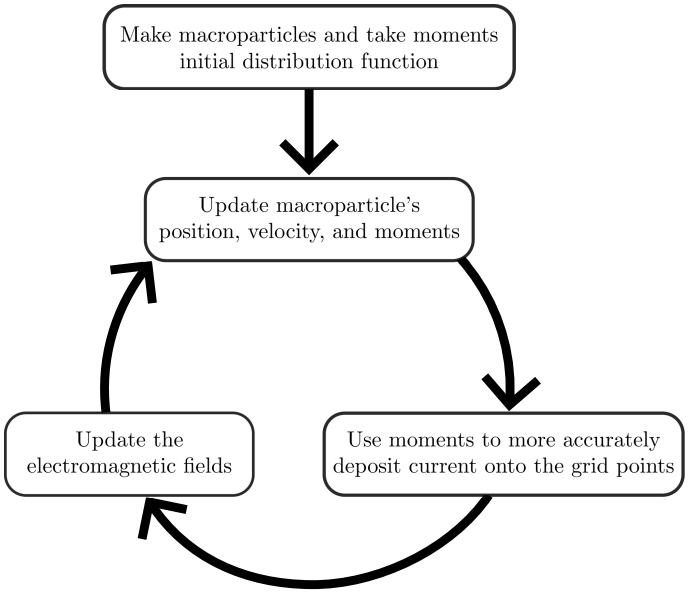

Figure 1.3: *The algorithm for a particle-in-cell code with moment tracking. The electromagnetic field solver is the same in both the standard particle-in-cell and moment tracking models.*

position space, giving related, but different quantities. The transport of moments is used in wider fields where the Liouville equation holds, such as particle nucleation [50], crystal growth [51], nuclear collisions [52], and fluid dynamics [53].

To track moments, the PIC algorithm needs to be modified (figure 1.3). At each time step, as well as updating a macroparticle's position and velocity, the moments also need to be updated. This creates additional computational overhead. In a standard PIC code, the current of a macroparticle is deposited onto grid points by assuming the macroparticle has a 'shape function', which weights how the current is placed onto the grid points (this is known as the *cloud-in-cell* method) [54, 55]. By using moments instead of a shape function, a more accurate current distribution function within the macroparticle can be found. This in turn feeds into Maxwell's equations for updating the electromagnetic fields, which gives a more accurate electromagnetic field with which to update the macroparticle's position, velocity, and moments. Thus by using macroparticles with moment tracking, the accuracy within a PIC code can

be improved, at the expense of computational overhead.

Order of moments tracked	**Information known**	**Number of differential equations to solve**	**Number of differential equations to solve relative to a standard macro-particle**
Monopole (zeroth order)	x^μ, u^μ	6	1
Dipole (first order)	x^μ, u^μ, V^a	12	2
Quadrupole (second order)	x^μ, u^μ, V^a, V^{ab}	33	5.5
Octopole (third order)	x^μ, u^μ, V^a, V^{ab}, V^{abc}	89	14.83
Hexadecapole (fourth order)	x^μ, u^μ, V^a, V^{ab}, V^{abc}, V^{abcd}	215	35.83

Table 1.1: *The amount of information in a macroparticle that tracks moments compared to a standard macroparticle. The increased information results in more memory usage and a larger number of first order differential equations to solve. Since there are six differential equations per time step for a standard macroparticle, the fourth column is the third column divided by six.*

Tracking more moments is more computationally expensive, as these moments come with additional computational work (both more differential equations to solve at each time step and more memory usage per macroparticle). This increased computational work is balanced by reducing the total number of macroparticles in the simulation. At the quadrupole (second) order there are 33 equations to solve at each time step (21 quadrupole moments, 6 dipole (first order) moments, 3 components of velocity and 3 components of position). This increases to 215 equations if the expansion is carried out to the hexadecapole level (fourth order) (table 1.1).

To perfectly track the moments, an infinite set of moments is required. This is because, as is shown in this thesis, higher order moments generate lower order moments. Since it is not possible to track an infinite set of moments, a *truncation* is required. There are multiple possibilities for this truncation. One possible method

is to directly track only a certain number of moments, and then approximate the higher order moments using these lower order moments [43]. Another truncation is to only consider a finite number of moments, neglecting the contribution from moments of a higher order than the truncation. This is the truncation used in this thesis. Care must be taken to ensure the truncation is of as low an order as possible to minimise computational load, whilst also ensuring that neglecting the higher order moments does not significantly impact accuracy. This thesis calculates all moments to quadrupole order, although all results presented can be generalised to arbitrary order.

1.3 Coordinate transformations of moments

Since the conception of black holes by Schwarzschild [56] as a consequence of Einstein's theory of general relativity, there has been a fascination with the concept of black holes in both modern physics [14, 57] and modern culture [58]. Recently, there has been a focus on using PIC codes to model the dynamics of plasma around black holes [34, 59, 60, 61]. Such plasmas may be important in active galactic nuclei, pulsars and gamma-ray bursts [61, 62, 63]. Reference [14] contains a full review of these studies. In such systems, there is not a preferred coordinate system i.e. when modelling a static uncharged black hole, there is a choice to work in Schwarzschild coordinates, or Kruskal-Szekeres coordinates, amongst others. As there is a choice, it is useful to be able to transform between different coordinate systems, especially where the time and space coordinates are mixed together (such as the coordinate transformation between Kruskal-Szekeres and Schwarzschild coordinates, shown in figure 1.4a). Coordinate transformations that mix space and time coordinates also appear in particle accelerators. When simulating the motion of a linearly accelerating bunch in a particle accelerator, the transformation into the instantaneous rest frame of an accelerating bunch mixes space and time coordinates (figure 1.4b), so the spacetime coordinate transformations presented in this work

are necessary.

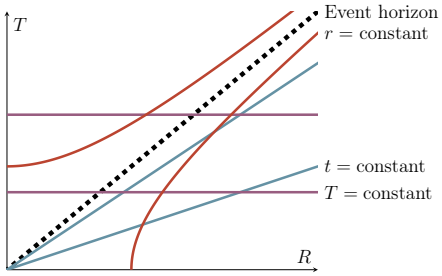

(a) *A spacetime diagram in Kruskal-Szekeres coordinates of a particle travelling at a constant r in Schwarzschild coordinates (the orange hyperbola). The diagonal blue lines are time slicings in Schwarzschild coordinates (constant t), and the horizontal purple lines are time slicings in Kruskal-Szekeres coordinates (constant T). The dashed black line represents the event horizon.*

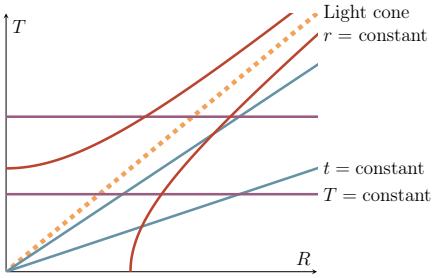

(b) *A spacetime diagram in the lab frame of an accelerating bunch showing particles that are accelerating according to a lab observer (the orange hyperbola). The diagonal blue lines are time slicings in the instantaneous rest frame coordinates (constant t), and the horizontal purple lines are time slicings in the lab frame (constant T). The dashed yellow line represents the light cone.*

Figure 1.4: *Spacetime diagrams showing the difference in time slicing between Kruskal-Szekeres and Schwarzschild coordinates, and between the lab frame and instantaneous rest frames of an accelerating bunch. The moments in a given coordinate system have no components in the direction of the time slicing in that coordinate system.*

The moments of a macroparticle depend on the choice of *time slicing* (figure 1.5). This time slicing is a foliation given by spatial hypersurfaces of constant coordinate time. In all coordinate systems considered in this thesis, the global *coordinate time* will be used as the time slicing. In general, different coordinate systems will give different time slicings. This means when transforming between coordinate systems that mix temporal and spatial coordinates, for example, transforming between

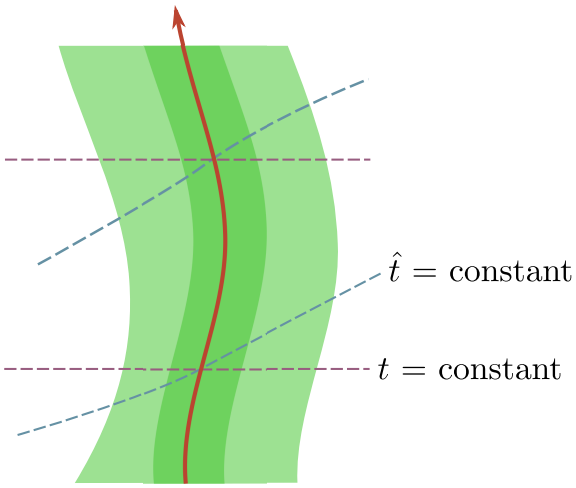

Figure 1.5: *An example of two different time slicings. When taking moments, the time slicing is the hypersurface the moments are integrated over. By using a different time slicing (e.g. either the horizontal dashed purple lines t or the curved dashed blue lines $\hat{t}$), the distance between the centre of the macroparticle (the orange arrow) and the nearby particles the macroparticle is representing (the green contours) is different, so different moments will be found.*

Schwarzschild and Kruskal-Szekeres coordinates, the time slicing will change (figure 1.4a). Additionally, it will be shown in chapter 4 that this time slicing is required to allow alternative representations of moments to be defined uniquely.

There are several choices for the time slicing. One time slicing may be the global Killing timelike vector in relativistic scenarios, the lab time in non-relativistic models, or the parameter of the beamline in a particle accelerator. Another possible time slicing is the backward light cone of an observer, which is the frame used when making astrophysical observations. A choice of time slicing commonly used in modelling plasma around black holes is found in the *fiducial observer* (FIDO) scheme, where the time slicing is given relative to local moving observers [64, 65]. A fourth possible time slicing is to take all the vectors orthogonal to the velocity of the world line. By using geodesics to propagate the vectors to the world line, they can be used for the Dixon representation of a multipole [66]. The proper time of the

initial centre of charge of a bunch cannot be used as a time slicing, as this is not an inertial frame [67].

One of the key results of this thesis is the formula for the coordinate transformation of moments between coordinate systems that mix space and time coordinates. The standard integral representation of moments cannot transform moments between coordinate systems where the time slicing changes. Simply transforming the moments into the new coordinate system does not take into account the change in time slicing. In principle, if one were to use the standard representation of moments, an 'effective' coordinate transformation could be performed. This is the process of reconstructing the distribution function from the moments, transforming the distribution function into the new coordinate system and retaking the moments in the new coordinate system. This requires a *model function*, which is a function that is used as a basis for reconstructing the distribution function. This process is outlined in chapter 6.

In order to find the coordinate transformations that change the time slicing, a different representation of moments must be used, in terms of Schwartz distributions [68, 69]. In this representation of moments, the moments are transformed into the new coordinate system, then *projected* onto the new time slicing to find the full coordinate transformation.

1.4 Finding the charge and current distribution from a set of moments

Tracking the moments is only one step of the particle-in-cell algorithm. As shown in figure 1.3, the next step is to use the moments to find the current of each macroparticle. In a standard PIC code, macroparticles are represented with a 'shape function', which does not change over time [54, 55]. By using the moments, the

distribution function of particles within a macroparticle can be approximated. This creates a more accurate current distribution within a macroparticle. Additionally by tracking the moments, this current distribution can change over time, in contrast to the shape function approach, where the current distribution is constant.

In general, even with an infinite set of moments, it is not possible to exactly reconstruct the original distribution used to create these moments [70]. This inability to exactly reconstruct a distribution from a set of moments is known as the moment problem. The most general of these problems assumes the original distribution function is integrable from $-\infty$ to ∞, and is known as the Hamburger problem [70]. In the case that the distribution function is compact, i.e. the bounds of integration are finite, then given an infinite set of moments, the function can be exactly reconstructed [71].

Given only a finite set of moments, it is not possible to exactly reconstruct the distribution used to generate the moments. Instead, some approximation to the original distribution function must be made. There are several existing approaches to approximating the reconstruction of a function given a set of moments. One method is to reconstruct the distribution by approximating the initial distribution as a set of splines, and give this set of splines the same moments as the initial distribution [72, 73]. Another approach models the distribution function as a series of orthogonal polynomials, which can in turn be related to the moments [74, 75]. Machine learning has also been applied to this problem, using the moments of a bunch to reconstruct the phase space distribution within a particle accelerator [76, 77].

The reconstruction of moments has a vast field of applications, including particle crystallisation and nucleation [50, 72, 73], 2D image reconstruction [78, 79], biophysics [80, 81], aerosols [82], the analysis of phonons [83, 84], and in the study

of ferrofluids [85].

Most studies for reconstructing model functions have been limited to either one or two dimensions. As far as the author is aware, there is little literature on how to reconstruct a function in an arbitrary number of dimensions using analytic methods. This thesis presents a method in which the original distribution function in an arbitrary number of dimensions can be reconstructed by creating a new function with the same moments as the original function. An alternative way of finding the 4-current from a given distributional 7-current is presented. This is done by integrating over the velocity space and using this reduced 7-current (a distributional 4-current) to reconstruct the source 4-current directly.

1.5 Thesis structure, conventions, and notation

This thesis is structured as follows: Chapter 2 introduces the seven-dimensional time-phase space, and the Vlasov equation, which describes the dynamics of collisionless charged particles. Chapter 3 introduces moments, and the existing methods for modelling them. Chapter 4 introduces a distributional representation of moments in terms of derivatives of Dirac delta functions and uses this representation to show the time evolution of moments. Several tests are done analytically, showing that the moment tracking equations agree with the transition matrix approach for modelling a quadrupole magnet; that moment tracking conserves phase space volume; and a limitation of the moment tracking model due to the truncation. The coordinate transformations for the moments are also found in this chapter. Chapter 5 numerically validates the moment tracking and coordinate transformation equations, through a computational model of uncharged particles circling a black hole. Chapter 6 shows how the moments can be used to find the charge and a current of a macroparticle, and numerically tests two different methods for finding this current. Chapter 7 discusses what further work needs to be taken to create a full

PIC code, and considers the specific application of the moment tracking model for simulating a klystron. Lastly, chapter 8 uses the language of differential geometry and de Rham currents to present the Vlasov equation, the transport equations, coordinate transformations, and current and charge reconstruction in this language. Whilst this approach gives a more geometric approach to deriving these equations, which may be considered philosophically nicer, there are no new results in this chapter, and as such this chapter can be skipped by a reader not familiar with the language of differential geometry. Alternatively, a reader familiar with the language of differential geometry may prefer to read chapter 8 first, to gain a more geometric interpretation of the mathematical results presented in this thesis.

Throughout the thesis, several complex proofs will be shown. These begin with *Proof.* and end with the □ symbol. These proofs may be skipped at first reading.

The calculations necessary to study plasma are performed in seven-dimensional time-phase space. Therefore, different summation conventions for indices are needed: summations over time, space, and velocity; time and space but not velocity; space and velocity but not time; just space, and just velocity. Because of this, the following summation conventions will be used:

- Latin indices a, b, c represent summations over $0, \ldots, 6$.
- Greek indices μ, ν, ρ represent summations over $0, \ldots, 3$.
- An underlined index means there is no summation over the 0 index, i.e. $\underline{a} = 1, \ldots, 6$ and $\underline{\mu} = 1, 2, 3$.
- Bold capital Latin indices $\mathbf{I}, \mathbf{K}$ and Greek indices $\mathbf{\Sigma}, \mathbf{\Lambda}$ represent multi-index lists, with capital Latin letters representing lists including spatial and velocity coordinates and capital Greek letters representing lists over just spatial coordinates. These lists are defined in section 6.2.

Additionally the following conventions and notations will be used:

- Dimensions are used such that $c = G = 1$.
- The metric signature of spacetime is $(-,+,+,+)$.
- The notation $f|_p$ represents the evaluation of a function at a point, i.e. $f|_p$ is f evaluated at p.
- After their introduction, the arguments of a function will not be written, unless needed for emphasis.
- An underlined variable represents a set of three components e.g. $\underline{x}$ represents the set of x^1, x^2, x^3.
- A doubly underlined variable represents a set of six components e.g. $\underline{\underline{\xi}}$ represents the set of $\xi^1, \xi^2, \xi^3, \xi^4, \xi^5, \xi^6$.
- A column vector will be denoted in bold font (e.g. $\mathbf{a}, \mathbf{E}$).
- A tilde underneath a variable (e.g. $\underset{\sim}{u}$) represents a vector at a point.
- A tensor density of weight one will be denoted in Fraktur (e.g. $\mathfrak{f}, \mathfrak{J}$) or calligraphic (e.g. $\mathcal{I}, \mathcal{J}$) font.
- In chapter 8, the evaluation of a vector field on a scalar field shall be denoted using angled brackets, e.g. if $W = W^a \partial_a$, then $W\langle f \rangle = W^a \partial_a f$ represents the vector field W acting on the scalar field f.

Chapter 2

The Vlasov equation and the transport equations

2.1 Seven-dimensional time-phase space

To model the complex dynamics of plasmas, it is necessary to work on a 7 dimensional *time-phase space*. These dimensions are time, three spatial dimensions and three proper velocity (4-velocity) dimensions. The time-phase space will be denoted by $\mathcal{E}$. It is often necessary to integrate over a specific time slice of $\mathcal{E}$. An integral over a specific time slice will be denoted Σ for an arbitrary time t or Σ_{t_0} for the evaluation at a specific time t_0. The coordinates of this dimension are $(t, x^{\underline{\mu}}, u^{\underline{\mu}})$ where t is the global time, $x^{\underline{\mu}}$ is a space coordinate, and $u^{\underline{\mu}}$ is a spatial coordinate of 4-velocity, defined such that

$$u^\mu = u^0 v^\mu, \tag{2.1.1}$$

where v^μ is the 3-velocity, and u^0 is the positive solution to the quadratic equation

$$g_{\mu\nu} u^\mu u^\nu = -1 \tag{2.1.2}$$

where g is the metric. In the specific example of Minkowski spacetime with Cartesian coordinates, u^0 is the Lorentz factor in special relativity, given by

$$u^0 = \left(1 + \sum_{\underline{\mu}=1}^{3} u^{\underline{\mu}} u^{\underline{\mu}}\right)^{\frac{1}{2}}. \tag{2.1.3}$$

The notation $(\xi^{\underline{a}})$ will be used to represent a general coordinate, such that

$$\xi^0 = t, \quad \xi^{\underline{\mu}} = x^{\underline{\mu}}, \quad \xi^{\underline{\mu}+3} = u^{\underline{\mu}} \tag{2.1.4}$$

i.e. $\xi^4 = u^1$, etc.

This thesis exclusively works in frames where t is a global time coordinate. As previously stated in the introduction, these frames are required to allow the moments to be defined (figure 1.5). It is assumed a global time coordinate always exists, at least near the world line. It will be shown in section 8.2 that the natural induced coordinates on $\mathcal{E}$ when using a global time coordinate are actually the Newtonian velocities $v^{\underline{\mu}}$, rather than the spatial component $u^{\underline{\mu}}$ of 4-velocity. For computational purposes it is more convenient to work with 4-velocity as this moves the singularity from $c = 1$ to infinity, removing the numerical floating point rounding error from particles travelling very close to the speed of light. The removal of this singularity is particularly useful for modelling particle accelerators, where speeds are often close to the speed of light. Using the 4-velocity does not affect any of the analytic results in this thesis.

Any integral of a scalar field must contain a measure Ω. The inclusion of the measure ensures that the evaluation of an integral is coordinate independent. This measure is given by

$$\Omega = \Omega_0 \, dt \, d^3x \, d^3u. \tag{2.1.5}$$

On $\mathcal{E}$, Ω_0 is given by

$$\Omega_0 = \frac{\det(g)}{(u^0)^4 u_0} \tag{2.1.6}$$

where the lack of square root in the determinant is because the integrals are over both position and velocity space, and the $1/(u^0)^4 u_0$ term comes from using 4-velocity as the velocity coordinates instead of Newtonian velocity. When integrating over a specific time slice, the measure becomes

$$\Omega_{0_\Sigma} = \Omega_0|_t = \left.\frac{\det(g)}{(u^0)^4 u_0}\right|_t . \tag{2.1.7}$$

This evaluation at specific time t will be implicit, and will not be stated in the integrals to enhance readability, as it does not affect any results in the thesis. In the specific case of special relativity, the measure can be written as

$$\Omega_0 = \frac{-\det(g)}{\gamma^5} \tag{2.1.8}$$

where γ is the Lorentz factor. These measures are derived in section 8.2, by pulling back the natural measure on the tangent bundle.

2.2 The Vlasov equation

As discussed in the introduction, one method to model the complicated dynamics of plasmas is to treat the plasma as collisionless. This method was first pioneered by Vlasov in 1938 to model the dispersion of waves in electron gases [86] (This paper is translated in ref. [26]).

To formulate a fully relativistic Vlasov equation, consider a group of charged particles, each with charge q and mass m. The distribution function of this group of particles is denoted $f(t, \underline{x}, \underline{u})$. Note that since f represents a group of particles, the support of f is closed. Consider an arbitrary spacetime with metric $g_{\mu\nu}(t, \underline{x})$, Christoffel symbols $\Gamma^\mu_{\nu\rho}(t, \underline{x})$ and electromagnetic 2-form $F_{\mu\nu}(t, \underline{x})$. Let $C(t)$ be a world line parameterised by t, the same parameter as the global time ξ^0. Let η be the prolongation of C, that is a curve on $\mathcal{E}$ such that

$$\eta^0(t) = C^0(t) = t, \quad \eta^{\underline{\mu}}(t) = C^{\underline{\mu}}(t), \quad \eta^{\underline{\mu}+3}(t) = \frac{dC^{\underline{\mu}}(t)}{dt}. \tag{2.2.1}$$

For a given value of t, $\eta(t)$ is a point in seven-dimensional time-phase space. In terms of coordinate functions $(t, x^{\underline{\mu}}, u^{\underline{\mu}})$, this can be represented as

$$\eta^0(t) = C^0(t) = t, \quad \eta^{\underline{\mu}}(t) = C^{\underline{\mu}}(t) = x^{\underline{\mu}}|_{\eta(t)}, \quad \eta^{\underline{\mu}+3} = \frac{dC^{\underline{\mu}}(t)}{dt} = \left.\frac{u^{\underline{\mu}}}{u^0}\right|_{\eta(t)}. \quad (2.2.2)$$

In general, $\eta(t)$ is a curve in time-phase space. In this thesis $\eta(t)$ will be the curve moments are taken around. In particle accelerators, the ideal orbit is a natural choice for $\eta(t)$. This choice does not exist in plasmas; in these cases choices for $\eta(t)$ could be the position of the macroparticle, or a trajectory based on the initial centre of charge of the macroparticle.

The Vlasov vector field, $W = W^a\partial_a$, where $\partial_a = \partial/\partial\xi^a$, is defined such that η is an integral curve of W,

$$W^a|_{\eta(t)} = \frac{d}{dt}\eta^a(t). \quad (2.2.3)$$

Finding the derivatives of η gives 7 ordinary differential equations (ODEs),

$$W^0|_{\eta(t)} = \left.\frac{dC^0(t)}{dt}\right|_{\eta(t)} = 1, \quad W^{\underline{\mu}}|_{\eta(t)} = \frac{dC^{\underline{\mu}}(t)}{dt} = \left.\frac{u^{\underline{\mu}}}{u^0}\right|_{\eta(t)}, \quad W^{\underline{\mu}+3}|_{\eta(t)} = \frac{d^2C^{\underline{\mu}}(t)}{dt^2}. \quad (2.2.4)$$

To find the acceleration, note that the parameterisation of $\eta(t)$, the global time coordinate t, is not affine. This means this acceleration is calculated using the pregeodesic equation combined with the (pre-)Lorentz force,

$$\left.\frac{d^2C^\mu(t)}{dt^2}\right|_\eta + \left.\left(\Gamma^\mu_{\nu\rho}\frac{dC^\nu(t)}{dt}\frac{dC^\rho(t)}{dt}\right)\right|_\eta = \left.\left(\kappa\frac{dC^\mu(t)}{dt}\right)\right|_\eta + \left.\left(\frac{q}{m}\frac{1}{u^0}F_{\nu\rho}g^{\underline{\mu}\nu}\frac{dC^\rho(t)}{dt}\right)\right|_\eta \quad (2.2.5)$$

where both the first term on the right hand side, and the $1/u^0$ term in the Lorentz force arise from using coordinate time as the parameterisation, rather than proper time. To find $\kappa(t)$, note $C^0 = t$, hence $d^2C^0/dt^2 = 0$, solving this gives

$$\kappa = \Gamma^0_{\nu\rho}\frac{dC^\nu(t)}{dt}\frac{dC^\rho(t)}{dt} - \frac{q}{m}\frac{1}{u^0}F_{\nu\rho}g^{0\nu}\frac{dC^\rho(t)}{dt}. \quad (2.2.6)$$

From this, solving equation (2.2.4) for all η gives

$$\begin{aligned} W^0 = 1, W^{\underline{\mu}} &= \frac{u^{\underline{\mu}}}{u^0}, \\ W^{\underline{\mu}+3} = &-\Gamma^{\underline{\mu}}_{\nu\rho}\frac{u^\nu}{u^0}\frac{u^\rho}{u^0} + \frac{q}{m}\frac{1}{u^0}F_{\nu\rho}g^{\underline{\mu}\nu}\frac{u^\rho}{u^0} + \Gamma^0_{\nu\rho}\frac{u^\nu}{u^0}\frac{u^\rho}{u^0}\frac{u^{\underline{\mu}}}{u^0} - \frac{q}{m}\frac{1}{u^0}F_{\nu\rho}g^{0\nu}\frac{u^\rho}{u^0}\frac{u^{\underline{\mu}}}{u^0}. \end{aligned} \tag{2.2.7}$$

Combining these terms together and acting on the particle distribution function f gives the Vlasov equation,

$$W^a\partial_a f = 0 \tag{2.2.8}$$

where $\partial_a = \partial/\partial\xi^a$. Rearranging this gives an important formulation of the Vlasov equation for calculating the dynamics of moments in the integral representation of moments in section 3.2,

$$\frac{\partial f}{\partial t} = -W^{\underline{a}}\frac{\partial f}{\partial \xi^{\underline{a}}}. \tag{2.2.9}$$

Since $W^{\underline{\mu}}|_{\eta(t)}$ and $W^{\underline{\mu}+3}|_{\eta(t)}$ correspond to the velocity and acceleration of a particle with the world line C, rewriting the Vlasov equation defined through a prolongation allows it to be compared to the more common formulation of the Vlasov equation (e.g. the Vlasov equation presented in refs. [10, 87]),

$$\frac{\partial f}{\partial t} + W^{\underline{\mu}}\frac{\partial f}{\partial x^{\underline{\mu}}} + W^{\underline{\mu}+3}\frac{\partial f}{\partial u^{\underline{\mu}}} = 0. \tag{2.2.10}$$

In general, the Vlasov field is parameterisation dependent. This thesis will work exclusively in the *coordinate time* frames. These are frames where the parameterisation t of $\eta(t)$ is the same as the time coordinate. This is true for the lab time in non-relativistic models, the Killing time in relativistic models, and the parameterisation of the beamline in a model of a particle accelerator. In any coordinate time frame, the Vlasov vector field will take the form of equation (2.2.7). If proper time is used as the parameterisation, then a different Vlasov vector field will be found [88, 89]. This formulation of the Vlasov vector field is also distinct from the $3+1$ formalism used in the *fiducial observer* (FIDO) scheme used when modelling plasma around strongly gravitating objects [64, 65]. The moment tracking and coordinate transformations found in this thesis will work in the FIDO scheme,

but will not work in the proper time parameterisation.

The Vlasov equation does not model a full PIC code on its own, and needs to be 'coupled' together with other equations to get a complete system. One choice is to couple the Vlasov equation to Maxwell's equations. By coupling to the dynamical Maxwell's equations (both Faraday's law and Ampère's law) a full electrodynamic PIC code can be developed. This will be the coupling for the full PIC code presented in chapter 7, and is the coupling in most PIC codes [36, 37]. Alternatively in cases where the magnetic force between particles is small compared to the external forces, only Gauss's law or Ampère's law is needed for the coupling, to allow an electrostatic PIC code to be developed [87, 90]. Another option is to integrate the Vlasov equation over velocity space to get equations for the plasma moments [35, 91]. This couples the Vlasov equation to the plasma moments, although it is stressed that these moments are only integrated over velocity space, so are distinct from the moments discussed in the rest of this thesis.

2.3 The transport equations

Rather than modelling the distribution function f, the *7-current* $\mathfrak{J}^a$ can be studied. This 7-current is related to the distribution function as

$$\mathfrak{J}^a = f\Omega_0 W^a = \mathfrak{f} W^a, \tag{2.3.1}$$

where

$$\mathfrak{f} = f\Omega_0 \tag{2.3.2}$$

is the distribution function density. Whilst f can be used in the integral representation of moments in chapter 3; to use the Ellis and geometric representations of moments in chapters 4 and 8, the distribution of particles needs to be represented as the 7-current.

To find the dynamics of the 7-current, there are two equations. Firstly, the conservation of charge,

$$\partial_a \mathfrak{J}^a = 0. \tag{2.3.3}$$

Secondly, the Vlasov equation,

$$\mathfrak{J}^a W^b - \mathfrak{J}^b W^a = 0. \tag{2.3.4}$$

These two equations will be referred to as the *transport equations*, since they define the transport of the 7-current over time. These equations follow from the Vlasov equation and the condition

$$\partial_a(\Omega_0 W^a) = 0. \tag{2.3.5}$$

Equation (2.3.5) will not be shown directly. In section 3.2 it is shown that this equation (2.3.5) corresponds to the conservation of charge. Equation (2.3.5) will also be shown in chapter 8. This is done by showing the equivalent equation on the tangent bundle is true, and pulling back this equation back onto $\mathcal{E}$.

To show the conservation of charge from the 7-current (equation (2.3.3)), insert equation (2.3.1) into equation (2.3.3),

$$\partial_a \mathfrak{J}^a = \partial_a \left(f \Omega_0 W^a \right) = \Omega_0 W^a \partial_a(f) + f \partial_a \left(\Omega_0 W^a \right) = 0 \tag{2.3.6}$$

where the Vlasov equation is used on the first term of the final step. To show the Vlasov equation for the 7-current (equation (2.3.4)), insert equation (2.3.1) into equation (2.3.4),

$$\mathfrak{J}^a W^b - \mathfrak{J}^b W^a = f \Omega_0 W^a W^b - f \Omega_0 W^b W^a = 0. \tag{2.3.7}$$

These transport equations will be used in chapter 4 to give the dynamics for the moments in a distributional representation.

Chapter 3

The integral representation of moments

3.1 Moments

One way of representing the bulk properties of a collection of particles are with their moments. The zeroth order moment, called the *monopole*, is given by

$$q = \int_{\Sigma} \mathfrak{f}(t, x, u)\, d^3x\; d^3u \tag{3.1.1}$$

and represents the total number of particles described by f. Note that, since charge is conserved, whilst the monopole is integrated at a specific moment in time, it is actually a constant, this will be proven when finding the dynamics of the moments in section 3.2, and equivalently shown in sections 4.3 and 8.3.2.

The first order moment, called the *dipole*, is given by

$$\begin{aligned} V^{\underline{\mu}}(t) &= \int_{\Sigma} \Big(x^{\underline{\mu}} - \eta^{\underline{\mu}}(t)\Big)\mathfrak{f}(t, x, u)\, d^3x\; d^3u, \\ V^{\underline{\mu}+3}(t) &= \int_{\Sigma} \Big(u^{\underline{\mu}} - \frac{dC^{\underline{\mu}}}{dt}(t)\Big)\mathfrak{f}(t, x, u)\, d^3x\; d^3u. \end{aligned} \tag{3.1.2}$$

These can be combined into a single equation,

$$V^{\underline{a}}(t) = \int_{\Sigma} \Big(\xi^{\underline{a}} - \eta^{\underline{a}}(t)\Big)\mathfrak{f}(t, x, u)\, d^6\xi \tag{3.1.3}$$

where $\xi^{\underline{a}}$ and $\eta^{\underline{a}}$ are defined by (2.1.4) and (2.2.2) respectively, $d^6\xi = d^3x\ d^3u$, and recall that an underlined latin index represents a summation over $1 \dots 6$. The dipole moment corresponds to the deviation of the centre of charge from the centre of the macroparticle. If the initial centre of the macroparticle is chosen such that the dipole moments are initially zero, then whilst the centre of the macroparticle will obey the Lorentz force equation, the centre of charge will not [67]. Hence, the two paths will diverge. The dipole moment represents the difference between these. The exact centre of charge, $\xi^{\underline{a}}_{\mathrm{CoC}}$, is given by

$$\xi^{\underline{a}}_{\mathrm{CoC}} = \frac{1}{q} V^{\underline{a}} + \eta^{\underline{a}}. \tag{3.1.4}$$

The second order moment, called the *quadrupole*, is given by

$$V^{\underline{ab}}(t) = \int_{\Sigma} \Big(\xi^{\underline{a}} - \eta^{\underline{a}}(t)\Big)\Big(\xi^{\underline{b}} - \eta^{\underline{b}}(t)\Big) \mathfrak{f}(t,x,u)\, d^6\xi. \tag{3.1.5}$$

The quadrupole moments are related to the variance of the macroparticle. The covariance matrix of the macroparticle is given by

$$(\text{Covariance})^{\underline{ab}} = (V^{\underline{ab}} - V^{\underline{a}} V^{\underline{b}}). \tag{3.1.6}$$

Note in the case the dipole is negligible compared to the quadrupole, then the quadrupole moments approximately represent the covariance of the macroparticle.

This formalism for the moments can be generalised to the nth order moment,

$$V^{\underline{a}_1,\dots,\underline{a}_n}(t) = \int_{\Sigma} \Big(\Big(\xi^{\underline{a}_1} - \eta^{\underline{a}_1}(t)\Big) \dots \Big(\xi^{\underline{a}_n} - \eta^{\underline{a}_n}(t)\Big)\Big) \mathfrak{f}(t,x,u)\, d^6\xi \tag{3.1.7}$$

where V is totally symmetric. Moments represented in this way will be called the *integral representation* of moments. Note the sums are only over space and velocity coordinates, and there are no corresponding 'time' moments. The naming convention for multipoles scales as 2^k, so the zeroth order moment is the monopole, then the dipole, quadrupole, octopole etc. (table 1.1). The octopole moment corresponds to the skew of the macroparticle, and the hexadecapole moment corresponds to

the kurtosis of the macroparticle. In contrast to this naming convention, moments in the context of magnetic multipoles scales as $2k$ (dipole, quadrupole, sextupole, octopole etc.). To avoid ambiguity, magnetic multipoles will always be explicitly named as such e.g. a quadrupole magnet refers to a quadrupole magnetic field, whilst a quadrupole refers to quadrupole moments.

As previously stated, the moments in this work are integrated over both position and momentum space, in contrast to the conventional moment equations for plasmas, which are just integrated over velocity space [10]. This definition of moments is often used to give physical properties of the plasma, like the current, temperature and pressure. It is possible to find the moments used in this work by integrating these quantities over position space. To go from the integral representation of moments back to the conventional moment equations for plasmas, you must reconstruct the original distribution function, and then integrate this over velocity space. This is done to find the current for solving Maxwell's equations in chapter 6.

3.2 Dynamics of moments

Using the Vlasov equation, it is possible to calculate the dynamics of moments using the integral representation. This was first done by Dymnikov and Perelshtein in 1978 [41]. It was also done through an equivalent but distinct method by Channell in 1983 [42], which was then implemented by Channell into the moment tracking code BEDLAM [43].

Both of these methods give the differential equations for the moments as an infinite series. As using an infinite series of moments is not practical, a truncation is required. This truncation is the highest order of moments considered, where moments beyond the truncation order are assumed to be zero. The choice of this truncation is one the largest sources of error in a moment tracking code, as will be shown in chapter

5. In practical codes, the simplest choice is to perform the truncation and neglect the higher order moments, however in certain moment tracking codes, for example in BEDLAM [43], higher order moments are approximated using the lower order moments, such as

$$V^{\underline{abc}} \approx \frac{1}{3}\left(V^{\underline{a}}V^{\underline{bc}} + V^{\underline{b}}V^{\underline{ac}} + V^{\underline{c}}V^{\underline{ba}}\right) \tag{3.2.1}$$

where $V^{\underline{abc}}$ is the octopole moment. This thesis will not take this approach, instead performing the truncation and neglecting the higher moments. This is because the focus of the computational results will be on how the truncation affects the convergence of the moment tracking model.

As a starting example to demonstrate Dymnikov and Perelshtein's method, the constancy of the monopole will be shown. Begin by differentiating equation (3.1.1) with respect to time

$$\frac{dq}{dt} = \frac{d}{dt}\int_{\Sigma} f(t,x,u)\,\Omega_0\,d^6\xi \tag{3.2.2}$$

where the scalar distribution is used rather than the density distribution. Since the domain of the integral is a time slice of the time-phase space $\mathcal{E}$, the derivative with respect to time can be passed inside the integral,

$$\frac{dq}{dt} = \int_{\Sigma} \frac{df}{dt}\,\Omega_0\,d^6\xi. \tag{3.2.3}$$

Next, using equation (2.2.9),

$$\frac{dq}{dt} = -\int_{\Sigma} W^{\underline{a}}\frac{\partial f}{\partial \xi^{\underline{a}}}\,\Omega_0\,d^6\xi. \tag{3.2.4}$$

Integrating by parts gives

$$\frac{dq}{dt} = \int_{\Sigma} f\partial_{\underline{a}}\left(W^{\underline{a}}\Omega_0\right)\,d^6\xi \tag{3.2.5}$$

where the evaluation of f on the boundaries of Σ vanishes since the support of f is closed. This vanishes if and only if $\partial_{\underline{a}}(W^{\underline{a}}\Omega_0) = 0$. The rate of change of the monopole must be zero as this corresponds to the conservation of charge. Thus, as previously stated, the condition $\partial_{\underline{a}}(W^{\underline{a}}\Omega_0) = 0$ must be true for charge to be

conserved. A more formal proof that this term vanishes will be done in chapter 8 through pulling back the measure on the tangent bundle.

To replicate Dymnikov and Perelshtein's result for the rate of change of the dipole, begin by differentiating equation (3.1.3) with respect to time and use equation (2.2.9),

$$\frac{dV^{\underline{a}}}{dt} = \frac{d}{dt}\int_\Sigma (\xi^{\underline{a}} - \eta^{\underline{a}})\, f\, \Omega_0\, d^6\xi \tag{3.2.6}$$

$$= -\int_\Sigma \dot{\eta}^{\underline{a}}\, f\, \Omega_0\, d^6\xi + \int_\Sigma (\xi^{\underline{a}} - \eta^{\underline{a}})\, \frac{df}{dt}\, \Omega_0\, d^6\xi \tag{3.2.7}$$

$$= -\dot{\eta}^{\underline{a}} \int_\Sigma f\, \Omega_0\, d^6\xi - \int_\Sigma (\xi^{\underline{a}} - \eta^{\underline{a}})\, W^{\underline{c}} \partial_{\underline{c}} f\, \Omega_0\, d^6\xi \tag{3.2.8}$$

where $\dot{\eta}^{\underline{a}}(t)$ are functions of t only, so they can be pulled out the integral. Next, integrate the last term by parts, using $\partial_{\underline{c}}(W^{\underline{c}}\Omega_0) = 0$, $\partial_b \xi^a = \delta^a_b$, and $\partial_{\underline{c}}\eta^{\underline{a}} = 0$ (since $\eta^a(t)$ is a function of time only), giving

$$\frac{dV^{\underline{a}}}{dt} = -\dot{\eta}^{\underline{a}} q + \int_\Sigma \partial_{\underline{c}}(\xi^{\underline{a}}) W^{\underline{c}} f\, \Omega_0\, d^6\xi \tag{3.2.9}$$

$$= -\dot{\eta}^{\underline{a}} q + \int_\Sigma W^{\underline{a}} f\, \Omega_0\, d^6\xi. \tag{3.2.10}$$

Next, Taylor expand $W^{\underline{a}}$ about η,

$$W^{\underline{a}} = \sum_{m=0}^{\infty} \frac{1}{m!} (\xi^{b_1} - \eta^{b_1}) \dots (\xi^{b_m} - \eta^{b_m}) \partial_{b_1} \dots \partial_{b_m} W^{\underline{a}}|_\eta. \tag{3.2.11}$$

Insert this expansion into $dV^{\underline{a}}/dt$,

$$\frac{dV^a}{dt} = -\dot{\eta}^{\underline{a}} q + \sum_{m=0}^{\infty} \frac{1}{m!} \partial_{\underline{c}_1} \dots \partial_{\underline{c}_m} W^{\underline{a}}|_\eta \int_\Sigma (\xi^{\underline{c}_1} - \eta^{\underline{c}_1}) \dots (\xi^{\underline{c}_m} - \eta^{\underline{c}_m})\, f\, \Omega_0\, d^6\xi \tag{3.2.12}$$

$$= -\dot{\eta}^{\underline{a}} q + \sum_{m=0}^{\infty} \frac{1}{m!} V^{\underline{c}_1 \dots \underline{c}_m} \partial_{\underline{c}_1} \dots \partial_{\underline{c}_m} W^{\underline{a}}|_\eta. \tag{3.2.13}$$

The first term in the expansion contains no derivatives, and the moment corresponding to $m = 0$ is the monopole q. This means the first term in the expansion is $\dot{\eta}^{\underline{a}} q$

(since $W^{\underline{a}}|_\eta = \dot{\eta}^{\underline{a}}$), cancelling the first term on the right hand side. This gives the differential equation for the dipole moment as

$$\frac{dV^{\underline{a}}}{dt} = \sum_{m=1}^{\infty} V^{\underline{c}_1 \cdots \underline{c}_m} \partial_{\underline{c}_1} \ldots \partial_{\underline{c}_m} W^{\underline{a}}|_\eta. \tag{3.2.14}$$

This has an important property: higher order moments generate lower order moments.

Before showing the differential equations for a general moment, it is worth showing the equation for the quadrupole first, to show how the process changes for higher order moments. Begin by differentiating equation (3.1.5),

$$\begin{aligned}
\frac{dV^{\underline{ab}}}{dt} = & -\int_{\mathcal{E}} \dot{\eta}^{\underline{a}} \left(\xi^{\underline{b}} - \eta^{\underline{b}}\right) f \, \Omega_0 \, d^6\xi - \int_{\Sigma} \dot{\eta}^{\underline{b}} \left(\xi^{\underline{a}} - \eta^{\underline{a}}\right) f \, \Omega_0 \, d^6\xi \qquad (3.2.15) \\
& + \int_{\Sigma} \left(\xi^{\underline{a}} - \eta^{\underline{a}}\right) \left(\xi^{\underline{b}} - \eta^{\underline{b}}\right) \frac{df}{dt} \, \Omega_0 \, d^6\xi \\
= & -\dot{\eta}^{\underline{a}} V^{\underline{b}} - \dot{\eta}^{\underline{b}} V^{\underline{a}} - \int_{\Sigma} \left(\xi^{\underline{a}} - \eta^{\underline{a}}\right) \left(\xi^{\underline{b}} - \eta^{\underline{b}}\right) W^{\underline{c}} \partial_{\underline{c}} f \, \Omega_0 \, d^6\xi \qquad (3.2.16) \\
= & -\dot{\eta}^{\underline{a}} V^{\underline{b}} - \dot{\eta}^{\underline{b}} V^{\underline{a}} + \int_{\Sigma} \left(\xi^{\underline{b}} - \eta^{\underline{b}}\right) W^{\underline{a}} f \, \Omega_0 \, d^6\xi + \int_{\Sigma} \left(\xi^{\underline{a}} - \eta^{\underline{a}}\right) W^{\underline{b}} f \, \Omega_0 \, d^6\xi \qquad (3.2.17)
\end{aligned}$$

where equation (2.2.9) is used, followed by integration by parts. Expanding $W^{\underline{a}}$ around η,

$$\begin{aligned}
\frac{dV^{\underline{ab}}}{dt} = & -\dot{\eta}^{\underline{a}} V^{\underline{b}} - \dot{\eta}^{\underline{b}} V^{\underline{a}} \\
& + \int_{\Sigma} \sum_{m=0}^{\infty} \frac{1}{m!} \partial_{\underline{c}_1} \ldots \partial_{\underline{c}_m} W^{\underline{a}}|_\eta \left(\xi^{\underline{c}_1} - \eta^{\underline{c}_1}\right) \ldots \left(\xi^{\underline{c}_m} - \eta^{\underline{c}_m}\right) \left(\xi^{\underline{b}} - \eta^{\underline{b}}\right) f \, \Omega_0 \, d^6\xi \\
& + \int_{\Sigma} \sum_{m=0}^{\infty} \frac{1}{m!} \partial_{\underline{c}_1} \ldots \partial_{\underline{c}_m} W^{\underline{b}}|_\eta \left(\xi^{\underline{c}_1} - \eta^{\underline{c}_1}\right) \ldots \left(\xi^{\underline{c}_m} - \eta^{\underline{c}_m}\right) \left(\xi^{\underline{a}} - \eta^{\underline{a}}\right) f \, \Omega_0 \, d^6\xi. \qquad (3.2.18)
\end{aligned}$$

The $m = 0$ terms of these sums cancel the first two terms of the right hand side, and simplifying the remaining terms gives

$$\frac{dV^{\underline{ab}}}{dt} = \sum_{m=1}^{\infty} \frac{1}{m!} \left(\partial_{\underline{c}_1} \ldots \partial_{\underline{c}_m} W^{\underline{a}}|_\eta V^{\underline{b}\underline{c}_1 \cdots \underline{c}_m} + \partial_{\underline{c}_1} \ldots \partial_{\underline{c}_m} W^{\underline{b}}|_\eta V^{\underline{a}\underline{c}_1 \cdots \underline{c}_m}\right). \tag{3.2.19}$$

To generalise this to the arbitrary order moment, begin by differentiating equation (3.1.7) with respect to time,

$$\frac{dV^{\underline{a}_1\cdots\underline{a}_n}}{dt} = \sum_{k=1}^{n}\int_{\Sigma} -\dot{\eta}^{\underline{a}_k}\left(\xi^{\underline{a}_1}-\eta^{\underline{a}_1}\right)\ldots\left(\xi^{\underline{a}_{k-1}}-\eta^{\underline{a}_{k-1}}\right) \times\left(\xi^{\underline{a}_{k+1}}-\eta^{\underline{a}_{k+1}}\right)\ldots\left(\xi^{\underline{a}_n}-\eta^{\underline{a}_n}\right) f\, d^6\xi + \int_{\Sigma}\left(\xi^{\underline{a}_1}-\eta^{\underline{a}_1}\right)\ldots\left(\xi^{\underline{a}_n}-\eta^{\underline{a}_n}\right)\frac{df}{dt}\,\Omega_0\, d^6\xi. \quad (3.2.20)$$

Using equation (2.2.9),

$$\frac{dV^{\underline{a}_1\cdots\underline{a}_n}}{dt} = -\sum_{k=1}^{n}\dot{\eta}^{\underline{a}_k}V^{\underline{a}_1\cdots\underline{a}_{k-1}\underline{a}_{k+1}\cdots\underline{a}_n} - \int_{\Sigma}\left(\xi^{\underline{a}_1}-\eta^{\underline{a}_1}\right)\ldots\left(\xi^{\underline{a}_n}-\eta^{\underline{a}_n}\right)W^{\underline{c}}\partial_{\underline{c}}f\,\Omega_0\, d^6\xi. \quad (3.2.21)$$

Integrating by parts,

$$\frac{dV^{\underline{a}_1\cdots\underline{a}_n}}{dt} = -\sum_{k=1}^{n}\dot{\eta}^{\underline{a}_k}V^{\underline{a}_1\cdots\underline{a}_{k-1}\underline{a}_{k+1}\cdots\underline{a}_n} + \sum_{k=1}^{n}\int_{\Sigma}\left(\xi^{\underline{a}_1}-\eta^{\underline{a}_1}\right)\ldots\left(\xi^{\underline{a}_{k-1}}-\eta^{\underline{a}_{k-1}}\right) \times\left(\xi^{\underline{a}_{k+1}}-\eta^{\underline{a}_{k+1}}\right)\ldots\left(\xi^{\underline{a}_n}-\eta^{\underline{a}_n}\right)W^{\underline{a}_k}f\,\Omega_0\, d^6\xi. \quad (3.2.22)$$

Inserting the Taylor expansion for W, introducing the substitution $\zeta^{\underline{a}}(t)=\xi^{\underline{a}}-\eta^{\underline{a}}(t)$ for brevity,

$$\frac{dV^{\underline{a}_1\cdots\underline{a}_n}}{dt} = -\sum_{k=1}^{n}\dot{\eta}^{\underline{a}_k}V^{\underline{a}_1\cdots\underline{a}_{k-1}\underline{a}_{k+1}\cdots\underline{a}_n} + \sum_{k=1}^{n}\sum_{m=0}^{\infty}\frac{1}{m!}\int_{\Sigma} f\zeta^{\underline{a}_1}\ldots\zeta^{\underline{a}_{k-1}}\zeta^{\underline{a}_{k+1}}\ldots\zeta^{\underline{a}_n}\zeta^{\underline{c}_1}\ldots\zeta^{\underline{c}_m}\partial_{\underline{c}_1}\ldots\partial_{\underline{c}_m}W^{\underline{a}_k}|_{\eta}\,\Omega_0\, d^6\xi. \quad (3.2.23)$$

Separating out the $m=0$ term, and pulling the differentials of $W^{\underline{a}_k}$ outside the

integral (since they are evaluated at η, so are functions of time only),

$$\frac{dV^{\underline{a}_1\cdots\underline{a}_n}}{dt} = -\sum_{k=1}^{n}\dot{\eta}^{\underline{a}_k}V^{\underline{a}_1\cdots\underline{a}_{k-1}\underline{a}_{k+1}\cdots\underline{a}_n} + \sum_{k=1}^{n}\dot{\eta}^{\underline{a}_k}\int_\Sigma \zeta^{\underline{a}_1}\ldots\zeta^{\underline{a}_{k-1}}\zeta^{\underline{a}_{k+1}}\ldots\zeta^{\underline{a}_n}\,\Omega_0\,d^6\xi$$
$$+\sum_{k=1}^{n}\sum_{m=1}^{\infty}\frac{1}{m!}\partial_{\underline{c}_1}\ldots\partial_{\underline{c}_m}W^{\underline{a}_k}|_\eta\int_\Sigma \zeta^{\underline{a}_1}\ldots\zeta^{\underline{a}_{k-1}}\zeta^{\underline{a}_{k+1}}\ldots\zeta^{\underline{a}_n}\zeta^{\underline{c}_1}\ldots\zeta^{\underline{c}_m}f\,\Omega_0\,d^6\xi. \tag{3.2.24}$$

The remaining integrals are simply moments, so first and second sums cancel, giving the remaining terms as

$$\frac{dV^{\underline{a}_1\cdots\underline{a}_n}}{dt} = \sum_{k=1}^{n}\sum_{m=1}^{\infty}\frac{1}{m!}V^{\underline{a}_1\cdots\underline{a}_{k-1}\underline{a}_{k+1}\cdots\underline{a}_n\underline{c}_1\cdots\underline{c}_m}\partial_{\underline{c}_1}\ldots\partial_{\underline{c}_m}W^{\underline{a}_k}|_\eta. \tag{3.2.25}$$

This is the general equation of motion for an arbitrary order moment.

As stated before, it is not possible to track an infinite set of moments. As such, a truncation is introduced, choosing the highest set of moments that will be considered. In this thesis, this truncation will be at the quadrupole level. After the truncation at the quadrupole level, the differential equations for the dipole and the quadrupole become

$$\frac{dV^{\underline{a}}}{dt} = V^{\underline{b}}\partial_{\underline{b}}W^{\underline{a}} + \frac{1}{2}V^{\underline{bc}}\partial_{\underline{b}}\partial_{\underline{c}}W^{\underline{a}} \tag{3.2.26}$$
$$\frac{dV^{\underline{ab}}}{dt} = V^{\underline{cb}}\partial_{\underline{c}}W^{\underline{a}} + V^{\underline{ac}}\partial_{\underline{c}}W^{\underline{b}}. \tag{3.2.27}$$

In these equations, the dipole generated by the quadrupole can clearly be seen. As previously stated, the moments of order octopole and higher have been assumed to be negligible as part of the truncation. The accuracy of this assumption is discussed in chapter 5.

Dymnikov and Perelshtein's method is not the only way to derive the differential equations for the moments through the integral representation. Channell's method [42] uses a similar approach, but begins by multiplying the Vlasov equation by some

set of points $(\xi^{\underline{a}} - \eta^{\underline{a}})$,

$$\left(\left(\xi^{\underline{a}_1} - \eta^{\underline{a}_1}(t)\right) \dots \left(\xi^{\underline{a}_n} - \eta^{\underline{a}_n}(t)\right)\right) \frac{\partial f}{\partial t} = -\left(\left(\xi^{\underline{a}_1} - \eta^{\underline{a}_1}(t)\right) \dots \left(\xi^{\underline{a}_n} - \eta^{\underline{a}_n}(t)\right)\right) W^{\underline{a}} \partial_{\underline{a}} f. \tag{3.2.28}$$

Multiplying by the measure and integrating across a time slice of time-phase space,

$$\int_\Sigma \zeta^{\underline{a}_1} \dots \zeta^{\underline{a}_n} \frac{\partial f}{\partial t} \, \Omega_0 \, d^6\xi = -\int_\Sigma \zeta^{\underline{a}_1} \dots \zeta^{\underline{a}_n} W^{\underline{a}} \Omega_0 \partial_{\underline{a}}(f) \, d^6\xi \tag{3.2.29}$$

where the substitution $\zeta^{\underline{a}}(t) = \xi^{\underline{a}} - \eta^{\underline{a}}(t)$ is used for brevity. Next, pulling the $\partial/\partial t$ out of the integral on the left hand side, noting that $d\zeta^{\underline{a}}/dt = \dot{\eta}^{\underline{a}}$, and integrating by parts on the right hand side,

$$\begin{aligned} \frac{d}{dt} \int_\Sigma \zeta^{\underline{a}_1} \dots \zeta^{\underline{a}_n} f \, \Omega_0 \, d^6\xi + \sum_{k=1}^{n} \int_\Sigma \dot{\eta}^{\underline{a}_k} \zeta^{\underline{a}_1} \dots \zeta^{\underline{a}_{k-1}} \zeta^{\underline{a}_{k+1}} \dots \zeta^{\underline{a}_n} f \, \Omega_0 \, d^6\xi \\ = \sum_{k=1}^{n} \int_\Sigma \zeta^{\underline{a}_1} \dots \zeta^{\underline{a}_{k-1}} \dots \zeta^{\underline{a}_{k+1}} \zeta^{\underline{a}_n} W^{\underline{a}_k} f \, \Omega_0 \, d^6\xi. \end{aligned} \tag{3.2.30}$$

The term on the left hand side and the first term on the right hand side are moments,

$$\begin{aligned} \frac{dV^{\underline{a}_1 \dots \underline{a}_n}}{dt} = -\sum_{k=1}^{n} \dot{\eta}^{\underline{a}_k} V^{\underline{a}_1 \dots \underline{a}_{k-1} \underline{a}_{k+1} \dots \underline{a}_n} \\ + \sum_{k=1}^{n} \int_\Sigma \zeta^{\underline{a}_1} \dots \zeta^{\underline{a}_{k-1}} \dots \zeta^{\underline{a}_{k+1}} \zeta^{\underline{a}_n} W^{\underline{a}_k} f \, \Omega_0 \, d^6\xi. \end{aligned} \tag{3.2.31}$$

At this point this is equivalent to equation (3.2.22) from the Dymnikov and Perelshtein approach, and by Taylor expanding $W^{\underline{a}_k}$, equation (3.2.25) can be found.

3.3 Coordinate transformations of moments where the time slicing is preserved

In general, the coordinate transformations for moments are complex [66, 68, 69]. As the integral representation of moments relies on integrals to define the moments, they are highly coordinate dependent objects. For the specific case of coordinate transformations where the time coordinate is unchanged, the integral representation

of the moments can be used to find the coordinate transformation. In coordinate transformations where the time and spatial coordinates are mixed together, then the integral representation of moments cannot be used, and an alternative representation of moments presented in chapter 4 must be used.

Consider two coordinate systems ξ^a and $\hat{\xi}^a$. If a coordinate transformation does not change the time slicing i.e. $\hat{t} = t$, it is possible to calculate the transformation of moments through the integral representation of moments. Since there is no change in time coordinate, the manifold Σ being integrated over is the same, $\hat{\Sigma} = \Sigma$. This means that the bounds of integration are the same.

As previously stated, $\mathfrak{f}$ transforms as a density, so

$$\hat{\mathfrak{f}} = \mathfrak{f}\frac{d^7\xi}{d^7\hat{\xi}} = \mathfrak{f}\frac{d^6\xi}{d^6\hat{\xi}}\frac{dt}{d\hat{t}} = \mathfrak{f}\frac{d^6\xi}{d^6\hat{\xi}} \tag{3.3.1}$$

since $\hat{t} = t$. From this, it is trivial to see that the monopole is invariant under a coordinate transformation, since

$$q = \int_\Sigma \mathfrak{f}\, d^6\xi = \int_\Sigma \hat{\mathfrak{f}}\, d^6\hat{\xi}. \tag{3.3.2}$$

To find the coordinate transformation of the dipole and quadrupole, observe that $\xi^{\underline{a}}(\hat{\xi}^{\underline{a}})$ gives $\xi^{\underline{a}}$ as a function in the new coordinate system. Consider the expansion of $\xi^{\underline{a}}$ in $\hat{\xi}^{\underline{a}}$ about $\eta^{\underline{a}}(\hat{t})$,

$$\xi^{\underline{a}} = \sum_{n=0}^{\infty} \frac{1}{n!}\left(\hat{\xi}^{\underline{b}_1} - \hat{\eta}^{\underline{b}_1}\right)\ldots\left(\hat{\xi}^{\underline{b}_n} - \hat{\eta}^{\underline{b}_n}\right)\frac{\partial}{\partial\hat{\xi}^{\underline{b}_1}}\ldots\frac{\partial}{\partial\hat{\xi}^{\underline{b}_n}}\xi^{\underline{a}}|_\eta. \tag{3.3.3}$$

Inserting these expansions into the expression for the dipole,

$$V^{\underline{a}} = \int_\Sigma \mathfrak{f}\,(\xi^{\underline{a}} - \eta^{\underline{a}})\, d^6\xi \tag{3.3.4}$$

$$= \int_\Sigma \hat{\mathfrak{f}}\left(\sum_{n=0}^{\infty} \frac{1}{n!}\left(\hat{\xi}^{\underline{b}_1} - \hat{\eta}^{\underline{b}_1}\right)\ldots\left(\hat{\xi}^{\underline{b}_n} - \hat{\eta}^{\underline{b}_n}\right)\frac{\partial}{\partial\hat{\xi}^{\underline{b}_1}}\ldots\frac{\partial}{\partial\hat{\xi}^{\underline{b}_n}}\xi^{\underline{a}}|_\eta - \eta^{\underline{a}}\right) d^6\hat{\xi}. \tag{3.3.5}$$

Pulling the derivatives of ξ out of the integral give an expansion in terms of an infinite series of moments,

$$V^{\underline{a}} = \int_\Sigma \hat{\mathfrak{f}} \left(\sum_{n=1}^{\infty} \frac{1}{n!} \left(\hat{\xi}^{\underline{b}_1} - \hat{\eta}^{\underline{b}_1} \right) \dots \left(\hat{\xi}^{\underline{b}_n} - \hat{\eta}^{\underline{b}_n} \right) \right) d^6\hat{\xi} \frac{\partial}{\partial \hat{\xi}^{\underline{b}_1}} \dots \frac{\partial}{\partial \hat{\xi}^{\underline{b}_n}} \xi^{\underline{a}}|_\eta + \int_\Sigma (\xi^{\underline{a}}|_\eta - \eta^{\underline{a}})\, d^6\hat{\xi}. \quad (3.3.6)$$

Evaluating this integral as the moments of $\hat{\mathfrak{f}}$,

$$V^{\underline{a}} = \sum_{n=1}^{\infty} \frac{1}{n!} \hat{V}^{\underline{b}_1 \dots \underline{b}_n} \frac{\partial}{\partial \hat{\xi}^{\underline{b}_1}} \dots \frac{\partial}{\partial \hat{\xi}^{\underline{b}_n}} \xi^{\underline{a}}|_\eta. \quad (3.3.7)$$

As with the differential equations for the moments, the coordinate transformation is also an infinite series of moments in the original coordinate system. This means again a truncation must be performed. Performing the truncation at the quadrupole level,

$$V^{\underline{a}} = \hat{V}^{\underline{b}} \left. \frac{\partial \xi^{\underline{a}}}{\partial \hat{\xi}^{\underline{b}}} \right|_\eta + \frac{1}{2} \hat{V}^{\underline{bc}} \left. \frac{\partial^2 \xi^{\underline{a}}}{\partial \hat{\xi}^{\underline{c}} \partial \hat{\xi}^{\underline{b}}} \right|_\eta. \quad (3.3.8)$$

The coordinate transformation of the quadrupole is found through a similar procedure,

$$V^{\underline{ab}} = \int_\Sigma \left(\xi^{\underline{a}} - \eta^{\underline{a}} \right) \left(\xi^{\underline{b}} - \eta^{\underline{b}} \right) \mathfrak{f}\, d^6\xi \quad (3.3.9)$$

$$= \int_\Sigma \left(\sum_{n=0}^{\infty} \frac{1}{n!} \left(\hat{\xi}^{\underline{c}_1} - \hat{\eta}^{\underline{c}_1} \right) \dots \left(\hat{\xi}^{\underline{c}_n} - \hat{\eta}^{\underline{c}_n} \right) \frac{\partial}{\partial \hat{\xi}^{\underline{c}_1}} \dots \frac{\partial}{\partial \hat{\xi}^{\underline{c}_n}} \xi^{\underline{a}}|_\eta - \eta^{\underline{a}} \right) \times \left(\sum_{m=0}^{\infty} \frac{1}{m!} \left(\hat{\xi}^{\underline{d}_1} - \hat{\eta}^{\underline{d}_1} \right) \dots \left(\hat{\xi}^{\underline{d}_m} - \hat{\eta}^{\underline{d}_m} \right) \frac{\partial}{\partial \hat{\xi}^{\underline{d}_1}} \dots \frac{\partial}{\partial \hat{\xi}^{\underline{d}_m}} \xi^{\underline{b}}|_\eta - \eta^{\underline{b}} \right) \hat{\mathfrak{f}}\, d^6\hat{\xi}. \quad (3.3.10)$$

Noting that the $n = 0$ and $m = 0$ terms of the sums cancel with the $\eta^{\underline{a}}$ and $\eta^{\underline{b}}$ terms, and pulling out the derivatives,

$$V^{\underline{ab}} = \sum_{n=1}^{\infty} \sum_{m=1}^{\infty} \frac{1}{n!} \frac{1}{m!} \int_\Sigma \left(\hat{\xi}^{\underline{c}_1} - \hat{\eta}^{\underline{c}_1} \right) \dots \left(\hat{\xi}^{\underline{c}_n} - \hat{\eta}^{\underline{c}_n} \right) \times \left(\hat{\xi}^{\underline{d}_1} - \hat{\eta}^{\underline{d}_1} \right) \dots \left(\hat{\xi}^{\underline{d}_m} - \hat{\eta}^{\underline{d}_m} \right) \hat{\mathfrak{f}}\, d^6\hat{\xi} \times \left(\frac{\partial}{\partial \hat{\xi}^{\underline{c}_1}} \dots \frac{\partial}{\partial \hat{\xi}^{\underline{c}_n}} \xi^{\underline{a}}|_\eta \right) \left(\frac{\partial}{\partial \hat{\xi}^{\underline{d}_1}} \dots \frac{\partial}{\partial \hat{\xi}^{\underline{d}_m}} \xi^{\underline{b}}|_\eta \right). \quad (3.3.11)$$

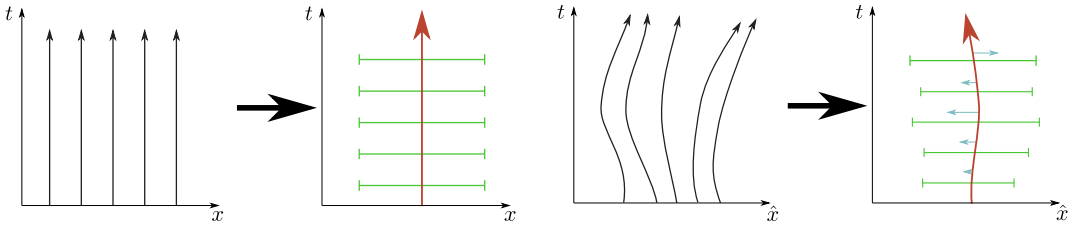

(a) *The original coordinate system.* **(b)** *The transformed coordinate system.*

Figure 3.1: *An example of a coordinate transformation where the dipole moment (the blue horizontal arrows) is zero in the original coordinate system, and non-zero in the transformed coordinate system. This dipole is generated by the quadrupole (the green error bars) when transforming coordinates.*

Evaluating these integrals,

$$V^{\underline{ab}} = \sum_{n=1}^{\infty}\sum_{m=1}^{\infty}\frac{1}{n!}\frac{1}{m!}\hat{V}^{\underline{c}_1\cdots\underline{c}_n\underline{d}_1\cdots\underline{d}_m}\left(\frac{\partial}{\partial\hat{\xi}^{\underline{c}_1}}\cdots\frac{\partial}{\partial\hat{\xi}^{\underline{c}_n}}\xi^{\underline{a}}|_\eta\right)\left(\frac{\partial}{\partial\hat{\xi}^{\underline{d}_1}}\cdots\frac{\partial}{\partial\hat{\xi}^{\underline{d}_m}}\xi^{\underline{b}}|_\eta\right). \tag{3.3.12}$$

This is the infinite sum of the coordinate transformation. Truncating this at the quadrupole level gives only the $n=1, m=1$ term of the summation,

$$V^{\underline{ab}} = \hat{V}^{\underline{cd}}\left.\frac{\partial\xi^{\underline{a}}}{\partial\hat{\xi}^{\underline{c}}}\right|_\eta\left.\frac{\partial\xi^{\underline{b}}}{\partial\hat{\xi}^{\underline{d}}}\right|_\eta. \tag{3.3.13}$$

It is worth stressing that whilst the quadrupole appears to be tensorial, it is only tensorial because of the truncation. If the truncation was at a higher order, the transformation for the quadrupole would depend on the higher order moments.

Since the coordinate transformation of moments depends on higher order moments, if a dipole moment is zero in one coordinate system it is not zero in all coordinate systems (figure 3.1).

In the case where the time coordinate changes, $\hat{\Sigma} \neq \Sigma$. Because of this, it is no longer possible to to relate the two manifolds together (figure 1.5). This means it is not possible to calculate the coordinate transformation where the time slicing changes using the integral representation of moments. In chapter 4 we will show a method

of calculating the coordinate transformation when the time slicing changes, by introducing a projection to transfer the moments from one time slicing to another.

Chapter 4

The Ellis representation of moments

4.1 Defining Ellis multipoles

Rather than defining moments explicitly through spatial integrals (equation (3.1.7)), an alternative representation of moments is through derivatives of Dirac delta functions. This means that rather than modelling a macroparticle as just a Dirac delta function and using a shape function to deposit charge (the cloud-in-cell approach), the macroparticle is represented as a set of derivatives of Dirac delta functions.

By using the language of the Schwartz distributions presented in this section, any coordinate transformation of the moments can be calculated, including those mixing space and time coordinates, which, as previously stated in section 3.3, cannot be done through equation (3.1.7). This coordinate transformation is done by projecting the moments from the original time slicing to the new time slicing.

Representing a multipole expansion using derivatives of a Dirac delta function is known as the *Ellis representation* of a multipole [46, 69, 92]. This thesis uses a specific *adapted Ellis representation* where there is a foliation given by the global time coordinate. In terms of Dirac delta functions the expansion to the second order

(the quadrupole), $\mathcal{J}^a$, is

$$\mathcal{J}^a = \frac{1}{2}\int_{\mathbb{R}} \dot{\eta}^a\, V^{\underline{bc}} \left(\partial_{\underline{b}}\partial_{\underline{c}}\delta^{(6)}(\xi-\eta)\right) dt - \int_{\mathbb{R}} \delta^a_{\underline{b}}\, X^{\underline{bc}} \left(\partial_{\underline{c}}\delta^{(6)}(\xi-\eta)\right) dt$$
$$- \int_{\mathbb{R}} \dot{\eta}^a\, V^{\underline{b}} \left(\partial_{\underline{b}}\delta^{(6)}(\xi-\eta)\right) dt + \int_{\mathbb{R}} \delta^a_{\underline{b}}\, X^{\underline{b}}\, \delta^{(6)}(\xi-\eta) dt + \int_{\mathbb{R}} \dot{\eta}^a\, q\, \delta^{(6)}(\xi-\eta) dt \quad (4.1.1)$$

where we recall that η is a fixed curve along $\mathcal{E}$ and that the differentiation is with respect to ξ i.e. $\partial_{\underline{b}} = \partial/\partial\xi^{\underline{b}}$, and

$$\delta^{(6)}(\xi-\eta) = \delta(\xi^1-\eta^1)\ldots\delta(\xi^6-\eta^6) \quad (4.1.2)$$

and

$$V^{\underline{bc}}(t) = \int_\Sigma (\xi^{\underline{b}}-\eta^{\underline{b}})(\xi^{\underline{c}}-\eta^{\underline{c}})\, \mathfrak{f}\, d^6\xi, \quad V^{\underline{b}}(t) = \int_\Sigma (\xi^{\underline{b}}-\eta^{\underline{b}})\, \mathfrak{f}\, d^6\xi, \quad q = \int_\Sigma \mathfrak{f}\, d^6\xi,$$
$$X^{\underline{ab}}(t) = V^{\underline{ac}}\partial_{\underline{c}}W^{\underline{b}}, \quad X^{\underline{a}}(t) = V^{\underline{b}}\partial_{\underline{b}}W^{\underline{a}} + \frac{1}{2}V^{\underline{bc}}\partial_{\underline{b}}\partial_{\underline{c}}W^{\underline{a}}. \quad (4.1.3)$$

Note q has no dependence on time due to the conservation of charge. In contrast with the quadrupoles presented in [69], the coordinate system is not chosen such that η is always along the origin. This means that equation (4.1.1) cannot be simplified to remove the integrals.

The terms $q, V^{\underline{a}}, X^{\underline{a}}, V^{\underline{ab}}$, and $X^{\underline{ab}}$ are called the *components* of a multipole. As this definition involves partial derivatives of Dirac delta functions, they are defined by their action on test functions $(\phi_0,\ldots,\phi_6)$ which are the components of a covector, and have compact support. Equation (4.1.1) acting on ϕ_a gives

$$\int_{\mathcal{E}} \mathcal{J}^a\phi_a d^7\xi = \frac{1}{2}\int_{\mathbb{R}} \dot{\eta}^a V^{\underline{bc}} \left(\partial_{\underline{c}}\partial_{\underline{b}}\phi_a|_{\eta(t)}\right) dt + \int_{\mathbb{R}} X^{\underline{ab}} \left(\partial_{\underline{b}}\phi_{\underline{a}}|_{\eta(t)}\right) dt$$
$$+ \int_{\mathbb{R}} \dot{\eta}^a V^{\underline{b}} \left(\partial_{\underline{b}}\phi_a|_{\eta(t)}\right) dt + \int_{\mathbb{R}} X^{\underline{a}}\phi_{\underline{a}}|_{\eta(t)} dt + \int_{\mathbb{R}} \dot{\eta}^a\, q\, \phi_a|_{\eta(t)} dt. \quad (4.1.4)$$

The evaluation of the test form at η will not be explicitly written in future representations of $\mathcal{J}^a$, but is implicitly present.

An alternative representation of moments uses covariant derivatives, rather than partial derivatives. This is known as the Dixon representation of a multipole [66,

69, 93]. This is not possible here due to the lack of a natural covariant derivative on $\mathcal{E}$.

Recall that the components in (4.1.3) are only over $(1, \ldots, 6)$ (there are no terms of the form V^0 or V^{01}). We shall see below that by writing a multipole in this way the components of a multipole are unique. This is due to the adapted Ellis representation used, with the specific time slicing.

The components of $\mathcal{J}^a$ can be extracted using the following test forms:

$$
\begin{aligned}
q|_{t_0} &= \lim_{\epsilon\to 0}\ \frac{1}{\epsilon}\ \int_{\mathcal{E}} \mathcal{J}^a\ \delta^0_a\ \psi\left(\frac{t-t_0}{\epsilon}\right) \prod_{i=1}^{6} \psi\left(\xi^i - \eta^i\right) d^7\xi \\
V^{\underline{b}}|_{t_0} &= \lim_{\epsilon\to 0}\ \frac{1}{\epsilon}\ \int_{\mathcal{E}} \mathcal{J}^a\ \delta^0_a\ \psi\left(\frac{t-t_0}{\epsilon}\right) \left(\xi^{\underline{b}} - \eta^{\underline{b}}\right) \prod_{i=1}^{6} \psi\left(\xi^i - \eta^i\right) d^7\xi \\
V^{\underline{bc}}|_{t_0} &= \lim_{\epsilon\to 0}\ \frac{2}{\epsilon}\ \int_{\mathcal{E}} \mathcal{J}^a\ \delta^0_a\ \psi\left(\frac{t-t_0}{\epsilon}\right) \left(\xi^{\underline{b}} - \eta^{\underline{b}}\right)\left(\xi^{\underline{c}} - \eta^{\underline{c}}\right) \prod_{i=1}^{6} \psi\left(\xi^i - \eta^i\right) d^7\xi \qquad (4.1.5) \\
\left(X^{\underline{b}} + q\dot{\eta}^{\underline{b}}\right)|_{t_0} &= \lim_{\epsilon\to 0}\ \frac{1}{\epsilon}\ \int_{\mathcal{E}} \mathcal{J}^a\ \delta^{\underline{b}}_a\ \psi\left(\frac{t-t_0}{\epsilon}\right) \prod_{i=1}^{6} \psi\left(\xi^i - \eta^i\right) d^7\xi \\
\left(X^{\underline{bc}} + V^{\underline{b}}\dot{\eta}^{\underline{c}}\right)|_{t_0} &= \lim_{\epsilon\to 0}\ \frac{1}{\epsilon}\ \int_{\mathcal{E}} \mathcal{J}^a\ \delta^{\underline{c}}_a\ \psi\left(\frac{t-t_0}{\epsilon}\right) \left(\xi^{\underline{b}} - \eta^{\underline{b}}\right)\ \prod_{i=1}^{6} \psi\left(\xi^i - \eta^i\right) d^7\xi
\end{aligned}
$$

where $\psi : \mathbb{R} \to \mathbb{R}$ is a test function such that $\psi_1(0) = 1$, it is flat about zero and $\int_{\mathbb{R}} \psi_1(t)dt = 1$, t_0 is the point at which the moments are evaluated.

Proof. Only the $V^{\underline{bc}}$ term and $X^{\underline{bc}} + V^{\underline{b}}\dot{\eta}^{\underline{c}}$ term will be shown as the other terms can be found similarly.

Consider $\mathcal{J}^a$ acting on the $V^{\underline{bc}}$ equation of (4.1.5). The only non-zero derivatives are the $\xi^{\underline{b}}$ and $\xi^{\underline{c}}$ terms. There are three possibilities, each $\xi^{\underline{b}}$ or $\xi^{\underline{c}}$ can either not be differentiated, differentiated once, or differentiated twice. If it is not differentiated, then the evaluation at η gives $(\xi^{\underline{b}} - \eta^{\underline{b}})|_\eta = \eta^{\underline{b}} - \eta^{\underline{b}} = 0$. If it is differentiated exactly once, then $\partial_{\underline{a}}(\xi^{\underline{b}} - \eta^{\underline{b}}) = \delta^{\underline{b}}_{\underline{a}}$, a Kronecker delta. If this is differentiated twice, then

the derivative of a Kronecker delta will vanish. Thus the only non zero term when acting $\mathcal{J}^a$ on the $V^{\underline{bc}}$ equation of (4.1.5) is the term where the number of derivatives matches the number of $\xi^{\underline{b}}$ terms. In this case this happens when there are exactly two partial derivatives. This gives

$$\lim_{\epsilon\to 0}\ \frac{2}{\epsilon}\ \int_{\mathcal{E}} \mathcal{J}^a\ \delta^0_a\ \psi\left(\frac{t-t_0}{\epsilon}\right)\left(\xi^{\underline{b}}-\eta^{\underline{b}}\right)\left(\xi^{\underline{c}}-\eta^{\underline{c}}\right)\prod_{i=1}^{6}\psi\left(\xi^i-\eta^i\right)d^7\xi$$
$$=\lim_{\epsilon\to 0}\ \frac{1}{\epsilon}\ \int_{\mathbb{R}}\dot{\eta}^0 V^{\underline{bc}}\psi\left(\frac{t-t_0}{\epsilon}\right)\prod_{i=1}^{6}\psi(\xi^i|_\eta-\eta^i)dt. \quad (4.1.6)$$

Noting $\xi^a|_\eta=\eta^a$, $\dot{\eta}^0=1$, $V^{\underline{bc}}=V^{\underline{bc}}(t)$ and introducing the substitution $t=t_0+\epsilon t'$ gives

$$\lim_{\epsilon\to 0}\ \frac{2}{\epsilon}\ \int_{\mathcal{E}} \mathcal{J}^a\ \delta^0_a\ \psi\left(\frac{t-t_0}{\epsilon}\right)\left(\xi^{\underline{b}}-\eta^{\underline{b}}\right)\left(\xi^{\underline{c}}-\eta^{\underline{c}}\right)\prod_{i=1}^{6}\psi\left(\xi^i-\eta^i\right)d^7\xi$$
$$=\lim_{\epsilon\to 0}\int_{\mathbb{R}} V^{\underline{bc}}(t_0+\epsilon t')\psi\left(t'\right)\left(\psi(0)\right)^6 dt'. \quad (4.1.7)$$

Integrating and taking the limit, noting $\psi(0)=1$ gives

$$\lim_{\epsilon\to 0}\ \frac{2}{\epsilon}\ \int_{\mathcal{E}} \mathcal{J}^a\ \delta^0_a\ \psi\left(\frac{t-t_0}{\epsilon}\right)\left(\xi^{\underline{b}}-\eta^{\underline{b}}\right)\left(\xi^{\underline{c}}-\eta^{\underline{c}}\right)\prod_{i=1}^{6}\psi\left(\xi^i-\eta^i\right)d^7\xi = V^{\underline{bc}}|_{t_0} \quad (4.1.8)$$

as required. In the extension to a higher order multipole, this still works as the δ^0_a term isolates only the $V^{\underline{ab}}$ term.

To isolate the $X^{\underline{bc}}+V^{\underline{b}}\dot{\eta}^{\underline{c}}$ term of $\mathcal{J}^a$, consider $\mathcal{J}^a$ acting on the $X^{\underline{bc}}+V^{\underline{b}}\dot{\eta}^{\underline{c}}$ equation of (4.1.5),

$$\lim_{\epsilon\to 0}\ \frac{1}{\epsilon}\ \int_{\mathcal{E}} \mathcal{J}^a\ \delta^{\underline{c}}_a\ \psi\left(\frac{t-t_0}{\epsilon}\right)\left(\xi^{\underline{b}}-\eta^{\underline{b}}\right)\ \prod_{i=1}^{6}\psi\left(\xi^i-\eta^i\right)d^7\xi$$
$$=\lim_{\epsilon\to 0}\ \frac{1}{\epsilon}\ \int_{\mathbb{R}}\dot{\eta}^{\underline{a}}V^{\underline{b}}\psi\left(\frac{t-t_0}{\epsilon}\right)\prod_{i=1}^{6}\psi(\xi^i|_\eta-\eta^i)dt$$
$$+\lim_{\epsilon\to 0}\ \frac{1}{\epsilon}\int_{\mathbb{R}} X^{\underline{ab}}\psi\left(\frac{t-t_0}{\epsilon}\right)\prod_{i=1}^{6}\psi(\xi^i|_\eta-\eta^i)dt. \quad (4.1.9)$$

Repeating the previous process gives

$$\lim_{\epsilon\to 0}\ \frac{1}{\epsilon}\ \int_{\mathcal{E}} \mathcal{J}^a\ \delta^{\underline{c}}_{a}\ \psi\left(\frac{t-t_0}{\epsilon}\right)\left(\xi^{\underline{b}}-\eta^{\underline{b}}\right)\ \prod_{i=1}^{6}\psi\left(\xi^i-\eta^i\right)d^7\xi = \left(X^{\underline{bc}}+V^{\underline{b}}\dot{\eta}^{\underline{c}}\right)|_{t_0}. \tag{4.1.10}$$

$X^{\underline{ab}}$ can be isolated after finding $V^{\underline{a}}$ using the appropriate test form. Since the components $V^{\underline{a}}, V^{\underline{ab}}, X^{\underline{a}}$ and $X^{\underline{ab}}$ can all be extracted using test forms, the components of $\mathcal{J}^a$ are unique. □

If the V^0 terms etc. were included in the multipole, then there can be multiple components which correspond to the same multipole (the components are not unique). To see this, consider the integral

$$\int_{\mathbb{R}}\left(U^{ab}+k^a\dot{\eta}^b\right)\left(\partial_b\phi_a|_\eta\right)dt \tag{4.1.11}$$

where k^a are constants. Noting that $\dot{\eta}^b\partial_b\phi_a|_\eta = d\phi_a/dt|_\eta$, this integral evaluates as

$$\begin{aligned}
\int_{\mathbb{R}}\left(U^{ab}+k^a\dot{\eta}^b\right)\left(\partial_b\phi_a|_\eta\right)dt &= \int_{\mathbb{R}}U^{ab}\left(\partial_b\phi_a|_\eta\right)dt+\int_{\mathbb{R}}k^a\left(\dot{\eta}^b\partial_b\phi_a|_\eta\right)dt && (4.1.12)\\
&= \int_{\mathbb{R}}U^{ab}\left(\partial_b\phi_a|_\eta\right)dt+\int_{\mathbb{R}}k^a\left.\frac{d\phi_a}{dt}\right|_\eta dt && (4.1.13)\\
&= \int_{\mathbb{R}}U^{ab}\left(\partial_b\phi_a|_\eta\right)dt-\int_{\mathbb{R}}\frac{d}{dt}\left(k^a\right)\phi_a|_\eta\,dt && (4.1.14)\\
&= \int_{\mathbb{R}}U^{ab}\left(\partial_b\phi_a|_\eta\right)dt. && (4.1.15)
\end{aligned}$$

This shows that if the indices run over $(0,\ldots,6)$, there is a gauge-like invariance that means it is impossible to uniquely define the moments. In the case k^a are not constants, this method can be used to project components into other components. This will be used in section 4.4 when calculating the coordinate transformation, to project the transformed multipole onto the new time slicing.

4.2 Relating the components of Ellis multipoles and moments

To show the relationship between the components of (4.1.4) and the moments of f (equation (4.1.3)), the distribution function f is *squeezed*. This is the process of representing a function using a Dirac delta function and the derivative of Dirac delta functions . The moments of f are the coefficients of this expansion. By doing this, it can be shown that the moments of the distribution function f naturally appear in the components of the Ellis representation of a multipole.

Squeezing a distribution can be shown using the language of differential geometry. Consider a smooth 6-form, J, that describes the flow of particles in a collisionless plasma,

$$J = \mathfrak{f}\, i_W\, d^7\xi = \mathfrak{f}\, W^a i_a\, d^7\xi = \mathfrak{f}\, d\xi^{1\ldots6} - \mathfrak{f}\, W^{\underline{a}} dt \wedge i_{\underline{a}} d\xi^{1\ldots6} \tag{4.2.1}$$

where $\wedge$ is the wedge product, i_W is an internal contraction with respect to W, and $i_{\underline{a}}$ is an internal contraction with respect to $\partial_{\underline{a}}$,

$$d\xi^{1\ldots6} = d\xi^1 \wedge d\xi^2 \wedge d\xi^3 \wedge d\xi^4 \wedge d\xi^5 \wedge d\xi^6. \tag{4.2.2}$$

The 6-form J is called the *current 6-form*, and is investigated in more detail in chapter 8.

A one parameter family of smooth 6-forms J_ε can be defined as

$$J_\varepsilon\big|_{\left(t,\underline{\underline{\xi}}\right)} = \frac{1}{\varepsilon^6}\,\mathfrak{f}\left(t, \frac{\underline{\underline{\xi}} - \underline{\underline{\eta}}}{\varepsilon}\right) d\xi^{1\ldots6}\bigg|_{\left(t,\underline{\underline{\eta}}\right)} - \frac{1}{\varepsilon^6}\left(\mathfrak{f}\left(t, \frac{\underline{\underline{\xi}} - \underline{\underline{\eta}}}{\varepsilon}\right) W^{\underline{a}}\right) dt \wedge i_{\underline{a}} d\xi^{1\ldots6}\bigg|_{\left(t,\underline{\underline{\xi}}\right)} \tag{4.2.3}$$

where $\underline{\underline{\xi}}$ refers to the combination of all spatial coordinates. This is not the only choice of one parameter family for J. This particularly choice of one parameter family is used as it corresponds to the time slicing, since the dependence of J_ε on the global time coordinate is not affected by ε.

By expanding J_ε about $\epsilon = 0$,

$$\phi \wedge J_\varepsilon = \bar{\mathcal{J}}^a \phi_a + \mathcal{O}(\varepsilon^3) \tag{4.2.4}$$

where ϕ is a test form (a form with compact support) $\phi_a d\xi^a$, and

$$\begin{aligned}\bar{\mathcal{J}}^a = \frac{1}{2}\int_{\mathbb{R}} \dot{\eta}^a \, \bar{V}^{\underline{bc}} \left(\partial_{\underline{b}}\partial_{\underline{c}}\delta^{(6)}(\xi-\eta)\right) dt - \int_{\mathbb{R}} \delta^a_{\underline{b}} \, \bar{X}^{\underline{bc}} \left(\partial_{\underline{c}}\delta^{(6)}(\xi-\eta)\right) dt \\ - \int_{\mathbb{R}} \dot{\eta}^a \, \bar{V}^{\underline{b}} \left(\partial_{\underline{b}}\delta^{(6)}(\xi-\eta)\right) dt + \int_{\mathbb{R}} \delta^a_{\underline{b}} \, \bar{X}^{\underline{b}} \, \delta^{(6)}(\xi-\eta) dt \\ + \int_{\mathbb{R}} \dot{\eta}^a \, q \, \delta^{(6)}(\xi-\eta) dt\end{aligned} \tag{4.2.5}$$

where

$$\begin{aligned} q = \int_\Sigma \mathfrak{f}\left(t, \underline{\bar{\xi}}\right) d\bar{\xi}^{1\ldots6}, \quad \bar{V}^{\underline{a}} = \varepsilon \int_\Sigma \mathfrak{f}\left(t, \underline{\bar{\xi}}\right) \left(\bar{\xi}^{\underline{a}} - \eta^{\underline{a}}\right) d\bar{\xi}^{1\ldots6}, \\ \bar{V}^{\underline{ab}} = \varepsilon^2 \int_\Sigma \mathfrak{f}\left(t, \underline{\bar{\xi}}\right) \left(\bar{\xi}^{\underline{a}} - \eta^{\underline{a}}\right) \left(\bar{\xi}^{\underline{b}} - \eta^{\underline{b}}\right) d\bar{\xi}^{1\ldots6}, \\ \bar{X}^{\underline{a}} = \bar{V}^{\underline{b}}(\partial_{\underline{b}} W^{\underline{a}})|_\eta + \frac{1}{2}\bar{V}^{\underline{bc}}(\partial_{\underline{b}}\partial_{\underline{c}} W^{\underline{a}})|_\eta, \quad \bar{X}^{\underline{ab}} = \bar{V}^{\underline{bc}}(\partial_{\underline{c}} W^{\underline{a}})|_\eta, \end{aligned} \tag{4.2.6}$$

where Σ is the spatial part of $\mathcal{E}$. Note $\bar{X}^{\underline{a}}$ is inhomogeneous in ε, since $V^{\underline{a}}$ contains an ε term whilst $V^{\underline{ab}}$ contains an ε^2 term.

Proof. Begin by wedging J_ε against a test form $\phi = \phi_a d\xi^a$,

$$\begin{aligned} \phi \wedge J_\varepsilon|_{\left(t,\underline{\underline{\xi}}\right)} = \; & \frac{1}{\varepsilon^6}\mathfrak{f}\left(t, \frac{\underline{\underline{\xi}} - \eta}{\varepsilon}\right) \phi_0 \, dt \wedge d\xi^{1\ldots6}\Big|_{\left(t,\underline{\underline{\xi}}\right)} \qquad (4.2.7) \\ & - \frac{1}{\varepsilon^6}\mathfrak{f}\left(t, \frac{\underline{\underline{\xi}} - \eta}{\varepsilon}\right) W^{\underline{a}}\phi_{\underline{b}} \, d\xi^{\underline{b}} \wedge dt \wedge i_{\underline{a}} d\xi^{1\ldots6}\Big|_{\left(t,\underline{\underline{\xi}}\right)} \\ = \; & \frac{1}{\varepsilon^6}\mathfrak{f}\left(t, \frac{\underline{\underline{\xi}} - \eta}{\varepsilon}\right) \phi_0 \, dt \wedge d\xi^{1\ldots6}\Big|_{\left(t,\underline{\underline{\xi}}\right)} \qquad (4.2.8) \\ & + \frac{1}{\varepsilon^6}\mathfrak{f}\left(t, \frac{\underline{\underline{\xi}} - \eta}{\varepsilon}\right) W^{\underline{a}}\phi_{\underline{b}} \, dt \wedge d\xi^{\underline{b}} \wedge i_{\underline{a}} d\xi^{1\ldots6}\Big|_{\left(t,\underline{\underline{\xi}}\right)} \\ = \; & \frac{1}{\varepsilon^6}\mathfrak{f}\left(t, \frac{\underline{\underline{\xi}} - \eta}{\varepsilon}\right) \phi_0\left(\underline{\underline{\xi}}\right) dt \wedge d\xi^{1\ldots6}\Big|_{\left(t,\underline{\underline{\xi}}\right)} \qquad (4.2.9) \\ & + \frac{1}{\varepsilon^6}\mathfrak{f}\left(t, \frac{\underline{\underline{\xi}} - \eta}{\varepsilon}\right) W^{\underline{a}}\phi_{\underline{a}} \, dt \wedge d\xi^{1\ldots6}\Big|_{\left(t,\underline{\underline{\xi}}\right)}. \end{aligned}$$

Making the substitution $\underline{\bar{\xi}} = (\underline{\xi} - \eta)/\varepsilon$, and making the evaluation at $(t, \underline{\xi})$ implicitly,

$$\begin{aligned}\phi \wedge J_\varepsilon|_{\left(t,\underline{\xi}\right)} &= \frac{1}{\varepsilon^6}\mathfrak{f}\left(t,\underline{\bar{\xi}}\right)\phi_0\left(t,\eta+\varepsilon\underline{\bar{\xi}}\right)\varepsilon^6 dt\wedge d\bar{\xi}^{1\ldots6} \\ &\quad+\frac{1}{\varepsilon^6}\mathfrak{f}\left(t,\underline{\bar{\xi}}\right)W^{\underline{a}}\left(\eta+\varepsilon\underline{\bar{\xi}}\right)\phi_{\underline{a}}\left(t,\eta+\varepsilon\underline{\bar{\xi}}\right)\varepsilon^6 dt\wedge d\bar{\xi}^{1\ldots6} \qquad (4.2.10)\\ &= \mathfrak{f}\left(t,\underline{\bar{\xi}}\right)\phi_0\left(t,\eta+\varepsilon\underline{\bar{\xi}}\right)dt\wedge d\bar{\xi}^{1\ldots6} \\ &\quad+\mathfrak{f}\left(t,\underline{\bar{\xi}}\right)W^{\underline{a}}\left(t,\eta+\varepsilon\underline{\bar{\xi}}\right)\phi_{\underline{a}}\left(t,\eta+\varepsilon\underline{\bar{\xi}}\right)dt\wedge d\bar{\xi}^{1\ldots6}. \qquad (4.2.11)\end{aligned}$$

Taylor expanding $\phi_0, \phi_{\underline{a}}$, and $W^{\underline{a}}$ around η, noting there are only spatial derivatives as $\xi^0|_\eta - \eta^0 = t - t = 0$,

$$\begin{aligned}\phi \wedge J_\varepsilon|_{\left(t,\underline{\xi}\right)} &= \mathfrak{f}\left(t,\underline{\bar{\xi}}\right)\phi_0|_\eta\, dt\wedge d\bar{\xi}^{1\ldots6}+\mathfrak{f}\left(t,\underline{\bar{\xi}}\right)W^{\underline{a}}|_\eta\phi_{\underline{a}}|_\eta\, dt\wedge d\bar{\xi}^{1\ldots6} \\ &+\mathfrak{f}\left(t,\underline{\bar{\xi}}\right)\varepsilon\left(\bar{\xi}^{\underline{b}}-\eta^{\underline{b}}\right)\partial_{\underline{b}}\phi_0|_\eta\, dt\wedge d\bar{\xi}^{1\ldots6}+\mathfrak{f}\left(t,\underline{\bar{\xi}}\right)\varepsilon\left(\bar{\xi}^{\underline{b}}-\eta^{\underline{b}}\right)\partial_{\underline{b}}(\phi_{\underline{a}}W^{\underline{a}})|_\eta\, dt\wedge d\bar{\xi}^{1\ldots6} \\ &+\frac{1}{2}\mathfrak{f}\left(t,\underline{\bar{\xi}}\right)\varepsilon^2\left(\bar{\xi}^{\underline{b}}-\eta^{\underline{b}}\right)\left(\bar{\xi}^{\underline{c}}-\eta^{\underline{c}}\right)\partial_{\underline{b}}\partial_{\underline{c}}\phi_0|_\eta\, dt\wedge d\bar{\xi}^{1\ldots6} \\ &+\frac{1}{2}\mathfrak{f}\left(t,\underline{\bar{\xi}}\right)\varepsilon^2\left(\bar{\xi}^{\underline{b}}-\eta^{\underline{b}}\right)\left(\bar{\xi}^{\underline{c}}-\eta^{\underline{c}}\right)\partial_{\underline{b}}\partial_{\underline{c}}(\phi_{\underline{a}}W^{\underline{a}})|_\eta\, dt\wedge d\bar{\xi}^{1\ldots6}+\mathcal{O}(\varepsilon^3). \qquad (4.2.12)\end{aligned}$$

Next, integrate this over $\mathcal{E}$, splitting $\mathcal{E}$ into $\mathbb{R}\times\Sigma$. The terms only depending on $\underline{\bar{\xi}}$ can be integrated out,

$$\begin{aligned}\int_{\mathcal{E}}\phi\wedge J_\varepsilon|_{\left(t,\underline{\xi}\right)} &= \int_{\mathbb{R}}\left(\int_\Sigma\mathfrak{f}\left(t,\underline{\bar{\xi}}\right)d\bar{\xi}^{1\ldots6}\right)\phi_0|_\eta\, dt+\int_{\mathbb{R}}\left(\int_\Sigma\mathfrak{f}\left(t,\underline{\bar{\xi}}\right)d\bar{\xi}^{1\ldots6}\right)W^{\underline{a}}|_\eta\phi_{\underline{a}}|_\eta\, dt \\ &+\int_{\mathbb{R}}\left(\varepsilon\int_\Sigma\mathfrak{f}\left(t,\underline{\bar{\xi}}\right)\left(\bar{\xi}^{\underline{b}}-\eta^{\underline{b}}\right)d\bar{\xi}^{1\ldots6}\right)\partial_{\underline{b}}\phi_0|_\eta\, dt \\ &+\int_{\mathbb{R}}\left(\varepsilon\int_\Sigma\mathfrak{f}\left(t,\underline{\bar{\xi}}\right)\left(\bar{\xi}^{\underline{b}}-\eta^{\underline{b}}\right)d\bar{\xi}^{1\ldots6}\right)\partial_{\underline{b}}(\phi_{\underline{a}}W^{\underline{a}})|_\eta\, dt \\ &+\frac{1}{2}\int_{\mathbb{R}}\left(\varepsilon^2\int_\Sigma\mathfrak{f}\left(t,\underline{\bar{\xi}}\right)\left(\bar{\xi}^{\underline{b}}-\eta^{\underline{b}}\right)\left(\bar{\xi}^{\underline{c}}-\eta^{\underline{c}}\right)d\bar{\xi}^{1\ldots6}\right)\partial_{\underline{b}}\partial_{\underline{c}}\phi_0|_\eta\, dt \\ &+\frac{1}{2}\int_{\mathbb{R}}\left(\varepsilon^2\int_\Sigma\mathfrak{f}\left(t,\underline{\bar{\xi}}\right)\left(\bar{\xi}^{\underline{b}}-\eta^{\underline{b}}\right)\left(\bar{\xi}^{\underline{c}}-\eta^{\underline{c}}\right)d\bar{\xi}^{1\ldots6}\right)\partial_{\underline{b}}\partial_{\underline{c}}(\phi_{\underline{a}}W^{\underline{a}})|_\eta\, dt+\mathcal{O}(\varepsilon^3). \qquad (4.2.13)\end{aligned}$$

Using the definitions of $q, \bar{V}^{\underline{a}}$, and $\bar{V}^{\underline{ab}}$ from equation (4.2.6),

$$\begin{aligned}\int_{\mathcal{E}}\phi\wedge J_\varepsilon|_{\left(t,\underline{\xi}\right)} &= \int_{\mathbb{R}}q\phi_0|_\eta\, dt+\int_{\mathbb{R}}qW^{\underline{a}}|_\eta\phi_{\underline{a}}|_\eta\, dt+\int_{\mathbb{R}}\bar{V}^{\underline{b}}\partial_{\underline{b}}\phi_0|_\eta\, dt \\ &+\int_{\mathbb{R}}\bar{V}^{\underline{b}}\partial_{\underline{b}}(\phi_{\underline{a}}W^{\underline{a}})|_\eta\, dt+\frac{1}{2}\int_{\mathbb{R}}\bar{V}^{\underline{bc}}\partial_{\underline{b}}\partial_{\underline{c}}\phi_0|_\eta\, dt+\frac{1}{2}\int_{\mathbb{R}}\bar{V}^{\underline{bc}}\partial_{\underline{b}}\partial_{\underline{c}}(\phi_{\underline{a}}W^{\underline{a}})|_\eta\, dt+\mathcal{O}(\varepsilon^3).\end{aligned} \qquad (4.2.14)$$

Next, expand the partial derivatives, and note $W^{\underline{a}}|_\eta = \dot{\eta}^{\underline{a}}$,

$$\begin{aligned}\int_{\mathcal{E}} \phi \wedge J_\varepsilon\big|_{\left(t,\underline{\xi}\right)} = &\int_{\mathbb{R}} q\phi_0|_\eta \, dt + \int_{\mathbb{R}} q\dot{\eta}^{\underline{a}}\phi_{\underline{a}}|_\eta \, dt + \int_{\mathbb{R}} \bar{V}^{\underline{b}}\partial_{\underline{b}}\phi_0|_\eta \, dt \\ &+ \int_{\mathbb{R}} \bar{V}^{\underline{b}}\dot{\eta}^{\underline{a}}\partial_{\underline{b}}\phi_{\underline{a}}|_\eta \, dt + \int_{\mathbb{R}} \bar{V}^{\underline{b}}\phi_{\underline{a}}|_\eta(\partial_{\underline{b}}W^{\underline{a}})|_\eta \, dt + \frac{1}{2}\int_{\mathbb{R}} \bar{V}^{\underline{bc}}\partial_{\underline{b}}\partial_{\underline{c}}\phi_0|_\eta \, dt \\ &+ \frac{1}{2}\int_{\mathbb{R}} \bar{V}^{\underline{bc}}\dot{\eta}^{\underline{a}}\partial_{\underline{b}}\partial_{\underline{c}}\phi_{\underline{a}}|_\eta \, dt + \int_{\mathbb{R}} \bar{V}^{\underline{bc}}(\partial_{\underline{c}}W^{\underline{a}})|_\eta(\partial_{\underline{b}}\phi_{\underline{a}})|_\eta \, dt \\ &+ \frac{1}{2}\int_{\mathbb{R}} \bar{V}^{\underline{bc}}\phi_{\underline{a}}|_\eta(\partial_{\underline{b}}\partial_{\underline{c}}W^{\underline{a}})|_\eta \, dt + \mathcal{O}(\varepsilon^3). \quad (4.2.15)\end{aligned}$$

Recalling the definitions of $\bar{X}^{\underline{a}}$ and $\bar{X}^{\underline{ab}}$ from equation (4.2.6),

$$\begin{aligned}\int_{\mathcal{E}} \phi \wedge J_\varepsilon\big|_{\left(t,\underline{\xi}\right)} = &\int_{\mathbb{R}} q\phi_0|_\eta \, dt + \int_{\mathbb{R}} q\dot{\eta}^{\underline{a}}\phi_{\underline{a}}|_\eta \, dt + \int_{\mathbb{R}} \bar{V}^{\underline{b}}\partial_{\underline{b}}\phi_0|_\eta \, dt \\ &+ \int_{\mathbb{R}} \bar{V}^{\underline{b}}\dot{\eta}^{\underline{a}}\partial_{\underline{b}}\phi_{\underline{a}}|_\eta \, dt + \int_{\mathbb{R}} \bar{X}^{\underline{a}}\phi_{\underline{a}}|_\eta \, dt + \frac{1}{2}\int_{\mathbb{R}} \bar{V}^{\underline{bc}}\partial_{\underline{b}}\partial_{\underline{c}}\phi_0|_\eta \, dt \\ &+ \frac{1}{2}\int_{\mathbb{R}} \bar{V}^{\underline{bc}}\dot{\eta}^{\underline{a}}\partial_{\underline{b}}\partial_{\underline{c}}\phi_{\underline{a}}|_\eta \, dt + \frac{1}{2}\int_{\mathbb{R}} \bar{X}^{\underline{ac}}(\partial_{\underline{c}}\phi_{\underline{a}})|_\eta \, dt + \mathcal{O}(\varepsilon^3). \quad (4.2.16)\end{aligned}$$

Recalling $\dot{\eta}^0 = 1$, this can be further simplified,

$$\begin{aligned}\int_{\mathcal{E}} \phi \wedge J_\varepsilon\big|_{\left(t,\underline{\xi}\right)} = &\int_{\mathbb{R}} q\phi_0|_\eta \, dt + \int_{\mathbb{R}} q\dot{\eta}^{\underline{a}}\phi_{\underline{a}}|_\eta \, dt + \int_{\mathbb{R}} \bar{V}^{\underline{b}}\dot{\eta}^{a}\partial_{\underline{b}}\phi_{a}|_\eta \, dt + \int_{\mathbb{R}} \bar{X}^{\underline{a}}\phi_{\underline{a}}|_\eta \, dt \\ &+ \frac{1}{2}\int_{\mathbb{R}} \bar{V}^{\underline{bc}}\dot{\eta}^{a}\partial_{\underline{b}}\partial_{\underline{c}}\phi_{a}|_\eta \, dt + \int_{\mathbb{R}} \bar{X}^{\underline{ac}}(\partial_{\underline{c}}\phi_{\underline{a}})|_\eta \, dt + \mathcal{O}(\varepsilon^3). \quad (4.2.17)\end{aligned}$$

This is the same as $\bar{\mathcal{J}}^a\phi_a$, as required. □

Thus there is a close relationship between the components of a multipole and the moments of f.

4.3 Dynamics of moments

4.3.1 Time evolution of moments

Having defined the Ellis representation of the quadrupole, we are now in a position to calculate the dynamics of the Ellis quadrupole. The transport equations for $\mathcal{J}^a$ given by equation (4.1.1) are found by considering the transport equations for $\mathfrak{J}^a$.

Since they are linear, they can be directly applied to distributions. The conservation of charge is given by

$$\partial_a \mathcal{J}^a = 0, \tag{4.3.1}$$

and the Vlasov equation is given by

$$\mathcal{J}^a W^b - \mathcal{J}^b W^a = 0. \tag{4.3.2}$$

These can be used to find the dynamics of the moments. The transport equations can also be defined by their actions on test forms λ and α_{ab},

$$\int_{\mathcal{E}} \mathcal{J}^a \partial_a \lambda \, d^7\xi = 0, \quad \int_{\mathcal{E}} \mathcal{J}^a W^b \alpha_{ab} \, d^7\xi = 0 \tag{4.3.3}$$

where α_{ab} is antisymmetric, both λ and α_{ab} have compact support, and recall that $\mathcal{E}$ is the time-phase space.

Proof. Acting $\partial_a \mathcal{J}^a$ on a test function λ and integrating by parts,

$$\int_{\mathcal{E}} \partial_a \mathcal{J}^a \lambda \, d^7\xi = -\int_{\mathcal{E}} \mathcal{J}^a \partial_a \lambda \, d^7\xi \tag{4.3.4}$$

so these conditions are equivalent. For the Vlasov equation, consider

$$\mathcal{J}^a W^b \alpha_{ab} = \frac{1}{2}\left(\mathcal{J}^a W^b + \mathcal{J}^b W^a\right)\alpha_{ab} + \frac{1}{2}\left(\mathcal{J}^a W^b - \mathcal{J}^b W^a\right)\alpha_{ab}. \tag{4.3.5}$$

Since α_{ab} is antisymmetric, the contraction $(\mathcal{J}^a W^b + \mathcal{J}^b W^a)\alpha_{ab}$ vanishes, leaving

$$\mathcal{J}^a W^b \alpha_{ab} = \frac{1}{2}\left(\mathcal{J}^a W^b - \mathcal{J}^b W^a\right)\alpha_{ab} \tag{4.3.6}$$

hence the second part of (4.3.3). □

The transport equations for $\mathcal{J}^a$ (equation (4.3.3)) can be used to find the dynamics of the moments, which are given by

$$\frac{dV^{\underline{ab}}}{dt} = X^{\underline{ab}} + X^{\underline{ba}}, \quad \frac{dV^{\underline{a}}}{dt} = X^{\underline{a}}, \quad \frac{dq}{dt} = 0, \tag{4.3.7a}$$

$$X^{\underline{ab}} = V^{\underline{bc}} \partial_{\underline{c}} W^{\underline{a}}, \quad X^{\underline{a}} = V^{\underline{b}} \partial_{\underline{b}} W^{\underline{a}} + \frac{1}{2} V^{\underline{bc}} \partial_{\underline{b}} \partial_{\underline{c}} W^{\underline{a}}. \tag{4.3.7b}$$

Proof. Begin by considering the conservation of charge (equation (4.3.1)), and act on a test form λ,

$$\int_{\mathcal{E}} \mathcal{J}^a \partial_a \lambda d^7\xi = \frac{1}{2}\int_{\mathbb{R}} V^{\underline{ab}} \dot{\eta}^c \partial_{\underline{a}}\partial_{\underline{b}}\partial_c \lambda dt + \int_{\mathbb{R}} X^{\underline{ab}} \partial_{\underline{b}}\partial_{\underline{a}}\lambda dt + \int_{\mathbb{R}} V^{\underline{a}} \dot{\eta}^b \partial_{\underline{a}}\partial_b \lambda dt + \int_{\mathbb{R}} X^{\underline{a}} \partial_{\underline{a}}\lambda dt + \int_{\mathbb{R}} q\dot{\eta}^a \partial_a \lambda dt = 0. \quad (4.3.8)$$

From here, note

$$\dot{\eta}^a \frac{\partial \lambda}{\partial \xi^a} = \left.\frac{d\lambda}{dt}\right|_\eta \quad (4.3.9)$$

so integration by parts can be used to pass a derivative onto the $V^{\underline{a}}$ and $V^{\underline{ab}}$ terms. This gives

$$\int_{\mathcal{E}} \mathcal{J}^a \partial_a \lambda d^7\xi = -\frac{1}{2}\int_{\mathbb{R}} \frac{dV^{\underline{ab}}}{dt}\partial_{\underline{a}}\partial_{\underline{b}}\lambda dt + \int_{\mathbb{R}} X^{\underline{ab}}\partial_{\underline{b}}\partial_{\underline{a}}\lambda dt - \int_{\mathbb{R}} \frac{dV^{\underline{a}}}{dt}\partial_{\underline{a}}\lambda dt + \int_{\mathbb{R}} X^{\underline{a}}\partial_{\underline{a}}\lambda dt + \int_{\mathbb{R}} \frac{dq}{dt}\lambda dt = 0. \quad (4.3.10)$$

Collecting terms based on derivatives of λ gives the first line of (4.3.7).

To consider the effects of the Vlasov equation (equation (4.3.2)), act $\mathcal{J}^a$ on $W^b\alpha_{ab}$, and expand the partial derivatives,

$$\begin{aligned}\int_{\mathcal{E}} \mathcal{J}^a W^b \alpha_{ab} d^7\xi = \frac{1}{2}\int_{\mathbb{R}} V^{\underline{cb}}\dot{\eta}^a \big(&\alpha_{ad}\partial_{\underline{b}}\partial_{\underline{c}}W^d + \partial_{\underline{b}}\alpha_{ad}\partial_{\underline{c}}W^d \\ &+ \partial_{\underline{c}}\alpha_{ad}\partial_{\underline{b}}W^d + W^d\partial_{\underline{b}}\partial_{\underline{c}}\alpha_{ad}\big)\,dt + \int_{\mathbb{R}} X^{\underline{ab}}\left(W^c\partial_{\underline{b}}\alpha_{\underline{a}c} + \alpha_{\underline{a}c}\partial_{\underline{b}}W^c\right)dt \\ + \int_{\mathbb{R}} V^{\underline{b}}\dot{\eta}^a\left(W^c\partial_{\underline{b}}\alpha_{ac} + \alpha_{ac}\partial_{\underline{b}}W^c\right)dt + \int_{\mathbb{R}} X^{\underline{a}}W^b\alpha_{\underline{a}b}dt + \int_{\mathbb{R}} qW^b\dot{\eta}^c\alpha_{bc}dt.\end{aligned} \quad (4.3.11)$$

Next, look at terms of the form

$$W^a\dot{\eta}^b\alpha_{ab}, \quad (4.3.12)$$

recalling the implicit evaluation at η, $W|_\eta = \dot{\eta}^a$. Since α_{ab} is antisymmetric,

$$W^a\dot{\eta}^b\alpha_{ab} = 0. \quad (4.3.13)$$

This is true for the derivatives of α_{ab} as well, since the derivatives are also antisymmetric. This means terms of the form $W^d\dot{\eta}^a\partial_{\underline{b}}\partial_{\underline{c}}\alpha_{ad}$ etc. vanish. Rearranging

the remaining terms in derivatives of α_{ab} gives

$$\int_{\mathcal{E}} \mathcal{J}^a W^b \alpha_{ab} d^7\xi = \int_{\mathbb{R}} \left(V^{\underline{cb}}\partial_{\underline{c}} W^{\underline{a}} - X^{\underline{ab}}\right) \dot{\eta}^d \partial_{\underline{b}} \alpha_{d\underline{a}}\, dt + \int_{\mathbb{R}} \left(V^{\underline{cb}}\partial_{\underline{c}} W^0\right) \dot{\eta}^d \partial_{\underline{b}} \alpha_{d0}\, dt + \int_{\mathbb{R}} X^{\underline{ab}} \partial_{\underline{b}} W^d \alpha_{\underline{a}d}\, dt + \int_{\mathbb{R}} \left(V^{\underline{b}}\partial_{\underline{b}} W^{\underline{a}} + \frac{1}{2} V^{\underline{bc}}\partial_{\underline{b}}\partial_{\underline{c}} W^{\underline{a}} - X^{\underline{a}}\right) \dot{\eta}^d \alpha_{d\underline{a}}\, dt + \int_{\mathbb{R}} \left(\frac{1}{2} V^{\underline{bc}}\partial_{\underline{b}}\partial_{\underline{c}} W^0 + V^{\underline{b}}\partial_{\underline{b}} W^0\right) \dot{\eta}^d \alpha_{d0}\, dt \quad (4.3.14)$$

where the minus sign in the $X^{\underline{a}}$ and $X^{\underline{ab}}$ terms comes from flipping the $\alpha_{a\underline{b}}$ indices. Next, note that calculations are in a frame where $W^0 = 1$, so derivatives of W^0 vanish. Two of the remaining terms give the required differential equations,

$$X^{\underline{ab}} = V^{\underline{bc}}\partial_{\underline{c}} W^{\underline{a}}, \quad (4.3.15)$$

$$X^{\underline{a}} = V^{\underline{b}}\partial_{\underline{b}} W^{\underline{a}} + \frac{1}{2} V^{\underline{bc}}\partial_{\underline{b}}\partial_{\underline{c}} W^{\underline{a}}. \quad (4.3.16)$$

Lastly, for the remaining integral, the third integral of equation (4.3.14), taking the antisymmetric part of $X^{\underline{ab}}\partial_{\underline{b}} W^{\underline{d}}$ gives

$$X^{\underline{ab}}\partial_{\underline{b}} W^{\underline{d}} \alpha_{\underline{ad}} = \left(X^{\underline{ab}}\partial_{\underline{b}} W^{\underline{d}} - X^{\underline{db}}\partial_{\underline{b}} W^{\underline{a}}\right) \alpha_{\underline{ad}} \quad (4.3.17)$$

$$= \left(V^{\underline{bc}}\partial_{\underline{b}} W^{\underline{a}}\partial_{\underline{c}} W^{\underline{d}} - V^{\underline{cb}}\partial_{\underline{c}} W^{\underline{a}}\partial_{\underline{b}} W^{\underline{d}}\right) \alpha_{\underline{ad}} \quad (4.3.18)$$

$$= 0. \quad (4.3.19)$$

So the differential equations in the bottom line of (4.3.7) uniquely solve the system, giving the equations of motion for the moments through the Ellis representation of multipoles. □

As a corollary, inserting equation (4.3.7b) into equation (4.3.7a) give equations (3.2.26) and (3.2.27), so the Ellis representation can also be used to find the differential equations for the moments. These differential equations are the same as directly differentiating (3.1.7).

Whilst the integral representation and Ellis representation find the same dynamics of the moments, there is a different philosophy to each approach. The method

presented in section 3.2 gives an infinite Taylor expansion, and picks the truncation point at the end of the method. Alternatively, the Ellis representation makes the choice of truncation when first performing the multipole expansion to a specific order. This order of expansion is then kept throughout. Whilst this work only carries out this expansion to quadrupole order, it is simple to extend this result to higher orders.

4.3.2 Comparison with transition matrices for a beam passing through a quadrupole magnet

Before modelling the moments numerically, this section analyses the differential equations to see if the models give the expected trends when comparing them to existing, simpler methods.

In a particle accelerator, the dynamics of individual particles through an element of a particle accelerator (drift space, dipole magnet, quadrupole magnet, RF cavity, etc.) are calculated using *transition matrices*. Transition matrices approximate the final position and velocity of a particle through an accelerator element. This formulation can be done in (3+3)D position-velocity phase space, but for ease of reading, only one spatial and one velocity dimension will be considered. This position and velocity can be denoted as a column vector, with their final state being given after passing through a transition matrix T,

$$\begin{pmatrix} x_{\text{fin}} \\ \frac{dx_{\text{fin}}}{ds} \end{pmatrix} = T \begin{pmatrix} x_{\text{init}} \\ \frac{dx_{\text{init}}}{ds} \end{pmatrix} \tag{4.3.20}$$

where s is a global parameter defining position along the beamline, and dx/ds gives the rate of change of the particle's position with respect to s along the beamline. This quantity will be related to velocity later in this section. For more information on how these matrices are formulated, the reader is directed to references [94] and [95]. Transition matrices are different for each accelerator element.

A focussing quadrupole magnet has the magnetic field

$$\mathbf{B}_{\text{quad}} = \begin{pmatrix} Gy & Gx & 0 \end{pmatrix} \tag{4.3.21}$$

where $G > 0$. This has the transition matrix

$$T_{\text{quad}} = \begin{pmatrix} \cos(\sqrt{K}s) & \frac{1}{\sqrt{K}}\sin(\sqrt{K}s) \\ -\sqrt{K}\sin(\sqrt{K}s) & \cos(\sqrt{K}s) \end{pmatrix} \tag{4.3.22}$$

where $K = qG/m\gamma$, and s is the parameter of the beamline.

The quadrupole moments, Ξ, of a bunch of n particles, each with individual position x_i and velocity dx_i/ds, can be calculated as

$$\Xi = \sum_{i=1}^{n} \begin{pmatrix} x_i \\ \frac{dx_i}{ds} \end{pmatrix} \begin{pmatrix} x_i \\ \frac{dx_i}{ds} \end{pmatrix}^T = \begin{pmatrix} \Xi^{11} & \Xi^{12} \\ \Xi^{12} & \Xi^{22} \end{pmatrix}. \tag{4.3.23}$$

Thus the moments after the bunch has passed through an accelerator element can be found using the transition matrices,

$$\Xi_{\text{fin}} = \sum_{i=1}^{n} \left(T \begin{pmatrix} x_{i,\text{init}} \\ \frac{dx_{i,\text{init}}}{ds} \end{pmatrix} \right) \left(T \begin{pmatrix} x_{i,\text{init}} \\ \frac{dx_{i,\text{init}}}{ds} \end{pmatrix} \right)^T \tag{4.3.24}$$

$$= \sum_{i=1}^{n} T \begin{pmatrix} x_{i,\text{init}} \\ \frac{dx_{i,\text{init}}}{ds} \end{pmatrix} \begin{pmatrix} x_{i,\text{init}} \\ \frac{dx_{i,\text{init}}}{ds} \end{pmatrix}^T T^T \tag{4.3.25}$$

$$= T\, \Xi_{\text{init}}\, T^T \tag{4.3.26}$$

so the dynamics of the moments of a bunch can also be found through the transition matrices. These equations give the moments after an accelerator element of finite thickness has been travelled through. This can be turned into an infinitesimal rate of change by considering differentiation from first principles as an accelerator element becomes infinitely thin,

$$\frac{d\Xi}{ds} = \lim_{s\to 0} \frac{\Xi_{\text{fin}} - \Xi_{\text{init}}}{s}. \tag{4.3.27}$$

Using this equation allows the rates of change for the moments to be found through the transition matrix approach. These should match, to leading order, those found

through the differential equations (3.2.26) and (3.2.27).

For the quadrupole magnet,

$$\frac{d\Xi}{ds} = \begin{pmatrix} 2\Xi^{12} & \Xi^{22} - K\Xi^{11} \\ \Xi^{22} - K\Xi^{11} & -2K\Xi^{12} \end{pmatrix}. \tag{4.3.28}$$

Proof. Using equation (4.3.26) with the focussing quadrupole magnet transition matrix gives

$$\Xi^{11}{}_{\text{fin}} = \cos^2(\sqrt{K}s)\Xi^{11} + \sin^2(\sqrt{K}s)\frac{\Xi^{22}}{K} + \frac{2}{\sqrt{K}}\cos(\sqrt{K}s)\sin(\sqrt{K}s)\Xi^{12} \tag{4.3.29}$$

$$\Xi^{12}{}_{\text{fin}} = \left(\cos^2(\sqrt{K}s) - \sin^2(\sqrt{K}s)\right)\Xi^{12} + \frac{\sin(\sqrt{K}s)\cos(\sqrt{K}s)}{\sqrt{K}}\Xi^{22} - \sqrt{K}\sin(\sqrt{K}s)\cos(\sqrt{K}s)\Xi^{11} \tag{4.3.30}$$

$$\Xi^{22}{}_{\text{fin}} = K\sin^2(\sqrt{K}s)\Xi^{11} + \cos^2(\sqrt{K}s)\Xi^{22} - 2\sqrt{K}\sin(\sqrt{K}s)\cos(\sqrt{K}s)\Xi^{12}. \tag{4.3.31}$$

To find the rate of change of the moments, use equation (4.3.27). To find the limits, use the standard results that for small s, $\cos(\sqrt{K}s) \approx 1$, $\sin(\sqrt{K}s) \approx \sqrt{K}s$, thus

$$\frac{d\Xi^{11}}{ds} = \lim_{s\to 0}\frac{1}{s}\left(\Xi^{11} + \frac{s^2\Xi^{22}}{K} + 2s\Xi^{14}\right) - \frac{\Xi^{11}}{s} = 2\Xi^{12} \tag{4.3.32}$$

$$\frac{d\Xi^{12}}{ds} = \lim_{s\to 0}\frac{1}{s}\left(\Xi^{12} - Ks^2\,\Xi^{12} + s\,\Xi^{22} - Ks\,\Xi^{11}\right) - \frac{\Xi^{12}}{s} = \Xi^{22} - K\,\Xi^{11} \tag{4.3.33}$$

$$\frac{d\Xi^{22}}{ds} = \lim_{s\to 0}\frac{1}{s}\left(K^2s^2\,\Xi^{11} + \Xi^{22} - 2Ks\,\Xi^{12}\right) - \frac{\Xi^{22}}{s} = -2K\,\Xi^{12}. \tag{4.3.34}$$

□

These are the leading order contributions to the transition matrices for the moments.

This can be compared to the rates of change found through tracking the moments directly. There are two ways to calculate the dynamics of the moments from equations (3.2.26) and (3.2.27). Firstly, the Vlasov equation in Frenet-Serret coordinates (a coordinate system defined relative to the ideal orbit) could be found and the moment tracking equations could be calculated directly in the same

coordinate system as the particle accelerator. Alternatively, since the ideal orbit through a pure quadrupole magnet is a straight line, the Vlasov field calculated in section 2.2 can be used, and the transformation for the moments between the two coordinate systems calculated at the end. This latter approach is what will be done here.

In the quadrupole magnetic field, the rates of change for the V^{11}, V^{14}, and V^{44} moments are given by

$$\frac{dV^{11}}{dt} = 2V^{14}\left(\frac{1}{\gamma} - \frac{u_x^2}{\gamma^3}\right) - \frac{2V^{15}u_y u_x}{\gamma^3} - \frac{2V^{16}u_z u_x}{\gamma^3} \tag{4.3.35}$$

$$\frac{dV^{14}}{dt} = -V^{11}Ku_z + \frac{V^{14}Kxu_x u_z}{\gamma^2} + \frac{V^{15}Ku_x u_y x}{\gamma^2} + V^{16}K\left(\frac{xu_z^2}{\gamma^2} - \frac{x}{\gamma}\right) + V^{44}\left(\frac{1}{\gamma} - \frac{u_x^2}{\gamma^3}\right) - \frac{V^{45}u_y u_x}{\gamma^3} - \frac{V^{46}u_z u_x}{\gamma^3} \tag{4.3.36}$$

$$\frac{dV^{44}}{dt} = -2V^{14}Ku_z + \frac{2V^{44}Ku_z u_x x}{\gamma^2} + \frac{2V^{45}Ku_z u_y x}{\gamma^2} + 2V^{46}K\left(\frac{u_z^2 x}{\gamma^2} - x\right). \tag{4.3.37}$$

These expressions were found using the symbolic algebra software Maple.

To compare these expressions to those found using the transition matrices, recall that the moments are taken along the ideal orbit, so x, u_x, and u_y are zero, and it is assumed that $u_z \approx \gamma$ i.e. the particles are ultra-relativistic. This gives

$$\frac{dV^{11}}{dt} = \frac{2V^{14}}{\gamma} \tag{4.3.38}$$

$$\frac{dV^{14}}{dt} = \frac{V^{44}}{\gamma} - V^{11}K\gamma \tag{4.3.39}$$

$$\frac{dV^{44}}{dt} = -2V^{14}K\gamma. \tag{4.3.40}$$

To compare these two results, note that the velocities in the transition matrix approach are dx/ds, rather than u_x. To make comparisons between the different

methods, introduce the following substitutions,

$$\frac{d}{ds} = c\frac{d}{dt} = \frac{d}{dt}, \quad \frac{dx}{ds} = \frac{dx}{dt} = \frac{u_x}{\gamma}, \quad \Xi^{11} = V^{11}, \quad \Xi^{12} = \frac{V^{14}}{\gamma}, \quad \Xi^{22} = \frac{V^{44}}{\gamma^2}. \tag{4.3.41}$$

These equalities hold for dV/ds since γ is constant in magnetic fields. Inserting these into $d\Xi/ds$ (equation (4.3.28)) gives

$$\frac{d\Xi^{11}}{ds} = 2\Xi^{14} \rightarrow \frac{dV^{11}}{dt} = \frac{2V^{14}}{\gamma} \tag{4.3.42}$$

$$\frac{d\Xi^{14}}{ds} = \Xi^{44} - K\,\Xi^{11} \rightarrow \frac{1}{\gamma}\frac{dV^{14}}{dt} = \frac{V^{44}}{\gamma^2} - KV^{11} \rightarrow \frac{dV^{14}}{dt} = \frac{V^{44}}{\gamma} - K\gamma V^{11} \tag{4.3.43}$$

$$\frac{d\Xi^{44}}{ds} = -2K\,\Xi^{14} \rightarrow \frac{1}{\gamma^2}\frac{dV^{44}}{dt} = -\frac{2KV^{14}}{\gamma} \rightarrow \frac{dV^{44}}{dt} = 2KV^{14}\gamma \tag{4.3.44}$$

which is equivalent to equations (4.3.35), (4.3.36), and (4.3.37), thus the transition matrix approach and moment tracking approach give the same results.

For dipole magnets (magnets that bend the trajectory radially) the coordinate systems are too distinct for this approach to work. This is because the moment tracking method uses Cartesian coordinates, so bending the trajectory in a dipole magnet involves mixing z and x coordinates. In contrast, the transition matrix approach uses Frenet-Serret coordinates, which are defined relative to the centre of the bunch, so the bending from the dipole magnetic moment is not considered. Whilst it may be possible to use this approach to compare the moment tracking with other transition matrices, this is only useful as a test that the theory gives existing results. It is instead more important to test this code numerically, to see if the extra effects included through using more complex electromagnetic and gravitational fields give new results.

4.3.3 Conservation of non-relativistic emittance

The volume a bunch of particles occupies in phase space is known as the *emittance*. This emittance, ϵ, is the determinant of the quadrupole moments, and is defined in the non-relativistic limit as

$$\epsilon = \det(V) \tag{4.3.45}$$

where V is the 6×6 matrix of quadrupole moments given by $V^{\underline{ab}}$. In a purely conservative system in flat space, emittance is conserved. The conservation of emittance follows from Liouville's theorem [96]. In an arbitrary coordinate system, emittance will not necessarily be conserved. Using the differential equations for the moments, the rate of change of emittance is given by

$$\frac{d\epsilon}{dt} = 2\det(V)\partial_{\underline{c}}W^{\underline{c}}. \tag{4.3.46}$$

Proof. The rate of change of emittance can be shown by differentiating ϵ with respect to time,

$$\begin{aligned}
\frac{d\epsilon}{dt} &= \frac{d}{dt}\det(V) && (4.3.47)\\
&= \det(V)(V^{-1})_{\underline{ab}}\frac{dV^{\underline{ab}}}{dt} && (4.3.48)\\
&= \det(V)(V^{-1})_{\underline{ab}}\left(V^{\underline{ac}}\partial_{\underline{c}}W^{\underline{b}} + V^{\underline{ac}}\partial_{\underline{c}}W^{\underline{b}}\right) && (4.3.49)\\
&= \det(V)\left(\delta^{\underline{c}}_{\underline{b}}\partial_{\underline{c}}W^{\underline{b}} + \delta^{\underline{ac}}\partial_{\underline{c}}W^{\underline{b}}\right) && (4.3.50)\\
&= 2\det(V)\partial_{\underline{c}}W^{\underline{c}}. && (4.3.51)
\end{aligned}$$

as required. □

Recall equation (2.3.5), in the system of a linear particle accelerator where it is assumed the system is non-relativistic, $|\det(g)| = 1$, so equation (2.3.5) becomes $\partial_{\underline{c}}W^{\underline{c}} = 0$, hence emittance is constant under these assumptions. For cases where the effects of γ are important, then the choice of coordinate system becomes more important. Switching between the Frenet-Serret coordinate system, where this definition of emittance is defined, and the lab time coordinate system used in the

moment tracking, is not straightforward. In cases where curvature matters, i.e. $\det(g) \neq 1$, then in general emittance will not be conserved, since phase space volume is not conserved in curved spacetimes.

4.3.4 Limitations of moment tracking

Moment tracking will not work well when the field around η is not accurately modelled by a small number of derivatives (figure 4.1). This is due to the truncation error. Specifically, when modelling only up to quadrupole moments, the dipole moment will not be modelled well when the field cannot be accurately modelled by only two derivatives. The quadrupole moments will not be modelled well when the field cannot be modelled by only a single derivative. As an example of this, consider a sextupole magnetic field (recalling that the naming convention for magnetic field multipoles scales as $2k$), given by

$$\mathbf{B}_{\text{sextupole}} = \left(Sxy, \quad \tfrac{S}{2}\left(x^2 - y^2\right), \quad 0 \right) \tag{4.3.52}$$

where S is the sextupole field strength. This field is quadratic, which means that, when evaluated along the ideal orbit η, where $x = y = 0$, the field and its first derivatives vanish. This means there is no contribution to the quadrupole moments from the sextupole magnetic field.

This effect will be studied in more detail in chapter 5 where the effects of the truncation on the error convergence will be examined.

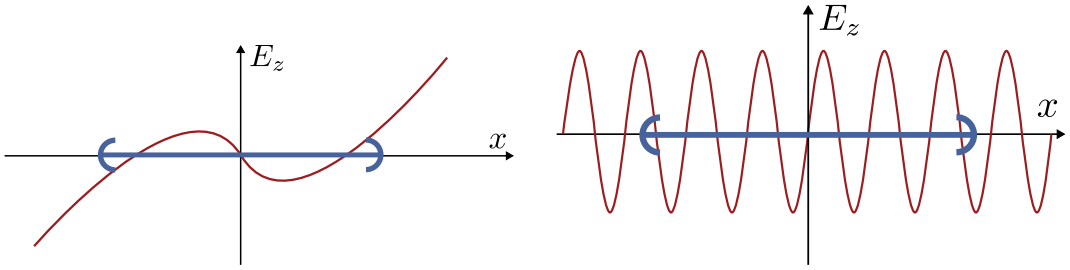

(a) *An electric field where moment tracking will work well.*

(b) *An electric field where moment tracking will not work well.*

Figure 4.1: *Examples of electric fields where the moment tracking method will work well and will not work well. When the fields (the red curves) rapidly change across the extent the macroparticle represents, (the support of f, indicated by the horizontal blue line), the moment tracking method will not work well.*

4.4 Coordinate transformations of multipoles where the time slicing changes

Having introduced the Ellis representation of the quadrupole, we are now in a position to calculate the coordinate transformations where the time slicing changes. As previously stated, this cannot be done using the integral representation of moments. This means that equations (4.4.22) and (4.4.23), below, are a new result. Consider a new coordinate system denoted by hatted coordinates $(\hat{t}, \hat{\xi}^{\hat{\underline{a}}})$, where the time coordinate is changed i.e. $\hat{t}(t, \xi^{\underline{a}})$ is a function of both t and $\xi^{\underline{a}}$. Hatted indices will be used to remind the reader that the quantity is in the new coordinate system. To find the transformation rules of a multipole, it is assumed $\mathcal{J}^a$ transforms as a tensor density, i.e.

$$\hat{\mathcal{J}}^{\hat{b}} = \mathcal{J}^a \frac{\partial \hat{\xi}^{\hat{b}}}{\partial \xi^a} \frac{d^7\xi}{d^7\hat{\xi}} \tag{4.4.1}$$

such that

$$\int_{\mathcal{E}} \mathcal{J}^a \phi_a d^7\xi = \int_{\mathcal{E}} \hat{\mathcal{J}}^{\hat{a}} \hat{\phi}_{\hat{a}} d^7\hat{\xi} \tag{4.4.2}$$

is an invariant quantity.

Since $\dot{\eta}^{\underline{a}}$ are functions on a world line, they transform as

$$\dot{\hat{\eta}}^{\hat{a}} = \frac{\partial \hat{\xi}^{\hat{a}}}{\partial \xi^{\underline{b}}} \frac{d\hat{t}}{dt} \dot{\eta}^{\underline{b}} \tag{4.4.3}$$

where

$$\dot{\hat{\eta}}^{\hat{a}}(\hat{t}) = \frac{d\hat{\eta}^{\hat{a}}(\hat{t})}{d\hat{t}}. \tag{4.4.4}$$

Recall ϕ_a and ∂_a are tensorial, so the transformation rules for these are

$$\hat{\phi}_{\hat{a}} = \frac{\partial \xi^{\underline{b}}}{\partial \hat{\xi}^{\hat{a}}} \phi_{\underline{b}}, \quad \frac{\partial}{\partial \hat{\xi}^{\hat{a}}} = \frac{\partial \xi^{\underline{b}}}{\partial \hat{\xi}^{\underline{a}}} \frac{\partial}{\partial \xi^{\underline{b}}}. \tag{4.4.5}$$

Note that although a quantity may only have indices over $(1, \ldots, 6)$ in the original coordinate system, when it is transformed into the new new coordinate system its indices will run over $(0, \ldots, 6)$. This means that the moments will have indices over $(0, \ldots, 6)$ in the transformed coordinate system, and, as such, the components will not be unique (as shown in section 4.1). Since the components are not unique, they will not be denoted with $V^{\underline{a}}$ and $X^{\underline{a}}$ etc., and instead denoted with U^a and Y^a respectively. Using these transformation rules gives

$$\begin{aligned} \int_{\mathcal{E}} \mathcal{J}^a \phi_a d^7\xi = \int_{\mathcal{E}} \hat{\mathcal{J}}^{\hat{a}} \hat{\phi}_{\hat{a}} d^7\hat{\xi} = \frac{1}{2} \int_{\mathbb{R}} \dot{\hat{\eta}}^{\hat{a}} \hat{U}^{\hat{c}\hat{b}} \hat{\partial}_{\hat{b}} \hat{\partial}_{\hat{c}} (\hat{\phi}_{\hat{a}}) d\hat{t} + \int_{\mathbb{R}} \hat{Y}^{\hat{a}\hat{b}} \hat{\partial}_{\hat{c}} \hat{\phi}_{\hat{a}} d\hat{t} \\ + \int_{\mathbb{R}} \dot{\hat{\eta}}^{\hat{a}} \hat{U}^{\hat{b}} \hat{\partial}_{\hat{b}} \hat{\phi}_{\hat{a}} dt + \int_{\mathbb{R}} \hat{Y}^{\hat{a}} \hat{\phi}_{\hat{a}} d\hat{t} + \int_{\mathbb{R}} \dot{\hat{\eta}}^{\hat{a}} q \hat{\phi}_{\hat{a}} d\hat{t} \end{aligned} \tag{4.4.6}$$

where $\hat{\partial}_a = \partial / \partial \hat{\xi}^{\hat{a}}$, and the components of $\hat{\mathcal{J}}^{\hat{a}}$ are given by

$$\begin{aligned} \hat{U}^{\hat{b}\hat{c}} &= V^{\underline{de}} A^{\hat{b}}_{\underline{d}} A^{\hat{c}}_{\underline{e}}, \\ \hat{Y}^{\hat{c}\hat{d}} &= \left(X^{\underline{ab}} A^{\hat{c}}_{\underline{b}} A^{\hat{d}}_{\underline{a}} + \frac{1}{2} V^{\underline{ef}} \dot{\eta}^a \partial_a \left(A^{\hat{d}}_{\underline{f}} A^{\hat{c}}_{\underline{e}} \right) \right) \frac{dt}{d\hat{t}}, \\ \hat{U}^{\hat{a}} &= V^{\underline{b}} A^{\hat{a}}_{\underline{b}} + \frac{1}{2} V^{\underline{bc}} A^{\hat{a}}_{\underline{bc}}, \\ \hat{Y}^{\hat{c}} &= \left(X^{\underline{d}} A^{\hat{c}}_{\underline{d}} + V^{\underline{b}} \dot{\eta}^a \partial_a (A^{\hat{c}}_{\underline{b}}) + X^{\underline{ab}} A^{\hat{c}}_{\underline{ab}} + \frac{1}{2} V^{\underline{de}} \dot{\eta}^a \partial_a \left(A^{\hat{c}}_{\underline{de}} \right) \right) \frac{dt}{d\hat{t}} \end{aligned} \tag{4.4.7}$$

and the notation

$$A^{\hat{a}}_{\underline{c}} = \frac{\partial \hat{\xi}^{\hat{a}}}{\partial \xi^{\underline{c}}}, \quad A^{\hat{a}}_{\underline{bc}} = \frac{\partial^2 \hat{\xi}^{\hat{a}}}{\partial \xi^{\underline{b}} \partial \xi^{\underline{c}}} \tag{4.4.8}$$

is used. A hatted index is used to make the $A^{\hat{a}}_{\underline{c}}$ notation distinct from $A^{\underline{c}}_{\hat{a}}$.

Proof. Proceed term by term using the transformation rules for $\dot{\eta}^{\underline{a}}$ (equation (4.4.3)), and $\partial_{\underline{a}}$ and ϕ_a (equation (4.4.5)). For the V^{ab} term,

$$\int_{\mathbb{R}} V^{\underline{bc}} \dot{\eta}^a \partial_{\underline{b}} \partial_{\underline{c}} \phi_a dt = \int_{\mathbb{R}} V^{\underline{bc}} \dot{\hat{\eta}}^{\hat{d}} A^a_{\hat{d}} \frac{dt}{d\hat{t}} A^{\hat{e}}_{\underline{b}} \hat{\partial}_{\hat{e}} \left(A^{\hat{f}}_{\underline{c}} \hat{\partial}_{\hat{f}} \left(A^{\hat{g}}_a \hat{\phi}_{\hat{g}} \right) \right) \frac{dt}{d\hat{t}} d\hat{t}. \tag{4.4.9}$$

Performing these derivatives gives

$$\begin{aligned}
\int_{\mathbb{R}} V^{\underline{bc}} \dot{\eta}^a \partial_{\underline{b}} \partial_{\underline{c}} \phi_a dt = & \int_{\mathbb{R}} V^{\underline{bc}} \dot{\hat{\eta}}^{\hat{d}} A^a_{\hat{d}} \frac{dt}{d\hat{t}} A^{\hat{g}}_{a\underline{bc}} \hat{\phi}_{\hat{g}} \frac{dt}{d\hat{t}} d\hat{t} + \int_{\mathbb{R}} V^{\underline{bc}} \dot{\hat{\eta}}^{\hat{d}} A^a_{\hat{d}} \frac{dt}{d\hat{t}} A^{\hat{e}}_{\underline{b}} A^{\hat{g}}_{a\underline{c}} \hat{\partial}_{\hat{e}} (\hat{\phi}_{\hat{g}}) \frac{dt}{d\hat{t}} d\hat{t} \\
& + \int_{\mathbb{R}} V^{\underline{bc}} \dot{\hat{\eta}}^{\hat{d}} A^a_{\hat{d}} \frac{dt}{d\hat{t}} A^{\hat{e}}_{\underline{c}} A^{\hat{f}}_{a\underline{b}} \hat{\partial}_{\hat{e}} (\hat{\phi}_{\hat{f}}) \frac{dt}{d\hat{t}} d\hat{t} + \int_{\mathbb{R}} V^{\underline{bc}} \dot{\hat{\eta}}^{\hat{d}} A^a_{\hat{d}} \frac{dt}{d\hat{t}} A^{\hat{e}}_{\underline{b}} A^{\hat{f}}_{\underline{c}} A^{\hat{g}}_a \hat{\partial}_{\hat{e}} \hat{\partial}_{\hat{f}} (\hat{\phi}_{\hat{g}}) \frac{dt}{d\hat{t}} d\hat{t} \\
& + \int_{\mathbb{R}} V^{\underline{bc}} \dot{\hat{\eta}}^{\hat{d}} A^a_{\hat{d}} \frac{dt}{d\hat{t}} A^{\hat{f}}_{\underline{cb}} A^h_{\hat{f}} A^{\hat{g}}_{ah} \hat{\phi}_{\hat{g}} \frac{dt}{d\hat{t}} d\hat{t} + \int_{\mathbb{R}} V^{\underline{bc}} \dot{\hat{\eta}}^{\hat{d}} A^a_{\hat{d}} \frac{dt}{d\hat{t}} A^{\hat{f}}_{\underline{cb}} A^{\hat{g}}_a \hat{\partial}_{\hat{f}} (\hat{\phi}_{\hat{g}}) \frac{dt}{d\hat{t}} d\hat{t}.
\end{aligned} \tag{4.4.10}$$

Simplifying these terms down

$$\begin{aligned}
\int_{\mathbb{R}} V^{\underline{bc}} \dot{\eta}^a \partial_{\underline{b}} \partial_{\underline{c}} \phi_a dt = & \int_{\mathbb{R}} V^{\underline{bc}} \dot{\eta}^a \partial_a \left(A^{\hat{g}}_{\underline{bc}} \right) \hat{\phi}_{\hat{g}} \frac{dt}{d\hat{t}} d\hat{t} + \int_{\mathbb{R}} V^{\underline{bc}} A^{\hat{e}}_{\underline{b}} \dot{\eta}^a \partial_a \left(A^{\hat{g}}_{\underline{c}} \right) \hat{\partial}_{\hat{e}} (\hat{\phi}_{\hat{g}}) \frac{dt}{d\hat{t}} d\hat{t} \\
& + \int_{\mathbb{R}} V^{\underline{bc}} A^{\hat{e}}_{\underline{c}} \dot{\eta}^a \partial_a \left(A^{\hat{f}}_{\underline{b}} \right) \hat{\partial}_{\hat{e}} (\hat{\phi}_{\hat{f}}) \frac{dt}{d\hat{t}} d\hat{t} + \int_{\mathbb{R}} V^{\underline{bc}} \dot{\hat{\eta}}^{\hat{d}} A^{\hat{e}}_{\underline{b}} A^{\hat{f}}_{\underline{c}} \hat{\partial}_{\hat{e}} \hat{\partial}_{\hat{f}} (\hat{\phi}_{\hat{d}}) d\hat{t} + \int_{\mathbb{R}} V^{\underline{bc}} \dot{\hat{\eta}}^{\hat{d}} A^{\hat{f}}_{\underline{cb}} \hat{\partial}_{\hat{f}} (\hat{\phi}_{\hat{d}}) d\hat{t}.
\end{aligned} \tag{4.4.11}$$

For the $X^{\underline{ab}}$ term,

$$\int_{\mathbb{R}} X^{\underline{ab}} \partial_{\underline{b}} \phi_{\underline{a}} dt = \int_{\mathbb{R}} X^{\underline{ab}} A^{\hat{c}}_{\underline{b}} \hat{\partial}_{\hat{c}} \left(A^{\hat{d}}_{\underline{a}} \hat{\phi}_{\hat{d}} \right) \frac{dt}{d\hat{t}} d\hat{t} \tag{4.4.12}$$

$$= \int_{\mathbb{R}} X^{\underline{ab}} A^{\hat{d}}_{\underline{ab}} \hat{\phi}_{\hat{d}} \frac{dt}{d\hat{t}} d\hat{t} + \int_{\mathbb{R}} X^{\underline{ab}} A^{\hat{c}}_{\underline{b}} A^{\hat{d}}_{\underline{a}} \hat{\partial}_{\hat{c}} (\hat{\phi}_{\hat{d}}) \frac{dt}{d\hat{t}} d\hat{t}. \tag{4.4.13}$$

For the V^a term,

$$\int_{\mathbb{R}} \dot{\eta}^a V^{\underline{b}} \partial_{\underline{b}} \phi_{\underline{a}} dt = \int_{\mathbb{R}} \dot{\hat{\eta}}^{\hat{c}} A^a_{\hat{c}} \frac{d\hat{t}}{dt} V^{\underline{b}} A^{\hat{d}}_{\underline{b}} \hat{\partial}_{\hat{d}} \left(A^{\hat{e}}_a \hat{\phi}_{\hat{e}} \right) \frac{d\hat{t}}{dt} dt \tag{4.4.14}$$

$$= \int_{\mathbb{R}} \dot{\eta}^a V^{\underline{b}} A^{\hat{e}}_{\underline{b}a} \hat{\phi}_{\hat{e}} \frac{d\hat{t}}{dt} dt + \int_{\mathbb{R}} \dot{\hat{\eta}}^{\hat{c}} A^a_{\hat{c}} V^{\underline{b}} A^{\hat{d}}_{\underline{b}} A^{\hat{e}}_a \hat{\partial}_{\hat{d}} \hat{\phi}_{\hat{e}} dt \tag{4.4.15}$$

$$= \int_{\mathbb{R}} V^{\underline{b}} \dot{\eta}^a \partial_a (A^{\hat{e}}_{\underline{c}}) \hat{\phi}_{\hat{e}} \frac{d\hat{t}}{dt} dt + \int_{\mathbb{R}} \dot{\hat{\eta}}^{\hat{c}} V^{\underline{b}} A^{\hat{d}}_{\underline{b}} \hat{\partial}_{\hat{d}} \hat{\phi}_{\hat{c}} dt. \tag{4.4.16}$$

For the $X^{\underline{a}}$ term,

$$\int_{\mathbb{R}} X^{\underline{d}} \phi_{\underline{d}} dt = \int_{\mathbb{R}} X^{\underline{d}} A^{\hat{c}}_{\underline{d}} \hat{\phi}_{\hat{c}} \frac{d\hat{t}}{dt} dt. \tag{4.4.17}$$

Summing all these terms together gives the transformed quadrupole,

$$\begin{aligned}\int_{\mathcal{E}} \mathcal{J}^a \phi_a d^7\xi = \int_{\mathcal{E}} \hat{\mathcal{J}}^{\hat{a}} \hat{\phi}_{\hat{a}} d^7\hat{\xi} = \frac{1}{2}\int_{\mathbb{R}} V^{\underline{bc}} \dot{\hat{\eta}}^{\hat{d}} A^{\hat{e}}_{\underline{b}} A^{\hat{f}}_{\underline{c}} \hat{\partial}_{\hat{e}} \hat{\partial}_{\hat{f}} (\hat{\phi}_{\hat{d}}) d\hat{t} \\ + \int_{\mathbb{R}} \left(X^{\underline{ab}} A^{\hat{c}}_{\underline{b}} A^{\hat{d}}_{\underline{a}} + \frac{1}{2} V^{\underline{ef}} A^{\hat{c}}_{\underline{e}} \dot{\eta}^a \partial_a \left(A^{\hat{d}}_{\underline{f}} \right) + \frac{1}{2} V^{\underline{ef}} A^{\hat{d}}_{\underline{f}} \dot{\eta}^a \partial_a \left(A^{\hat{c}}_{\underline{e}} \right) \right) \hat{\partial}_{\hat{c}} (\hat{\phi}_{\hat{d}}) \frac{dt}{d\hat{t}} d\hat{t} \\ + \int_{\mathbb{R}} \dot{\hat{\eta}}^{\hat{a}} \left(V^{\underline{b}} A^{\hat{d}}_{\underline{b}} + \frac{1}{2} V^{\underline{bc}} A^{\hat{a}}_{\underline{cb}} \right) \hat{\partial}_{\hat{d}} \hat{\phi}_{\hat{a}} dt \\ + \int_{\mathbb{R}} \left(X^{\underline{d}} A^{\hat{c}}_{\underline{d}} + V^{\underline{b}} \dot{\eta}^a \partial_a (A^{\hat{c}}_{\underline{b}}) + X^{\underline{ab}} A^{\hat{c}}_{\underline{ab}} + \frac{1}{2} V^{\underline{de}} \dot{\eta}^a \partial_a \left(A^{\hat{c}}_{\underline{de}} \right) \right) \hat{\phi}_{\hat{c}} \frac{dt}{d\hat{t}} d\hat{t}. \quad (4.4.18)\end{aligned}$$

This gives equation (4.4.7) as required, where the components of the quadrupole in the new coordinate system are no longer unique. □

As previously stated, U^a, U^{ab}, Y^a, and Y^{ab} have indices ranging over $(0, \ldots, 6)$, not just $(1, \ldots, 6)$. As shown in section 4.1, for the components of a multipole to be unique, the components must only range over $(1, \ldots, 6)$. The reason that the multipole contains terms of the form U^0 etc. is because it is still adapted to the time slicing t from the original coordinate system. To adapt the components to the new time slicing, and find the full coordinate transformation, they are projected onto the new time coordinate $\hat{t}$. Consider differentiating along a world line,

$$\partial_{\dot{\eta}} = \dot{\eta}^a \partial_a = \partial_0 + \dot{\eta}^{\underline{a}} \partial_{\underline{a}}. \quad (4.4.19)$$

By rearranging this for ∂_0, these terms are projected onto components along $\partial_{\underline{a}}$, and components along the world line,

$$\partial_0 = \partial_{\dot{\eta}} - \dot{\eta}^{\underline{a}} \partial_{\underline{a}}. \quad (4.4.20)$$

Since U^a are functions along a world line,

$$\partial_{\dot{\eta}} U^{\underline{a}} = \frac{dU^{\underline{a}}}{dt} \quad (4.4.21)$$

with similar relations for U^{ab}, Y^a, Y^{ab}, and $\phi|_\eta$. By using this projection, terms like U^{00} get projected into terms in $\hat{V}^{\underline{ab}}$, $\hat{X}^{\underline{ab}}$, $\hat{V}^{\underline{a}}$, and $\hat{X}^{\underline{a}}$.

Using this projection allows multipoles to be adapted to the time slicing $\hat{t}$ in the new coordinate system, i.e. adapted such that the components indices only range over $(1,\ldots,6)$, giving the full coordinate transformation. The new moments are

$$\begin{aligned}\hat{V}^{\hat{a}\hat{b}} &= V^{\underline{cd}}A^{\hat{a}}_{\underline{c}}A^{\hat{b}}_{\underline{d}} - \dot{\eta}^e V^{\underline{cd}}A^{\hat{0}}_{\underline{c}}A^{\hat{b}}_{\underline{d}}A^{\hat{a}}_{\underline{e}}\frac{d\hat{t}}{dt} \\ &\quad - \dot{\eta}^e V^{\underline{cd}}A^{\hat{a}}_{\underline{c}}A^{\hat{0}}_{\underline{d}}A^{\hat{b}}_{\underline{e}}\frac{d\hat{t}}{dt} + \dot{\eta}^e\dot{\eta}^f V^{\underline{cd}}A^{\hat{0}}_{\underline{c}}A^{\hat{0}}_{\underline{d}}A^{\hat{a}}_{\underline{e}}A^{\hat{b}}_{\underline{f}}\left(\frac{d\hat{t}}{dt}\right)^2, \end{aligned} \tag{4.4.22}$$

$$\begin{aligned}\hat{V}^{\hat{a}} &= V^{\underline{b}}A^{\hat{a}}_{\underline{b}} + \frac{1}{2}V^{\underline{bc}}A^{\hat{a}}_{\underline{bc}} - \dot{\eta}^d V^{\underline{b}}A^{\hat{0}}_{\underline{b}}A^{\hat{a}}_{\underline{d}}\frac{d\hat{t}}{dt} - \frac{1}{2}\dot{\eta}^d V^{\underline{bc}}A^{\hat{0}}_{\underline{bc}}A^{\hat{a}}_{\underline{d}}\frac{d\hat{t}}{dt} \\ &\quad + \frac{1}{2}V^{\underline{bc}}\frac{dt}{d\hat{t}}\frac{d}{dt}\left(\dot{\eta}^b A^{\hat{a}}_{\underline{d}}A^{\hat{0}}_{\underline{b}}A^{\hat{0}}_{\underline{c}}\frac{d\hat{t}}{dt}\right) + \frac{1}{2}\dot{\eta}^b\frac{dV^{\underline{bc}}}{dt}A^{\hat{a}}_{\underline{b}}A^{\hat{0}}_{\underline{b}}A^{\hat{0}}_{\underline{c}} \\ &\quad - \left(X^{\underline{cb}}A^{\hat{a}}_{\underline{b}}A^{\hat{0}}_{\underline{c}} + \frac{1}{2}V^{\underline{ef}}\dot{\eta}^c\partial_c\left(A^{\hat{0}}_{\underline{f}}A^{\hat{a}}_{\underline{e}}\right)\right)\frac{dt}{d\hat{t}}. \end{aligned} \tag{4.4.23}$$

To calculate terms of the form $dA^{\hat{a}}_{\underline{d}}/dt$, recall the implicit evaluation at η, so

$$\left.\frac{dA^{\hat{a}}_{\underline{d}}}{dt}\right|_{\eta} = \dot{\eta}^b\partial_b A^{\hat{a}}_{\underline{d}}. \tag{4.4.24}$$

Additionally, note

$$\frac{d\dot{\eta}^{\underline{a}}}{dt} = \frac{d^2\eta^{\underline{a}}(t)}{dt^2} \tag{4.4.25}$$

which, in contrast to $\dot{\eta}^a$, does not transform as a vector.

Similar terms exist for $\hat{X}^{\hat{a}\hat{b}}$ and $\hat{X}^{\hat{a}}$ such that (4.3.7) is still satisfied, and are given by

$$\begin{aligned}\hat{X}^{\hat{a}\hat{b}} &= \left(X^{\underline{cd}}A^{\hat{a}}_{\underline{c}}A^{\hat{b}}_{\underline{d}} + \frac{1}{2}V^{\underline{ef}}A^{\hat{a}}_{\underline{e}}\dot{\eta}^c\partial_c\left(A^{\hat{b}}_{\underline{f}}\right) + \frac{1}{2}V^{\underline{ef}}A^{\hat{b}}_{\underline{f}}\dot{\eta}^c\partial_c\left(A^{\hat{a}}_{\underline{e}}\right)\right)\frac{dt}{d\hat{t}} \\ &\quad - \left(X^{\underline{cd}}A^{\hat{a}}_{\underline{c}}A^{\hat{0}}_{\underline{d}} + \frac{1}{2}V^{\underline{ef}}A^{\hat{a}}_{\underline{e}}\dot{\eta}^c\partial_c\left(A^{\hat{0}}_{\underline{f}}\right) + \frac{1}{2}V^{\underline{ef}}A^{\hat{0}}_{\underline{f}}\dot{\eta}^c\partial_c\left(A^{\hat{a}}_{\underline{e}}\right)\right)\dot{\eta}^g A^{\hat{b}}_{\underline{g}} \\ &\quad - \left(X^{\underline{cd}}A^{\hat{0}}_{\underline{c}}A^{\hat{b}}_{\underline{d}} + \frac{1}{2}V^{\underline{ef}}A^{\hat{0}}_{\underline{e}}\dot{\eta}^c\partial_c\left(A^{\hat{b}}_{\underline{f}}\right) + \frac{1}{2}V^{\underline{ef}}A^{\hat{b}}_{\underline{f}}\dot{\eta}^c\partial_c\left(A^{\hat{0}}_{\underline{e}}\right)\right)\dot{\eta}^g A^{\hat{a}}_{\underline{g}} \\ &\quad + \left(X^{\underline{cd}}A^{\hat{0}}_{\underline{c}}A^{\hat{0}}_{\underline{d}} + \frac{1}{2}V^{\underline{ef}}A^{\hat{0}}_{\underline{e}}\dot{\eta}^c\partial_c\left(A^{\hat{0}}_{\underline{f}}\right) + \frac{1}{2}V^{\underline{ef}}A^{\hat{0}}_{\underline{f}}\dot{\eta}^c\partial_c\left(A^{\hat{0}}_{\underline{e}}\right)\right)\dot{\eta}^g\dot{\eta}^h A^{\hat{a}}_{\underline{g}}A^{\hat{b}}_{\underline{h}}\frac{d\hat{t}}{dt} \\ &\quad + \dot{\eta}^f V^{\underline{de}}A^{\hat{0}}_{\underline{d}}A^{\hat{0}}_{\underline{e}}A^{\hat{b}}_{\underline{f}}\frac{d}{dt}\left(\dot{\eta}^g A^{\hat{a}}_{\underline{g}}\frac{d\hat{t}}{dt}\right) - V^{\underline{de}}A^{\hat{b}}_{\underline{d}}A^{\hat{0}}_{\underline{e}}\frac{dt}{d\hat{t}}\frac{d}{dt}\left(\dot{\eta}^c A^{\hat{a}}_{\underline{c}}\frac{d\hat{t}}{dt}\right), \end{aligned} \tag{4.4.26}$$

and

$$\begin{aligned}\hat{X}^{\hat{\underline{a}}} = &\left(X^{\underline{d}}A^{\hat{\underline{a}}}_{\underline{d}} + V^{\underline{b}}\dot{\eta}^e\partial_e(A^{\hat{\underline{a}}}_{\underline{b}}) + X^{\underline{cb}}A^{\hat{\underline{a}}}_{\underline{cb}} + \frac{1}{2}V^{\underline{de}}\dot{\eta}^c\partial_c\left(A^{\hat{\underline{a}}}_{\underline{de}}\right)\right)\frac{dt}{d\hat{t}}\\ &- \frac{d}{dt}\left(\dot{\eta}^eV^{\underline{b}}A^{\hat{0}}_{\underline{b}}A^{\hat{\underline{a}}}_{\underline{e}}\frac{d\hat{t}}{dt} + \frac{1}{2}\dot{\eta}^eV^{\underline{bc}}A^{\hat{0}}_{\underline{bc}}A^{\hat{\underline{a}}}_{\underline{e}}\frac{d\hat{t}}{dt}\right)\\ &+ \frac{1}{2}\left(\frac{dt}{d\hat{t}}\right)^2\frac{d^2}{dt^2}\left(\dot{\eta}^fV^{\underline{de}}A^{\hat{0}}_{\underline{d}}A^{\hat{0}}_{\underline{e}}A^{\hat{\underline{a}}}_{\underline{f}}\frac{d\hat{t}}{dt}\right) + \frac{1}{2}\frac{d^2t}{d\hat{t}^2}\frac{d}{dt}\left(\dot{\eta}^fV^{\underline{de}}A^{\hat{0}}_{\underline{d}}A^{\hat{0}}_{\underline{e}}A^{\hat{\underline{a}}}_{\underline{f}}\frac{d\hat{t}}{dt}\right)\\ &- \frac{dt}{d\hat{t}}\frac{d}{dt}\left(\left(X^{\underline{cd}}A^{\hat{\underline{a}}}_{\underline{d}}A^{\hat{0}}_{\underline{c}} + \frac{1}{2}V^{\underline{ef}}A^{\hat{\underline{a}}}_{\underline{e}}\dot{\eta}^c\partial_c\left(A^{\hat{0}}_{\underline{f}}\right) + \frac{1}{2}V^{\underline{ef}}A^{\hat{0}}_{\underline{f}}\dot{\eta}^c\partial_c\left(A^{\hat{\underline{a}}}_{\underline{e}}\right)\right)\frac{dt}{d\hat{t}}\right). \quad (4.4.27)\end{aligned}$$

These terms can also be found using equation (4.1.3) in the new coordinate system.

Proof. Consider the non-unique quadrupole, where, as this is all in the new coordinate system, hats have been removed from the indices temporarily to aid readability,

$$\begin{aligned}\int_{\mathcal{E}}\mathcal{J}^a\phi_ad^7\xi = &\frac{1}{2}\int_{\mathbb{R}}\dot{\eta}^aU^{bc}\partial_b\partial_c\phi_adt + \int_{\mathbb{R}}Y^{ab}\partial_{\underline{b}}\phi_{\underline{a}}dt\\ &+ \int_{\mathbb{R}}\dot{\eta}^aU^{\underline{b}}\partial_{\underline{b}}\phi_adt + \int_{\mathbb{R}}Y^{\underline{a}}\phi_{\underline{a}}dt + \int_{\mathbb{R}}\dot{\eta}^aq\phi_adt. \quad (4.4.28)\end{aligned}$$

Use the projection (equation (4.4.20)) and proceed term by term. Starting with the U^{ab} term, noting the symmetry of U^{ab},

$$\begin{aligned}\int_{\mathbb{R}}\dot{\eta}^aU^{bc}\partial_b\partial_c\phi_adt = &\int_{\mathbb{R}}\dot{\eta}^aU^{\underline{bc}}\partial_{\underline{b}}\partial_{\underline{c}}\phi_adt \quad (4.4.29)\\ &+ 2\int_{\mathbb{R}}\dot{\eta}^aU^{\underline{b}0}\partial_{\underline{b}}\partial_0\phi_adt + \int_{\mathbb{R}}\dot{\eta}^aU^{00}\partial_0\partial_0\phi_adt\\ = &\int_{\mathbb{R}}\dot{\eta}^aU^{\underline{bc}}\partial_{\underline{b}}\partial_{\underline{c}}\phi_adt + 2\int_{\mathbb{R}}\dot{\eta}^aU^{\underline{b}0}\partial_{\dot{\eta}}\partial_{\underline{b}}\phi_adt \quad (4.4.30)\\ &- 2\int_{\mathbb{R}}\dot{\eta}^a\dot{\eta}^{\underline{d}}U^{\underline{b}0}\partial_{\underline{b}}\partial_{\underline{d}}\phi_adt + \int_{\mathbb{R}}\dot{\eta}^aU^{00}\partial_{\dot{\eta}}\partial_0\phi_adt\\ &- \int_{\mathbb{R}}\dot{\eta}^a\dot{\eta}^{\underline{b}}U^{00}\partial_0\partial_{\underline{b}}\phi_adt.\end{aligned}$$

Recalling that $\partial_{\dot{\eta}}\phi_a = d\phi_a/dt$, and then integrating by parts gives

$$\begin{aligned}\int_{\mathbb{R}}\dot{\eta}^aU^{bc}\partial_b\partial_c\phi_adt = &\int_{\mathbb{R}}\dot{\eta}^a\left(U^{\underline{bc}} - 2\dot{\eta}^{\underline{c}}U^{\underline{c}0}\right)\partial_{\underline{b}}\partial_{\underline{c}}\phi_adt\\ &- 2\int_{\mathbb{R}}\frac{d}{dt}\left(\dot{\eta}^aU^{\underline{b}0}\right)\partial_{\underline{b}}\phi_adt + \int_{\mathbb{R}}\frac{d}{dt}\left(\dot{\eta}^aU^{00}\right)\partial_0\phi_adt\\ &- \int_{\mathbb{R}}\dot{\eta}^a\dot{\eta}^{\underline{b}}U^{00}\partial_{\underline{b}}\partial_0\phi_adt. \quad (4.4.31)\end{aligned}$$

Projecting the remaining ∂_0 terms gives

$$\begin{aligned}\int_{\mathbb{R}} \dot{\eta}^a U^{bc} \partial_b \partial_c \phi_a dt = &\int_{\mathbb{R}} \dot{\eta}^a \left(U^{b\underline{c}} - 2\dot{\eta}^{\underline{c}} U^{\underline{c}0} \right) \partial_{\underline{b}} \partial_{\underline{c}} \phi_a dt - 2 \int_{\mathbb{R}} \frac{d}{dt} \left(\dot{\eta}^a U^{\underline{b}0} \right) \partial_{\underline{b}} \phi_a dt \\ &+ \int_{\mathbb{R}} \frac{d}{dt} \left(\dot{\eta}^a U^{00} \right) \partial_{\dot{\eta}} \phi_a dt + \int_{\mathbb{R}} \frac{d}{dt} \left(\dot{\eta}^a U^{00} \right) \dot{\eta}^{\underline{b}} \partial_{\underline{b}} \phi_a dt \\ &- \int_{\mathbb{R}} \dot{\eta}^a \dot{\eta}^{\underline{b}} U^{00} \partial_{\dot{\eta}} \partial_{\underline{b}} \phi_a dt + \int_{\mathbb{R}} \dot{\eta}^a \dot{\eta}^{\underline{b}} \dot{\eta}^{\underline{c}} U^{00} \partial_{\underline{b}} \partial_{\underline{c}} \phi_a dt. \end{aligned} \tag{4.4.32}$$

Integrating by parts and simplifying,

$$\begin{aligned}\int_{\mathbb{R}} \dot{\eta}^a U^{bc} \partial_b \partial_c \phi_a dt = &\int_{\mathbb{R}} \dot{\eta}^a \left(U^{b\underline{c}} - 2\dot{\eta}^{\underline{c}} U^{\underline{c}0} + \dot{\eta}^{\underline{b}} \dot{\eta}^{\underline{c}} U^{00} \right) \partial_{\underline{b}} \partial_{\underline{c}} \phi_a dt \\ &- 2 \int_{\mathbb{R}} \frac{d}{dt} \left(\dot{\eta}^a U^{\underline{b}0} \right) \partial_{\underline{b}} \phi_a dt + \int_{\mathbb{R}} \frac{d^2}{dt^2} \left(\dot{\eta}^a U^{00} \right) \phi_a dt \\ &+ \int_{\mathbb{R}} \frac{d}{dt} \left(\dot{\eta}^a U^{00} \right) \dot{\eta}^{\underline{b}} \partial_{\underline{b}} \phi_a dt - \int_{\mathbb{R}} \frac{d}{dt} \left(\dot{\eta}^a \dot{\eta}^{\underline{b}} U^{00} \right) \partial_{\underline{b}} \phi_a dt. \end{aligned} \tag{4.4.33}$$

For the Y^{ab} term,

$$\int_{\mathbb{R}} Y^{ab} \partial_b \phi_a dt = \int_{\mathbb{R}} Y^{a\underline{b}} \partial_{\underline{b}} \phi_a dt + \int_{\mathbb{R}} Y^{a0} \partial_0 \phi_a dt \tag{4.4.34}$$

$$= \int_{\mathbb{R}} Y^{a\underline{b}} \partial_{\underline{b}} \phi_a dt + \int_{\mathbb{R}} Y^{a0} \partial_{\dot{\eta}} \phi_a dt - \int_{\mathbb{R}} Y^{a0} \dot{\eta}^{\underline{b}} \partial_{\underline{b}} \phi_a dt \tag{4.4.35}$$

$$= \int_{\mathbb{R}} \left(Y^{a\underline{b}} - Y^{a0} \dot{\eta}^{\underline{b}} \right) \partial_{\underline{b}} \phi_a dt - \int_{\mathbb{R}} \frac{d}{dt} Y^{a0} \phi_a dt. \tag{4.4.36}$$

For the U^a term,

$$\int_{\mathbb{R}} \dot{\eta}^a U^b \partial_b \phi_a dt = \int_{\mathbb{R}} \dot{\eta}^a U^0 \partial_0 \phi_a dt + \int_{\mathbb{R}} \dot{\eta}^a U^{\underline{b}} \partial_{\underline{b}} \phi_a dt \tag{4.4.37}$$

$$= \int_{\mathbb{R}} \dot{\eta}^a U^0 \partial_{\dot{\eta}} \phi_a dt - \int_{\mathbb{R}} \dot{\eta}^a U^0 \dot{\eta}^{\underline{a}} \partial_{\underline{b}} \phi_a dt + \int_{\mathbb{R}} \dot{\eta}^a U^{\underline{b}} \partial_{\underline{b}} \phi_a dt \tag{4.4.38}$$

$$= -\int_{\mathbb{R}} \frac{d}{dt} \left(\dot{\eta}^a U^0 \right) \phi_a dt + \int_{\mathbb{R}} \dot{\eta}^a \left(U^{\underline{b}} - U^0 \dot{\eta}^{\underline{b}} \right) \partial_{\underline{b}} \phi_a dt. \tag{4.4.39}$$

Summing all these terms together,

$$\begin{aligned}\int_{\mathcal{E}} \mathcal{J}^a \phi_a d^7\xi = \frac{1}{2}\int_{\mathbb{R}} \dot\eta^a \left(U^{\underline{bc}} - 2\dot\eta^{\underline{c}} U^{\underline{c}0} + \dot\eta^{\underline{b}}\dot\eta^{\underline{c}} U^{00}\right)\partial_{\underline{b}}\partial_{\underline{c}}\phi_a dt \\ - \int_{\mathbb{R}} \frac{d}{dt}\left(\dot\eta^a U^{\underline{b}0}\right)\partial_{\underline{b}}\phi_a dt + \frac{1}{2}\int_{\mathbb{R}} \frac{d^2}{dt^2}\left(\dot\eta^a U^{00}\right)\phi_a dt \\ + \frac{1}{2}\int_{\mathbb{R}} \frac{d}{dt}\left(\dot\eta^a U^{00}\right)\dot\eta^{\underline{b}}\partial_{\underline{b}}\phi_a dt - \frac{1}{2}\int_{\mathbb{R}} \frac{d}{dt}\left(\dot\eta^a \dot\eta^{\underline{b}} U^{00}\right)\partial_{\underline{b}}\phi_a dt \\ + \int_{\mathbb{R}} \left(Y^{a\underline{b}} - Y^{a0}\dot\eta^{\underline{b}}\right)\partial_{\underline{b}}\phi_a dt - \int_{\mathbb{R}} \frac{d}{dt} Y^{a0}\phi_a dt - \int_{\mathbb{R}} \frac{d}{dt}\left(\dot\eta^a U^0\right)\phi_a dt \\ + \int_{\mathbb{R}} \dot\eta^a \left(U^{\underline{b}} - U^0\dot\eta^{\underline{b}}\right)\partial_{\underline{b}}\phi_a dt + \int_{\mathbb{R}} Y^a \phi_a dt + \int_{\mathbb{R}} \dot\eta^a q \phi_a dt. \quad (4.4.40)\end{aligned}$$

Grouping terms together,

$$\begin{aligned}\int_{\mathcal{E}} \mathcal{J}^a \phi_a d^7\xi = \frac{1}{2}\int_{\mathbb{R}} \dot\eta^a \left(U^{\underline{bc}} - 2\dot\eta^{\underline{c}} U^{\underline{c}0} + \dot\eta^{\underline{b}}\dot\eta^{\underline{c}} U^{00}\right)\partial_{\underline{b}}\partial_{\underline{c}}\phi_a dt \\ + \int_{\mathbb{R}} \left(Y^{a\underline{b}} - Y^{a0}\dot\eta^{\underline{b}} - \frac{d}{dt}\left(\dot\eta^a U^{\underline{b}0}\right) + \frac{1}{2}\frac{d}{dt}\left(\dot\eta^a \dot\eta^{\underline{b}} U^{00}\right)\right)\partial_{\underline{b}}\phi_a dt \\ + \frac{1}{2}\int_{\mathbb{R}} \frac{d^2}{dt^2}\left(\dot\eta^a U^{00}\right)\phi_a dt + \frac{1}{2}\int_{\mathbb{R}} \frac{d}{dt}\left(\dot\eta^a U^{00}\right)\dot\eta^{\underline{b}}\partial_{\underline{b}}\phi_a dt - \int_{\mathbb{R}} \frac{d}{dt} Y^{a0}\phi_a dt \\ + \int_{\mathbb{R}} \dot\eta^a \left(U^{\underline{b}} - U^0\dot\eta^{\underline{b}}\right)\partial_{\underline{b}}\phi_a dt + \int_{\mathbb{R}} \left(Y^a - \frac{d}{dt}\left(\dot\eta^a U^0\right)\right)\phi_a dt + \int_{\mathbb{R}} \dot\eta^a q \phi_a dt. \quad (4.4.41)\end{aligned}$$

Calculating some derivatives and symmetrising $U^{0\underline{b}}$ gives

$$\begin{aligned}\int_{\mathcal{E}} \mathcal{J}^a \phi_a d^7\xi = \frac{1}{2}\int_{\mathbb{R}} \dot\eta^a \left(U^{\underline{bc}} - \dot\eta^{\underline{b}} U^{\underline{c}0} - \dot\eta^{\underline{c}} U^{\underline{b}0} + \dot\eta^{\underline{b}}\dot\eta^{\underline{c}} U^{00}\right)\partial_{\underline{b}}\partial_{\underline{c}}\phi_a dt \\ + \int_{\mathbb{R}} \left(Y^{a\underline{b}} - Y^{a0}\dot\eta^{\underline{b}} - \dot\eta^a \frac{d}{dt}\left(U^{\underline{b}0}\right) + \frac{1}{2}\dot\eta^a \dot\eta^{\underline{b}} \frac{d}{dt}\left(U^{00}\right)\right)\partial_{\underline{b}}\phi_a dt \\ + \int_{\mathbb{R}} \left(-U^{\underline{b}0}\frac{d}{dt}\left(\dot\eta^a\right) + \frac{1}{2}U^{00}\frac{d}{dt}\left(\dot\eta^a \dot\eta^{\underline{b}}\right)\right)\partial_{\underline{b}}\phi_a dt \\ + \frac{1}{2}\int_{\mathbb{R}} \frac{d^2}{dt^2}\left(\dot\eta^a U^{00}\right)\phi_a dt + \frac{1}{2}\int_{\mathbb{R}} \frac{d}{dt}\left(\dot\eta^a U^{00}\right)\dot\eta^{\underline{b}}\partial_{\underline{b}}\phi_a dt - \int_{\mathbb{R}} \frac{d}{dt} Y^{a0}\phi_a dt \\ + \int_{\mathbb{R}} \dot\eta^a \left(U^{\underline{b}} - U^0\dot\eta^{\underline{b}}\right)\partial_{\underline{b}}\phi_a dt + \int_{\mathbb{R}} \left(Y^a - \frac{d}{dt}\left(\dot\eta^a U^0\right)\right)\phi_a dt + \int_{\mathbb{R}} \dot\eta^a q \phi_a dt. \quad (4.4.42)\end{aligned}$$

Noting $dU^{ab}/dt = Y^{ab} + Y^{ba}$ gives

$$\begin{aligned}\int_{\mathcal{E}} \mathcal{J}^a \phi_a d^7\xi = \frac{1}{2}\int_{\mathbb{R}} \dot{\eta}^a \left(U^{\underline{bc}} - \dot{\eta}^{\underline{b}} U^{\underline{c}0} - \dot{\eta}^{\underline{c}} U^{\underline{b}0} + \dot{\eta}^{\underline{b}}\dot{\eta}^{\underline{c}} U^{00}\right) \partial_{\underline{b}}\partial_{\underline{c}}\phi_a dt \\ + \int_{\mathbb{R}} \left(Y^{a\underline{b}} - Y^{a0}\dot{\eta}^{\underline{b}} - \dot{\eta}^a Y^{\underline{b}0} - \dot{\eta}^a Y^{0\underline{b}} + \dot{\eta}^a\dot{\eta}^{\underline{b}} Y^{00}\right) \partial_{\underline{b}}\phi_a dt \\ + \int_{\mathbb{R}} \left(\frac{1}{2} U^{00}\frac{d}{dt}\left(\dot{\eta}^a\dot{\eta}^{\underline{b}}\right) - U^{\underline{b}0}\frac{d}{dt}\left(\dot{\eta}^a\right)\right) \partial_{\underline{b}}\phi_a dt \\ + \frac{1}{2}\int_{\mathbb{R}} \frac{d^2}{dt^2}\left(\dot{\eta}^a U^{00}\right)\phi_a dt + \frac{1}{2}\int_{\mathbb{R}} \frac{d}{dt}\left(\dot{\eta}^a U^{00}\right)\dot{\eta}^{\underline{b}}\partial_{\underline{b}}\phi_a dt \\ - \int_{\mathbb{R}} \frac{d}{dt} Y^{a0}\phi_a dt + \int_{\mathbb{R}} \dot{\eta}^a\left(U^{\underline{b}} - U^0\dot{\eta}^{\underline{b}}\right)\partial_{\underline{b}}\phi_a dt + \int_{\mathbb{R}} \left(Y^a - \frac{d}{dt}\left(\dot{\eta}^a U^0\right)\right)\phi_a dt \\ + \int_{\mathbb{R}} \dot{\eta}^a q\phi_a dt. \quad (4.4.43)\end{aligned}$$

Rearranging for clarity, and reinserting hats over quantities,

$$\begin{aligned}\int_{\mathcal{E}} \hat{\mathcal{J}}^{\hat{a}}\hat{\phi}_{\hat{a}} d^7\hat{\xi} = \frac{1}{2}\int_{\mathbb{R}} \dot{\hat{\eta}}^{\hat{a}}\left(\hat{U}^{\hat{\underline{b}}\hat{\underline{c}}} - \dot{\hat{\eta}}^{\hat{\underline{b}}}\hat{U}^{\hat{\underline{c}}\hat{0}} - \dot{\hat{\eta}}^{\hat{\underline{c}}}\hat{U}^{\hat{\underline{b}}\hat{0}} + \dot{\hat{\eta}}^{\hat{\underline{b}}}\dot{\hat{\eta}}^{\hat{\underline{c}}}\hat{U}^{\hat{0}\hat{0}}\right)\hat{\partial}_{\hat{\underline{b}}}\hat{\partial}_{\hat{\underline{c}}}\hat{\phi}_{\hat{a}} d\hat{t} \\ + \int_{\mathbb{R}} \left(\hat{Y}^{\hat{a}\hat{\underline{b}}} - \hat{Y}^{\hat{a}\hat{0}}\dot{\hat{\eta}}^{\hat{\underline{b}}} - \dot{\hat{\eta}}^{\hat{a}}\hat{Y}^{\hat{0}\hat{\underline{b}}} + \dot{\hat{\eta}}^{\hat{a}}\dot{\hat{\eta}}^{\hat{\underline{b}}}\hat{Y}^{\hat{0}\hat{0}}\right)\hat{\partial}_{\hat{\underline{b}}}\hat{\phi}_{\hat{a}} d\hat{t} \\ + \int_{\mathbb{R}} \left(\hat{U}^{\hat{0}\hat{0}}\dot{\hat{\eta}}^{\hat{\underline{b}}}\frac{d}{d\hat{t}}\left(\dot{\hat{\eta}}^{\hat{a}}\right) - \hat{U}^{\hat{\underline{b}}\hat{0}}\frac{d}{d\hat{t}}\left(\dot{\hat{\eta}}^{\hat{a}}\right)\right)\hat{\partial}_{\hat{\underline{b}}}\hat{\phi}_{\hat{a}} d\hat{t} \\ + \int_{\mathbb{R}} \dot{\hat{\eta}}^a\left(\hat{U}^{\hat{\underline{b}}} - \hat{U}^{\hat{0}}\dot{\hat{\eta}}^{\hat{\underline{b}}} + \frac{1}{2}\frac{d}{d\hat{t}}\left(\dot{\hat{\eta}}^{\hat{\underline{b}}}\hat{U}^{\hat{0}\hat{0}}\right) - \hat{Y}^{\hat{\underline{b}}\hat{0}}\right)\hat{\partial}_{\hat{\underline{b}}}\hat{\phi}_{\hat{a}} d\hat{t} \\ + \int_{\mathbb{R}} \left(\hat{Y}^{\hat{a}} - \frac{d}{d\hat{t}}\left(\dot{\hat{\eta}}^{\hat{a}}\hat{U}^{\hat{0}}\right) + \frac{1}{2}\frac{d^2}{d\hat{t}^2}\left(\dot{\hat{\eta}}^{\hat{a}}\hat{U}^{\hat{0}\hat{0}}\right) - \frac{d}{d\hat{t}}\hat{Y}^{\hat{a}\hat{0}}\right)\hat{\phi}_{\hat{a}} d\hat{t}. \quad (4.4.44)\end{aligned}$$

By noting $\dot{\eta}^0 = 1$, the $Y^{0\underline{a}}, Y^{\underline{a}0}, Y^{00}$, and Y^0 components cancel. Additionally, transform the relevant $\dot{\hat{\eta}}^{\hat{\underline{a}}}$ and $d/d\hat{t}$ terms back into the original coordinate system, noting

$$\frac{d}{d\hat{t}^2} = \left(\frac{dt}{d\hat{t}}\right)^2 \frac{d^2}{dt^2} + \frac{d^2t}{d\hat{t}^2}\frac{d}{dt}. \quad (4.4.45)$$

This is done so the full coordinate transformation is defined relative to the original

coordinate system. Doing this transformation gives the projected moments,

$$\begin{aligned}
\hat{V}^{\hat{\underline{b}}\hat{\underline{c}}} &= \hat{U}^{\hat{\underline{b}}\hat{\underline{c}}} - \dot{\eta}^a \hat{U}^{\hat{\underline{c}}\hat{0}} A^{\hat{\underline{b}}}_{\underline{a}} \frac{d\hat{t}}{dt} - \dot{\eta}^a \hat{U}^{\hat{\underline{b}}\hat{0}} A^{\hat{\underline{c}}}_{\underline{a}} \frac{d\hat{t}}{dt} + \dot{\eta}^a \dot{\eta}^d \hat{U}^{\hat{0}\hat{0}} A^{\hat{\underline{b}}}_{\underline{a}} A^{\hat{\underline{c}}}_{\underline{d}} \left(\frac{d\hat{t}}{dt}\right)^2, \\
\hat{X}^{\hat{\underline{a}}\hat{\underline{b}}} &= \hat{Y}^{\hat{\underline{a}}\hat{\underline{b}}} - \dot{\eta}^c \hat{Y}^{\hat{\underline{a}}\hat{0}} A^{\hat{\underline{b}}}_{\underline{c}} \frac{d\hat{t}}{dt} - \dot{\eta}^c \hat{Y}^{\hat{0}\hat{\underline{b}}} A^{\hat{\underline{a}}}_{\underline{c}} \frac{d\hat{t}}{dt} + \dot{\eta}^c \dot{\eta}^d \hat{Y}^{\hat{0}\hat{0}} A^{\hat{\underline{a}}}_{\underline{c}} A^{\hat{\underline{b}}}_{\underline{d}} \left(\frac{d\hat{t}}{dt}\right)^2 \\
&\quad + \dot{\eta}^c \hat{U}^{\hat{0}\hat{0}} A^{\hat{\underline{b}}}_{\underline{c}} \frac{d}{dt}\left(\dot{\eta}^c A^{\hat{\underline{a}}}_{\underline{c}} \frac{d\hat{t}}{dt}\right) - \hat{U}^{\hat{\underline{b}}\hat{0}} \frac{dt}{d\hat{t}} \frac{d}{dt}\left(\dot{\eta}^c A^{\hat{\underline{a}}}_{\underline{c}} \frac{d\hat{t}}{dt}\right), \\
\hat{V}^{\hat{\underline{b}}} &= \hat{U}^{\hat{\underline{b}}} - \dot{\eta}^a \hat{U}^{\hat{0}} A^{\hat{\underline{b}}}_{\underline{a}} \frac{d\hat{t}}{dt} + \frac{1}{2} \frac{dt}{d\hat{t}} \frac{d}{dt}\left(\dot{\eta}^a \hat{U}^{\hat{0}\hat{0}} A^{\hat{\underline{b}}}_{\underline{a}} \frac{d\hat{t}}{dt}\right) - \hat{Y}^{\hat{\underline{b}}\hat{0}}, \\
\hat{X}^{\hat{\underline{a}}} &= \hat{Y}^{\hat{\underline{a}}} - \frac{dt}{d\hat{t}} \frac{d}{dt}\left(\dot{\eta}^b \hat{U}^{\hat{0}} A^{\hat{\underline{a}}}_{\underline{b}} \frac{d\hat{t}}{dt}\right) + \frac{1}{2}\left(\frac{dt}{d\hat{t}}\right)^2 \frac{d^2}{d\hat{t}^2}\left(\dot{\eta}^c \hat{U}^{\hat{0}\hat{0}} A^{\hat{\underline{a}}}_{\underline{c}} \frac{d\hat{t}}{dt}\right) \\
&\quad + \frac{d^2 t}{d\hat{t}^2} \frac{d}{dt}\left(\dot{\eta}^c \hat{U}^{\hat{0}\hat{0}} A^{\hat{\underline{a}}}_{\underline{c}} \frac{d\hat{t}}{dt}\right) - \frac{dt}{d\hat{t}} \frac{d}{dt} \hat{Y}^{\hat{\underline{a}}\hat{0}}.
\end{aligned} \tag{4.4.46}$$

Combining this with (4.4.7) gives the full coordinate transformations for the quadrupole. □

Equation (4.4.22) and equation (4.4.23) are a new result, and are numerically tested in the next chapter to show their validity. In a coordinate transformation where there is no change in the time coordinate, $A^{\hat{0}}_{\underline{b}} = 0$. This reduces equations (4.4.22) and equation (4.4.23) to equations (3.3.7) and (3.3.13) respectively. This work has transformed between two coordinate time frames, but can be generalised to any frame, not just one where $\dot{\eta}^0 = 1$, with a more general projection

$$\partial_0 = \frac{1}{\dot{\eta}^0} \partial_{\dot{\eta}} - \frac{\dot{\eta}^{\underline{a}}}{\dot{\eta}^0} \partial_{\underline{a}}. \tag{4.4.47}$$

Chapter 5

Numerical validation of the moment tracking and cooordinate transformations around a black hole

5.1 Developing the simulation

To test the accuracy of the moment tracking and coordinate transformation equations, a computational model was developed. The code tests whether the truncation to quadrupole order is acceptable, or if a higher order multipole expansion should be used for practical cases. The results presented here are an example of a coordinate transformation that mixes time and space coordinates, focussing on the particularly challenging case of black holes. It is important to stress that whilst black holes are the focus of this numerical validation, the applications of this work are not solely limited to plasma around black holes. In particular, the moment tracking can be applied to any plasma, and to particle accelerators.

In all cases, only uncharged particles will be tracked. To calculate the inter-macroparticle forces needed for a full PIC code, a method to use the moments to deposit the charge from a macroparticle onto the grid must be developed. Two

different methods to do this are presented in chapter 6.

To develop the code, the derivatives of the Vlasov equation were calculated using the symbolic algebra software Maple. The simulation itself was written in C++. There are 36 first derivatives of the Vlasov equation and 126 second derivatives. Each of these derivatives are very complex, hence the need to calculate them using symbolic algebra software. To give an example of this complexity, in Schwarzschild coordinates $(t, r, \theta, \phi, u_r, u_\theta, u_\phi)$, one derivative of the Vlasov field is

$$\begin{aligned}\frac{\partial W^4}{\partial u_\theta} = &-\frac{1}{u^0}\left(-\frac{(r-r_s)\,r_s u_\theta}{r\left(-1+\frac{r_s}{r}\right)}+2\left(-r+r_s\right)u_\theta\right)\\ &-\frac{2}{u^0}\frac{\left(\frac{(r-r_s)r_s u^0}{2r^3}-\frac{r_s\,u_r^2}{2r(r-r_s)}\right)r^2 u_\theta}{\left(-1-\frac{u_r^2}{1-\frac{r_s}{r}}-r^2u_\theta^2-r^2\left(\sin^2(\theta)\right)u_\phi^2\right)}\\ &-\frac{2}{u^0}\frac{\left(\left(-r+r_s\right)u_\theta^2-\left(r-r_s\right)\left(\sin^2(\theta)\right)u_\phi^2\right)r^2u_\theta}{\left(-1-\frac{u_r^2}{1-\frac{r_s}{r}}-r^2u_\theta^2-r^2\left(\sin^2(\theta)\right)u_\phi^2\right)}\\ &+\frac{2}{u^0}\frac{rr_s u_r^2 u_\theta}{\left(r-r_s\right)\left(-1-\frac{u_r^2}{1-\frac{r_s}{r}}-r^2u_\theta^2-r^2\left(\sin^2(\theta)\right)u_\phi^2\right)}.\end{aligned} \tag{5.1.1}$$

The model uses the forward Euler method to integrate both the particle motion and the moment equations [97]. Particle positions are updated using the 3-velocities $u^{\underline{\mu}}/u^0$, and the 4-velocities are updated using the geodesic equation,

$$x^{\underline{\mu}}_{\text{new}} = x^{\underline{\mu}}_{\text{old}} + \frac{u^{\underline{\mu}}_{\text{old}}}{u^0_{\text{old}}}\Delta t, \tag{5.1.2a}$$

$$u^{\underline{\mu}}_{\text{new}} = u^{\underline{\mu}}_{\text{old}} - \Gamma^{\underline{\mu}}_{\nu\rho}u^{\nu}_{\text{old}}u^{\rho}_{\text{old}}\,\Delta t, \tag{5.1.2b}$$

where u^0 is defined by equation (2.1.2) and Δt is the time step size. Moments are updated using the equations

$$V^{\underline{a}}_{\text{new}} = V^{\underline{b}}_{\text{old}}\partial_{\underline{b}}W^{\underline{a}}_{\text{old}}\,\Delta t + \frac{1}{2}V^{\underline{bc}}_{\text{old}}\partial_{\underline{b}}\partial_{\underline{c}}W^{\underline{a}}_{\text{old}}\,\Delta t, \tag{5.1.3a}$$

$$V^{\underline{ab}}_{\text{new}} = \left(V^{\underline{ac}}_{\text{old}}\partial_{\underline{b}}W^{\underline{b}}_{\text{old}} + V^{\underline{cb}}_{\text{old}}\partial_{\underline{b}}W^{\underline{a}}_{\text{old}}\right)\Delta t. \tag{5.1.3b}$$

Despite the high numerical error associated with the forward Euler method, it is acceptable for use as a test to assess the validity of the equations, as the dominating

error is not numerical.

5.2 The spacetimes modelled

To validate the model, tests were performed in both Schwarzschild and Kruskal-Szekeres coordinates. The coordinates in Schwarzschild coordinates are denoted with lowercase letters $\xi^{\mu}_{(\mathrm{Sw})} = (t, r, \theta, \phi, u_r, u_\theta, u_\phi)$, with metric

$$\begin{gathered} g^{(\mathrm{Sw})}_{00} = -\left(1 - \frac{r_s}{r}\right), \quad g^{(\mathrm{Sw})}_{11} = \frac{1}{1 - \frac{r_s}{r}}, \\ g^{(\mathrm{Sw})}_{22} = r^2, \quad g^{(\mathrm{Sw})}_{33} = r^2 \sin^2(\theta), \end{gathered} \tag{5.2.1}$$

where $g^{(\mathrm{Sw})}_{\mu\nu}$ is the metric in Schwarzschild coordinates.

Coordinates in Kruskal-Szekeres will be denoted with a capital letter, such that the coordinates in Kruskal-Szekeres are $\xi^{\mu}_{(\mathrm{KS})} = (T, R, \Theta, \Phi, U_R, U_\Theta, U_\Phi)$. The transformation from Schwarzschild coordinates to Kruskal-Szekeres coordinates (shown in figure 1.4a) is given by

$$R = \sqrt{\frac{r}{r_s} - 1}\, \exp\left(\frac{r}{2r_s}\right) \cosh\left(\frac{t}{2r_s}\right), \tag{5.2.2}$$

$$T = \sqrt{\frac{r}{r_s} - 1}\, \exp\left(\frac{r}{2r_s}\right) \sinh\left(\frac{t}{2r_s}\right), \tag{5.2.3}$$

$$U^{\underline{\mu}} = u^{\nu} \frac{\partial \xi^{\underline{\mu}}_{(\mathrm{KS})}}{\partial \xi^{\nu}_{(\mathrm{Sw})}} \tag{5.2.4}$$

where the subscript (KS) indicates the coordinates in Kruskal-Szekeres. The metric in Kruskal-Szekeres coordinates is given by

$$\begin{gathered} g^{(\mathrm{KS})}_{00} = -\frac{4r_s^3}{r} \exp\left(\frac{-r}{r_s}\right), \quad g^{(\mathrm{KS})}_{11} = \frac{4r_s^3}{r} \exp\left(\frac{-r}{r_s}\right), \\ g^{(\mathrm{KS})}_{22} = r^2, \quad g^{(\mathrm{KS})}_{33} = r^2 \sin^2(\theta), \end{gathered} \tag{5.2.5}$$

where r, the radial coordinate in Schwarzschild coordinates, can be found by the inverse transformation

$$r = r_s \left(1 + W_0\left(\frac{R^2 - T^2}{e}\right)\right) \tag{5.2.6}$$

where W_0 is the principal branch of the Lambert W function.

The numerical testing performed in this article uses moments on a scale that may be considered small on astrophysical scales. This is because for numerical simulations in Kruskal-Szekeres coordinates, it is impossible to run the model with large moments, or for large amounts of time. As R is updated, the particle will eventually cross the event horizon (the point $T^2 - R^2 = 1$) due to numerical errors from updating the position of the particle. This will happen with any numerical differential equation solver that overestimates the true value. This is another reason it is important to transform coordinates, so a full PIC simulation can be performed in Schwarzschild coordinates, then transformed to Kruskal-Szekeres coordinates at the end, avoiding these numerical issues. Although the variation in the metric over the domain represented by the macroparticle and its moments may be small, this does not mean the derivatives of the metric, which the moments couple to, are small.

5.3 Computational results

To test the model, the motion of 200 particles that began normally distributed at $r = 30000$ in Schwarzschild coordinates with Schwarzschild radius $r_s = 3000$, and a time step size of $\Delta t = 0.01$ were modelled. These particles were also transformed into Kruskal-Szekeres coordinates. In both spacetimes, the particles were tracked using equation (5.1.2) and the moments taken at $t = 10$. Moments were also taken at $t = 0$ and tracked using equation (5.1.3). When taking the moments, recall that $\mathfrak{f}$ is a density, so the effect of curved spacetime adding a measure to the integrals is included in the definition of $\mathfrak{f}$. Running the simulation until $t = 10$ corresponds to 0.001% of an orbit around the black hole. Whilst this is small, it is required because of the very small numerical time step required for stability in Kruskal-Szekeres coordinates, and because of the relatively large number of particles being tracked on a single core.

By modelling particles at a radius of $10\,r_s$, the accretion disc of the black hole can be studied. Once the accuracy of the moment tracking model at this distance from the black hole has been established, the accuracy of our model in the extreme environments close to the Schwarzschild radius can be examined.

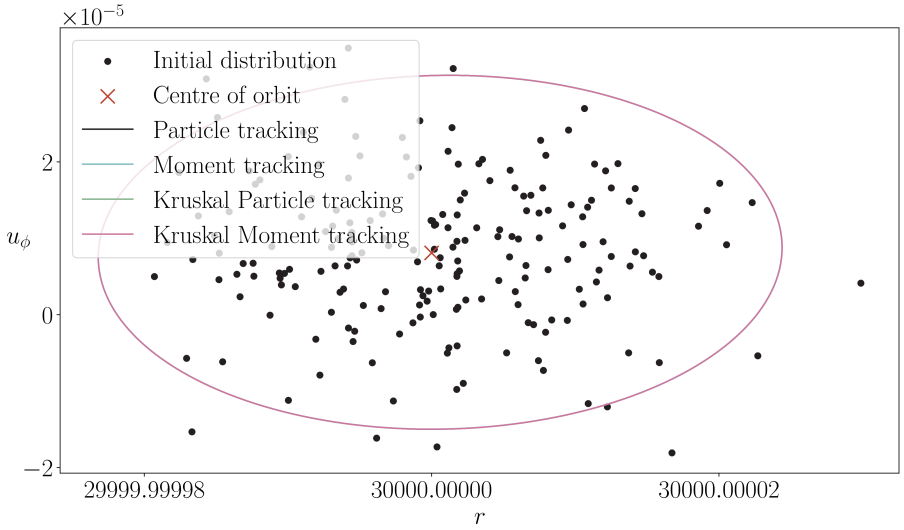

(a) $t = 0$, *all ellipses overlap.*

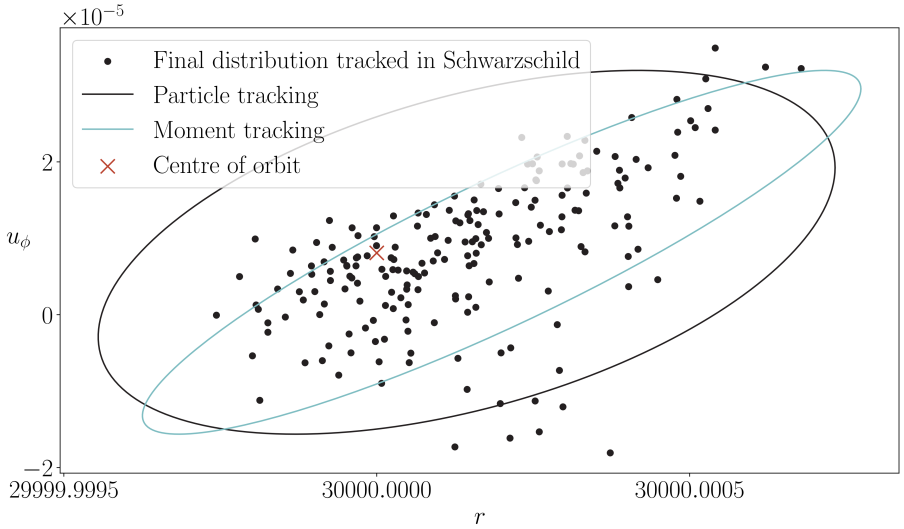

(b) $t = 10$ *showing particles and moments tracked in Schwarzschild coordinates.*

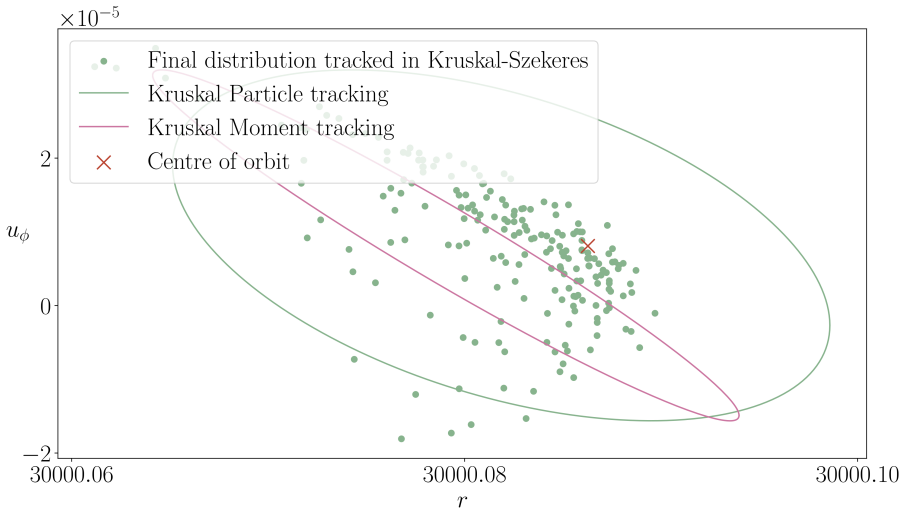

(c) $t = 10$ *showing the same particles transformed to Kruskal-Szekeres coordinates, then the moments and particles tracked, then transformed back to Schwarzschild coordinates.*

Figure 5.1: *The (r, u_ϕ) phase space portraits in Schwarzschild coordinates for the individual particles, the centre of orbit with the path η, and the ellipses used to visualise the actual moments and tracked moments of these particles. Also shown are the ellipses generated from tracking the same particles and their moments in Kruskal-Szekeres coordinates, then the moments coordinate transformed back into Schwarzschild coordinates. These ellipses show the range that 95% of particles will be within, if the particles are normally distributed. The reason that 95% of particles are not within the ellipses in 5.1c and 5.1b is because the data is no longer normally distributed. Note that if just a standard macroparticle was tracked, only the centre of orbit would be known. [Associated dataset available at http://dx.doi.org/10.5281/zenodo.8082181] (Ref. [98]).*

The results of the tracking are shown in figure 5.1, with the moments used to calculate confidence ellipses in Schwarzschild spacetime. Figure 5.1 shows two things: firstly, whilst there is some deviation between the moment tracking and particle tracking ellipses, neither accurately reflect the underlying distribution of particles. This is because the data develops a large skew, as the faster particles orbits get thrown radially outwards. This means the particle distribution is no longer normally distributed, and as such, cannot be modelled accurately with just the first and second order moments. To improve this, higher order moments will also need to be tracked. All models correctly predict the spread in the radial coordinate, such that if the r and u_ϕ axes were equally scaled, all models would correctly predict a long, horizontally thin ellipse. The second feature is that whilst the data is initially uncoupled, the velocity and position very quickly develop a covariance (a V^{16} moment), coupling the u_ϕ and r motion together. This is an expected result, as particles with a larger magnitude of u_ϕ than the one required for a circular orbit are spiralling away from the event horizon.

There is a noticeable displacement in the radial coordinate in the Kruskal-Szekeres coordinates tracking (figure 5.1b) from 30000 to 30000.08. This is because in Kruskal-Szekeres coordinates, small errors from the numerical integration will compound, and result in the ideal orbit drifting from its expected position. This compounding of errors is because Kruskal-Szekeres coordinates involve exponential functions, so small deviations can result in substantial offsets, which cannot be reduced by decreasing step size. This effect is small, and can be avoided by prescribing η beforehand, if it is known. If η is cannot be prescribed before the simulation is run this is still only a minor issue, as the offset from these numerical factors is likely to be small compared to the other effects within a plasma.

To quantify the error in the model, there are six different errors that are analysed: $\epsilon_{\mathbf{sp-sm}}, \epsilon_{\mathbf{sp-kp}}, \epsilon_{\mathbf{sp-km}}, \epsilon_{\mathbf{kp-km}}, \epsilon_{\mathbf{kp-sp}}$, and $\epsilon_{\mathbf{kp-sm}}$. These errors are defined in table 5.1. The subscript **sp** represents that particles were tracked, then the moments taken at the end of the simulation, all in Schwarzschild coordinates. A subscript **km** represents moments being tracked in Kruskal-Szekeres coordinates. These subscripts are defined pictorially in figure 5.2. A hatted V in table 5.1 represents a coordinate transformation. As an example, $\epsilon_{\mathbf{sp-sm}}$ represents the difference between tracking the group of particles and taking their moments at the end (the black ellipse in figure 5.1b), compared to tracking the moments using equations (3.2.26) and (3.2.27) (the blue ellipse in figure 5.1b), all in Schwarzschild coordinates. These errors assess either the error in the moment tracking model, the error in the coordinate transformations, or the combined error of both. These six errors allow both the errors in moment tracking and coordinate transformations to be quantified and measured over time.

The error $\epsilon_{\mathbf{km-sm}}$ could also be calculated, to show the error in the coordinate transformations between two different sets of tracked moments. The origin of this error would not be discernible, as it would be impossible to distinguish between errors caused by moment tracking in either coordinate system, or the error from the coordinate transformation.

To examine the error, another simulation was performed, again around a black hole with Schwarzschild radius $r_s = 3000$, and an ideal circular orbit at $r = 30000$ in Schwarzschild coordinates. For these simulations the number of particles was decreased to 20, and the time step used was increased to $\Delta t = 0.1$, with 10^6 total iterations. This adjustment was made to allow the simulation to run for more iterations, to obtain information about the long term behaviour of the model. Note the time step size is in the respective frame, so $t = 10000$ in Schwarzschild coordinates corresponds to $T = 1200$ in Kruskal-Szekeres coordinates. This amount

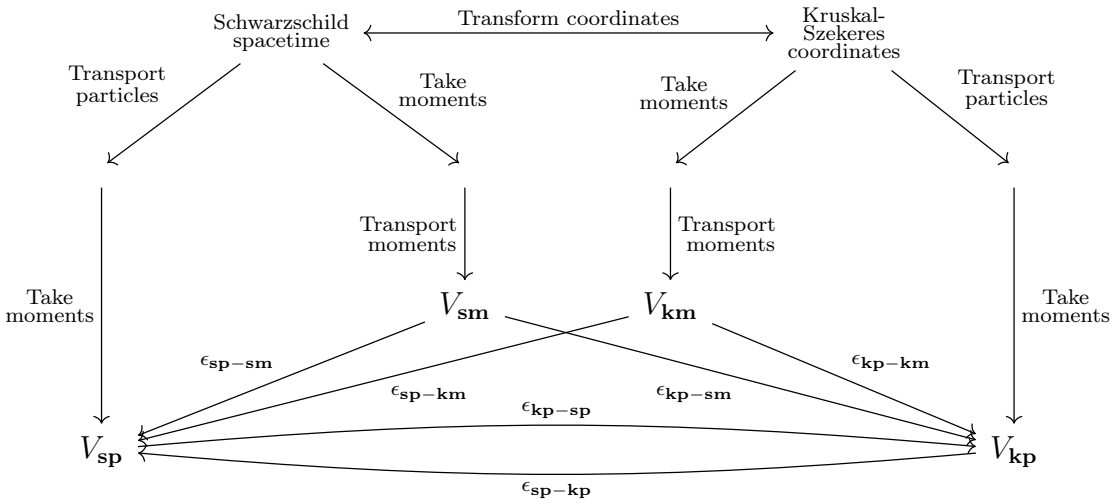

Figure 5.2: *The model used to test the moment tracking and coordinate transformation theories. The error in the moment tracking model is the difference between transporting the moments and transporting the particles then taking moments. The error in coordinate transforming is the difference between transporting particles then taking moments in each frame. The combined error is the difference between transporting the moments in one frame, compared to tracking particle in the other. The errors are defined algebraically in table 5.1.*

of time corresponds to 1.1% of a complete orbit. Whilst this is again small, it is required due to the numerical instability of Kruskal-Szekeres coordinates. Figure 5.3 shows the three different total errors as functions of time, where the particles are normally distributed around the ideal orbit with variance 10^{-20} in all dimensions.

In all cases the error rapidly grows, before stabilising. This is because, as shown in figure 5.1b, there is a large radial dipole moment after only a small amount of time. Because the V^1 moment is large, a small error then dominates compared to all other errors. Despite this, the total error is still relatively small.

The error from the coordinate transformations is more substantial than the error from the moment tracking. It is postulated that this increased error is because the

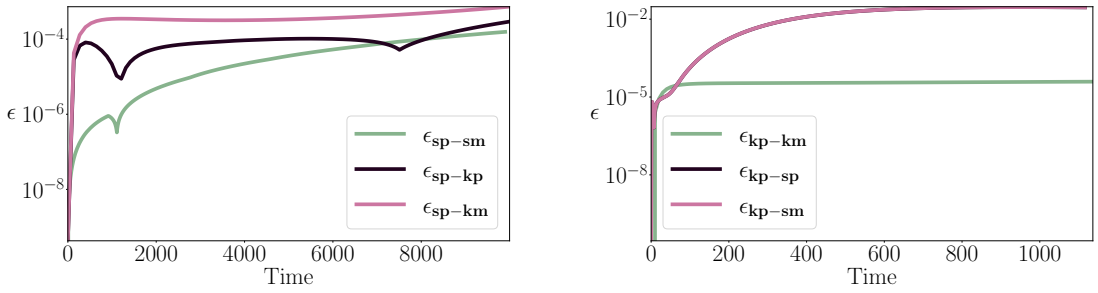

(a) *Schwarzschild coordinates.*

(b) *Kruskal-Szekeres coordinates. Note both blue and pink lines overlap.*

Figure 5.3: *The total error as a function of time for the different types of errors the theory can generate. [Associated dataset available at http://dx.doi.org/10.5281/zenodo.8082181] (Ref. [98]).*

higher order moments affect the coordinate transformations twice: once during the coordinate transformation (during equation (4.4.7)), and once during the projection (during equation (4.4.20)). This suggests that for a moment tracking code that also incorporates a coordinate transformation, a higher order of moments will be needed. The bumps and discontinuities in the results are due to particles passing the macroparticle centre. If a particle is travelling faster than the macroparticle centre, the particle tracking moments (e.g. $V_{\mathbf{sp}}$) will decrease, then increase once the particle passes the macroparticle centre. The moment tracking code will not see this behaviour, and will track the moments as always either decreasing or increasing, rather than the true mixture of both. These discontinuities are an intrinsic part of modelling moments. They can be avoided by sorting the particles before the modelling starts, so higher speed particles are ahead of the macroparticle centre, but this is no longer realistic.

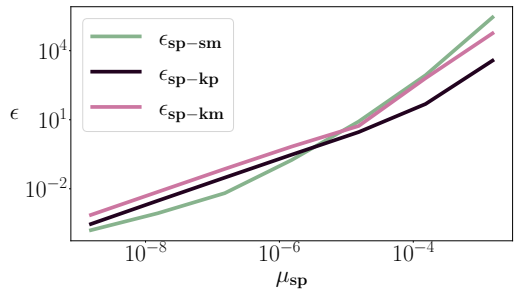

(a) *Schwarzschild coordinates.*

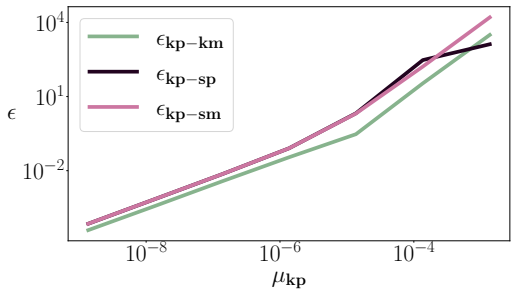

(b) *Kruskal-Szekeres coordinates. Note blue and pink lines overlap for* $\mu_{\boldsymbol{kp}} < 10^{-5}$.

Figure 5.4: *The total error as a function of* μ*, the initial total moment, for the different kinds of errors the model can create. The gradient of the lines is approximately linear in low* μ*, and approximately 1.7 for larger* μ*. [Associated dataset available at http://dx.doi.org/10.5281/zenodo.8082181] (Ref. [98]).*

To study the magnitude of the error, rather than just the shape, three main sources of error can be identified: floating point errors, numerical errors (the error arising from finite step size in numerical integration), and truncation errors (the error arising from truncating the multipole expansion at second order). These errors will dominate in different ways depending on the size of the total initial moments μ, where

$$\mu = \sum_{\underline{a}} \left| V^{\underline{a}}|_{t=0} \right|^2 + \sum_{\underline{ab}} \left| V^{\underline{ab}}|_{t=0} \right| . \tag{5.3.1}$$

Floating point errors can arise from a sufficiently small time step and small number of iterations in any numerical differential equation solver, but in the case of this work they also dominate if the moments are very small i.e. $\mu \approx 10^{-15}$. Numerical errors arise from the choice of integrator used, and in the case of forward Euler, are linear in Δt. The truncation errors arise from only running the moment tracking code up to quadrupole order. There is an infinite expansion of moments, which is truncated to quadrupole order in this thesis. Including more moments will decrease the total error. At the quadrupole level, the truncation error is quadratic. This

means total error $\epsilon(\mu) \approx \mu^2$. This is verified in figure 5.4. The error is linear in the low μ regime, where numerical errors dominate, and as μ increases, the total error increases at about $\epsilon(\mu) \approx \mu^{1.7}$. This is a combination of the predicted quadratic increase, and the numerical error. This quadratic behaviour suggests that if the moments are half the size, the total error will be quartered.

Error and description of the error
$\epsilon_{\mathbf{sp-sm}} = \sqrt{\sum_{\underline{a}} \left\|V^{\underline{a}}_{\mathbf{sp}} - V^{\underline{a}}_{\mathbf{sm}}\right\|^2 + \sum_{\underline{ab}} \left\|V^{\underline{ab}}_{\mathbf{sp}} - V^{\underline{ab}}_{\mathbf{sm}}\right\|}$ The error between tracking particles then taking moments, compared to tracking moments, both in Schwarzschild coordinates.
$\epsilon_{\mathbf{sp-kp}} = \sqrt{\sum_{\underline{a}} \left\|V^{\underline{a}}_{\mathbf{sp}} - \hat{V}^{\underline{a}}_{\mathbf{kp}}\right\|^2 + \sum_{\underline{ab}} \left\|V^{\underline{ab}}_{\mathbf{sp}} - \hat{V}^{\underline{ab}}_{\mathbf{kp}}\right\|}$ The error between tracking particles and taking moments in Kruskal-Szekeres coordinates then transforming these into moments in Schwarzschild coordinates, compared to tracking particles and taking moments in Schwarzschild coordinates.
$\epsilon_{\mathbf{sp-km}} = \sqrt{\sum_{\underline{a}} \left\|V^{\underline{a}}_{\mathbf{sp}} - \hat{V}^{\underline{a}}_{\mathbf{km}}\right\|^2 + \sum_{\underline{ab}} \left\|V^{\underline{ab}}_{\mathbf{sp}} - \hat{V}^{\underline{ab}}_{\mathbf{km}}\right\|}$ The error between tracking moments in Kruskal-Szekeres coordinates then transforming these into moments in Schwarzschild coordinates, compared to tracking moments in Schwarzschild coordinates.
$\epsilon_{\mathbf{kp-km}} = \sqrt{\sum_{\underline{a}} \left\|V^{\underline{a}}_{\mathbf{kp}} - V^{\underline{a}}_{\mathbf{km}}\right\|^2 + \sum_{\underline{ab}} \left\|V^{\underline{ab}}_{\mathbf{kp}} - V^{\underline{ab}}_{\mathbf{km}}\right\|}$ The error between tracking particles then taking moments, compared to tracking moments, both in Kruskal-Szekeres coordinates.
$\epsilon_{\mathbf{kp-sp}} = \sqrt{\sum_{\underline{a}} \left\|V^{\underline{a}}_{\mathbf{kp}} - \hat{V}^{\underline{a}}_{\mathbf{sp}}\right\|^2 + \sum_{\underline{ab}} \left\|V^{\underline{ab}}_{\mathbf{kp}} - \hat{V}^{\underline{ab}}_{\mathbf{sp}}\right\|}$ The error between tracking particles and taking moments in Schwarzschild coordinates then transforming these into moments in Kruskal-Szekeres coordinates, compared to tracking particles and taking moments in Kruskal-Szekeres coordinates.
$\epsilon_{\mathbf{kp-sm}} = \sqrt{\sum_{\underline{a}} \left\|V^{\underline{a}}_{\mathbf{kp}} - \hat{V}^{\underline{a}}_{\mathbf{sm}}\right\|^2 + \sum_{\underline{ab}} \left\|V^{\underline{ab}}_{\mathbf{kp}} - \hat{V}^{\underline{ab}}_{\mathbf{sm}}\right\|}$ The error between tracking moments in Schwarzschild coordinates then transforming these into moments in Kruskal-Szekeres coordinates, compared to tracking moments in Kruskal-Szekeres coordinates.

Table 5.1: *The types of error the numerical testing generates. These errors show the accuracy of both the moment tracking model and the coordinate transformations by comparing the results to a particle tracking model. Figure 5.2 shows these errors diagrammatically.*

Chapter 6

Constructing a charge and current from a set of moments

6.1 Introduction

The differential equations for the moments are only one step of a PIC code using moment tracking. The next step is to use a set of moments to find the charge and current distributions of a macroparticle (figure 1.3). In this chapter, two different methods will be presented to do this. The first method approximates the original distribution function used to find the moments, then integrates this to find the charge and current. The second method integrates the Ellis representation of the 7-current over velocity space, to find the Ellis representation of the 4-current. Finding the 4-current needed to create this distributional 4-current gives another method to find the charge and current from the distributional 7-current. The chapter is concluded by numerically testing both methods to assess their accuracy, then discussing the advantages and disadvantages of each method.

6.2 Multi-index notation

The reconstruction method presented here can be generalised to arbitrary dimensions, and using arbitrarily large order of multipoles. This requires a notation that collects a set of quantities into a single column vector. These column vectors will be defined by a symbol, representing a dimension and a maximum order.

Capitalised boldface Latin characters $\mathbf{I}, \mathbf{K}$ denote a column vector of dimension 6 and maximum order 2, such that $\boldsymbol{\xi}^{\mathbf{I}}$ is a column vector of length 28, given by

$$\begin{aligned}\boldsymbol{\xi}^{\mathbf{I}} = \big(&1, \xi^1, \xi^2, \xi^3, \xi^4, \xi^5, \xi^6, \xi^1\xi^1, \xi^1\xi^2, \xi^1\xi^3, \xi^1\xi^4, \xi^1\xi^5, \xi^1\xi^6, \xi^2\xi^2, \xi^2\xi^3, \xi^2\xi^4, \\ &\xi^2\xi^5, \xi^2\xi^6, \xi^3\xi^3, \xi^3\xi^4, \xi^3\xi^5, \xi^3\xi^6, \xi^4\xi^4, \xi^4\xi^5, \xi^4\xi^6, \xi^5\xi^5, \xi^5\xi^6, \xi^6\xi^6\big)^T . \end{aligned} \tag{6.2.1}$$

Capitalised boldface Greek characters $\boldsymbol{\Sigma}, \boldsymbol{\Lambda}$ denote denote a column vector of dimension 3 and maximum order 2, such that $\boldsymbol{\xi}^{\boldsymbol{\Sigma}}$ is a column vector of length 10, given by

$$\boldsymbol{\xi}^{\boldsymbol{\Sigma}} = \big(1, \xi^1, \xi^2, \xi^3, \xi^1\xi^1, \xi^1\xi^2, \xi^1\xi^3, \xi^2\xi^2, \xi^2\xi^3, \xi^3\xi^3\big)^T . \tag{6.2.2}$$

If the index is a superscript it represents a set of powers, as above. If the index is a subscript this column vector is just a set of scalar fields, for example

$$\boldsymbol{\varphi}_{\mathbf{I}} = (\varphi_\varnothing, \varphi_1, \varphi_2, \ldots, \varphi_6, \varphi_{11}, \varphi_{12}, \varphi_{13}, \ldots, \varphi_{66})^T \tag{6.2.3}$$

Since the location of an index indicates whether it is a set of numbers or a list of powers, summations over these indices are written explicitly. An example summation over $\mathbf{I}$ is

$$\sum_{\mathbf{I}} \boldsymbol{\xi}^{\mathbf{I}} \varphi_{\mathbf{I}} = \varphi_\varnothing + \varphi_{\underline{a}} \xi^{\underline{a}} + \varphi_{\underline{ab}} \xi^{\underline{a}} \xi^{\underline{b}}. \tag{6.2.4}$$

By using this notation, multipoles can be collected into a single index, which is useful for the reconstruction algorithms presented in this chapter.

6.3 The reconstruction algorithm

In this section, a method for reconstructing a distribution function from a set of moments is proposed. This method was outlined in one dimension by Wright [99]. Consider a distribution function density $\mathfrak{f}$. This section shows how a distribution function density $\hat{\mathfrak{f}}$ that has the same moments as the initial $\mathfrak{f}$ can be constructed. The reconstructed distribution function density is defined as

$$\hat{\mathfrak{f}}\left(\underline{\underline{\xi}}\right) = \sum_{\mathbf{K}} c_{\mathbf{K}} \varphi_{\mathbf{K}}\left(\underline{\underline{\xi}}\right) \tag{6.3.1}$$

where $\varphi_{\mathbf{K}}$ are model densities, and $c_{\mathbf{K}}$ are weighting coefficients. These model densities are a set of scalar field densities that is used to approximate the original distribution function $\mathfrak{f}$. Picking a model density is a choice, and will depend on the situation. The simplest choice of model density is to use a top-hat function in every dimension,

$$\varphi_{\mathbf{K}}\left(\underline{\underline{\xi}}\right) = \xi^{\mathbf{K}} \varphi_0 \tag{6.3.2}$$

$$\varphi_0 = \begin{cases} 1 & \text{if} \quad \underline{\underline{\xi_-}} < \underline{\underline{\xi}} < \underline{\underline{\xi_+}} \\ 0 & \text{otherwise} \end{cases} \tag{6.3.3}$$

where $\underline{\underline{\xi_-}}$ and $\underline{\underline{\xi_+}}$ give the width of the top-hat function. Appropriate values for $\underline{\underline{\xi_-}}$ and $\underline{\underline{\xi_+}}$ will depend on the original $\mathfrak{f}$ being reconstructed. A top-hat function is not the only choice. If the original distribution function is known to be a Gaussian, it may make more sense to choose φ_0 to be a Gaussian. The quadrupole moments can be used to define the covariances needed for a multi-dimensional Gaussian. In this thesis only top-hat model densities will be used.

Since $\hat{\mathfrak{f}}$ is defined to have the same moments as $\mathfrak{f}$,

$$\int_\Sigma (\xi - \eta)^{\mathbf{I}} \, \mathfrak{f} \, d^6\xi = \int_\Sigma (\xi - \eta)^{\mathbf{I}} \, \hat{\mathfrak{f}} \, d^6\xi = \sum_{\mathbf{K}} \int_\Sigma (\xi - \eta)^{\mathbf{I}} \, c_{\mathbf{K}} \, \varphi_{\mathbf{K}} \, d^6\xi \tag{6.3.4}$$

denoting the column-vector of moments on the left hand side as $a_{\mathbf{I}}$, and pulling the

$c_{\mathbf{K}}$ coefficients out of the integral,

$$a_{\mathbf{I}} = \sum_{\mathbf{K}} c_{\mathbf{K}} \int_{\Sigma} (\xi - \eta)^{\mathbf{I}} \varphi_{\mathbf{K}} d^6\xi \tag{6.3.5}$$

$$= \sum_{\mathbf{K}} c_{\mathbf{K}} B_{\mathbf{KI}} \tag{6.3.6}$$

where

$$B_{\mathbf{KI}} = \int_{\Sigma} (\xi - \eta)^{\mathbf{I}} \varphi_{\mathbf{K}} d^6\xi \tag{6.3.7}$$

so there is a linear system of equations which can be solved to find $c_{\mathbf{K}}$. This gives the reconstructed $\hat{\mathfrak{f}}$, which can then be used to find various physical quantities of the plasma.

Physical quantities associated with the plasma (plasma moments) can be found by integrating the reconstructed distribution function density over the velocity space, the charge $\mathfrak{p}$ and current $\mathfrak{T}^{\underline{\mu}}$ are given by

$$\mathfrak{p} = q \int_{\mathcal{E}_p} \mathfrak{f}\, d^3u \tag{6.3.8}$$

$$\mathfrak{T}^{\underline{\mu}} = q \int_{\mathcal{E}_p} \frac{u^{\underline{\mu}}}{\gamma} \mathfrak{f}\, d^3u \tag{6.3.9}$$

where the charge and currents are scalar field densities, rather than just scalar fields, and $\mathcal{E}_p$ denotes the integration bounds of velocity space (formally this is the fibre associated with point p). Higher order plasma moments can also be found from this. The pressure tensor of a plasma, $\mathfrak{t}^{\underline{\mu\nu}}$, is given by

$$\mathfrak{t}^{\underline{\mu\nu}} = q \int_{\mathcal{E}_p} \frac{u^{\underline{\mu}}}{\gamma} \frac{u^{\underline{\nu}}}{\gamma} \mathfrak{f} d^3u. \tag{6.3.10}$$

It does not make sense to construct a plasma moment of an order higher than the moments used to reconstruct $\hat{\mathfrak{f}}$. This is because there is no control over the high order moments when finding $\hat{\mathfrak{f}}$, so there is no guarantee they will be similar to the original moments of $\mathfrak{f}$. The approximation to a plasma moment of the same order as the highest moment tracked may not be accurate, as it is likely the truncation will affect the accuracy of this reconstruction. The accuracy of this reconstruction algorithm for higher order moments has not been studied, and is future work.

6.3.1 A 1D example

To explain the multi-index notation used in this section, it is worth doing a simple one-dimensional example of the reconstruction algorithm, as this will allow an understanding of the notation, and some properties of the reconstruction algorithm to be seen.

Consider $\mathfrak{f}(x)$, where $\mathfrak{f}$ is now a function of $x \in \mathbb{R}$ only. Taking moments around some point x_0 gives the moments

$$\mathbf{a} = \begin{pmatrix} q \\ V^1 \\ V^{11} \end{pmatrix} = \begin{pmatrix} \int_{\mathbb{R}} \mathfrak{f}\, dx \\ \int_{\mathbb{R}} (x - x_0)\, \mathfrak{f}\, dx \\ \int_{\mathbb{R}} (x - x_0)^2\, \mathfrak{f}\, dx \end{pmatrix}. \tag{6.3.11}$$

The model function reconstructing this, $\hat{\mathfrak{f}}$, is given by

$$\hat{\mathfrak{f}}(x) = \begin{pmatrix} \varphi_0(x) & x\,\varphi_0(x) & x^2\,\varphi_0(x) \end{pmatrix} \begin{pmatrix} c_\varnothing \\ c_1 \\ c_{11} \end{pmatrix}. \tag{6.3.12}$$

To take the moments of this, premultiply both sides by $(x - x_0)^{\mathbf{I}}$, recalling that $\hat{\mathfrak{f}}$ has the same moments as $\mathfrak{f}$, and integrate,

$$\mathbf{a} = \int_{\mathbb{R}} \begin{pmatrix} 1 \\ (x - x_0) \\ (x - x_0)^2 \end{pmatrix} \begin{pmatrix} \varphi_0 & x\,\varphi_0 & x^2\,\varphi_0 \end{pmatrix} \begin{pmatrix} c_\varnothing \\ c_1 \\ c_{11} \end{pmatrix} dx. \tag{6.3.13}$$

Multiplying the first terms together to give a matrix, and pulling the integral into the matrix as $\mathbf{c}$ are constants,

$$\mathbf{a} = \begin{pmatrix} \int_{\mathbb{R}} \varphi_0 dx & \int_{\mathbb{R}} x\,\varphi_0 dx & \int_{\mathbb{R}} x^2\,\varphi_0 dx \\ \int_{\mathbb{R}} (x - x_0)\,\varphi_0 dx & \int_{\mathbb{R}} (x - x_0)\,x\,\varphi_0 dx & \int_{\mathbb{R}} (x - x_0)\,x^2\,\varphi_0 dx \\ \int_{\mathbb{R}} (x - x_0)^2\,\varphi_0 dx & \int_{\mathbb{R}} (x - x_0)^2\,x\,\varphi_0 dx & \int_{\mathbb{R}} (x - x_0)^2\,x^2\,\varphi_0 dx \end{pmatrix} \begin{pmatrix} c_\varnothing \\ c_1 \\ c_{11} \end{pmatrix} \tag{6.3.14}$$

giving the equation

$$\mathbf{a} = B\mathbf{c}. \tag{6.3.15}$$

Solving this linear system of equations gives $\mathbf{c}$, in turn giving $\hat{\mathfrak{f}}$.

As a explicit example, consider the specific example of a parabola,

$$\mathfrak{f} = \begin{cases} ax^2 + bx + c & \text{if} \quad x_- \leq x \leq x_+ \\ 0 & \text{otherwise} \end{cases} \tag{6.3.16}$$

where x_- and x_+ are the two roots of the parabola (it shall be assumed these are not repeating and are real). Taking the moments of $\mathfrak{f}$ about $x_0 = 0$ (for simplicity) gives

$$\mathbf{a} = \begin{pmatrix} q \\ V^1 \\ V^{11} \end{pmatrix} = \begin{pmatrix} \int_{\mathbb{R}} (ax^2 + bx + c)dx \\ \int_{\mathbb{R}} (ax^3 + bx^2 + cx)dx \\ \int_{\mathbb{R}} (ax^4 + bx^3 + cx^2)dx \end{pmatrix}. \tag{6.3.17}$$

Rearranging this into a matrix equation,

$$\mathbf{a} = \begin{pmatrix} \int_{\mathbb{R}} 1\,dx & \int_{\mathbb{R}} x\,dx & \int_{\mathbb{R}} x^2\,dx \\ \int_{\mathbb{R}} x\,dx & \int_{\mathbb{R}} x^2\,dx & \int_{\mathbb{R}} x^3\,dx \\ \int_{\mathbb{R}} x^2\,dx & \int_{\mathbb{R}} x^3\,dx & \int_{\mathbb{R}} x^4\,dx \end{pmatrix} \begin{pmatrix} c \\ b \\ a \end{pmatrix} \tag{6.3.18}$$

where terms have been rearranged into this order to compare to the reconstruction formula. Assuming the model top-hat function φ_0 has the same width as the support of $\mathfrak{f}$, then comparing this to equation (6.3.14) gives

$$\mathbf{c} = \begin{pmatrix} c_\varnothing \\ c_1 \\ c_{11} \end{pmatrix} = \begin{pmatrix} c \\ b \\ a \end{pmatrix} \tag{6.3.19}$$

so if the width of the model function matches the width of the parabola exactly, then the reconstruction algorithm is exact for a parabola. This provides a useful sanity check for verifying the model numerically in section 6.5.

6.4 Using the Ellis representation of moments to deposit charge and current

The method discussed for finding the 4-current using moments reconstructs the entire distribution function $\mathfrak{f}$, then integrates this over velocity space. An alternative method directly finds the 4-current from the moments in a single step. This is done by creating a distributional 4-current, and finding a current that when squeezed, is related to that distribution. By doing this, the integrals over velocity space can be avoided.

The 7-current can be reduced to a 4-current $\mathfrak{T}^\mu$ by integrating across velocity space,

$$\mathfrak{T}^\mu|_p = \int_{\mathcal{E}_p} \mathfrak{J}^\mu d^3u. \tag{6.4.1}$$

The choice to only take the spatial components of $\mathfrak{J}^a$ is because these correspond to the components of the 4-current. In section 8.5 it is shown through differential geometry that the velocity components of the 7-current vanish when the 7-current is projected from $\mathcal{E}$ onto the base spatial manifold.

The 4-current $\mathfrak{T}^\mu$ is the source term in Maxwell's equations, although care must be taken to check if the electric and magnetic fields are densities of weight 1 or densities of weight 0. In this thesis the electric and magnetic fields are densities of weight 0. This means that the 4-current must be divided by the measure Ω_0 to be used in the continuous Maxwell's equations. Alternatively, it can be integrated across a cell. This gives a discretised current, used in the finite difference Maxwell's equations (this process is discussed in more detail in section 7.3.4).

Similarly, the Ellis representation of the 7-current can be reduced to the Ellis representation of the 4-current, $\mathcal{I}^\mu$, by integrating over velocity space,

$$\mathcal{I}^\mu = \int_{\mathcal{E}_p} \mathcal{J}^\mu d^3u. \tag{6.4.2}$$

This gives

$$\begin{aligned}\mathcal{I}^\mu = \frac{1}{2}\int_{\mathbb{R}} \dot{C}^\mu\, V^{\underline{\nu}\underline{\rho}} \left(\partial_{\underline{\nu}}\partial_{\underline{\rho}}\delta^{(3)}(x-C)\right)\, dt \\ - \int_{\mathbb{R}} \delta^\mu_{\underline{\nu}}\, X^{\underline{\nu}\underline{\rho}} \left(\partial_{\underline{\rho}}\delta^{(3)}(x-C)\right)\, dt - \int_{\mathbb{R}} \dot{C}^\mu\, V^{\underline{\nu}} \left(\partial_{\underline{\nu}}\delta^{(3)}(x-C)\right)\, dt \\ + \int_{\mathbb{R}} \delta^\mu_{\underline{\nu}}\, X^{\underline{\nu}}\, \delta^{(3)}(x-C)\, dt + \int_{\mathbb{R}} \dot{C}^\mu\, q\, \delta^{(3)}(x-C)\, dt.\end{aligned} \tag{6.4.3}$$

where

$$\delta^{(3)}(x-C) = \delta(x^1-C^1)\,\delta(x^2-C^2)\,\delta(x^3-C^3). \tag{6.4.4}$$

Proof. To calculate the integral over velocity space, note two properties of the Dirac delta function, for some function of time only $h(t)$,

$$\int_{\mathbb{R}} h(t)\delta(x)dx = h(t), \quad \int_{\mathbb{R}} h(t)\frac{d}{dx}\delta(x)dx = -\int_{\mathbb{R}} \frac{\partial h(t)}{\partial x}\delta(x)dx = 0. \tag{6.4.5}$$

Using these properties,

$$\begin{aligned}\mathcal{I}^\mu = \frac{1}{2}\int_{\mathbb{R}}\int_{\mathcal{E}_p} \dot{\eta}^\mu\, V^{\underline{b}\underline{c}} \left(\partial_{\underline{b}}\partial_{\underline{c}}\delta^{(6)}(\xi-\eta)\right) d^3u\, dt - \int_{\mathbb{R}}\int_{\mathcal{E}_p} \delta^\mu_{\underline{b}}\, X^{\underline{b}\underline{c}} \left(\partial_{\underline{c}}\delta^{(6)}(\xi-\eta)\right) d^3u\, dt \\ - \int_{\mathbb{R}}\int_{\mathcal{E}_p} \dot{\eta}^\mu\, V^{\underline{b}} \left(\partial_{\underline{b}}\delta^{(6)}(\xi-\eta)\right) d^3u\, dt + \int_{\mathbb{R}}\int_{\mathcal{E}_p} \delta^\mu_{\underline{b}}\, X^{\underline{b}}\, \delta^{(6)}(\xi-\eta) d^3u\, dt \\ + \int_{\mathbb{R}}\int_{\mathcal{E}_p} \dot{\eta}^\mu\, q\, \delta^{(6)}(\xi-\eta) d^3u\, dt.\end{aligned} \tag{6.4.6}$$

Splitting $V^{\underline{b}\underline{c}}$ into $V^{\underline{\mu}\underline{\nu}}$, $2V^{\underline{\nu}(\underline{\rho}+3)}$ (the factor of two is due to symmetry), and

$V^{(\underline{\nu}+3)(\underline{\rho}+3)}$; and splitting $X^{\underline{b}\underline{c}}$ into $X^{\underline{b}\underline{\rho}}$ and $X^{\underline{b}(\underline{\rho}+3)}$ gives

$$\begin{aligned}\mathcal{I}^{\mu} = \frac{1}{2}\int_{\mathbb{R}}\int_{\mathcal{E}_p} \dot{\eta}^{\mu}\, V^{\underline{\nu}\underline{\rho}} \left(\partial_{\underline{\nu}}\partial_{\underline{\rho}}\delta^{(6)}(\xi-\eta)\right) d^3u\, dt \\ + \int_{\mathbb{R}}\int_{\mathcal{E}_p} \dot{\eta}^{\mu}\, V^{\underline{\nu}(\underline{\rho}+3)} \left(\partial_{\underline{b}}\partial_{\underline{\rho}+3}\delta^{(6)}(\xi-\eta)\right) d^3u\, dt \\ + \frac{1}{2}\int_{\mathbb{R}}\int_{\mathcal{E}_p} \dot{\eta}^{\mu}\, V^{(\underline{\nu}+3)(\underline{\rho}+3)} \left(\partial_{\underline{\nu}+3}\partial_{\underline{\rho}+3}\delta^{(6)}(\xi-\eta)\right) d^3v\, dt \\ - \int_{\mathbb{R}}\int_{\mathcal{E}_p} \delta^{\mu}_{\underline{b}}\, X^{\underline{b}\underline{\rho}} \left(\partial_{\underline{\rho}}\delta^{(6)}(\xi-\eta)\right) d^3u\, dt - \int_{\mathbb{R}}\int_{\mathcal{E}_p} \delta^{\mu}_{\underline{b}}\, X^{\underline{b}(\underline{\rho}+3)} \left(\partial_{\underline{\rho}+3}\delta^{(6)}(\xi-\eta)\right) d^3u\, dt \\ - \int_{\mathbb{R}}\int_{\mathcal{E}_p} \dot{\eta}^{\mu}\, V^{\underline{\nu}} \left(\partial_{\underline{\nu}}\delta^{(6)}(\xi-\eta)\right) d^3u\, dt - \int_{\mathbb{R}}\int_{\mathcal{E}_p} \dot{\eta}^{\mu}\, V^{\underline{\nu}+3} \left(\partial_{\underline{b}+3}\delta^{(6)}(\xi-\eta)\right) d^3u\, dt \\ + \int_{\mathbb{R}}\int_{\mathcal{E}_p} \delta^{\mu}_{\underline{b}}\, X^{\underline{b}}\, \delta^{(6)}(\xi-\eta) d^3u\, dt + \int_{\mathbb{R}}\int_{\mathcal{E}_p} \dot{\eta}^{\mu}\, q\, \delta^{(6)}(\xi-\eta) d^3u\, dt. \quad (6.4.7)\end{aligned}$$

Performing all the integrals, using the Dirac delta function identities given in equation (6.4.5), gives

$$\begin{aligned}\mathcal{I}^{\mu} = \frac{1}{2}\int_{\mathbb{R}} \dot{\eta}^{\mu}\, V^{\underline{\nu}\underline{\rho}} \left(\partial_{\underline{\nu}}\partial_{\underline{\rho}}\delta^{(3)}(x-C)\right) dt \\ - \int_{\mathbb{R}} \delta^{\mu}_{\underline{b}}\, X^{\underline{b}\underline{\rho}} \left(\partial_{\underline{\rho}}\delta^{(3)}(x-C)\right) dt - \int_{\mathbb{R}} \dot{\eta}^{\mu}\, V^{\underline{\nu}} \left(\partial_{\underline{\nu}}\delta^{(3)}(x-C)\right) dt \\ + \int_{\mathbb{R}} \delta^{\mu}_{\underline{b}}\, X^{\underline{b}}\, \delta^{(3)}(x-C)\, dt + \int_{\mathbb{R}} \dot{\eta}^{\mu}\, q\, \delta^{(3)}(x-C)\, dt \quad (6.4.8)\end{aligned}$$

since

$$\delta(\xi^1-\eta^1)\,\delta(\xi^2-\eta^2)\,\delta(\xi^3-\eta^3) = \delta(x^1-C^1)\,\delta(x^2-C^2)\,\delta(x^3-C^3) = \delta^{(3)}(x-C). \quad (6.4.9)$$

Note that whilst terms of the form $X^{\underline{\mu}+3}$ are still present, it is impossible to extract these components since the Kronecker delta upper index only ranges from $0-3$. Additionally, since $\dot{\eta}^{\mu} = \dot{C}^{\mu}$, this can also be rewritten. Combining these gives equation (6.4.3). □

This acts on test functions $\phi_{\mu}(t, \underline{x})$, to give

$$\begin{aligned}\int_M \mathcal{I}^{\mu}\phi_{\mu} d^4x = \frac{1}{2}\int_{\mathbb{R}} \dot{C}^{\mu}\, V^{\underline{\nu}\underline{\rho}}\partial_{\underline{\nu}}\partial_{\underline{\rho}}\phi_{\mu}|_C\, dt - \int_{\mathbb{R}} X^{\underline{\nu}\underline{\rho}}\partial_{\underline{\rho}}\phi_{\underline{\nu}}|_C\, dt \\ - \int_{\mathbb{R}} \dot{C}^{\mu}\, V^{\underline{\nu}}\partial_{\underline{\nu}}\phi_{\mu}|_C\, dt + \int_{\mathbb{R}} X^{\underline{\mu}}\,\phi_{\underline{\mu}}|_C\, dt + \int_{\mathbb{R}} \dot{C}^{\mu}\, q\,\phi_{\mu}|_C\, dt. \quad (6.4.10)\end{aligned}$$

This distributional 4-current is the distributional version of the 4-current $\mathfrak{T}^\mu$ used in Maxwell's equations. This means that if there is a 4-current such that, when squeezed, gives the same moments as $\mathcal{I}$, this 4-current is the 4-current associated with the macroparticle. This avoids having to create model functions in velocity space.

Using the language of differential forms, the 4-current 3-form is given by $\mathfrak{T}(t, \underline{x})$, where $\underline{x}$ are the spatial coordinates. Through a process analogous to the squeezing in section 4.2, there exists a one parameter family of smooth 3-forms adapted to the time slicing,

$$\mathfrak{T}_\epsilon = \frac{1}{\varepsilon^3}\mathfrak{T}^\mu\left(t, \frac{\underline{x} - C}{\varepsilon}\right) i_\mu dt \wedge dx^{1\ldots3}. \tag{6.4.11}$$

This can be wedged this against a test form ϕ,

$$\phi \wedge \mathfrak{T}_\varepsilon = \frac{1}{\varepsilon^3}\mathfrak{T}^\mu\left(t, \frac{\underline{x} - C}{\varepsilon}\right) \phi_\mu(t, \underline{x}) dt \wedge dx^{1\ldots3}. \tag{6.4.12}$$

Similarly to the squeezed distribution function $\mathfrak{f}$ in section 4.2,

$$\phi \wedge \mathfrak{T}_\varepsilon = \bar{\mathcal{I}}^\mu \phi_\mu + \mathcal{O}(\varepsilon^3) \tag{6.4.13}$$

where

$$\begin{aligned}\bar{\mathcal{I}}^\mu = \frac{1}{2}\int_{\mathbb{R}} \dot{C}^\mu \bar{V}^{\underline{\nu}\underline{\rho}} \left(\partial_{\underline{\nu}}\partial_{\underline{\rho}}\delta^{(3)}(\xi - \eta)\right) dt \\ - \int_{\mathbb{R}} \delta^\mu_{\underline{\nu}} \bar{X}^{\underline{\nu}\underline{\rho}} \left(\partial_{\underline{\rho}}\delta^{(3)}(\xi - \eta)\right) dt - \int_{\mathbb{R}} \dot{C}^\mu \bar{V}^{\underline{\nu}} \left(\partial_{\underline{\nu}}\delta^{(3)}(\xi - \eta)\right) dt \\ + \int_{\mathbb{R}} \delta^\mu_{\underline{\nu}} \bar{X}^{\underline{\nu}} \delta^{(3)}(\xi - \eta)\, dt + \int_{\mathbb{R}} \dot{C}^\mu\, q\, \delta^{(6)}(\xi - \eta)\, dt.\end{aligned} \tag{6.4.14}$$

The components of $\bar{\mathcal{I}}^{\mu}$ are given by

$$q = \int_{\mathcal{M}} \mathfrak{T}^0(t, \underline{\hat{x}}) d^3\hat{x} \tag{6.4.15a}$$

$$\bar{X}^{\underline{\mu}} + q\dot{C}^{\underline{\mu}} = \int_{\mathcal{M}} \mathfrak{T}^{\underline{\mu}}(t, \underline{\hat{x}}) d^3\hat{x} \tag{6.4.15b}$$

$$\bar{V}^{\underline{\mu}} = \epsilon \int_{\mathcal{M}} \mathfrak{T}^0(t, \underline{\hat{x}}) \left(\hat{x}^{\underline{\nu}} - C^{\underline{\nu}}\right) d^3\hat{x} \tag{6.4.15c}$$

$$\bar{X}^{\underline{\mu\nu}} + \dot{C}^{\underline{\mu}}\bar{V}^{\underline{\nu}} = \epsilon \int_{\mathcal{M}} \mathfrak{T}^{\underline{\mu}}(t, \underline{\hat{x}}) \left(\hat{x}^{\underline{\nu}} - C^{\underline{\nu}}\right) d^3\hat{x} \tag{6.4.15d}$$

$$\bar{V}^{\underline{\mu\nu}} = \epsilon^2 \int_{\mathcal{M}} \mathfrak{T}^0(t, \underline{\hat{x}}) \left(\hat{x}^{\underline{\nu}} - C^{\underline{\nu}}\right) \left(\hat{x}^{\underline{\rho}} - C^{\underline{\rho}}\right) d^3\hat{x} \tag{6.4.15e}$$

$$\dot{C}^{\underline{\mu}}\bar{V}^{\underline{\nu\rho}} = \epsilon^2 \int_{\mathcal{M}} \mathfrak{T}^{\underline{\mu}}(t, \underline{\hat{x}}) \left(\hat{x}^{\underline{\nu}} - C^{\underline{\nu}}\right) \left(\hat{x}^{\underline{\rho}} - C^{\underline{\rho}}\right) d^3\hat{x}. \tag{6.4.15f}$$

where $\mathcal{M}$ represents an integration over the spatial components of M.

Proof. Begin by introducing the substitution

$$\underline{\hat{x}} = \frac{\underline{x} - C}{\epsilon} \tag{6.4.16}$$

gives

$$\mathfrak{T}_\epsilon \wedge \phi = \mathfrak{T}^{\mu}(t, \underline{\hat{x}}) \phi_{\mu}(t, \epsilon\underline{\hat{x}} + C) d^4\hat{x}. \tag{6.4.17}$$

Now Taylor expand this about ϵ,

$$\begin{aligned}\mathfrak{T}_\epsilon \wedge \phi = \mathfrak{T}^{\mu}(t, \underline{\hat{x}}) \phi_{\mu}|_C d^4\hat{x} + \epsilon \mathfrak{T}^{\mu}(t, \underline{\hat{x}}) \left(\hat{x}^{\underline{\nu}} - C^{\underline{\nu}}\right) \left.\frac{\partial \phi_{\mu}}{\partial x^{\underline{\nu}}}\right|_C d^4\hat{x} \\ + \frac{1}{2}\epsilon^2 \mathfrak{T}^{\mu}(t, \underline{\hat{x}}) \left(\hat{x}^{\underline{\nu}} - C^{\underline{\nu}}\right) \left(\hat{x}^{\underline{\rho}} - C^{\underline{\rho}}\right) \left.\frac{\partial^2 \phi_{\mu}}{\partial x^{\underline{\rho}} \partial x^{\underline{\nu}}}\right|_C d^4\hat{x}.\end{aligned} \tag{6.4.18}$$

Integrating this, and splitting into the ϕ_0 and $\phi_{\underline{\mu}}$ terms,

$$\begin{aligned}\int_M \mathfrak{T}_\epsilon \wedge \phi = \int_M \mathfrak{T}^0(t, \underline{\hat{x}}) \phi_0|_C d^4\hat{x} + \int_M \mathfrak{T}^{\underline{\mu}}(t, \underline{\hat{x}}) \phi_{\underline{\mu}}|_C d^4\hat{x} \\ + \epsilon \int_M \mathfrak{T}^0(t, \underline{\hat{x}}) \left(\hat{x}^{\underline{\nu}} - C^{\underline{\nu}}\right) \left.\frac{\partial \phi_0}{\partial x^{\underline{\nu}}}\right|_C d^4\hat{x} + \epsilon \int_M \mathfrak{T}^{\underline{\mu}}(t, \underline{\hat{x}}) \left(\hat{x}^{\underline{\nu}} - C^{\underline{\nu}}\right) \left.\frac{\partial \phi_{\underline{\mu}}}{\partial x^{\underline{\nu}}}\right|_C d^4\hat{x} \\ + \frac{1}{2}\epsilon^2 \int_M \mathfrak{T}^0(t, \underline{\hat{x}}) \left(\hat{x}^{\underline{\nu}} - C^{\underline{\nu}}\right) \left(\hat{x}^{\underline{\rho}} - C^{\underline{\rho}}\right) \left.\frac{\partial^2 \phi_0}{\partial x^{\underline{\rho}} \partial x^{\underline{\nu}}}\right|_C d^4\hat{x} \\ + \frac{1}{2}\epsilon^2 \int_M \mathfrak{T}^{\underline{\mu}}(t, \underline{\hat{x}}) \left(\hat{x}^{\underline{\nu}} - C^{\underline{\nu}}\right) \left(\hat{x}^{\underline{\rho}} - C^{\underline{\rho}}\right) \left.\frac{\partial^2 \phi_{\underline{\mu}}}{\partial x^{\underline{\rho}} \partial x^{\underline{\nu}}}\right|_C d^4\hat{x}.\end{aligned} \tag{6.4.19}$$

Splitting these integrals up into spatial and temporal terms

$$\begin{aligned}\int_M \mathfrak{T}_\epsilon \wedge \phi = &\int_{\mathbb{R}} \left(\int_{\mathcal{M}} \mathfrak{T}^0(t, \underline{\hat{x}}) d^3\hat{x} \right) \phi_0|_C dt + \int_{\mathbb{R}} \left(\int_{\mathcal{M}} \mathfrak{T}^{\underline{\mu}}(t, \underline{\hat{x}}) d^3\hat{x} \right) \phi_{\underline{\mu}}|_C dt \\ &+ \int_{\mathbb{R}} \left(\epsilon \int_{\mathcal{M}} \mathfrak{T}^0(t, \underline{\hat{x}}) \left(\hat{x}^{\underline{\nu}} - C^{\underline{\nu}}\right) d^3\hat{x} \right) \left. \frac{\partial \phi_0}{\partial x^{\underline{\nu}}} \right|_C dt \\ &+ \int_{\mathbb{R}} \left(\epsilon \int_{\mathcal{M}} \mathfrak{T}^{\underline{\mu}}(t, \underline{\hat{x}}) \left(\hat{x}^{\underline{\nu}} - C^{\underline{\nu}}\right) d^3\hat{x} \right) \left. \frac{\partial \phi_{\underline{\mu}}}{\partial x^{\underline{\nu}}} \right|_C dt \\ &+ \frac{1}{2} \int_{\mathbb{R}} \left(\epsilon^2 \int_{\mathcal{M}} \mathfrak{T}^0(t, \underline{\hat{x}}) \left(\hat{x}^{\underline{\nu}} - C^{\underline{\nu}}\right) \left(\hat{x}^{\underline{\rho}} - C^{\underline{\rho}}\right) d^3\hat{x} \right) \left. \frac{\partial^2 \phi_0}{\partial x^{\underline{\rho}} \partial x^{\underline{\nu}}} \right|_C dt \\ &+ \frac{1}{2} \int_{\mathbb{R}} \left(\epsilon^2 \int_{\mathcal{M}} \mathfrak{T}^{\underline{\mu}}(t, \underline{\hat{x}}) \left(\hat{x}^{\underline{\nu}} - C^{\underline{\nu}}\right) \left(\hat{x}^{\underline{\rho}} - C^{\underline{\rho}}\right) d^3\hat{x} \right) \left. \frac{\partial^2 \phi_{\underline{\mu}}}{\partial x^{\underline{\rho}} \partial x^{\underline{\nu}}} \right|_C dt. \end{aligned} \tag{6.4.20}$$

Comparing this to equation (6.4.10), noting $\dot{C}^0 = 1$, gives equation (6.4.15), as required. □

This gives a method to find the 4-current, using each $\mathfrak{T}^\mu$ as a different test density, without needing reconstruct over the velocity coordinates.

Let $\hat{\mathfrak{T}}^\mu$ be the reconstructed 4-current, where, similarly to the previous section, it is defined as

$$\hat{\mathfrak{T}}^\mu = \sum_{\mathbf{\Sigma}} c_{\mathbf{\Sigma}} \phi^\mu_{\mathbf{\Sigma}}. \tag{6.4.21}$$

Taking the moments of this gives

$$a^\mu_{\mathbf{\Lambda}} = \sum_{\mathbf{\Sigma}} (x - C)^{\mathbf{\Sigma}} \int_{\mathcal{M}} c_{\mathbf{\Sigma}} \phi^\mu_{\mathbf{\Sigma}} d^3x = \sum_{\mathbf{\Sigma}} c_{\mathbf{\Sigma}} B^\mu_{\mathbf{\Sigma}\mathbf{\Lambda}} \tag{6.4.22}$$

where similarly to the previous section,

$$B^\mu_{\mathbf{\Sigma}\mathbf{\Lambda}} = \int_{\mathcal{M}} (x - C)^{\mathbf{\Lambda}} \phi^\mu_{\mathbf{\Sigma}} d^3x, \tag{6.4.23}$$

and $a^\mu_{\mathbf{\Lambda}}$ is defined from equations (6.4.15), i.e.

$$a^0_{\mathbf{\Lambda}} = \left(q, V^1, V^2, V^3, V^{11}, V^{12}, V^{13}, V^{22}, V^{23}, V^{33}\right)^T \tag{6.4.24}$$

$$\begin{aligned} a^1_{\mathbf{\Lambda}} = \Big(&X^1 + q\dot{C}^1, X^{11} + \dot{C}^1 V^1, X^{12} + \dot{C}^1 V^2, X^{13} + \dot{C}^1 V^3, \\ &\dot{C}^1 V^{11}, \dot{C}^1 V^{12}, \dot{C}^1 V^{13}, \dot{C}^1 V^{22}, \dot{C}^1 V^{23}, \dot{C}^1 V^{33} \Big)^T \end{aligned} \tag{6.4.25}$$

etc.

This gives 4 scalar fields that must be reconstructed to find the 4-current, in exchange the lack of integration over the velocity space means the reconstruction requires half the number of integrals. Additionally, by not integrating over velocity space, all integrals can be calculated analytically. This is in contrast to the reconstruction approach presented in section 6.3, where to find the current (equation (6.3.9)), an integral had to be performed including a $1/\gamma$ term, which can only be solved numerically.

In section 8.4, a more geometric approach to this deposition process will be shown, where the current 3-form will be derived through a projection of the 7-current onto the base spatial manifold.

6.5 Numerical validation of the moment reconstruction methods

To validate both methods of generating a 4-current from a set of moments, begin with some distribution function density $\mathfrak{f}$. The moments of $\mathfrak{f}$ can be taken, to give $\mathcal{J}^a$. From here there are two possible ways to find the 4-current. Firstly, $\hat{\mathfrak{f}}$ can be reconstructed using the method in section 6.3, and then the 4-current found using equation (6.3.9). This will be referred to as the *reconstruction method*. Alternatively, the projection method presented in section 6.4 can be used, and then a 4-current reconstructed from the distributional 4-current. This method will be referred to as the *projection method*. Both of these methods can then be compared to the 4-current found directly from using equation (6.3.9) with $\mathfrak{f}$, denoted as the *direct method*. This testing procedure is explained pictorially in figure 6.1.

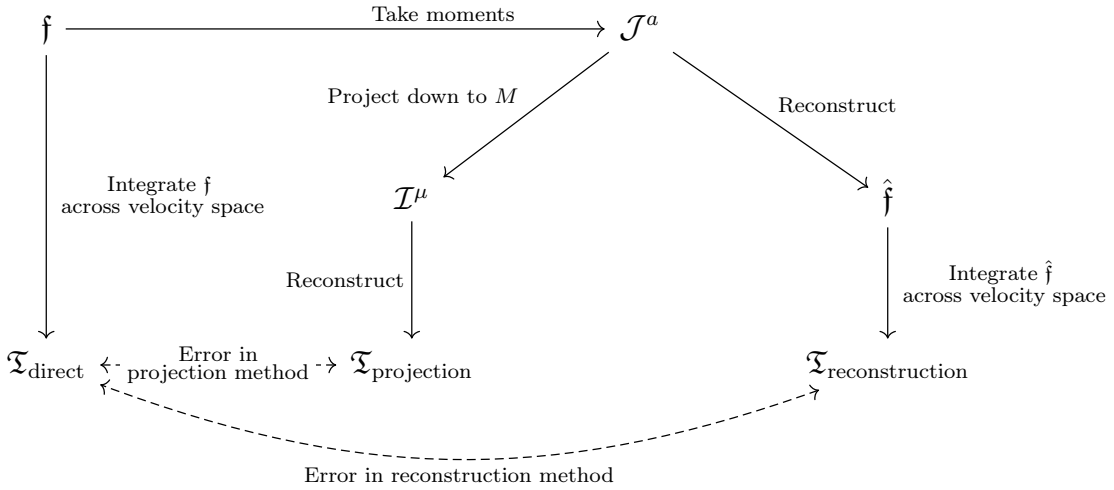

Figure 6.1: *The different ways to calculate the 4-current from a set of moments $\mathcal{J}^a$, which has moments generated by $\mathfrak{f}$. The error in the reconstruction method is the difference between the 4-current generated by reconstructing $\hat{\mathfrak{f}}$, compared to finding the 4-current directly from $\mathfrak{f}$. The error in the projection method is the difference between the 4-current found through projecting $\mathcal{J}^a$ onto M, compared to finding the 4-current directly from $\mathfrak{f}$.*

To reconstruct the functions, the algorithm was written in C++, so that it can be combined with the moment tracking code developed in chapter 5 as part of a full PIC code. The matrices and column vectors required for the reconstruction algorithms were implemented using the external library Eigen3 [100]. The linear system of equations was solved numerically using the LU factorisation method [97]. This algorithm is numerically slow, but highly accurate, so it the best choice for testing the accuracy of the reconstruction process. This is because errors in the results will be due to issues with the reconstruction or projection methods, rather than the numerical process used. Integrals over position space are solved analytically, whilst integrals over velocity space are solved numerically, using Gaussian quadrature [97].

In all cases, the choice of model function will be the function

$$\varphi_0 = \varphi_{0,x}(x)\,\varphi_{0,y}(y)\,\varphi_{0,z}(z)\,\varphi_{0,u_x}(u_x)\,\varphi_{0,u_y}(u_y)\,\varphi_{0,u_z}(u_z), \tag{6.5.1}$$

where

$$\begin{gathered}
\varphi_{0,x} = 1 \quad \text{if} \quad 0 \leq x \leq 10, \quad 0 \text{ otherwise} \\
\varphi_{0,y} = \delta(y) \\
\varphi_{0,z} = 1 \quad \text{if} \quad -5 \leq z \leq 5, \quad 0 \text{ otherwise} \\
\varphi_{0,u_x} = 1 \quad \text{if} \quad -3 \leq u_x \leq 3, \quad 0 \text{ otherwise} \\
\varphi_{0,u_y} = \delta(u_y) \\
\varphi_{0,u_z} = 1 \quad \text{if} \quad 1 \leq u_z \leq 5, \quad 0 \text{ otherwise},
\end{gathered} \tag{6.5.2}$$

where $\delta(y)$ and $\delta(u_y)$ represent Dirac delta functions. The projection method uses the same model function without the velocity components. This corresponds to a top-hat function in x, z, u_x, and u_z, and a Dirac delta function in y and u_y. Additionally to calculate $X^{\underline{\mu}\underline{\nu}}, X^{\underline{\mu}}$ and $\dot{C}^{\mu}$, it shall be assumed the particle is travelling in a straight line along $x = y = 0$, $u_x = u_y = 0$, and $u_z = 3$. The particles will be travelling in flat space, so $u^0 = \gamma$, the Lorentz factor. These assumptions show how simple functions affect the accuracy of the projection and reconstruction methods compared to the direct method.

First consider an $\mathfrak{f}$ that has a support identical to the support of the top hat model density. Figures 6.2 and 6.3 show the $\mathfrak{T}_x$ and $\mathfrak{T}_z$ components for a parabola and a bump function respectively. The reconstruction method parabola matches the direct method exactly. This is because when working up to quadrupole moments, the reconstructed model function becomes a parabola. This was shown in section 6.3.1 in the 1D case. The bump function is modelled well by the reconstruction method in the centre, and less well towards the edge. This is because a second order Taylor expansion of an exponential function will accurately model the centre of the bump function, but poorly model the edges of the bump function, when the

importance of higher order terms is significant.

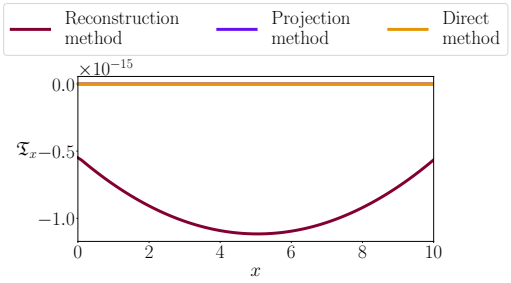

(a) $\mathfrak{T}_x$, *the projection method and direct method overlap.*

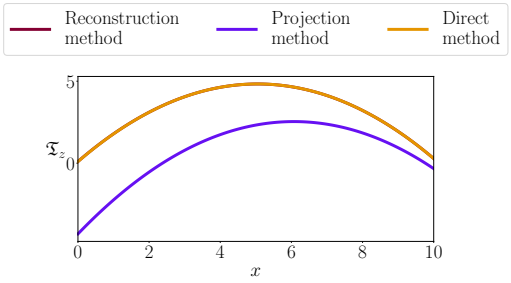

(b) $\mathfrak{T}_z$, *the reconstruction method and direct method overlap.*

Figure 6.2: *The* $\mathfrak{T}_x$ *and* $\mathfrak{T}_z$ *components from an initial distribution function* $\mathfrak{f} = -(x)(x-10)\,\varphi_0$ *through the direct method, the projection method, and the reconstruction method.*

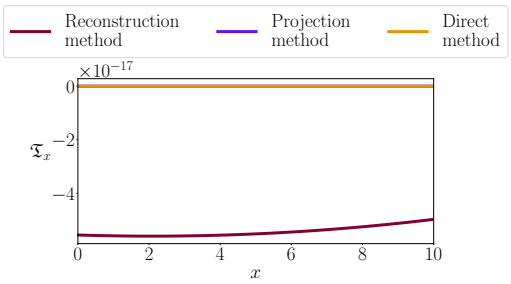

(a) $\mathfrak{T}_x$, *the projection method and direct method overlap.*

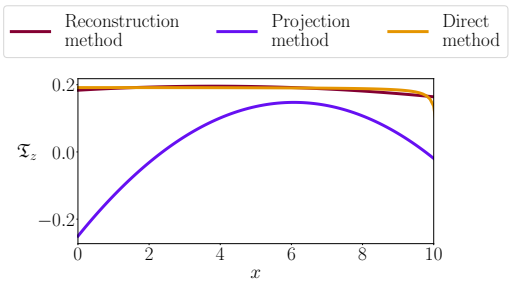

(b) $\mathfrak{T}_z$

Figure 6.3: *The* $\mathfrak{T}_x$ *and* $\mathfrak{T}_z$ *components from an initial distribution function* $\mathfrak{f} = \exp\left(\frac{1}{x^2-100}\right)\varphi_0$ *through the direct method, the projection method, and the reconstruction method.*

In figures 6.2a and 6.3a, the $\mathfrak{T}_x$ current found through both the direct method and projection method vanish. The reconstruction method $\mathfrak{T}_x$ current is not zero, but is incredibly small, so is only non-zero from numerical errors. This is the expected result; the distribution function $\mathfrak{f}$ is even in u_x, so the integrand in the 4-current

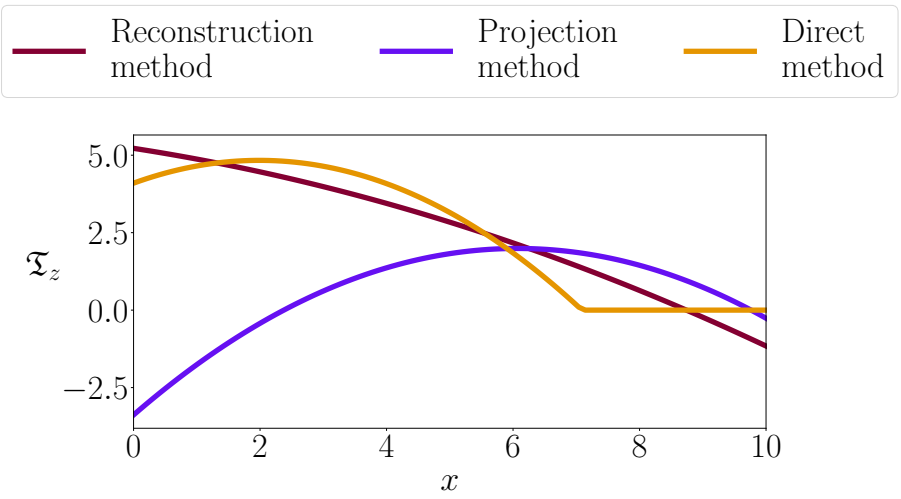

Figure 6.4: *The $\mathfrak{T}_z$ component of current from an initial distribution function $\mathfrak{f} = -(x+3)(x-7)\,\varphi_0$ if $0 \leq x \leq 7$, 0 otherwise, through the direct method, the projection method, and the reconstruction method.*

equation ($\mathfrak{f}u_x/\gamma$) is odd, so the integral vanishes. The $\mathfrak{T}_x$ component of 4-current will not be considered for the other symmetric distribution functions being tested.

Figure 6.4 shows a function where the width of the parabola is less than the width of the model function. In this case the reconstruction method fails to accurately reconstruct the function. This is because the reconstruction and projection methods assume the function they are approximating is spread across the whole width of the model function. This means care must be taken to make sure that the width of the model function is close to the width of the actual function. When choosing a model function, consideration must be made about its width. This will be a significant issue in a full PIC code, where the width of the original distribution function is unknown, and will change over time. By assuming the original distribution is parabolic, it may be possible to numerically approximate the width of the parabola. This is done by using the moments to solve a non-linear system of equations to find the roots of the quadratic equation used to create the parabola. By doing this, the top-hat model function can always be guaranteed to be the correct width.

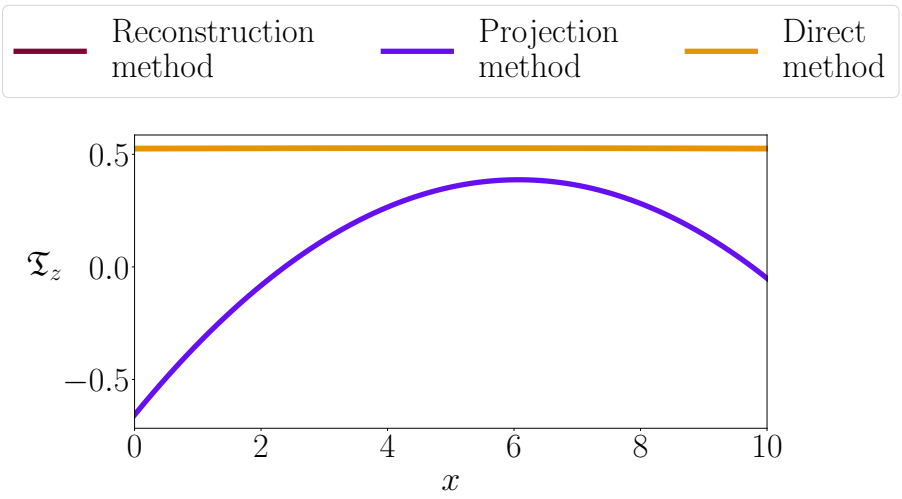

Figure 6.5: *The $\mathfrak{T}_z$ component of current from an initial distribution function $\mathfrak{f} = -(u_z - 1)(u_z - 5)\,\varphi_0$, through the direct method, the projection method, and the reconstruction method. The direct and reconstruction methods overlap.*

In the case that the original function is a top-hat function in position, but some non-flat function in the velocity coordinates, then the current will be constant, scaled by the integral of u^μ/γ. Figures 6.5 and 6.6 show this. Again the reconstruction method correctly models this to within numerical precision, whilst the projection method does not give an accurate current. In the case that the width of the original distribution in velocity space is less than the width of the model function used in the reconstruction method (figure 6.6), the reconstruction method is still accurate, at least in the non-relativistic limit. This is because whilst the velocity function might not be correctly reconstructed, the integral over velocity space is still the same (by definition of the algorithm).

In all cases, the projection method is inaccurate compared to the reconstruction method. The reason for this can be seen by considering the definition of the 4-current,

$$\mathfrak{T}^1_{\text{direct}} = \int_{\mathcal{E}_p} \frac{u^1}{\gamma} \mathfrak{f}\, d^3u. \tag{6.5.3}$$

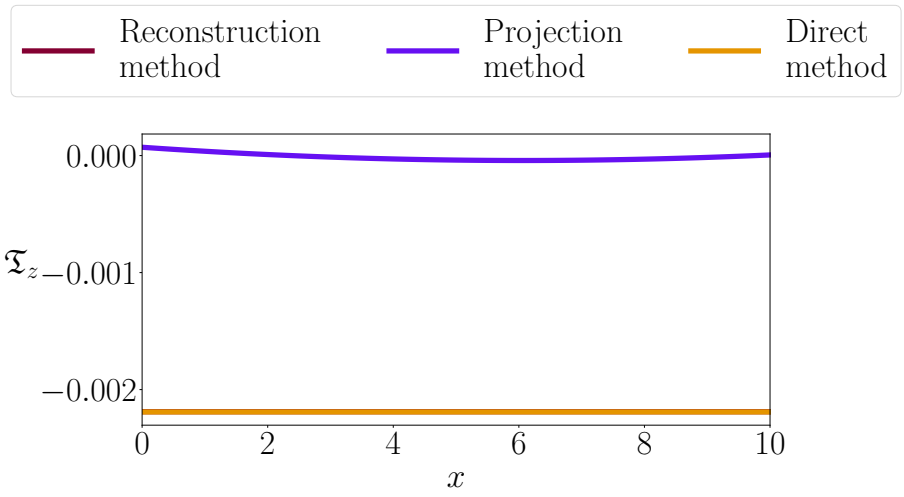

Figure 6.6: *The $\mathfrak{T}_z$ component of current from an initial distribution function $\mathfrak{f} = -(u_x - 0.1)(u_x + 0.1)\,\varphi_0$ for $-0.1 \leq u_x \leq 0.1$, 0 otherwise, through the direct method, the projection method, and the reconstruction method. The direct and reconstruction methods overlap.*

Consider a case where $\gamma \approx 1$, so that the factors of γ can be ignored. Integrating this function over position space $\mathcal{M}$,

$$\int_{\mathcal{M}} \mathfrak{T}^1_{\text{direct}}\, d^3x = \int_{\Sigma} u^1 \mathfrak{f}\, d^3u\, d^3x = V^4. \tag{6.5.4}$$

Compare this to (6.4.15b), using Maple to find X^1 in the case $\dot{C}^1 = 0, \dot{C}^2 = 0, x = 0, y = 0$, and $\gamma \approx 1$ gives

$$\int_{\mathcal{M}} \mathfrak{T}^1_{\text{projection}}\, d^3x = X^1 = V^4 - V^{46} u_z, \tag{6.5.5}$$

so there is a discrepancy between the two methods. Since the projection method uses X^1, this is an infinite series that has been truncated to the quadrupole level. This means the effect of higher order moments will be significant. How higher order moments affect the accuracy of the projection method is improved is outside the scope of this thesis, and is future work.

It is important to stress that even though the projection method is less accurate, it has significant computational benefits. As it does not involve any integrals over

velocity space, there is no numerical integration required to integrate the $u^{\underline{\mu}}/\gamma$ terms. Additionally, because there are no velocity integrals, the projection method involves solving a system of 10 equations 4 times, compared to the reconstruction method, which requires solving 28 simultaneous equations. Whilst this difference in computational time is small at the quadrupole level, when this algorithm is extended to higher order moments the effect will be significant. Additionally, since the error in the projection method is due to the truncation, it may be reduced by increasing the number of moments.

Chapter 7

Creating an axially symmetric full PIC code

7.1 Introduction

Having developed and numerically verified the theory for tracking moments and reconstructing charge and current from these moments, a full PIC code using moments can now be developed. Rather than simulating a full (3+3)D PIC code (3 spatial dimensions + 3 velocity dimensions), a simpler case is to simulate a '1.5D' PIC code. This 1.5D code models an axially symmetric system in cylindrical coordinates. This represents the motion of particles through a straight section of a particle accelerator, or an RF cavity. One particular application that is interesting to simulate is that of a klystron. These are used for generating RF signals, and consist of an electron gun, an RF cavity (the 'buncher cavity') to focus the electrons, and then a decelerating cavity (the 'catcher cavity'), where the RF signal is boosted due to the decelerating electrons (figure 7.1).

This chapter presents an outline of the steps needed to implement, test, and optimise a cylindrically symmetric 1.5D moment tracking PIC code. This chapter only outlines the code and how it can be tested and improved. No numerical results

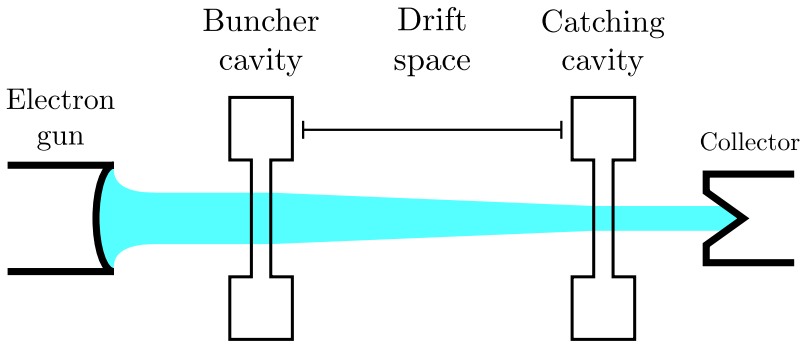

Figure 7.1: *The design principle of a klystron. An electron beam (the blue line) is emitted from an electron gun. This beam passes through a bunching cavity followed by a drift space, which longitudinally focusses the particles. They are then decelerated in the catcher cavity, emitting radiation of an amplitude greater than the initial signal used to accelerate the beam.*

from a full 1.5D PIC code are presented. The structure of this chapter as follows: Section 7.2 explains the 1.5D coordinate system used in the axially symmetric PIC code, and explains how this reduces the amount of information in the PIC code. Section 7.3 reviews existing techniques for updating the electromagnetic field, and interpolating fields in PIC codes. This section also introduces the algorithms that can be used for modelling the axially symmetric 1.5D PIC code. Section 7.4 explains how this PIC code will be tested, and how existing issues with PIC codes will be examined. Section 7.5 describes future work, outlining how features can be added to the PIC code to allow more moments to be tracked; and how structure within a macroparticle can be modelled.

7.2 The 1.5D coordinate system

The cylindrical coordinates will be denoted (r, ϕ, z). The 1.5D code models the motion of a macroparticle restricted to the $r = 0$ axis, so the only parameters that can be updated for the macroparticles motion are the z and u_z components. As the motion of the macroparticle is restricted to the z-direction, the value of the Lorentz

Order of moments tracked	**Information known**	**Number of differential equations to solve**	**Number of differential equations to solve relative to a standard macro-particle**
Monopole (zeroth order)	z, u_z	2	1
Dipole (first order)	z, u_z, V^a	6	3
Quadrupole (second order)	z, u_z, V^a, V^{ab}	16	8
Octopole (third order)	z,u_z, V^a, V^{ab}, V^{abc}	36	18
Hexadecapole (fourth order)	z, u_z, V^a, V^{ab}, V^{abc}, V^{abcd}	71	35.5

Table 7.1: *The amount of information in a macroparticle that also tracks moments compared to a standard macroparticle in the 1.5D model. Note, whilst the number of differential equations relative to a standard macroparticle (the fourth column) is larger than in the 3D case (table 1.1), there are less equations overall (the third column).*

factor, γ is given by

$$u^0 = \gamma = \sqrt{1 + u_z^2}. \tag{7.2.1}$$

The moments of the macroparticle will include both longitudinal and radial components. The system is axially symmetric, so these macroparticles with their moments can be thought of as representing 'rings' of charge. By excluding the axial moments, there is less information each at time step, as outlined in table 7.1. Since the angular components in sums can be ignored (due to the symmetry), they will not be considered in sums in this chapter. This means that in this chapter, Latin indices range over $1, 2, 3, 4$ and Greek indices will range over $1, 2$.

Since the beam being simulated is axially symmetric, the beam does not move in the angular direction. This restriction means that only certain components of Maxwell's equations need to be considered. Since the beam cannot rotate in the angular plane, there will not be an E_ϕ component of the electric field. Similarly, because of the symmetry, there cannot be a radial or longitudinal magnetic field unless one is added externally. Since the radial magnetic field is generated by dE_ϕ/dz or $dE_z/d\phi$ terms,

and the longitudinal magnetic field is generated by dE_ϕ/dr or $dE_r/d\phi$ terms; all of these terms vanish due to the axial symmetry. The B_z field will still be considered in the model, as low energy RF accelerators often include a solenoid to stop the beam diverging radially from space-charge effects.

There is a choice to be made in whether this 1.5D algorithm is constructed in 2 dimensions from the beginning, or if the axial coordinates are integrated out. These formulations will only differ by a factor of 2π in the moments. Since densities are used for all the integrations, this effect can be included. We shall choose to construct the system in 2 dimensions initially, since integrating axial coordinates at $r = 0$ is ill defined. This is due to the singularity axial coordinates have along the $r = 0$ axis.

7.3 The numerical methods needed for a full PIC code

7.3.1 Taking the initial moments

The first step of a PIC code is to split the initial distribution of particles into macroparticles (figures 1.1 and 1.3). In the case of a klystron, this initial distribution is the beam from the electron gun. This beam will provide a constant stream of particles in the z direction, and a distribution of particles in r, u_r and u_z. It it will be assumed that these particles are distributed as a parabola, since, as previously shown, this results in an accurate reconstruction of current. As previously mentioned, splitting the beam longitudinally results in each macroparticle representing a 'ring' of charge. An example of how these rings are shaped from the moments is given in figure 7.2.

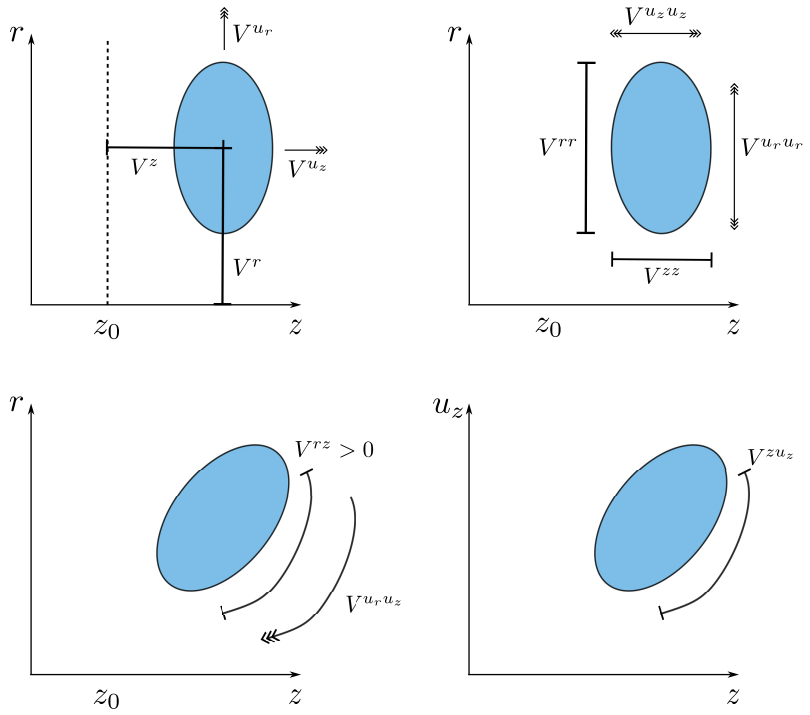

Figure 7.2: *An example of a ring represented by its moments. To picture this in 3 dimensions, the ring should be rotated around the z axis.*

7.3.2 The particle and moment updating algorithms

In a particle-in-cell code in Cartesian coordinates, particles position and velocity are updated by solving the Lorentz force,

$$\frac{d\mathbf{x}}{dt} = \frac{\mathbf{u}}{\gamma}, \tag{7.3.1}$$

$$\frac{d\mathbf{u}}{dt} = \frac{q}{m}\left(\mathbf{E} + \frac{\mathbf{u}\times\mathbf{B}}{\gamma}\right). \tag{7.3.2}$$

Note, this is not the same as the $W^{\underline{\mu}+3}$ terms in the Vlasov equation. This is because the coordinate being updated is $\mathbf{u}$, rather than $\mathbf{v}$. As previously discussed, $\mathbf{u}$ is the velocity coordinate as it moves the singularity from $v = c = 1$ to infinity, removing the machine precision rounding error that occurs as a particle moves very close to c.

In most PIC codes, the position and velocity are solved using the Boris algorithm [101]. This algorithm is a leapfrog algorithm, which means the position and velocity are not updated at the same time. The position is updated, then the velocity, then the position again. This improves the numerical stability. Whilst the PIC code presented in this chapter will not use the standard leapfrog algorithm used in many PIC codes, it is still possible to get the enhanced accuracy of the particle pusher section of the PIC code.

Recall the cylindrical symmetry, and that the centre of the macroparticle will always be along the $r = 0$ axis. This means only the z and u_z components of the motion need to be updated. Position is updated using the forward Euler algorithm,

$$z^{n+\frac{1}{2}} = z^{n-\frac{1}{2}} + \frac{u_z}{\gamma}\Delta t. \tag{7.3.3}$$

Note these are at half time step positions, to get the stability from the leapfrog algorithm. As there are no B_r or B_ϕ fields along the axis (they must vanish along the r-axis to be continuous), there will be no contribution to the motion of the particles due to the magnetic field. This means the velocities can be updated using a forward Euler method for the electric field,

$$u_z^{n+1} = u_z^n + \frac{q\Delta t}{m} E_z^{n+\frac{1}{2}} \tag{7.3.4}$$

where $E_z^{n+\frac{1}{2}}$ is the electric field found at the half time step position.

Moments are updated using the Forward Euler method,

$$\begin{aligned} V_{n+1}^{\underline{a}} &= V_n^{\underline{a}} + \frac{dV_n^{\underline{a}}}{dt}\Delta t, \\ V_{n+1}^{\underline{ab}} &= V_n^{\underline{ab}} + \frac{dV_n^{\underline{ab}}}{dt}\Delta t. \end{aligned} \tag{7.3.5}$$

Whilst this method is prone to numerical errors when using a large time step, chapter 5 showed the dominating error was the truncation error, rather than numerical finite time step integration errors. In the case that the error from using the forward Euler

method becomes significant, the integration can be improved by using algorithms such as implicit Runge-Kutta, although these are very computationally expensive. Alternatively, a multistep model such as Adams-Bashforth could be used. These solve the differential equations using several previous time steps, and have less computational complexity than Runge-Kutta, but require more memory [97].

Note that whilst the E_r and magnetic fields do not contribution to the position and velocity of the macroparticle, they do affect the motion of the moments, as well the E_z field itself, and hence must be included.

7.3.3 Updating the electromagnetic fields

7.3.3.1 Discretisation of space

In PIC codes, rather than a continuous electromagnetic (EM) field defined everywhere, the EM field is defined at discrete grid points. By discretising the electromagnetic field, the fields between particles are not defined by the Coulomb and Biot-Savart laws. Instead the current from a macroparticle is deposited onto nearby grid points. This current is used to solve discretised Maxwell's equations, which then are interpolated to the particle's position, to solve the Lorentz force.

Rather than defining all the components of the EM field at the same point, modern PIC codes use a staggered grid. This grid was first proposed by Yee [102], and has the advantage of ensuring that the divergence of the curl vanishes. By working in cylindrical coordinates with an axial symmetry, it is possible to reduce the 3D grid down to a 2D grid. This thesis uses the grid proposed in ref. [103]. By using a 2D grid the number of grid points scales as $\mathcal{O}(n^2)$, rather than $\mathcal{O}(n^3)$. This reduces both the computational time it takes to update the grid, and the amount of memory needed to store the grid points, without reducing the amount of information about the electromagnetic fields. The grid used is shown in figure 7.3. Note that only B_ϕ, B_z, E_r, and j_r are defined along the $r = 0$ axis. As previously mentioned, due

to the axial symmetry E_ϕ, B_r, and j_ϕ vanish everywhere.

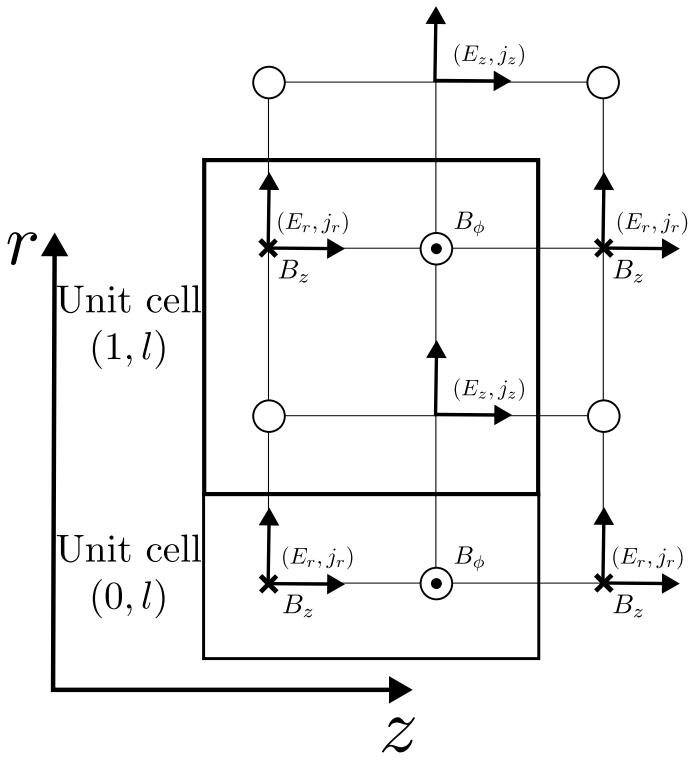

Figure 7.3: *The grid used for discretising Maxwell's equations, figure inspired by [103]. Since the grid is axially symmetric, this can be converted to a 3D grid by rotating the grid around the z axis. A black cross denotes the centre of a cell (the point radius is at evaluated at in the field updating equations). Due to the axial symmetry, the E_ϕ and B_r fields will always vanish.*

7.3.3.2 Updating the fields

Fields are updated by solving the dynamical Maxwell's equations

$$\frac{d\mathbf{E}}{dt} = \frac{1}{c^2}\nabla \times \mathbf{B} - \frac{1}{\varepsilon_0}\mathbf{j}, \tag{7.3.6}$$

$$\frac{d\mathbf{B}}{dt} = -\nabla \times \mathbf{E}. \tag{7.3.7}$$

There is no need to consider Gauss' law

$$\nabla \cdot \mathbf{E} = \frac{\rho}{\varepsilon_0} \tag{7.3.8}$$

since differentiating both sides with respect to time,

$$\frac{d}{dt}\left(\nabla \cdot \mathbf{E}\right) = \frac{d}{dt}\left(\frac{\rho}{\varepsilon_0}\right) \tag{7.3.9}$$

$$\nabla \cdot \frac{d\mathbf{E}}{dt} = \frac{1}{\varepsilon_0}\frac{d\rho}{dt}. \tag{7.3.10}$$

Using Ampère's Law (equation (7.3.6)),

$$\nabla \cdot \left(\nabla \times \mathbf{B} - \frac{1}{\varepsilon_0}\mathbf{j}\right) = \frac{1}{\varepsilon_0}\frac{d\rho}{dt} \tag{7.3.11}$$

$$\nabla \cdot \left(\nabla \times \mathbf{B}\right) - \frac{1}{\varepsilon_0}\nabla \cdot \mathbf{j} = \frac{1}{\varepsilon_0}\frac{d\rho}{dt} \tag{7.3.12}$$

$$\nabla \cdot \mathbf{j} = \frac{d\rho}{dt} \tag{7.3.13}$$

so if the divergence of $\mathbf{j}$ vanishes, charge is conserved.

To solve the relevant Maxwell's equations on a discretised grid, a finite-difference time domain (FDTD) algorithm is used. These algorithms solve partial differential equations that involve temporal and spatial derivatives by using the discretised spatial coordinates. In cylindrical coordinates, it is possible to exploit the rotational symmetry to simplify the FDTD equations, since the derivatives with respect to ϕ can be ignored. From [103], the equations used to update the electric fields are

$$E_r^{n+1}(k,l) = E_r^n(k,l) - \left(\frac{B_\phi^n(k,l) - B_\phi^n(k,l-1)}{\Delta z}\right)\Delta t - \frac{1}{\varepsilon_0}J_r^n(k,l)\Delta t \tag{7.3.14}$$

$$E_z^{n+1}(k,l) = E_z^n(k,l) + \left(\frac{r_k B_\phi^n(k,l) - r_{k-1}B_\phi^n(k-1,l)}{r_{k-\frac{1}{2}}\Delta r}\right)\Delta t - \frac{1}{\varepsilon_0}J_r^n(k,l)\Delta t. \tag{7.3.15}$$

where (k,l) is used to refer to the field component in the (k,l) cell (as in figure 7.3). The equations for updating the magnetic fields are

$$B_\phi^{n+1}(k,l) = B_\phi^n(k,l) - \left(\frac{E_r^n(k,l+1) - E_r^n(k,l)}{\Delta z}\right)\Delta t + \left(\frac{E_z^n(k+1,l) - E_z^n(k,l)}{\Delta r}\right)\Delta t \tag{7.3.16}$$

$$B_z^{n+1}(k,l) = B_z^n(k,l). \tag{7.3.17}$$

7.3.3.3 Boundary conditions

To solve the EM field equations, it is not sufficient to just use Maxwell's equations: boundary conditions to describe how the field behaves at the edges of the simulation must also be designed. There are several different options, depending on the physics described by the system. One possibility are periodic boundary conditions, where the edge of the simulation matches the opposite edge of the simulation [104]. For a simulation where electromagnetic fields can escape the system, absorbing boundary conditions must be used [105].

For an RF cavity, the most appropriate boundary conditions are metallic boundary conditions. This means that the electric field components tangent to the boundaries and the magnetic field components normal to the boundary vanish. Additionally, it shall be assumed that the electromagnetic fields within the walls vanish. It shall be the convention of this thesis that the boundaries of the cavities line up with the centre of the cells (the location of the B_z, E_r, and j_r components). This choice gives the boundary conditions as

$$\begin{aligned} E_\phi(k, z_{min}) = E_r(k, z_{min}) = B_z(k, z_{min}) = 0, \\ E_\phi(k, z_{max}) = E_r(k, z_{max}) = B_z(k, z_{max}) = 0, \\ B_\phi(k, z_{max}) = E_z(k, z_{max}) = 0, \end{aligned} \tag{7.3.18}$$

where the last line is due to assuming fields are zero within the cavity walls, and the use of the staggered grid.

There are no boundary conditions for the r_{max} boundary because the quantities defined at r_{max} (and not at the halfway point between the cells) are not zero on the boundary. These are instead corrected by using different differential equations to solve the boundaries. The simplest way to do this is to set the $E_z(k+1, l)$ term in (7.3.16) to zero. This is unstable, as this equates to using the backwards difference formula to calculate derivatives, which is not accurate. This is in contrast

to the FDTD equations for the bulk of the media, which use a more stable central difference formula. To update B_ϕ on the r_{max} boundary, use five points to calculate the derivative at the r_{max} boundary, using the formulae

$$B_\phi^{n+1}(r_{max}, l) = B_\phi^n(r_{max}, l) - \left(\frac{E_r^n(k, l+1) - E_r^n(k, l)}{\Delta z}\right)\Delta t - \left(\frac{35}{8\Delta x}E_z(r_{max}-1, l) + \frac{35}{24\Delta x}E_z(r_{max}-2, l) - \frac{21}{40\Delta x}E_z(r_{max}-3, l) + \frac{5}{56\Delta x}E_z(r_{max}-4, l)\right)\Delta t. \quad (7.3.19)$$

The numerical differentiation formula used to derive this is in appendix A.1.

To solve the fields along the $r = 0$ axis, use the cylindrical symmetry to note that for fields to be continuous, $E_r(0, j) = 0$, and $B_\phi(0, j) = 0$. The only non-zero field defined at a grid point along the axis is B_z. Since B_z is constant due to the cylindrical symmetry, this term does not need to be updated.

To test the field updater is working, an electric field with E_z component

$$E_z = E_0 J_0\left(\frac{2.405\, r}{a}\right) \quad (7.3.20)$$

can be modelled, where $J_0(r)$ is the zeroth Bessel function of the first kind, E_0 is the initial electromagnetic field strength and a is the radial width of the cavity. This corresponds to the TM_{010} mode of an accelerating cavity (see reference [95] for a derivation of this). Figure 7.4 shows the electric and magnetic fields for this cavity. There is no gain in oscillation amplitude over time, and the fields are 90° out of phase with each other, as is expected. This shows the electromagnetic field updater works correctly without the addition of current sources.

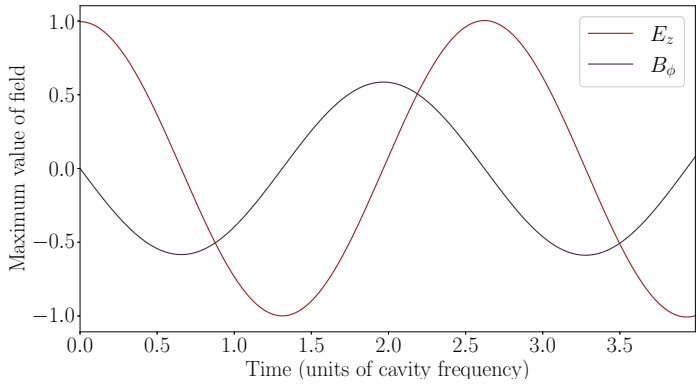

Figure 7.4: *The maximum values of electric and magnetic fields of a* TM_{010} *mode in a cylindrical cavity over time. The initial electric field is defined by equation* (7.3.20) *where* $E_0 = 1$*, and* $a = 1$*. The grid size simulated is* 10×10 *with a uniform spacing of* 0.1*, and a time step* $\Delta t = 0.001$*.*

7.3.4 Depositing current onto the grid points

Chapter 6 showed how to reconstruct the 4-current from a set of moments. These currents need to be deposited onto the grid points in order to solve the discretised Maxwell's equations. This is done by integrating $\mathfrak{T}^{\underline{\mu}}$ across the volume of the cell,

$$j^{\underline{\mu}}(k,l) = \int_{\text{cell}} \mathfrak{T}^{\underline{\mu}} d^2x \tag{7.3.21}$$

where $\int_{\text{cell}}$ represents integration over the area of the (k,l) cell, and the integration is only over 2 dimensions since the grid is 2D.

The bounds of the cell used for integration are the nearest staggered grid points adjacent to the grid point the current is defined at. These boundaries are shown pictorially in figure 7.5. Special consideration needs to be taken for the bounds of integration of the j_r current component along all of the boundaries. For the $r = 0$ axis, this is because the cell is only half as wide as the other cells at this point. For the other boundaries, this is because there is no current inside the cavity walls, so these regions should not be included in the integration.

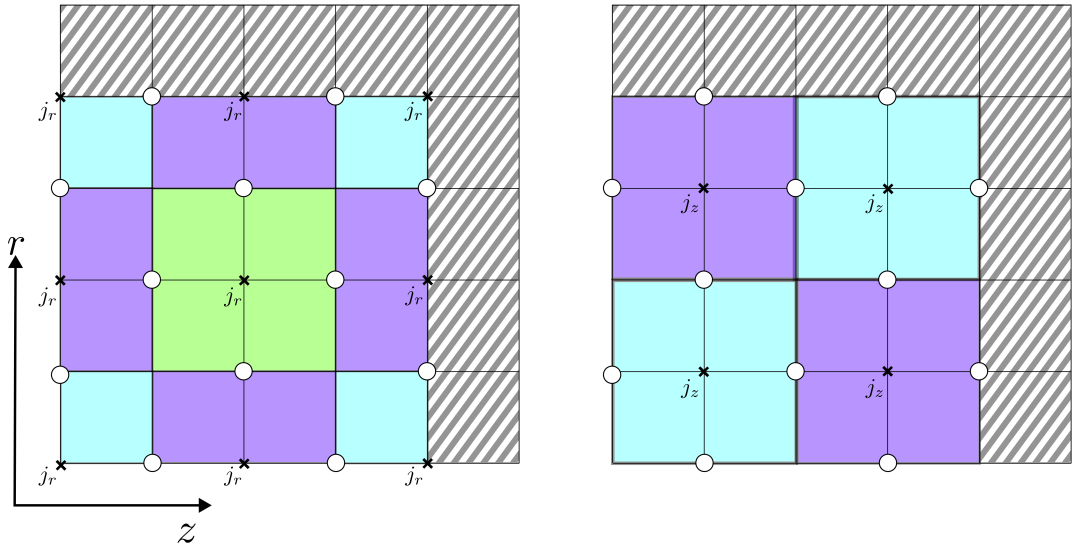

(a) *The j_r grid cell boundaries for depositing current to the grid. Since there is no current inside the cavity walls, these boundaries are only half cells.*

(b) *The j_z grid cell boundaries for depositing current to the grid. Since there are no j_z grid cells along the axis, there are only 2×2 grid points for the j_z to be evaluated on.*

Figure 7.5: *An example of the cell boundaries when integrating the current across a 3×3 grid. The colours are used to distinguish cells. The diagonal striped region represents the cavity walls, within which there is zero current. The leftmost grid points represent the z_{min} cell.*

Is is important to deposit over multiple grid cells, as this allows the structure from the charge distribution to be reflected across the extent of the macroparticle. The number of cells deposited across is determined by the width of the model function used to find the current through either the reconstruction or projection methods (equation (6.3.3)). The number of cells the current is deposited over covers the whole support of the model function (figure 7.6).

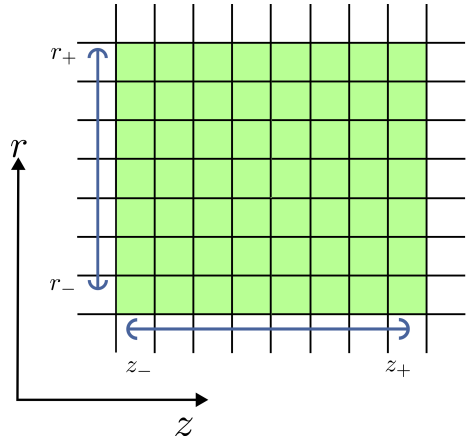

Figure 7.6: *The number of grid cells (highlighted in green) the current is deposited across. The number of grid cells the current is deposited across is determined by the width of the model function (equation* (6.3.3)*). The number of grid cells deposited across needs to cover the whole support of the model function (the blue lines).*

7.3.5 Interpolating the fields

As previously shown, the electromagnetic fields are calculated at points on the grid. To update the macroparticle's position, velocity, and moments; the EM fields and their derivatives must be interpolated to the current position of the macroparticle. There are several existing methods for interpolation. The simplest interpolation method is to linearly weight the field across the closest grid points [106]. This method can be improved be weighting over several grid points [36, 37]. An alternative method is to use splines to find a continuous function across the whole grid [107, 108]. Spline interpolation methods stitch together multiple low order polynomials to find the field across the whole grid. This is more accurate, but is more computationally intensive.

The linear weighting methods do not allow for the derivatives of the field to be accurately calculated. One method to use linear weighting to calculate the derivatives would be to find the derivatives at the grid points using numerical differentiation, and linearly interpolate these to the macroparticles location. The

spline methods use several polynomials, each of low order. This means that derivatives above this order will not be accurately calculated by the splines. An alternative method is to interpolate to the particles position by finding a polynomial approximation to the field. Consider a function $h(r,z)$, this can be approximated as a polynomial

$$h(r,z) \approx \sum_{i=0}^{n}\sum_{j=0}^{m} a_{ij} r^i z^j \tag{7.3.22}$$

where n and m are the number of r and z points being used for finding the interpolation polynomial. This allows a $nm \times nm$ square matrix of points,

$$\begin{pmatrix} h_{r_0,z_0} \\ h_{r_1,z_0} \\ \vdots \\ h_{r_n,z_0} \\ h_{r_0,z_1} \\ \vdots \\ h_{r_n,z_1} \\ \vdots \\ h_{r_n,z_m} \end{pmatrix} = \begin{pmatrix} r_0^0 z_0^0 & r_0^1 z_0^0 & \dots & r_0^n z_0^0 & r_0^0 z_0^1 & r_0^1 z_0^1 & r_0^n z_0^1 & \dots & r_0^n z_0^m \\ r_1^0 z_0^0 & r_1^1 z_0^0 & \dots & r_1^n z_0^0 & r_1^0 z_0^1 & r_1^1 z_0^1 & r_1^n z_0^1 & \dots & r_1^n z_0^m \\ \vdots & & & & & & & & \\ r_n^0 z_0^0 & r_n^1 z_0^0 & \dots & r_n^n z_0^0 & r_n^0 z_0^1 & r_n^1 z_0^1 & r_n^n z_0^1 & \dots & r_n^n z_0^m \\ r_0^0 z_1^0 & r_0^1 z_1^0 & \dots & r_0^n z_1^0 & r_0^0 z_1^1 & r_0^1 z_1^1 & r_0^n z_1^1 & \dots & r_0^n z_1^m \\ \vdots & & & & & & & & \\ r_n^0 z_1^0 & r_n^1 z_1^0 & \dots & r_n^n z_1^0 & r_n^0 z_1^1 & r_n^1 z_1^1 & r_n^n z_1^1 & \dots & r_n^n z_1^m \\ \vdots & & & & & & & & \\ r_n^0 z_m^0 & r_n^1 z_m^0 & \dots & r_n^n z_m^0 & r_n^0 z_m^1 & r_n^1 z_m^1 & r_n^n z_m^1 & \dots & r_n^n z_m^m \end{pmatrix} \begin{pmatrix} a_{0,0} \\ a_{1,0} \\ \vdots \\ a_{n,0} \\ a_{0,1} \\ \vdots \\ a_{n,1} \\ \vdots \\ a_{n,m} \end{pmatrix} \tag{7.3.23}$$

so by solving this system of equations, the coefficients $a_{i,j}$, and the approximation for h can be found. This also allows the derivatives of h to be found quickly, by analytically differentiating the polynomial for h.

Replacing h with each component of the electromagnetic field gives a mechanism for interpolating the electromagnetic field and its derivatives from the grid points to the position of the macroparticle.

The number of points used for interpolating the function is something that will be tested when the code is developed. Using too few points results in the derivatives of the function being inaccurately calculated. Using too many points results in not

only an increased computation time, but also less accurate results. This is because the interpolation becomes overfitted to the number of points, no longer accurately representing the fields between the grid points. This means there is an ideal number of points to get the most accurate interpolation.

7.4 How to numerically validate the 1.5D PIC code

Once the simulation has been developed, initial testing will examine the basic physical phenomena of a klystron, to ensure that the code works at a proof-of-principle level. This will involve testing the accelerating cavities of the klystron, to verify bunching occurs as expected. It is important to test the final cavity of the klystron, where the particles are decelerated, to verify that they radiate the electromagnetic radiation into the cavity as expected.

One aspect of the code that needs to be tested is how many macroparticles are appropriate for modelling a bunch. For the moments to be accurately modelled, the variation in the field across the extent the macroparticle represents (the width of the model functions used for reconstructing charge and current) will need to be small (figure 4.1). By increasing the number of macroparticles, each one will have a smaller width in the z space, meaning the variation of the fields across each macroparticle will be smaller. This will need to be balanced against the extra computational load from tracking more macroparticles. Part of the initial testing will be to gain intuition about the correct number of macroparticles. As the macroparticles represent rings of charge, adding more macroparticles will not affect the accuracy of the moment tracking in r space. This means that if there is a lot of variation in the radial fields, the moment tracking method can only be improved by including more moments.

It is difficult to check standard conserved quantities within the moment tracking PIC code. In a standard PIC code, energy will be conserved. Whilst this PIC code should conserve energy, it is difficult to verify this as it is unknown how to calculate the energy of a set of moments. As previously shown, the moment tracking PIC method should conserve emittance in the drift spaces of the klystron. It will not conserve emittance whilst being accelerated and decelerated, as these forces are not conservative, so Liouville's theorem is not valid [94, 95].

No additional charge is added to a PIC code from tracking moments. This is because when the charge and current is deposited to the grid, the reconstructed or projected charge has the same monopole moment as the original distribution, which corresponds to the same total charge. This does not mean charge is conserved in total (in general PIC codes do not conserve charge), because of errors associated with using a discretised grid. Whilst it is not known if the moment tracking PIC code presented in this thesis will also suffer from this issue, it is suspected it will. The extra charge created from the discretisation can be reduced through a process called *divergence cleaning* [109]. In a standard PIC code using Cartesian coordinates, it is possible to use shape functions devised by Villasenor and Buneman, and later Esirkepov [110, 111] that conserve charge exactly. These do not exist in this approach, since there are no shape functions for depositing charge. Despite this, for modelling a PIC code in cylindrical coordinates, standard PIC codes cannot use these charge conserving shape functions, since they do not work in curvilinear coordinates.

It is not known what the appropriate choice of grid size will be. The electromagnetic field solver is limited by the Courant-Friedrichs-Lewy condition [112],

$$(\Delta t)^2 \leq \left(\frac{1}{(\Delta r)^2} + \frac{1}{(\Delta z)^2} \right)^{-1}. \tag{7.4.1}$$

This limits the maximum time step used in a moment tracking PIC code, as the FDTD algorithm is still being used to update the fields. In a typical plasma, the maximum spatial grid size is typically given by the Debye length of the plasma

(the maximum width the electrons and ions oscillate from each other). It is not known if the Debye length of the plasma will be the limiting factor for the spatial resolution of a PIC code with moment tracking. The dominating source of error in the moment tracking is when the field cannot be accurately modelled by a small number of derivatives at the macroparticle centre. This means that one limit for the cell size will be based on the density of grid points required to accurately find the derivatives of the fields. Since the macroparticle has an internal structure, it needs to span over several cells. This allows the extra structure from tracking the moments to be reflected in the deposited charge and current. This is in contrast to existing methods, which deposit over several cells to reduce numerical instability [109, 113]. It may be that in cases where the fields can be approximated using a low resolution grid (figure 4.1a), that it is possible for a single macroparticle to be larger than the Debye length of the plasma. By tracking the moments, information about the structure within the macroparticle is known, and this affects how the charge and current will be deposited onto the grid points. By tracking moments, it may be that the effects of instabilities generated from using a finite grid (aliasing instabilities) [54, 109, 114, 115] are not as significant.

7.5 Future features

7.5.1 Considerations to be made when scaling the moment tracking approach to higher order moments

The multipoles in this thesis have all been truncated at the quadrupole level. As previously discussed, this can cause significant issues due to the truncation error. It is likely a practical PIC code using moment tracking will want to operate at at least the hexadecapole (fourth order) level. As shown in tables 1.1 and 7.1, this creates substantially more ODE's to solve each timestep for updating the moments, as well as more variables to store in memory. These cannot be avoided, and are one

of the expenses of using more moments in a PIC code. Optimisations can be made however, by parallelising the code to allow multiple macroparticles to be updated simultaneously.

To parallelise a standard PIC code, the grid is split between multiple CPU cores, with each core updating the macroparticles within its section of the grid in parallel [37]. This approach might not work for the moment tracking PIC code method, since it is required that each macroparticle spreads over several grid points. Instead, it might be more practical to allocate different macroparticles to individual cores. In the extreme case that there are only a small number of macroparticles, each with a very large number of moments, then multiple cores can run on a single macroparticle. The moment updating equations are all independent for each macroparticle, so can be run in parallel. Additionally, depositing over each grid point can be run independently, with different cores depositing the current onto different parts of the grid. Whilst the updating and depositing can be parallelised, the linear system of equations needed to solve both the projection and reconstruction methods have to be done on a single core. It may be possible to optimise this step for certain model functions, such that solving the linear system of equations can be avoided.

7.5.2 Modifying the transport equations to add internal structure to a macroparticle

In a low velocity RF system, such as the early stages of a particle accelerator or a klystron, space-charge effects within the bunch mean that the bunch blows itself apart radially over time. In real systems, this is suppressed by surrounding the system with a solenoid. This creates a constant B_z field through the cavity. This field, combined with the small u_r component, creates a angular velocity, causing the particles to move in small circles. The net effect of this results in the average radial position of the whole bunch oscillating over time. The effect of a bunch radially oscillating is known as *scalloping* [116, 117]. It is not possible to simulate scalloping

with the 1.5D model presented in this chapter. This is because the 1.5D model assumes there is no motion in the angular direction, so the u_ϕ component of the Lorentz force is not calculated, therefore no scalloping from the solenoid can occur. A full 3+3D PIC code would not have this issue, since angular forces are calculated. In order to include scalloping in the 1.5D code, a modification to the transport equations must be made, to allow for forces within a macroparticle to be included.

Consider the transport equation $\partial_a \mathfrak{J}^a = 0$, corresponding to the conservation of charge. All that matters for the conservation of charge is the conservation of the current across the spatial coordinates, rather than both spatial and velocity coordinates. Therefore the 4-current $\mathfrak{T}^\mu(t, \underline{x})$ needs to be conserved, rather than the full 7-current. This means that it is possible to create a more general transport equation that allows internal structure within a macroparticle to be modelled. This internal structure has already been modelled in previous moment tracking methods, for the specific cases of muon cooling (reduction of the emittance of a muon beam) [42], and space-charge [45]. By finding a general formula for effects that can be added to the multipoles, it will be possible to add other effects to the macroparticles, including scalloping. This section outlines how the transport equations can be modified to include an the arbitrary field to simulate internal structure, but it does not give any examples of testing these internal structures, as this is future work.

Given that only 4-current matters for conservation of charge, then the conservation of charge becomes

$$\partial_\mu \mathfrak{T}^\mu = 0 \tag{7.5.1}$$

where the sums are only over $0, \ldots, 3$. This equation is the continuity equation in electrodynamics, and follows from the definition of 4-current from the electromagnetic field tensor $\mathfrak{F}^{\mu\nu}$,

$$\mathfrak{T}^\mu = \partial_\nu \mathfrak{F}^{\mu\nu} \tag{7.5.2}$$

where $\mathfrak{F}^{\mu\nu}$ is antisymmetric. This gives

$$\partial_\mu \mathfrak{T}^\mu = \partial_\mu \partial_\nu \mathfrak{F}^{\mu\nu} = 0 \tag{7.5.3}$$

because of the antisymmetry [118].

Using the definition of $\mathfrak{T}^\mu$ from $\mathfrak{J}^\mu$ gives

$$\partial_\mu \int_{\mathcal{E}_p} \mathfrak{J}^\mu d^3u = \int_{\mathcal{E}_p} \partial_\mu \mathfrak{J}^\mu d^3u = 0 \tag{7.5.4}$$

since an integral over velocity space and differentiation over spatial coordinates commute. For the velocity components, use Stoke's theorem, and that the flux of $\mathfrak{J}^{\mu+3}$ through $\mathcal{E}_p$ is equal to $\mathfrak{J}^{\mu+3}$ evaluated at the boundaries of $\mathcal{E}_p$. Since $\mathfrak{J}^a$ has compact support from its definition (equation (2.3.1)), this vanishes, and, as such,

$$\int_{\mathcal{E}_p} \partial_{\underline{\mu}+3}\, \mathfrak{J}^{\underline{\mu}+3} = 0. \tag{7.5.5}$$

Combining equations (7.5.4) and (7.5.5) gives the the modified transport equation,

$$\partial_a \mathfrak{J}^a = \mathfrak{B}, \quad \int_{\mathcal{E}_p} \mathfrak{B}\, d^3u = 0, \tag{7.5.6}$$

where $\mathfrak{B}$ is some function chosen to add internal structure to the macroparticle.

By squeezing both sides, this can be promoted to the Ellis representation of a distribution,

$$\partial_a \mathcal{J}^a = \mathcal{B}, \quad \int_{\mathcal{E}_p} \mathcal{B}\, d^3u = 0, \tag{7.5.7}$$

where $\mathcal{B}$ is a distribution found by squeezing $\mathfrak{B}$. This can equivalently be defined through the action on a test form λ,

$$\int_{\mathcal{E}} \mathcal{J}^a \partial_a \lambda\, dt = \mathcal{B}, \quad \int_{\mathcal{E}_p} \mathcal{B}\, d^3u = 0. \tag{7.5.8}$$

This means that by suggesting some scalar field $\mathfrak{B}$ containing extra terms to add to the transport equation, and squeezing this into the distributional $\mathcal{B}$, it is possible to add internal dynamics into the moment tracking equations. Alternatively it may be possible to suggest some $\mathcal{B}$ that is not derived through squeezing $\mathfrak{B}$, based on the physical features one is aiming to simulate.

Chapter 8

A geometric interpretation of the multipole transport equations

In this chapter, the measure, the Vlasov equation, the transport equations, and the coordinate transformations of multipoles are presented, using the language of differential geometry and de Rham currents [68, 69]. Whilst several results necessary to prove the differential equations for the moments are shown in this chapter, they can be justified physically through the conservation of charge. Because of this, if a reader is unfamiliar with the language of differential geometry, this section is not necessary to understand the content of the thesis.

The language of differential geometry allows the measure and the conservation of charge to be calculated on the tangent bundle, then these results pulled back onto $\mathcal{E}$. This is advantageous as the calculations required on the tangent bundle are much simpler than those on $\mathcal{E}$. By working on the tangent bundle it provides results that are easier to calculate, and easier for the reader to understand.

By using the language of de Rham currents there is a clearer split between the $V^{\underline{a}}$ and $X^{\underline{ab}}$ components. This split makes it simpler to isolate each term when performing complex calculations that mix both terms, such as during coordinate

transformations. It also means the evolution of the moments can be described in a coordinate free way. This is in contrast to the integral representation of moments (e.g. equation (3.1.7)), which is highly dependent on the coordinate system, in particular the choice of time slicing. The Ellis method also requires a coordinate system to define the action on a test form.

Rather than integrating over the velocity space, the projection can be defined through the creation of a map from $\mathcal{E}$ to M. This map gives a geometric way to explain the relationship between the 7-current and the 4-current. Additionally, by working with differential forms instead of a set of scalar fields, it is clearer to see why the velocity components of $\mathfrak{J}^a$ and $\mathcal{J}^a$ are not considered when projecting to the base manifold.

8.1 Operations on the tangent bundle

Before finding quantities on the seven-dimensional time-phase space, the Vlasov equation and the measure shall be derived on the tangent bundle. By finding the measure on the tangent bundle, the measure on $\mathcal{E}$ can be derived. Additionally, in order to prove the conservation of charge (equation (2.3.5)), it must be proven on the tangent bundle first. This result is then pulled back onto $\mathcal{E}$ in section 8.2.

Consider a manifold M, with metric g and tangent bundle TM. The bundle of p-forms on TM is written $\Lambda^p TM$ such that a specific p-form (field) is denoted as $\alpha \in \Gamma\Lambda^p TM$. A vector field is denoted as $A \in \Gamma TTM$. The coordinates on the tangent bundle will be denoted $(x^\mu, \dot{x}^\mu)$.

A scalar lift is defined as

$$\dot{h} \in \Gamma\Lambda^0(TM), \quad \dot{h}|_{\underset{\sim}{u}} = \underset{\sim}{u}\langle h\rangle \text{ for } \underset{\sim}{u} \in TM, \quad h \in \Gamma\Lambda^0 M \tag{8.1.1}$$

where angled brackets represent the evaluation of a vector and a scalar field, and

$\underset{\sim}{u} \in TM$ is a vector at a point. In terms of coordinates, this is given by

$$\dot{h} = \dot{x}^\mu \frac{\partial h}{\partial x^\mu}. \tag{8.1.2}$$

Let $C_{TM} : \mathbb{R} \to M$, and be parameterised by τ, an affine parameter. The prolongation of C_{TM} onto TM, η_{TM}, gives a curve defined as

$$\eta^\mu_{TM}(\tau) = C^\mu_{TM}(\tau) = x^\mu|_{\eta_{TM}(\tau)}, \quad \eta^{\mu+4}_{TM}(\tau) = \dot{C}^\mu_{TM}(\tau) = \dot{x}^\mu|_{\eta_{TM}(\tau)}. \tag{8.1.3}$$

Let W_{TM} be the Vlasov vector field on TM. As on $\mathcal{E}$, η_{TM} is an integral curve of W_{TM}, so

$$W^\mu_{TM}|_{\eta_{TM}} = \frac{dC^\mu(\tau)}{d\tau}, \quad W^{\mu+4}_{TM}|_{\eta_{TM}} = \frac{d^2C^\mu(\tau)}{d\tau}. \tag{8.1.4}$$

To solve these derivatives, note that since τ is affine, it solves the geodesic equation with the Lorentz force,

$$\nabla_{\dot{C}} \dot{C} = \frac{q}{m} \widetilde{i_{\dot{C}} F}, \tag{8.1.5}$$

where $\nabla_{\dot{C}}\dot{C}$ represents a covariant derivative with respect to a vector field, and a tilde over a quantity represents the metric dual. This means

$$W^\mu_{TM}|_{\eta_{TM}} = \dot{x}^\mu|_{\eta_{TM}}, \quad W^{\mu+4}_{TM}|_{\eta_{TM}} = -\left(\Gamma^\mu_{\nu\rho}\dot{x}^\nu\dot{x}^\rho + \frac{q}{m}F_{\nu\rho}g^{\mu\nu}\dot{x}^\rho\right). \tag{8.1.6}$$

Combining these gives the Vlasov equation on TM,

$$W_{TM} = \dot{x}^\mu \frac{\partial}{\partial x^\mu} - \left(\Gamma^\mu_{\nu\rho}\dot{x}^\nu\dot{x}^\rho + \frac{q}{m}F_{\nu\rho}g^{\mu\nu}\dot{x}^\rho\right)\frac{\partial}{\partial \dot{x}^\mu}. \tag{8.1.7}$$

To find the natural measure on TM, begin by considering the cotangent bundle T^*M. The cotangent bundle has coordinates (x^μ, p^μ) where p^μ are the conjugate coordinates, and have the property

$$p_\mu|_\alpha = \alpha_\mu \tag{8.1.8}$$

where $\alpha = \alpha_\mu dx^\mu \in \Gamma\Lambda^1 M$. The canonical 1-form on the cotangent bundle is given by

$$\theta = p_\mu dx^\mu. \tag{8.1.9}$$

The symplectic 2-form is given by

$$\omega = d\theta = dp_\mu \wedge dx^\mu. \tag{8.1.10}$$

The measure on the cotangent bundle is given by the wedge product of the symplectic 2-form,

$$\Omega_{T^*M} = \omega^4 = \omega \wedge \omega \wedge \omega \wedge \omega = (-1)dp_0 \wedge \ldots \wedge dp_3 \wedge dx^0 \wedge \ldots \wedge dx^3 \tag{8.1.11}$$

where the factor of -1 comes from a choice of orientation such that the final measure Ω_{TM} will be a positive quantity (since the determinant of the metric is negative).

Let $\beta : TM \to T^*M$. For differential forms the pullback of β, β^*, is the metric dual. The measure on TM is given by pulling back the measure on the cotangent bundle,

$$\Omega_{TM} = \beta^*(\Omega_{T^*M}). \tag{8.1.12}$$

In terms of coordinates, the measure on TM is given by

$$\Omega_{TM} = -\det(g)dx^0 \wedge \ldots \wedge dx^3 \wedge d\dot{x}^0 \ldots \wedge d\dot{x}^3 = dx^{[0,1,2,3]} \wedge d\dot{x}^{[0,1,2,3]} \tag{8.1.13}$$

where

$$dx^{[0,1,2,3]} = dx^0 \wedge dx^1 \wedge dx^2 \wedge dx^3. \tag{8.1.14}$$

Proof. To calculate the pullback β^*, let $V \in \Gamma TM = \beta^*(\alpha)$, then

$$\beta^*(p_\mu|_\alpha) = \beta^*(\alpha_\mu) \tag{8.1.15}$$

$$(\beta^* p_\mu)|_V = V^\nu g_{\mu\nu} \tag{8.1.16}$$

$$\beta^*(p_\mu) = \dot{x}^\nu g_{\mu\nu} \tag{8.1.17}$$

where the last step follows from the definition of the scalar lift. Since the pullback commutes with the exterior derivative, the pullback of dp_μ is

$$\beta^*(dp_\mu) = d\beta^* p_\mu = d(\dot{x}^\nu g_{\mu\nu}) = g_{\mu\nu} d\dot{x}^\nu + \dot{x}^\nu \partial_\rho(g_{\mu\nu}) dx^\rho. \tag{8.1.18}$$

The pullback of dx^μ is simply $\beta^*(dx^\mu) = dx^\mu$. Using these pullbacks, the measure on TM can be found,

$$\Omega_{TM} = \beta^*(\Omega_{T^*M}) = \beta^*(-dp_0 \wedge \ldots \wedge dp_3 \wedge dx^0 \wedge \ldots \wedge dx^3) \tag{8.1.19}$$

$$= -\beta^*(dp_0) \wedge \ldots \wedge \beta^*(dp_3) \wedge \beta^*(dx^0) \wedge \ldots \wedge \beta^*(dx^3) \tag{8.1.20}$$

$$= -g_{\mu 0} d\dot{x}^0 \wedge \ldots \wedge g_{\mu 3} d\dot{x}^3 \wedge dx^0 \wedge \ldots \wedge dx^3 \tag{8.1.21}$$

$$= -g_{\mu 0} \ldots g_{\mu 3} d\dot{x}^0 \wedge \ldots \wedge d\dot{x}^3 \wedge dx^0 \wedge \ldots \wedge dx^3. \tag{8.1.22}$$

It is assumed that the order of the $d\dot{x}$ terms is increasing (if this is not assumed this approach is still valid, but the signature of the permutations needed to order the terms needs to be considered). This means that

$$g_{\mu 0} \ldots g_{\mu 3} d\dot{x}^0 \wedge \ldots \wedge d\dot{x}^3 = \det(g) d\dot{x}^0 \wedge \ldots \wedge d\dot{x}^3. \tag{8.1.23}$$

The last step is to permute the $d\dot{x}^\mu$ terms to the end of the wedge product, each term is moved through four terms, and this is done four times, so

$$\Omega_{TM} = -\det(g) d\dot{x}^0 \wedge \ldots \wedge d\dot{x}^3 \wedge dx^0 \wedge \ldots \wedge dx^3 \tag{8.1.24}$$

$$= \det(g)(-1)(-1)^{16} dx^0 \wedge \ldots \wedge dx^3 \wedge d\dot{x}^0 \wedge \ldots \wedge d\dot{x}^3 \tag{8.1.25}$$

$$= -\det(g) dx^0 \wedge \ldots \wedge dx^3 \wedge d\dot{x}^0 \wedge \ldots \wedge d\dot{x}^3. \tag{8.1.26}$$

as required. □

Using this measure, it can be shown that on the tangent bundle,

$$L_{W_{TM}} \Omega_{TM} = 0. \tag{8.1.27}$$

Proof. Begin by considering Cartan's identity, and that Ω_{TM} is a top-form, so

$$L_{W_{TM}}\Omega_{TM} = di_{W_{TM}}\Omega_{TM} \tag{8.1.28}$$

$$= -di_{W_{TM}}\det(g)dx^{[0,1,2,3]} \wedge d\dot{x}^{[0,1,2,3]} \tag{8.1.29}$$

$$= -dW^{\mu}_{TM}\det(g)i_{\mu}dx^{[0,1,2,3]} \wedge d\dot{x}^{[0,1,2,3]} \tag{8.1.30}$$

$$\quad - dW^{\mu+4}_{TM}\det(g)dx^{[0,1,2,3]} \wedge i_{\mu+4}d\dot{x}^{[0,1,2,3]}$$

$$= -\partial_{\mu}(W^{\mu}_{TM}\det(g))dx^{[0,1,2,3]} \wedge d\dot{x}^{[0,1,2,3]} \tag{8.1.31}$$

$$\quad - \partial_{\mu+4}(W^{\mu+4}_{TM}\det(g))dx^{[0,1,2,3]} \wedge d\dot{x}^{[0,1,2,3]}$$

$$= -\left(\partial_{\mu}(W^{\mu}_{TM}\det(g)) + \det(g)\partial_{\mu+4}(W^{\mu+4}_{TM})\right) dx^{[0,1,2,3]} \wedge d\dot{x}^{[0,1,2,3]}. \tag{8.1.32}$$

Since $W^{\mu}_{TM} = \dot{x}^{\mu}$,

$$\partial_{\mu}(W^{\mu}_{TM}\det(g)) = W^{\mu}_{TM}\partial_{\mu}(\det(g)) = 2\dot{x}^{\mu}\det(g)\Gamma^{\nu}_{\mu\nu}. \tag{8.1.33}$$

For the velocity components of the Vlasov equations, it is clearer to split the field into the electromagnetic part and the gravity part,

$$\partial_{\mu+4}W^{\mu+4}_{TM,\mathrm{EM}} = \frac{q}{m}\partial_{\mu+4}\left(F^{\mu}{}_{\nu}\dot{x}^{\nu}\right) = \frac{q}{m}F^{\mu}{}_{\nu}\delta^{\nu}_{\mu} = \frac{q}{m}F^{\mu}{}_{\mu} = 0 \tag{8.1.34}$$

since F is antisymmetric. For the gravity part,

$$\det(g)\partial_{\mu+4}W^{\mu+4}_{TM,\mathrm{grav}} = -\det(g)\partial_{\mu+4}\left(\Gamma^{\mu}_{\nu\rho}\dot{x}^{\nu}\dot{x}^{\rho}\right) = -2\det(g)\Gamma^{\mu}_{\nu\mu}\dot{x}^{\nu} \tag{8.1.35}$$

summing these together shows $L_{W_{TM}}\Omega_{TM} = 0$, as required. □

In this section the Vlasov field is parameterised by τ, an affine parameter, such that the motion of the world line C was described by the geodesic equation with the Lorentz force (equation (8.1.5)). This is in contrast to the Vlasov equation derived in section 2.2, which is parameterised by t, the global lab time coordinate. A Vlasov equation parameterised by τ is chosen to make the calculations easier to read, as there are less terms in this parameterisation. To go from a Vlasov field parameterised by τ to one parameterised by t, there are two possibilities. The Vlasov

field can be derived by considering the flow lines of η_{TM}, where the parameterisation is changed to use t instead of τ. Alternatively, to make it clearer that the results hold in both parameterisations, it is possible to calculate the Vlasov field between two parameterisations directly, by considering it as a spray. Chapter 12 of reference [119] explains this procedure. An explanation of this procedure is also available in reference [120].

8.2 Seven-dimensional time-phase space

Consider a scalar field $t \in \Gamma\Lambda^0 M$, which represents a global time. The coordinate time hypersurface is defined by this scalar field, defined such that

$$\mathcal{E} = \{Z \in TM \mid Z\langle t\rangle = 1\}\,. \tag{8.2.1}$$

As previously discussed, different time slicings will give different hypersurfaces. Using the definition of scalar lifts, equation (8.2.1) is equivalent to the condition $\dot{t} = 1$. The spatial coordinates (x^μ) are always chosen such that $x^0 = t$. Equation (8.2.1) means the natural choice of velocity coordinates on $\mathcal{E}$ are $(v^{\underline{\mu}})$. This is because in this choice of coordinates,

$$\dot{x}^0|_\eta = \left.\frac{dC^0}{dt}\right|_\eta = \left.\frac{dt}{dt}\right|_\eta = 1, \tag{8.2.2}$$

as required.

To find the Vlasov equation on $\mathcal{E}$, there are two possible ways to calculate it. The first is to use the definition

$$i_{W_\mathcal{E}}\mathcal{E}^*(\alpha) = \mathcal{E}^*(i_{W_{TM}}(\alpha)), \tag{8.2.3}$$

and the second is to calculate the prolongation of C directly on $\mathcal{E}$. Both approaches give the same result as the Vlasov equation calculated in section 2.2, with the second option being identical to the approach in section 2.2.

As stated in section 2.1, all integrals must contain a measure. The measure on $\mathcal{E}$ is found by pulling back the measure on TM,

$$\Omega_{\mathcal{E}} = \mathcal{E}^*(i_{\mathcal{V}}\Omega_{TM}) \tag{8.2.4}$$

where $\mathcal{V}$ is the vertical vector field

$$\mathcal{V} = \dot{x}^\mu \frac{\partial}{\partial \dot{x}^\mu} \tag{8.2.5}$$

and $\mathcal{E} : \mathcal{E} \to TM$. Equations (8.2.3) and (8.2.4) imply

$$L_{W_{\mathcal{E}}}\Omega_{\mathcal{E}} = 0. \tag{8.2.6}$$

Proof. The measure on $\mathcal{E}$ is given by

$$\Omega_{\mathcal{E}} = \mathcal{E}^*(i_{\mathcal{V}}\Omega_{TM}). \tag{8.2.7}$$

This means

$$L_{W_{\mathcal{E}}}\Omega_{\mathcal{E}} = L_{W_{\mathcal{E}}}\mathcal{E}^*(i_{\mathcal{V}}\Omega_{TM}). \tag{8.2.8}$$

Using equation (8.2.3),

$$L_{W_{\mathcal{E}}}\Omega_{\mathcal{E}} = \mathcal{E}^*(L_{W_{TM}} i_{\mathcal{V}}\Omega_{TM}). \tag{8.2.9}$$

Now using the identity

$$[L_X, i_Y] = i_{[X,Y]} \tag{8.2.10}$$

for all vector fields X and Y,

$$L_{W_{TM}} i_{\mathcal{V}} = i_{\mathcal{V}} L_{W_{TM}} - i_{[\mathcal{V}, W_{TM}]}. \tag{8.2.11}$$

To calculate this Lie bracket, consider $[\mathcal{V}, W_{TM}]$ acting on the scalar fields x^μ and $\dot{x}^\mu$ separately,

$$[\mathcal{V}, W_{TM}]\langle x^\mu \rangle = \mathcal{V}\langle W_{TM}\langle x^\mu \rangle\rangle - W_{TM}\langle \mathcal{V}\langle x^\mu \rangle\rangle \tag{8.2.12}$$

$$= \mathcal{V}\langle \dot{x}^\mu \rangle - (0) \tag{8.2.13}$$

$$= \dot{x}^\mu \tag{8.2.14}$$

and acting on $\dot{x}^\mu$,

$$[\mathcal{V}, W_{TM}]\langle\dot{x}^\mu\rangle = \mathcal{V}\langle W_{TM}\langle\dot{x}^\mu\rangle\rangle - W_{TM}\langle\mathcal{V}\langle\dot{x}^\mu\rangle\rangle \tag{8.2.15}$$

$$= \mathcal{V}\left\langle \frac{q}{m}F^\mu{}_\nu\dot{x}^\nu - \Gamma^\mu_{\nu\rho}\dot{x}^\nu\dot{x}^\rho\right\rangle - W_{TM}\langle\dot{x}^\mu\rangle \tag{8.2.16}$$

$$= \frac{q}{m}F^\mu{}_\nu\mathcal{V}\langle\dot{x}^\nu\rangle - 2\Gamma^\mu_{\nu\rho}\dot{x}^\nu\mathcal{V}\langle\dot{x}^\rho\rangle - W_{TM}\langle\dot{x}^\mu\rangle \tag{8.2.17}$$

$$= \frac{q}{m}F^\mu{}_\nu\dot{x}^\nu - 2\Gamma^\mu_{\nu\rho}\dot{x}^\nu\dot{x}^\rho - W_{TM}\langle\dot{x}^\mu\rangle \tag{8.2.18}$$

$$= \frac{q}{m}F^\mu{}_\nu\dot{x}^\nu - 2\Gamma^\mu_{\nu\rho}\dot{x}^\nu\dot{x}^\rho - \frac{q}{m}F^\mu{}_\nu\dot{x}^\nu + \Gamma^\mu_{\nu\rho}\dot{x}^\nu\dot{x}^\rho \tag{8.2.19}$$

$$= -\Gamma^\mu_{\nu\rho}\dot{x}^\nu\dot{x}^\rho. \tag{8.2.20}$$

Summing these together gives

$$[\mathcal{V}, W_{TM}] = \dot{x}^\mu\frac{\partial}{\partial x^\mu} - \Gamma^\mu_{\nu\rho}\dot{x}^\nu\dot{x}^\rho\frac{\partial}{\partial\dot{x}^\mu} = W_{TM}|_{\text{in absence of charges}}. \tag{8.2.21}$$

This means

$$L_{W_{TM}}i_\mathcal{V} = i_\mathcal{V}L_{W_{TM}} - i_{W_{TM}|_{\text{in absence of charges}}}. \tag{8.2.22}$$

This gives

$$L_{W_\mathcal{E}}\Omega_\mathcal{E} = \mathcal{E}^*(L_{W_{TM}}i_\mathcal{V}\Omega_{TM}) \tag{8.2.23}$$

$$= \mathcal{E}^*(i_\mathcal{V}L_{W_{TM}}\Omega_{TM}) - \mathcal{E}^*(i_{W_{TM}|_{\text{in absence of charges}}}\Omega_{TM}) \tag{8.2.24}$$

$$= (0) - i_{W_\mathcal{E}|_{\text{in absence of charges}}}\mathcal{E}^*(\Omega_{TM}) \tag{8.2.25}$$

$$= 0 \tag{8.2.26}$$

since $L_{W_{TM}}\Omega_{TM} = 0$, and the pullback of a form of higher degree than the manifold the pullback it maps onto vanishes. This shows $L_{W_\mathcal{E}}\Omega_\mathcal{E} = 0$, as required. □

Equation (8.2.6) is the geometric equivalent to the condition $\partial_a(W^a\Omega_0) = 0$ (equation (2.3.5)) corresponding to the conservation of charge used in deriving the transport equations (section 2.3), and in showing the constancy of the monopole (section 3.2).

In terms of coordinates, defining the measure through equation (8.2.4) gives the measure on $\mathcal{E}$ as

$$\Omega_{\mathcal{E}} = -\det(g)dt \wedge dx^1 \wedge dx^2 \wedge dx^3 \wedge dv^1 \wedge dx^2 \wedge dv^3 = -\det(g)dt \wedge dx^{[1,2,3]} \wedge dv^{[1,2,3]} \tag{8.2.27}$$

since

$$\begin{aligned} i_{\mathcal{V}}\Omega_{TM} = -\det(g)\big(&\dot{x}^0 dx^{[0,1,2,3]} \wedge d\dot{x}^{[1,2,3]} - \dot{x}^1 dx^{[0,1,2,3]} \wedge d\dot{x}^{[0,2,3]} \\ &+\dot{x}^2 dx^{[0,1,2,3]} \wedge d\dot{x}^{[0,1,3]} - \dot{x}^2 dx^{[0,1,2,3]} \wedge d\dot{x}^{[0,1,2]}\big) \end{aligned} \tag{8.2.28}$$

and $x^0 = t$, and since, on $\mathcal{E}$, $\dot{x}^0 = 1$, $\mathcal{E}^*(d\dot{x}^0) = 0$, and $\dot{x}^{\underline{\mu}} = v^{\underline{\mu}}$. Combining these gives equation (8.2.27). From here, a coordinate transformation from 3-velocity $v^{\underline{\mu}}$ to 4-velocity $u^{\underline{\mu}}$ must be performed, because, as previously discussed, $u^{\underline{\mu}}$ is a more suitable choice of velocity coordinates to perform numerical simulations in.

Recall the definition of $u^{\underline{\mu}}$ (equation (2.1.1)). Rearranging this gives

$$v^{\underline{\mu}} = \frac{u^{\underline{\mu}}}{u^0}. \tag{8.2.29}$$

This means that, in order to find the coordinate transformation from 3-velocity $v^{\underline{\mu}}$ to 4-velocity $u^{\underline{\mu}}$, du^0 needs to be calculated. Consider the definition of u^0, from equation (2.1.2),

$$d(g_{\mu\nu}u^\mu u^\nu) = u^\mu u^\nu dg_{\mu\nu} + 2u^\nu g_{\mu\nu}du^\mu \tag{8.2.30}$$

$$= u^\mu u^\nu \frac{\partial g_{\mu\nu}}{\partial x^\rho}dx^\rho + 2u^\nu g_{\underline{\mu}\nu}du^{\underline{\mu}} + 2u^\nu g_{0\nu}du^0 \tag{8.2.31}$$

since $g_{\mu\nu}u^\mu u^\nu = -1$, the exterior derivative of this should vanish, so equation (8.2.31) can be rearranged to find du^0,

$$du^0 = -\frac{1}{2u^\nu g_{0\nu}}u^\mu u^\nu \frac{\partial g_{\mu\nu}}{\partial x^\rho}dx^\rho - \frac{1}{u^\nu g_{0\nu}}u^\nu g_{\underline{\mu}\nu}du^{\underline{\mu}} \tag{8.2.32}$$

$$= -\frac{1}{2u_0}u^\mu u^\nu \frac{\partial g_{\mu\nu}}{\partial x^\rho}dx^\rho - \frac{1}{u_0}u_{\underline{\mu}}du^{\underline{\mu}}. \tag{8.2.33}$$

Equations (8.2.27) and (8.2.33) imply

$$\Omega_{\mathcal{E}} = \frac{1}{(u^0)^4 u_0}\det(g)dt \wedge dx^{[1,2,3]} \wedge du^{[1,2,3]}. \tag{8.2.34}$$

Proof. Consider $dv^{\underline{\mu}} = d(u^{\underline{\mu}}/u^0)$, this gives

$$d\left(\frac{u^{\underline{\mu}}}{u^0}\right) = \frac{1}{u^0}du^{\underline{\mu}} - \frac{1}{(u^0)^2}u^{\underline{\mu}}du^0 \tag{8.2.35}$$

$$= \frac{1}{u^0}du^{\underline{\mu}} + \frac{1}{(u^0)^2}u^{\underline{\mu}}\left(\frac{1}{2u_0}u^\sigma u^\nu \frac{\partial g_{\sigma\nu}}{\partial x^\rho}dx^\rho + \frac{1}{u_0}u_{\underline{\nu}}du^{\underline{\nu}}\right) \tag{8.2.36}$$

$$= \frac{1}{u^0}du^{\underline{\mu}} + \frac{1}{(u^0)^2u_0}u^{\underline{\mu}}u^\sigma u^\nu \frac{\partial g_{\sigma\nu}}{\partial x^\rho}dx^\rho + \frac{1}{(u^0)^2u_0}u^{\underline{\mu}}u_{\underline{\nu}}du^{\underline{\nu}} \tag{8.2.37}$$

$$= \frac{1}{(u^0)^2u_0}\left(u^0u_0\delta^{\underline{\mu}}_{\underline{\nu}} + u^{\underline{\mu}}u_{\underline{\nu}}\right)du^{\underline{\nu}} + \frac{1}{(u^0)^2u_0}u^{\underline{\mu}}u^\sigma u^\nu \frac{\partial g_{\sigma\nu}}{\partial x^\rho}dx^\rho \tag{8.2.38}$$

$$= \frac{1}{u^0}\left(\delta^{\underline{\mu}}_{\underline{\nu}} + \frac{u^{\underline{\mu}}u_{\underline{\nu}}}{u^0u_0}\right)du^{\underline{\nu}} + \frac{1}{(u^0)^2u_0}u^{\underline{\mu}}u^\sigma u^\nu \frac{\partial g_{\sigma\nu}}{\partial x^\rho}dx^\rho. \tag{8.2.39}$$

Wedging these together, considering only the velocity parts (the spatial parts will cancel out when the full measure is considered since they will all be terms of the form $dx^1 \wedge dx^1 = 0$), and writing out all the terms in the sums

$$d\left(\frac{u^1}{u^0}\right) \wedge \ldots \wedge d\left(\frac{u^3}{u^0}\right) = \frac{1}{u^0}\left(\delta^1_{\underline{\nu}} + \frac{u^1u_{\underline{\nu}}}{u^0u_0}\right)du^{\underline{\nu}} \wedge \ldots \wedge \frac{1}{u^0}\left(\delta^3_{\underline{\rho}} + \frac{u^3u_{\underline{\rho}}}{u^0u_0}\right)du^{\underline{\rho}}$$

(8.2.40)

$$= \frac{1}{(u^0)^3}\left(\delta^1_{\underline{\nu}} + \frac{u^1u_{\underline{\nu}}}{u^0u_0}\right)\ldots\left(\delta^3_{\underline{\nu}} + \frac{u^3u_{\underline{\nu}}}{u^0u_0}\right)du^{\underline{\nu}} \wedge \ldots \wedge du^{\underline{\rho}}$$

(8.2.41)

$$= \frac{1}{(u^0)^3}\sum_{\underline{\nu}\in S_3}\varepsilon(\underline{\nu})\left(\delta^1_{\underline{\nu}} + \frac{u^1u_{\underline{\nu}}}{u^0u_0}\right)\ldots\left(\delta^3_{\underline{\nu}} + \frac{u^3u_{\underline{\nu}}}{u^0u_0}\right) \tag{8.2.42}$$

$$\times du^1 \wedge du^2 \wedge du^3$$

$$= \frac{1}{(u^0)^3}\det(A)\,du^{[1,2,3]} \tag{8.2.43}$$

where $A^{\underline{\mu}}_{\underline{\nu}} = \delta^{\underline{\mu}}_{\underline{\nu}} + u^{\underline{\mu}}u_{\underline{\nu}}/(u^0u_0)$. To calculate this determinant, consider

$$A^{\underline{\mu}}_{\underline{\nu}}u_{\underline{\mu}} = u_{\underline{\nu}} + u^{\underline{\mu}}u_{\underline{\nu}}u_{\underline{\mu}} = \left(1 + \frac{u^{\underline{\mu}}u_{\underline{\mu}}}{u^0u_0}\right)u_{\underline{\nu}} \tag{8.2.44}$$

so $u_{\underline{\nu}}$ is an eigenvalue of A. For all metrics considered in this thesis, the metric is only defined along the diagonal, which means that A is symmetric. Since A is symmetric, it must be diagonalisable, which means there is set of orthonormal basis

vectors $(u_{\underline{\nu}}, a_{\underline{\nu},1} \dots a_{\underline{\nu},3})$ that are the eigenvectors of A. Consider

$$A^{\underline{\mu}}_{\underline{\nu}} a_{\underline{\mu},1} = a_{\underline{\nu},1} + u^{\underline{\mu}} u_{\underline{\nu}} a_{\underline{\mu},1} = a_{\underline{\nu},1} \tag{8.2.45}$$

since $u^{\underline{\mu}} a_{\underline{\mu},1} = 0$ (they are part of an orthonormal basis). This means $a_{\underline{\nu},1}$, and the remaining basis vectors, are eigenvectors with eigenvalue 1. This means that

$$\det(A) = 1 + \frac{u^{\underline{\mu}} u_{\underline{\mu}}}{u^0 u_0} \tag{8.2.46}$$

$$= 1 + \frac{u^\mu u_\mu}{u^0 u_0} - \frac{u^0 u_0}{u^0 u_0} \tag{8.2.47}$$

$$= -\frac{1}{u^0 u_0} \tag{8.2.48}$$

since $u^\mu u_\mu = -1$. Using this in equation (8.2.43) gives equation (8.2.34), as required.

□

To find the measure on an individual hypersurface Σ, let $\Sigma : \Sigma \to \mathcal{E}$, then

$$\Omega_\Sigma = \Sigma^* \left(i_{\partial/\partial t} \Omega_{\mathcal{E}} \right). \tag{8.2.49}$$

In terms of coordinates this becomes

$$\Omega_\Sigma = \Sigma^* \left(i_{\partial/\partial t} \frac{1}{(u^0)^4 u_0} \det(g) dt \wedge dx^{[1,2,3]} \wedge du^{[1,2,3]} \right) \tag{8.2.50}$$

$$= \Sigma^* \left(\frac{1}{(u^0)^4 u_0} \det(g)\, dx^{[1,2,3]} \wedge du^{[1,2,3]} \right) \tag{8.2.51}$$

$$= \left(\frac{1}{(u^0)^4 u_0} \det(g) \right) \Big|_t \, dx^{[1,2,3]} \wedge du^{[1,2,3]} \tag{8.2.52}$$

matching equation (2.1.7).

In this section the measure was calculated in four dimensions, however the computational model discussed in chapter 7 is in three dimensions. This is not an issue, as whenever an integration occurs (when first taking the moments, and when depositing the current onto grid points), the integrand is a tensor density of weight 1. This means by working with densities throughout this thesis, issues about the correct measure when switching from four to three dimensions are avoided.

8.2.1 The transport equations

By using the language of differential geometry, a more geometric approach to understanding the origin of the transport equations can be found. The current 6-form $J \in \Gamma\Lambda^6\mathcal{E}$ (where as J is a differential form, it is not a density) is given by

$$J = \mathfrak{J}^a i_a d^7\xi \tag{8.2.53}$$

and conversely

$$\mathfrak{J}^a d^7\xi = J \wedge d\xi^a \tag{8.2.54}$$

where i_a represents an internal contraction with respect to the vector field $\partial/\partial\xi^a$.

Using equation (8.2.53), the current 6-form is related to the distribution function $\mathfrak{f}$ as

$$J = \mathfrak{f} W^a i_a d^7\xi, \tag{8.2.55}$$

and

$$\mathfrak{f}\, d^7\xi = J \wedge dt \tag{8.2.56}$$

since $W^0 = 1$. Recall the current 6-form J was the 6-form that was squeezed in section 4.2 to show the relationship between distributional multipoles and moments.

To find the dynamics of multipoles defined through differential forms, the equivalent of equations (4.3.1) and (4.3.2) for distributions are used,

$$dJ = 0, \quad i_W J = 0, \tag{8.2.57}$$

where $W = W^a\partial_a$. The $dJ = 0$ condition corresponds to the conservation of charge, and the $i_W J$ condition says that the flow lines of J are the integral curves of the Vlasov field. These equations are the same as equations (4.3.1) and (4.3.2), i.e. it is equivalent to the Ellis representation.

Proof. Using equation (8.2.53) and Cartan's identity

$$\begin{aligned} dJ &= d\big(\mathfrak{J}^a i_a d^7\xi\big) = d\big(\mathfrak{J}^a\big) \wedge i_a d^7\xi + \mathfrak{J}^a L_a d^7\xi \\ &= (\partial_b \mathfrak{J}^a) d\xi^b \wedge i_a d^7\xi + (0) = (\partial_b \mathfrak{J}^a)\delta^b_a d^7\xi \\ &= \partial_a \mathfrak{J}^a d^7\xi. \end{aligned} \tag{8.2.58}$$

This is zero if, and only if, $\partial_a \mathfrak{J}^a = 0$, so $dJ = 0$ is equivalent to equation (4.3.1). For the $i_W \mathfrak{J}$ term,

$$\begin{aligned} i_W J = i_W\big(\mathfrak{J}^a i_a d^7\xi\big) &= \mathfrak{J}^a W^b i_b i_a d^7\xi \\ &= \frac{1}{2}\left(\mathfrak{J}^a W^b + \mathfrak{J}^b W^a\right) i_b i_a d^7\xi + \frac{1}{2}\left(\mathfrak{J}^a W^b - \mathfrak{J}^b W^a\right) i_b i_a d^7\xi. \end{aligned} \tag{8.2.59}$$

Since $i_b i_a$ is antisymmetric, the symmetric part of $\mathfrak{J}^a W^b$ contracting against it vanishes, leaving

$$i_W J = \frac{1}{2}\left(\mathfrak{J}^a W^b - \mathfrak{J}^b W^a\right) i_b i_a d^7\xi. \tag{8.2.60}$$

This is zero if, and only if, $\mathfrak{J}^a W^b - \mathfrak{J}^b W^a = 0$, so $i_W J = 0$ is equivalent to equation (4.3.2). □

8.3 De Rham current representation of multipoles

8.3.1 Introducing de Rham current distributions

In this section we will work in 7-dimensional time-phase space, but all results generalise to an arbitrary dimension space. A distributional p-form is defined by its action on a test $(7-p)$-form $\phi \in \Gamma\Lambda^{7-p}\mathcal{E}$, this is a $(7-p)$-form with compact support. Given $\eta : \mathbb{R} \to \mathcal{E}$ is a closed embedding parameterised by t, the de Rham pushforward with respect to η of a p-form $\alpha \in \Gamma\Lambda^p\mathbb{R}$ is given by the distribution

$$\eta_\varsigma(\alpha)[\phi] = \int_{\mathbb{R}} \eta^*(\phi) \wedge \alpha. \tag{8.3.1}$$

The definition of the wedge product, Lie derivatives, internal contractions and exterior derivatives for an arbitrary distribution Ψ are defined as

$$\begin{aligned}
(\Psi_1 + \Psi_2)[\phi] &= \Psi_1[\phi] + \Psi_2[\phi], \\
(\beta \wedge \Psi)[\phi] &= \Psi[\phi \wedge \beta], \\
i_B\Psi[\phi] &= -(-1)^{\deg\phi}\Psi[i_B\phi], \\
d\Psi[\phi] &= -(-1)^{\deg\phi}\Psi[d\phi], \\
L_B\Psi[\phi] &= -\Psi[L_B\phi]
\end{aligned} \tag{8.3.2}$$

where $\beta \in \Gamma\Lambda^q\mathcal{E}$ and $B \in \Gamma T\mathcal{E}$. These properties are defined such that they agree with regular distributions [68, 69]. The space of all relevant distributions we are considering in this thesis are those that can be constructed from equation (8.3.1) and a finite number of applications of equation (8.3.2).

The de Rham pushforward commutes with the exterior derivative,

$$d\eta_\varsigma(\alpha) = \eta_\varsigma(d\alpha). \tag{8.3.3}$$

Proof. Consider $d\eta_\varsigma(\alpha)$ acting on a test form ϕ,

$$\begin{aligned}
d\eta_\varsigma(\alpha)[\phi] &= -(-1)^{\deg\phi}\eta_\varsigma(\alpha)[d\phi] \\
&= -(-1)^{\deg\phi}\int_{\mathbb{R}} \eta^*(d\phi)\wedge\alpha = -(-1)^{\deg\phi}\int_{\mathbb{R}} d\eta^*(\phi)\wedge\alpha
\end{aligned} \tag{8.3.4}$$

since the exterior derivative commutes with the pullback. Using the properties of the external derivative,

$$d\eta^*(\phi)\wedge\alpha = d(\eta^*(\phi)\wedge\alpha) - (-1)^{\deg\phi}\phi\wedge d\alpha. \tag{8.3.5}$$

Integrating $d(\eta^*(\phi)\wedge\alpha)$, and using Stoke's theorem

$$\int_{\mathbb{R}} d(\eta^*(\phi)\wedge\alpha) = \int_{\partial\mathbb{R}} \eta^*(\phi)\wedge\alpha = 0 \tag{8.3.6}$$

where $\partial_{\mathbb{R}}$ is the boundary of $\mathbb{R}$, and the integral vanishes since ϕ has compact support. This means

$$d\eta^*(\phi)\wedge\alpha = (-1)^2(-1)^{2\deg\phi}\int_{\mathbb{R}} \eta^*(\phi)\wedge d\alpha = \eta_\varsigma(d\alpha)[\phi] \tag{8.3.7}$$

as required. □

Given two vector fields $A \in \Gamma T\mathbb{R}$ and $B \in \Gamma T\mathcal{E}$, such that $B = \eta_*(A)$, then

$$i_B \eta_\varsigma(\alpha) = \eta_\varsigma(i_A \alpha). \tag{8.3.8}$$

Proof. Consider $i_B\eta_\varsigma(\alpha)$ acting on a test form ϕ,

$$\begin{aligned} i_B\eta_\varsigma(\alpha)[\phi] &= -(-1)^{\deg\phi}\eta_\varsigma(\alpha)[i_B\phi] \\ &= -(-1)^{\deg\phi}\int_{\mathbb{R}} \eta^*(i_B\phi)\wedge\alpha = -(-1)^{\deg\phi}\int_{\mathbb{R}} i_A\eta^*(\phi)\wedge\alpha. \end{aligned} \tag{8.3.9}$$

Consider

$$i_A\eta^*(\phi)\wedge\alpha = i_A(\eta^*(\phi)\wedge\alpha) - (-1)^{\deg\phi}\eta^*(\phi)\wedge i_A\alpha. \tag{8.3.10}$$

From the properties of the de Rham pushforward, the degree of $i_A\eta^*(\phi)\wedge\alpha = 1$, the dimension of $\mathbb{R}$. This means that the degree of $\eta^*(\phi)\wedge\alpha = 2$, so vanishes. Thus

$$i_B\eta_\varsigma(\alpha)[\phi] = (-1)^2(-1)^{2\deg\phi}\int_{\mathbb{R}} \eta^*(\phi)\wedge i_A\alpha = \eta_\varsigma(i_A\alpha)[\phi] \tag{8.3.11}$$

as required. □

The integral curves of the Vlasov vector field are a specific example of this for the case of η, with

$$i_W\eta_\varsigma(\alpha) = \eta_\varsigma(i_{\frac{d}{dt}}\alpha) \tag{8.3.12}$$

since W is tangent to η.

Combining the rules for exterior derivatives and internal contractions, using Cartan's identity, gives the properties of Lie derivatives with the de Rham pushforward,

$$L_B\eta_\varsigma(\alpha) = di_B\eta_\varsigma(\alpha) + i_B d\eta_\varsigma(\alpha) = \eta_\varsigma(di_A\alpha) + \eta_\varsigma(i_A d\alpha) = \eta_\varsigma(L_A\alpha). \tag{8.3.13}$$

The degree of the distribution $\eta_\varsigma(\alpha)$ is $6 + \deg(\alpha)$. Since $\mathbb{R}$ is a curve, the degree of α is either 0 or 1, so the degree of $\eta_\varsigma(\alpha)$ is either 6 or 7. Similarly to differential forms, it can be shown that an internal contraction decreases the degree by one and an exterior derivative increases the degree by one. Lie derivatives do not affect the degree of a distribution.

The order of a p-form distribution over η is defined as follows. If

$$\begin{gathered}\Psi[\lambda^{k+1}\phi] = 0 \text{ for all } \phi \in \Gamma\Lambda^q\mathcal{E} \text{ with compact support and} \\ \lambda \in \Gamma\Lambda^0\mathcal{E} \text{ such that } \eta^*(\lambda) = 0\end{gathered} \tag{8.3.14}$$

where η^* is the pullback, then the order of Ψ is at most k. Note that a quadrupole (a distribution of order two) also includes the dipole and the monopole terms. It can be shown that, using this definition, Lie derivatives and exterior derivatives can both increase order of a distribution by one. Internal contractions do not affect the order of a distribution.

A distribution Ψ of degree 6 is a semi-multipole of order at most l if

$$\Psi[\lambda^l d\mu] = 0 \quad \text{for all } \lambda, \mu \in \Gamma\Lambda^0\mathcal{E} \text{ such that } \eta^*(\lambda) = \eta^*(\mu) = 0. \tag{8.3.15}$$

This work concerns the dynamics of a semi-quadrupole, which is a semi-multipole $\mathcal{J}$ of order 2 and degree 6. In coordinates, this is denoted as

$$\mathcal{J} = \frac{1}{2}L_{\underline{a}}L_{\underline{b}}\eta_\varsigma(V^{\underline{ab}}) - i_{\underline{a}}L_{\underline{b}}\eta_\varsigma(X^{\underline{ab}}dt) - L_{\underline{a}}\eta_\varsigma(V^{\underline{a}}) + i_{\underline{a}}\eta_\varsigma(X^{\underline{a}}dt) + \eta_\varsigma(q) \tag{8.3.16}$$

where $L_{\underline{a}}$ is the Lie derivative with respect to $\partial_{\underline{a}}$, and $i_{\underline{a}}$ is the internal contraction with respect to $\partial_{\underline{a}}$. It is trivial to show this satisfies the definition of quadrupole (equation (8.3.14) with $k = 2$), and the definition of a semi-quadrupole (equation (8.3.15) with $l = 2$). Note in this representation of the semi-quadrupole, the $X^{\underline{ab}}$ and $V^{\underline{a}}$ terms are easier to distinguish by the additional internal contraction, as opposed to the Ellis representation (equation (4.1.1)), in which the separation between the terms was not as clear.

Similarly to the relationship between the 7-current and current 6-form, the de Rham current representation of a multipole can be related to the Ellis representation through the relationship

$$\mathcal{J} = \mathcal{J}^a i_a d^7\xi, \tag{8.3.17}$$

and conversely

$$\mathcal{J}^a = \mathcal{J} \wedge d\xi^a. \tag{8.3.18}$$

In $\mathcal{J}$, there is no term of the form $i_{\underline{a}} L_{\underline{b}} L_{\underline{c}} \eta_\varsigma (X^{\underline{abc}} dt)$ even though this contains two Lie derivatives. Similarly, there is no $X^{\underline{abc}}$ term in the Ellis representation. This term is included if $\mathcal{J}$ is a full quadrupole, as opposed to a semi-quadrupole. The advantage of the coordinate free approach used in this section is that it can be shown that the $X^{\underline{abc}}$ term vanishes in a coordinate system adapted to η, and hence $\mathcal{J}$ is a semi-quadrupole in this adapted coordinate system. Since the definition of a semi-multipole is coordinate free, $\mathcal{J}$ is a semi-quadrupole in every coordinate system. The coordinate free semi-multipoles written in this form correspond to the electric multipoles of ref. [68], and the semi-multipoles of ref. [69].

8.3.2 Dynamics of moments

Similarly to the Ellis representation, the dynamics for the de Rham current representation of the quadrupole are found by considering the transport equations for differential forms (equation (8.2.57)). Since they are linear, they can be directly applied to the distributions. The equations are

$$d\mathcal{J} = 0, \tag{8.3.19}$$

$$i_W \mathcal{J} = 0. \tag{8.3.20}$$

These are satisfied if, and only if,

$$\frac{dV^{\underline{ab}}}{dt} = X^{\underline{ab}} + X^{\underline{ba}}, \quad \frac{dV^{\underline{a}}}{dt} = X^{\underline{a}}, \quad \frac{dq}{dt} = 0, \tag{8.3.21}$$

$$X^{\underline{ab}} = V^{\underline{bc}} \partial_{\underline{c}} W^{\underline{a}}, \tag{8.3.22}$$

$$X^{\underline{c}} = V^{\underline{b}} \partial_{\underline{b}} W^{\underline{c}} + \frac{1}{2} V^{\underline{ab}} \partial_{\underline{a}} \partial_{\underline{b}} W^{\underline{c}}. \tag{8.3.23}$$

Proof. Assume equation (8.3.21)

$$d\mathcal{J} = \frac{1}{2} L_{\underline{a}} L_{\underline{b}} \eta_\varsigma \left(\frac{dV^{\underline{ab}}}{dt} dt \right) - L_{\underline{a}} L_{\underline{b}} \eta_\varsigma (X^{\underline{ab}} dt) - L_{\underline{a}} \eta_\varsigma \left(\frac{dV^{\underline{a}}}{dt} dt \right) + L_{\underline{a}} \eta_\varsigma (X^{\underline{a}} dt) + \eta_\varsigma \left(\frac{dq}{dt} \right). \tag{8.3.24}$$

Note that

$$L_{\underline{a}}L_{\underline{b}}\eta_\varsigma(X^{\underline{ab}}dt) = \frac{1}{2}L_{\underline{a}}L_{\underline{b}}\eta_\varsigma((X^{\underline{ab}} + X^{\underline{ba}}dt). \tag{8.3.25}$$

Inserting equation (8.3.21) gives $d\mathcal{J} = 0$.

Working in reverse, from equation (8.3.24), consider

$$d\mathcal{J}[\lambda], \tag{8.3.26}$$

where $\lambda \in \Gamma_0\Lambda^0\mathcal{E}$. Evaluating this gives

$$d\mathcal{J}[\lambda] = \frac{1}{2}\eta_\varsigma\left(\frac{dV^{\underline{ab}}}{dt}dt\right)[\partial_{\underline{a}}\partial_{\underline{b}}\lambda] - \eta_\varsigma(X^{\underline{ab}}dt)[\partial_{\underline{a}}\partial_{\underline{b}}\lambda] - \eta_\varsigma\left(\frac{dV^{\underline{a}}}{dt}dt\right)[\partial_{\underline{a}}\lambda] \tag{8.3.27}$$

$$+ \eta_\varsigma(X^{\underline{a}}dt)[\partial_{\underline{a}}\lambda] + \eta_\varsigma\left(\frac{dq}{dt}\right)[\lambda]$$

$$= \frac{1}{2}\eta_\varsigma\left(\left(\frac{dV^{\underline{ab}}}{dt} - X^{\underline{ab}} - X^{\underline{ba}}\right)dt\right)[\partial_{\underline{a}}\partial_{\underline{b}}\lambda] \tag{8.3.28}$$

$$+ \eta_\varsigma\left(\left(\frac{dV^{\underline{a}}}{dt} - X^{\underline{a}}\right)dt\right)[\partial_{\underline{a}}\lambda] + \eta_\varsigma\left(\frac{dq}{dt}dt\right)[\lambda]$$

since λ can be any value, the only way this can vanish for all λ is if equation (8.3.21) is true.

Moving onto $i_W\Psi = 0$, to calculate this proceed term by term through equation (8.3.16), and use the relations

$$i_W\eta_\varsigma(\alpha) = \eta_\varsigma(i_0\alpha), \qquad [L_a, i_W] = i_{[a,W]} \tag{8.3.29}$$

giving

$$i_W L_{\underline{a}}L_{\underline{b}}\eta_\varsigma(V^{\underline{ab}}) = (L_{\underline{a}}i_W L_{\underline{b}} - i_{[\underline{a},W]}L_{\underline{b}})\eta_\varsigma(V^{\underline{ab}}) \tag{8.3.30}$$

$$= (L_{\underline{a}}L_{\underline{b}}i_W - L_{\underline{a}}i_{[\underline{b},W]} - L_{\underline{b}}i_{[\underline{a},W]} + i_{[\underline{b},[\underline{a},W]]})\eta_\varsigma(V^{\underline{ab}}) \tag{8.3.31}$$

$$= (0) - L_{\underline{a}}i_c\eta_\varsigma(V^{\underline{ab}}\partial_{\underline{b}}W^c) - L_{\underline{b}}i_c\eta_\varsigma(V^{\underline{ab}}\partial_{\underline{a}}W^c) + i_c\eta_\varsigma(V^{\underline{ab}}\partial_{\underline{a}}\partial_{\underline{b}}W^c) \tag{8.3.32}$$

$$= -L_{\underline{a}}i_b(2V^{\underline{ac}}\partial_{\underline{c}}W^b) + i_c\eta_\varsigma(V^{\underline{ab}}\partial_{\underline{a}}\partial_{\underline{b}}W^c). \tag{8.3.33}$$

The sums over the W^c terms range over $0, \ldots, 6$. Since the coordinate time frame has $W^0 = 1$, the derivatives of this vanish, so

$$i_W L_{\underline{a}} L_{\underline{b}} \eta_\varsigma(V^{\underline{ab}}) = -L_{\underline{a}} i_{\underline{b}}(2V^{\underline{ac}} \partial_{\underline{c}} W^{\underline{b}}) + i_{\underline{c}} \eta_\varsigma(V^{\underline{ab}} \partial_{\underline{a}} \partial_{\underline{b}} W^{\underline{c}}). \tag{8.3.34}$$

For brevity, in the remaining terms the step

$$i_{[\underline{a}, W]} = i_c \partial_{\underline{a}} W^c = i_{\underline{c}} \partial_{\underline{a}} W^{\underline{c}} \tag{8.3.35}$$

shall be done implicitly.

Moving onto the $X^{\underline{ab}}$ term,

$$\begin{aligned} i_W i_{\underline{a}} L_{\underline{b}} \eta_\varsigma(X^{\underline{ab}} dt) &= -i_{\underline{a}} i_W L_{\underline{b}} \eta_\varsigma(X^{\underline{ab}} dt) && (8.3.36)\\ &= -(i_{\underline{a}} L_{\underline{b}} i_W - i_{\underline{a}} i_{[\underline{b}, W]}) \eta_\varsigma(X^{\underline{ab}} dt) && (8.3.37)\\ &= -i_{\underline{a}} L_{\underline{b}} i_W \eta_\varsigma(X^{\underline{ab}} dt) - i_{\underline{a}} i_{\underline{c}} \eta_\varsigma(X^{\underline{ab}} \partial_{\underline{a}} W^{\underline{c}} dt) && (8.3.38)\\ &= -i_{\underline{a}} L_{\underline{b}} \eta_\varsigma(X^{\underline{ab}}) - i_{\underline{a}} i_{\underline{c}} \eta_\varsigma(X^{\underline{ab}} \partial_{\underline{a}} W^{\underline{c}} dt). && (8.3.39) \end{aligned}$$

The dipole terms,

$$\begin{aligned} -i_W L_{\underline{a}} \eta_\varsigma(V^{\underline{a}}) + i_W i_{\underline{a}} \eta_\varsigma(X^{\underline{a}} dt) &= -L_{\underline{a}} i_W \eta_\varsigma(V^{\underline{a}}) + i_{[\underline{a}, W]} \eta_\varsigma(V^{\underline{a}}) - i_{\underline{a}} i_W \eta_\varsigma(X^{\underline{a}} dt) && (8.3.40)\\ &= (0) - i_{\underline{c}} \eta_\varsigma(X^{\underline{c}} - V^{\underline{a}} \partial_{\underline{a}} W^{\underline{c}}). && (8.3.41) \end{aligned}$$

Summing all these terms together gives

$$\begin{aligned} i_W \mathcal{J} &= \frac{1}{2} i_W L_{\underline{a}} L_{\underline{b}} \eta_\varsigma(V^{\underline{ab}}) - i_W i_{\underline{a}} L_{\underline{b}} \eta_\varsigma(X^{\underline{ab}} dt) - i_W L_{\underline{a}} \eta_\varsigma(V^{\underline{a}}) + i_W i_{\underline{a}} \eta_\varsigma(X^{\underline{a}} dt)\\ &= L_{\underline{a}} i_{\underline{b}} \eta_\varsigma(X^{\underline{ba}} - V^{\underline{ac}} \partial_{\underline{c}} W^{\underline{b}}) + i_{\underline{c}} i_{\underline{b}} \eta_\varsigma(X^{\underline{ab}} \partial_{\underline{a}} W^{\underline{c}} dt)\\ &\quad + i_{\underline{c}} \eta_\varsigma(\frac{1}{2} V^{\underline{ab}} \partial_{\underline{a}} \partial_{\underline{b}} W^{\underline{c}} + V^{\underline{a}} \partial_{\underline{a}} W^{\underline{c}} - X^{\underline{c}}). \end{aligned} \tag{8.3.42}$$

Lastly, note $i_{\underline{b}} i_{\underline{c}}$ is antisymmetric, so taking the antisymmetric part of $X^{\underline{ab}} \partial_{\underline{a}} W^{\underline{c}}$,

$$\begin{aligned} i_W \mathcal{J} &= L_{\underline{a}} i_{\underline{b}} \eta_\varsigma \left(X^{\underline{ba}} - V^{\underline{ac}} \partial_{\underline{c}} W^{\underline{b}}\right) + i_{\underline{c}} i_{\underline{b}} \eta_\varsigma \left(\frac{1}{2} \left(X^{\underline{ab}} \partial_{\underline{a}} W^{\underline{c}} - X^{\underline{ac}} \partial_{\underline{a}} W^{\underline{b}}\right) dt\right)\\ &\quad + i_{\underline{c}} \eta_\varsigma \left(\frac{1}{2} V^{\underline{ab}} \partial_{\underline{a}} \partial_{\underline{b}} W^{\underline{c}} + V^{\underline{b}} \partial_{\underline{b}} W^{\underline{a}} - X^{\underline{c}}\right). \end{aligned} \tag{8.3.43}$$

Assume equations (8.3.23) and (8.3.22) are true. Inserting $X^{\underline{ab}}$ and $X^{\underline{a}}$ into equation (8.3.43) gives

$$\begin{aligned} i_W \mathcal{J} = L_{\underline{a}} i_{\underline{b}} \eta_\varsigma \left(V^{\underline{ac}} \partial_{\underline{c}} W^{\underline{b}} - V^{\underline{ac}} \partial_{\underline{c}} W^{\underline{b}} \right) \\ + i_{\underline{c}} i_{\underline{b}} \eta_\varsigma \left(\frac{1}{2} \left(V^{\underline{ad}} \partial_{\underline{d}} W^{\underline{b}} \partial_{\underline{a}} W^{\underline{c}} - V^{\underline{ad}} \partial_{\underline{d}} W^{\underline{c}} \partial_{\underline{a}} W^{\underline{b}} \right) dt \right) \\ + i_{\underline{c}} \eta_\varsigma \left(\frac{1}{2} V^{\underline{ab}} \partial_{\underline{a}} \partial_{\underline{b}} W^{\underline{c}} + V^{\underline{b}} \partial_{\underline{b}} W^{\underline{a}} - V^{\underline{a}} \partial_{\underline{a}} W^{\underline{c}} - \frac{1}{2} V^{\underline{ac}} \partial_{\underline{c}} W^{\underline{b}} \right) = 0 \end{aligned} \quad (8.3.44)$$

since $V^{\underline{ab}}$ is symmetric.

For the reverse, it is trivial to see that the only solution where the terms with only one internal contraction vanish is if equations (8.3.23) and (8.3.22) are true. As shown in equation (8.3.44), if equation (8.3.22) is true, then the term with two internal contractions also vanishes, so equations (8.3.23) and (8.3.22) uniquely solve $i_W \mathcal{J} = 0$. □

As previously discussed, since $\mathcal{J}$ is a semi-quadrupole, there is no term of the form $L_{\underline{a}} L_{\underline{b}} i_{\underline{c}} \eta_\varsigma (X^{\underline{abc}} dt)$. If $\mathcal{J}$ was a full quadrupole, then the $X^{\underline{abc}}$ term vanishes under the $i_W \mathcal{J}$ condition anyway. Consider passing the internal contraction through the Lie derivatives, giving

$$i_W i_{\underline{a}} L_{\underline{b}} L_{\underline{c}} \eta_\varsigma (X^{\underline{abc}} dt) = i_{\underline{a}} L_{\underline{b}} L_{\underline{c}} \eta_\varsigma (X^{\underline{abc}}) + \text{ terms with one or fewer Lie derivatives.} \quad (8.3.45)$$

Compare this to equation (8.3.43), where there are no terms containing two Lie derivatives, this means that the $X^{\underline{abc}}$ term must vanish for the full quadrupole to be subject to the transport equations. Hence, any full quadrupole subject to the transport equations is a semi-quadrupole.

8.3.3 Coordinate transformations of moments where the time slicing is preserved

The coordinate transformations of the quadrupole can also be found using the language of distributions. The coordinate transformations for internal contractions are given by

$$i_{\underline{a}}\alpha = A^{\hat{b}}_{\underline{a}} i_{\hat{b}}\alpha = \hat{i}_{\hat{b}}(A^{\hat{b}}_{\underline{a}}\alpha). \tag{8.3.46}$$

For Lie derivatives the coordinate transformations are

$$L_{\underline{a}}\alpha = A^{\hat{b}}_{\underline{a}} L_{\hat{b}}\alpha = \hat{L}_{\hat{b}}(A^{\hat{b}}_{\underline{a}}\alpha) - \alpha \wedge \hat{L}_{\hat{b}} A^{\hat{b}}_{\underline{a}} = \hat{L}_{\hat{b}}(A^{\hat{b}}_{\underline{a}}\alpha) - \hat{i}_{\hat{b}}\left(dA^{\hat{b}}_{\underline{a}} \wedge \alpha\right) \tag{8.3.47}$$

where the hat over the Lie derivatives and internal contractions is to make it clear that these are taken with respect to $\hat{\partial}_{\hat{\underline{a}}}$ in the new coordinate system. Note that similarly to the transformation of $\partial_{\underline{a}}$, the indices in the transformed coordinate system run from $(0, \ldots, 6)$, whilst the original indices only ran from $(1, \ldots, 6)$. By using the coordinate transformation rules for Lie derivatives and internal contractions, the coordinate transformations for the semi-quadrupole can be found. This is equivalent to the coordinate transformations found through the Ellis representation, and is given by

$$\hat{\mathcal{J}} = \mathcal{J} = \frac{1}{2}\hat{L}_{\hat{a}}\hat{L}_{\hat{b}}\eta_{\varsigma}(\hat{U}^{\hat{a}\hat{b}}) - \hat{i}_{\hat{a}}\hat{L}_{\hat{b}}\eta_{\varsigma}(\hat{Y}^{\hat{a}\hat{b}}d\hat{t}) - \hat{L}_{\hat{a}}\eta_{\varsigma}(\hat{U}^{\hat{a}}) + \hat{i}_{\hat{\underline{a}}}\eta_{\varsigma}(\hat{Y}^{\hat{a}}d\hat{t}) + \eta_{\varsigma}(q) \tag{8.3.48}$$

where $\hat{U}^{\hat{a}\hat{b}}, \hat{Y}^{\hat{a}\hat{b}}, \hat{U}^{\hat{a}}$, and $\hat{Y}^{\hat{a}}$ are given by equation (4.4.7).

Proof. Consider the de Rham representation of the semi-quadrupole,

$$\mathcal{J} = \frac{1}{2}L_{\underline{a}}L_{\underline{b}}\eta_{\varsigma}(V^{\underline{ab}}) - L_{\underline{a}}i_{\underline{b}}\eta_{\varsigma}(X^{\underline{ab}}dt) - L_{\underline{a}}\eta_{\varsigma}(V^{\underline{a}}) + i_{\underline{a}}\eta_{\varsigma}(X^{\underline{a}}dt) + \eta_{\varsigma}(q). \tag{8.3.49}$$

Using equations (8.3.46) and (8.3.47) to calculate this coordinate transformation, and proceed term by term. For the double Lie derivative term, use the standard differential geometry result

$$L_U(fg) = fL_U g + gL_U f \quad \forall f, g \in \Gamma\Lambda^0\mathcal{E}, U \in \Gamma T\mathcal{E} \tag{8.3.50}$$

to find

$$L_{\underline{a}}L_{\underline{b}}\alpha = L_{\underline{a}}\left(\hat{L}_{\hat{d}}(A^{\hat{d}}_{\underline{b}}\wedge\alpha) - \hat{i}_{\hat{d}}(dA^{\hat{d}}_{\underline{b}}\wedge\alpha)\right) \tag{8.3.51}$$

$$= \hat{L}_{\hat{c}}\left(A^{\hat{c}}_{\underline{a}}\wedge\left(\hat{L}_{\hat{d}}(A^{\hat{d}}_{\underline{b}}\wedge\alpha) - \hat{i}_{\hat{d}}(dA^{\hat{d}}_{\underline{b}}\wedge\alpha)\right)\right) \tag{8.3.52}$$

$$\begin{aligned} &- \hat{i}_{\hat{c}}\left(dA^{\hat{c}}_{\underline{a}}\wedge\left(\hat{L}_{\hat{d}}(A^{\hat{d}}_{\underline{b}}\wedge\alpha) - \hat{i}_{\hat{d}}(dA^{\hat{d}}_{\underline{b}}\wedge\alpha)\right)\right)\\ &= \hat{L}_{\hat{c}}\hat{L}_{\hat{d}}\left(A^{\hat{c}}_{\underline{a}}A^{\hat{d}}_{\underline{b}}\wedge\alpha\right) - \hat{L}_{\hat{c}}\left(\hat{i}_{\hat{d}}(dA^{\hat{c}}_{\underline{a}})\wedge A^{\hat{d}}_{\underline{b}}\wedge\alpha\right)\\ &- \hat{L}_{\hat{c}}\hat{i}_{\hat{d}}(A^{\hat{c}}_{\underline{a}}\wedge dA^{\hat{d}}_{\underline{b}}\wedge\alpha) - \hat{i}_{\hat{c}}\hat{L}_{\hat{d}}\left(dA^{\hat{c}}_{\underline{a}}\wedge A^{\hat{d}}_{\underline{b}}\wedge\alpha\right) + \hat{i}_{\hat{c}}\left((d\hat{i}_{\hat{d}}dA^{\hat{c}}_{\underline{a}})\wedge A^{\hat{d}}_{\underline{b}}\wedge\alpha\right)\\ &- \hat{i}_{\hat{c}}\hat{i}_{\hat{d}}\left(dA^{\hat{c}}_{\underline{a}}\wedge dA^{\hat{d}}_{\underline{b}}\wedge\alpha\right) + \hat{i}_{\hat{c}}\left(\hat{i}_{\hat{d}}dA^{\hat{c}}_{\underline{a}}\wedge dA^{\hat{d}}_{\underline{b}}\wedge\alpha\right) \end{aligned} \tag{8.3.53}$$

$$\begin{aligned} &= \hat{L}_{\hat{c}}\hat{L}_{\hat{d}}\left(A^{\hat{c}}_{\underline{a}}A^{\hat{d}}_{\underline{b}}\wedge\alpha\right) - \hat{L}_{\hat{c}}\hat{i}_{\hat{d}}\left(d\left(A^{\hat{c}}_{\underline{a}}A^{\hat{d}}_{\underline{b}}\right)\wedge\alpha\right) - \hat{L}_{\hat{c}}\left(\hat{\partial}_{\hat{d}}A^{\hat{c}}_{\underline{a}}\wedge A^{\hat{d}}_{\underline{b}}\wedge\alpha\right)\\ &+ \hat{i}_{\hat{c}}\left(d\left(\hat{\partial}_{\hat{d}}A^{\hat{c}}_{\underline{a}}\wedge A^{\hat{d}}_{\underline{b}}\right)\wedge\alpha\right) - \hat{i}_{\hat{c}}\hat{i}_{\hat{d}}\left(dA^{\hat{c}}_{\underline{a}}\wedge dA^{\hat{d}}_{\underline{b}}\wedge\alpha\right). \end{aligned} \tag{8.3.54}$$

Using $\partial_{\hat{d}}A^{\hat{c}}_{\underline{a}} = A^{e}_{\hat{d}}A^{\hat{c}}_{\underline{ab}}$, and noting that the $i_{\hat{c}}i_{\hat{d}}$ term vanishes (as the term inside the brackets is symmetric), gives

$$L_{\underline{a}}L_{\underline{b}}\alpha = \hat{L}_{\hat{c}}\hat{L}_{\hat{d}}\left(A^{\hat{c}}_{\underline{a}}A^{\hat{d}}_{\underline{b}}\wedge\alpha\right) - \hat{L}_{\hat{c}}\hat{i}_{\hat{d}}\left(d\left(A^{\hat{c}}_{\underline{a}}A^{\hat{d}}_{\underline{b}}\right)\wedge\alpha\right) - \hat{L}_{\hat{c}}\left(A^{\hat{c}}_{\underline{ab}}\wedge\alpha\right) + \hat{i}_{\hat{c}}\left(dA^{\hat{c}}_{\underline{ab}}\wedge\alpha\right). \tag{8.3.55}$$

This gives the coordinate transformation for the $V^{\underline{ab}}$ term,

$$\begin{aligned} L_{\underline{a}}L_{\underline{b}}\eta_{\varsigma}(V^{\underline{ab}}) = \hat{L}_{\hat{c}}\hat{L}_{\hat{d}}\eta_{\varsigma}\left(A^{\hat{c}}_{\underline{a}}A^{\hat{d}}_{\underline{b}}V^{\underline{ab}}\right) - \hat{L}_{\hat{c}}\hat{i}_{\hat{d}}\eta_{\varsigma}\left(d\left(A^{\hat{c}}_{\underline{a}}A^{\hat{d}}_{\underline{b}}\right)\wedge V^{\underline{ab}}\right)\\ - \hat{L}_{\hat{c}}\eta_{\varsigma}\left(A^{\hat{c}}_{\underline{ab}}V^{\underline{ab}}\right) + \hat{i}_{\hat{c}}\eta_{\varsigma}\left(dA^{\hat{c}}_{\underline{ab}}\wedge V^{\underline{ab}}\right). \end{aligned} \tag{8.3.56}$$

For the $X^{\underline{ab}}$ term,

$$i_{\underline{a}}L_{\underline{b}}\eta_{\varsigma}(X^{\underline{ab}}dt) = i_{\underline{a}}\hat{L}_{\hat{c}}\eta_{\varsigma}(A^{\hat{c}}_{\underline{b}}\wedge X^{\underline{ab}}dt) - i_{\underline{a}}\hat{i}_{\hat{c}}\left(\eta_{\varsigma}(dA^{\hat{c}}_{\underline{b}}\wedge X^{\underline{ab}}dt)\right) \tag{8.3.57}$$

$$= \hat{i}_{\hat{d}}A^{\hat{d}}_{\underline{a}}\hat{L}_{\hat{c}}\eta_{\varsigma}(A^{\hat{c}}_{\underline{b}}\wedge X^{\underline{ab}}dt) \tag{8.3.58}$$

$$= \hat{i}_{\hat{d}}\hat{L}_{\hat{c}}\eta_{\varsigma}(A^{\hat{d}}_{\underline{a}}A^{\hat{c}}_{\underline{b}}\wedge X^{\underline{ab}}dt) - \hat{i}_{\hat{d}}\eta_{\varsigma}\left(\hat{L}_{\hat{c}}(A^{\hat{d}}_{\underline{a}})\wedge A^{\hat{c}}_{\underline{b}}\wedge X^{\underline{ab}}dt\right) \tag{8.3.59}$$

$$= \hat{i}_{\hat{d}}\hat{L}_{\hat{c}}\eta_{\varsigma}(A^{\hat{d}}_{\underline{a}}A^{\hat{c}}_{\underline{b}}\wedge X^{\underline{ab}}dt) - \hat{i}_{\hat{d}}\eta_{\varsigma}(A^{\hat{d}}_{\underline{ab}}\wedge X^{\underline{ab}}dt) \tag{8.3.60}$$

$$= \hat{i}_{\hat{d}}\hat{L}_{\hat{c}}\eta_{\varsigma}\left(A^{\hat{d}}_{\underline{a}}A^{\hat{c}}_{\underline{b}}\wedge X^{\underline{ab}}\frac{dt}{d\hat{t}}d\hat{t}\right) - \hat{i}_{\hat{d}}\eta_{\varsigma}\left(A^{\hat{d}}_{\underline{ab}}\wedge X^{\underline{ab}}\frac{dt}{d\hat{t}}d\hat{t}\right) \tag{8.3.61}$$

where $dA^{\hat{c}}_{\underline{b}} \wedge X^{\underline{ab}} dt = 0$ is used. The $V^{\underline{a}}$ and $X^{\underline{a}}$ terms are more straightforward,

$$L_{\underline{a}}\eta_\varsigma(V^{\underline{a}}) = \hat{L}_{\hat{b}}\eta_\varsigma\left(A^{\hat{b}}_{\underline{a}} \wedge V^{\underline{a}}\right) - \hat{i}_{\hat{b}}\eta_\varsigma\left(dA^{\hat{b}}_{\underline{a}} \wedge V^{\underline{a}}\right) \tag{8.3.62}$$

$$i_{\underline{a}}\eta_\varsigma(X^{\underline{a}} dt) = \hat{i}_{\hat{b}}\eta_\varsigma\left(A^{\hat{b}}_{\underline{a}} X^{\underline{a}} \frac{dt}{d\hat{t}} d\hat{t}\right). \tag{8.3.63}$$

Summing these together (noting that the monopole term is invariant under transformation), gives

$$\begin{aligned}\mathcal{J} = \hat{\mathcal{J}} &= \frac{1}{2} L_{\underline{a}} L_{\underline{b}} \eta_\varsigma(V^{\underline{ab}}) - i_{\underline{a}} L_{\underline{b}} \eta_\varsigma(X^{\underline{ab}} dt) - L_{\underline{a}}\eta_\varsigma(V^{\underline{a}}) + i_{\underline{a}}\eta_\varsigma(X^{\underline{a}} dt) + \eta_\varsigma(q) \\ &= \frac{1}{2}\hat{L}_{\hat{a}}\hat{L}_{\hat{b}}\eta_\varsigma(\hat{U}^{\hat{a}\hat{b}}) - \hat{i}_{\hat{a}}\hat{L}_{\hat{b}}\eta_\varsigma(\hat{Y}^{\hat{a}\hat{b}} d\hat{t}) - \hat{L}_{\hat{a}}\eta_\varsigma(\hat{U}^{\hat{a}}) + \hat{i}_{\underline{\hat{a}}}\eta_\varsigma(\hat{Y}^{\hat{a}} d\hat{t}) + \eta_\varsigma(q). \end{aligned} \tag{8.3.64}$$

where $\hat{U}^{\hat{a}\hat{b}}$ and $\hat{U}^{\hat{a}}$ are defined by equation (4.4.7), and

$$\hat{Y}^{\hat{c}\hat{d}} = A^{\hat{c}}_{\underline{a}} A^{\hat{d}}_{\underline{b}} X^{\underline{ab}} \frac{dt}{d\hat{t}} d\hat{t} + \frac{1}{2} d\left(A^{\hat{c}}_{\underline{a}} A^{\hat{d}}_{\underline{b}}\right) V^{\underline{ab}} \tag{8.3.65}$$

$$\hat{Y}^{\hat{c}} = \left(A^{\hat{c}}_{\underline{a}} X^{\underline{a}} + A^{\hat{c}}_{\underline{ab}} X^{\underline{ab}}\right) \frac{dt}{d\hat{t}} d\hat{t} + d(A^{\hat{c}}_{\underline{a}}) V^{\underline{a}} + d(A^{\hat{c}}_{\underline{ab}}) V^{\underline{ab}}. \tag{8.3.66}$$

By taking the external derivatives, these are equivalent to (4.4.7). □

As before, the transformed quadrupole is still based on the original time slicing. In this case the projections to the new time slicing are based on the internal contraction and Lie derivatives along η. The projections are given by

$$i_0 = i_{\dot{\eta}} - \dot{\eta}^{\underline{a}} i_{\underline{a}}, \quad L_0 = L_{\dot{\eta}} - \dot{\eta}^{\underline{a}} L_{\underline{a}}. \tag{8.3.67}$$

Using these projections give the full coordinate transformation for the quadrupole,

$$\hat{\mathcal{J}} = \frac{1}{2}\hat{L}_{\underline{\hat{a}}}\hat{L}_{\underline{\hat{b}}}\eta_\varsigma(\hat{V}^{\underline{\hat{a}\hat{b}}}) - \hat{i}_{\underline{\hat{a}}}\hat{L}_{\underline{\hat{b}}}\eta_\varsigma(\hat{X}^{\underline{\hat{a}\hat{b}}} d\hat{t}) - \hat{L}_{\underline{\hat{a}}}\eta_\varsigma(\hat{V}^{\underline{\hat{a}}}) + \hat{i}_{\hat{a}}\eta_\varsigma(\hat{X}^{\hat{a}} d\hat{t}) + \eta_\varsigma(q). \tag{8.3.68}$$

where $\hat{V}^{\underline{\hat{a}\hat{b}}}$, $\hat{V}^{\underline{\hat{a}}}$, $\hat{X}^{\underline{\hat{a}\hat{b}}}$, and $\hat{X}^{\underline{\hat{a}}}$ are defined by equations (4.4.22), (4.4.23), (4.4.26), and (4.4.27) respectively.

Proof. The non-unique semi-quadrupole, where hats have been temporarily removed to aid readability, is given by

$$\mathcal{J} = \frac{1}{2} L_a L_b \eta_\varsigma(U^{ab}) - i_a L_b \eta_\varsigma(Y^{ab} dt) - L_a \eta_\varsigma(U^a) + i_a \eta_\varsigma(Y^a dt) + \eta_\varsigma(q). \tag{8.3.69}$$

To find the projections, proceed term by term, beginning with the L_aL_b term,

$$L_aL_b\eta_\varsigma(U^{ab}) = L_aL_{\underline{b}}\eta_\varsigma(U^{a\underline{b}}) + L_aL_0(U^{a0}) \tag{8.3.70}$$

$$= L_aL_{\underline{b}}\eta_\varsigma(U^{a\underline{b}}) + L_aL_{\dot\eta}(U^{a0}) - L_a\dot\eta^{\underline{b}}L_{\underline{b}}\eta_\varsigma(U^{a0}) \tag{8.3.71}$$

$$= L_aL_{\underline{b}}\eta_\varsigma(U^{a\underline{b}} - \dot\eta^{\underline{b}}U^{a0}) + L_a\eta_\varsigma\left(\frac{dU^{a0}}{dt}\right) + L_ai_{\underline{b}}\eta_\varsigma\left(U^{a0}d\dot\eta^{\underline{b}}\right). \tag{8.3.72}$$

Projecting the L_a term,

$$\begin{aligned} L_aL_b\eta_\varsigma(U^{ab}) &= L_{\underline{a}}L_{\underline{b}}\eta_\varsigma(U^{\underline{a}\underline{b}} - \dot\eta^{\underline{b}}U^{\underline{a}0}) + L_{\underline{b}}L_{\dot\eta}\eta_\varsigma(U^{0\underline{b}} - \dot\eta^{\underline{b}}U^{00}) \\ &- L_{\underline{b}}\dot\eta^{\underline{a}}L_{\underline{a}}\eta_\varsigma(U^{0\underline{b}} - \dot\eta^{\underline{b}}U^{00}) + L_{\underline{a}}\eta_\varsigma\left(\frac{dU^{\underline{a}0}}{dt}\right) + L_{\dot\eta}\eta_\varsigma\left(\frac{dU^{00}}{dt}\right) - \dot\eta^{\underline{a}}L_{\underline{a}}\eta_\varsigma\left(\frac{dU^{00}}{dt}\right) \\ &+ L_{\underline{a}}i_{\underline{b}}\eta_\varsigma\left(U^{\underline{a}0}d\dot\eta^{\underline{b}}\right) + i_{\underline{b}}L_{\dot\eta}\eta_\varsigma\left(U^{00}d\dot\eta^{\underline{b}}\right) - i_{\underline{b}}\dot\eta^{\underline{a}}L_{\underline{a}}\eta_\varsigma\left(U^{00}d\dot\eta^{\underline{b}}\right). \end{aligned} \tag{8.3.73}$$

Simplifying this gives

$$\begin{aligned} L_aL_b\eta_\varsigma(U^{ab}) &= L_{\underline{a}}L_{\underline{b}}\eta_\varsigma\left(U^{\underline{a}\underline{b}} - \dot\eta^{\underline{b}}U^{\underline{a}0} - \dot\eta^{\underline{a}}U^{\underline{b}0} + \dot\eta^{\underline{a}}\dot\eta^{\underline{b}}U^{00}\right) \\ &+ L_{\underline{b}}i_{\underline{a}}\eta_\varsigma\left((2U^{0\underline{b}} - 2\dot\eta^{\underline{b}}U^{00})d\dot\eta^{\underline{a}}\right) + L_{\underline{a}}\eta_\varsigma\left(2\frac{dU^{\underline{a}0}}{dt} - \dot\eta^{\underline{a}}\frac{dU^{00}}{dt} - \frac{d}{dt}\left(\dot\eta^{\underline{a}}U^{00}\right)\right) \\ &+ i_{\underline{a}}\eta_\varsigma\left(\frac{dU^{00}}{dt}d\dot\eta^{\underline{a}} + \frac{d}{dt}\left(U^{00}d\dot\eta^{\underline{a}}\right)\right) + \eta_\varsigma\left(\frac{d^2U^{00}}{dt^2}\right) \\ &+ i_{\underline{b}}i_{\underline{a}}\eta_\varsigma\left(U^{00}d\dot\eta^{\underline{a}}\wedge d\dot\eta^{\underline{b}}\right) \end{aligned} \tag{8.3.74}$$

and note the last term vanishes as $\mathbb{R}$ is only 1-dimensional. For the L_ai_b term,

$$L_bi_a\eta_\varsigma(Y^{ab}dt) = L_bi_{\underline{a}}\eta_\varsigma(Y^{\underline{a}b}dt) + L_ai_{\dot\eta}\eta_\varsigma(Y^{0b}dt) - L_a\dot\eta^{\underline{b}}i_{\underline{b}}\eta_\varsigma(Y^{0b}dt) \tag{8.3.75}$$

$$= L_bi_{\underline{a}}\eta_\varsigma(Y^{\underline{a}b}dt - \dot\eta^{\underline{a}}Y^{0b}dt) + L_b\eta_\varsigma(Y^{0b}). \tag{8.3.76}$$

Splitting the L_b term into $L_0 + L_{\underline{b}}$,

$$\begin{aligned} L_bi_a\eta_\varsigma(Y^{ab}dt) &= L_{\underline{b}}i_{\underline{a}}\eta_\varsigma(Y^{\underline{a}\underline{b}}dt - \dot\eta^{\underline{a}}Y^{0\underline{b}}dt) + L_0i_{\underline{a}}\eta_\varsigma(Y^{\underline{a}0}dt - \dot\eta^{\underline{a}}Y^{00}dt) \\ &+ L_{\underline{b}}\eta_\varsigma(Y^{0\underline{b}}) + L_0\eta_\varsigma(Y^{00}). \end{aligned} \tag{8.3.77}$$

Projecting out the L_0 term,

$$\begin{aligned} L_bi_a\eta_\varsigma(Y^{ab}dt) &= L_{\underline{b}}i_{\underline{a}}\eta_\varsigma(Y^{\underline{a}\underline{b}}dt - \dot\eta^{\underline{a}}Y^{0\underline{b}}dt) + L_{\dot\eta}i_{\underline{a}}\eta_\varsigma(Y^{\underline{a}0}dt - \dot\eta^{\underline{a}}Y^{00}dt) \\ &- \dot\eta^{\underline{b}}L_{\underline{b}}i_{\underline{a}}\eta_\varsigma(Y^{\underline{a}0}dt - \dot\eta^{\underline{a}}Y^{00}dt) + L_{\underline{b}}\eta_\varsigma(Y^{0\underline{b}}) + L_{\dot\eta}\eta_\varsigma(Y^{00}) - \dot\eta^{\underline{a}}L_{\underline{a}}\eta_\varsigma(Y^{00}). \end{aligned} \tag{8.3.78}$$

Simplifying,

$$\begin{aligned} L_b i_a \eta_\varsigma(Y^{ab}dt) &= L_{\underline{b}} i_{\underline{a}} \eta_\varsigma(Y^{\underline{ab}}dt - \dot\eta^{\underline{a}} Y^{0\underline{b}}dt) + L_{\dot\eta} i_{\underline{a}} \eta_\varsigma(Y^{\underline{a}0}dt - \dot\eta^{\underline{a}} Y^{00}dt) \\ &\quad - L_{\underline{b}} \dot\eta^{\underline{b}} i_{\underline{a}} \eta_\varsigma(Y^{\underline{a}0}dt - \dot\eta^{\underline{a}} Y^{00}dt) + L_{\underline{b}} \eta_\varsigma(Y^{0\underline{b}}) + L_{\dot\eta}\eta_\varsigma(Y^{00}) - L_{\underline{a}} \dot\eta^{\underline{a}} \eta_\varsigma(Y^{00}) \\ &\quad + i_{\underline{a}} \eta_\varsigma(Y^{00} d\dot\eta^{\underline{a}}) + i_{\underline{b}} i_{\underline{a}} \eta_\varsigma \left(d\dot\eta^{\underline{b}} \wedge (Y^{\underline{a}0} - \dot\eta Y^{00}) dt \right). \end{aligned} \tag{8.3.79}$$

Noting that the $i_{\underline{a}} i_{\underline{b}}$ term vanishes since $d\eta^{\underline{b}} \wedge dt = 0$ (since the wedge product is on a one-dimensional manifold),

$$\begin{aligned} &L_b i_a \eta_\varsigma(Y^{ab}dt) = L_{\underline{b}} i_{\underline{a}} \eta_\varsigma(Y^{\underline{ab}}dt - \dot\eta^{\underline{a}} Y^{0\underline{b}}dt - \dot\eta^{\underline{b}} Y^{\underline{a}0}dt + \dot\eta^{\underline{a}}\dot\eta^{\underline{b}} Y^{00}dt) \\ &+ L_{\underline{b}} \eta_\varsigma(Y^{0\underline{b}} - \dot\eta^{\underline{b}} Y^{00}) + i_{\underline{a}} \eta_\varsigma \left(\frac{dY^{\underline{a}0}}{dt} dt - \frac{d}{dt}\left(\dot\eta^{\underline{a}} Y^{00}\right) dt + Y^{00} d\dot\eta^{\underline{a}} \right) + \eta_\varsigma \left(\frac{dY^{00}}{dt} \right). \end{aligned} \tag{8.3.80}$$

The U^a term,

$$L_a \eta_\varsigma(U^a) = L_{\underline{a}} \eta_\varsigma(U^{\underline{a}}) + L_{\dot\eta}\eta_\varsigma(U^0) - \dot\eta^{\underline{a}} L_{\underline{a}} \eta_\varsigma(U^0) \tag{8.3.81}$$

$$= L_{\underline{a}} \eta_\varsigma(U^{\underline{a}} - \dot\eta^{\underline{a}} U^0) + i_{\underline{a}} \eta_\varsigma(U^0 d\dot\eta^{\underline{a}}) + \eta_\varsigma \left(\frac{dU^0}{dt} \right). \tag{8.3.82}$$

Lastly the Y^a term,

$$i_a \eta_\varsigma(Y^a dt) = i_{\underline{a}} \eta_\varsigma(Y^{\underline{a}} dt) + i_{\dot\eta}\eta_\varsigma(Y^0 dt) - i_{\underline{a}} \dot\eta^{\underline{a}} \eta_\varsigma(Y^0 dt) \tag{8.3.83}$$

$$= i_{\underline{a}} \eta_\varsigma(Y^{\underline{a}} dt - \dot\eta^{\underline{a}} Y^0 dt) + \eta_\varsigma(Y^0). \tag{8.3.84}$$

Summing these together,

$$\begin{aligned} \mathcal{J} &= \frac{1}{2} L_{\underline{a}} L_{\underline{b}} \eta_\varsigma \left(U^{\underline{ab}} - \dot\eta^{\underline{b}} U^{\underline{a}0} - \dot\eta^{\underline{a}} U^{\underline{b}0} + \dot\eta^{\underline{a}}\dot\eta^{\underline{b}} U^{00} \right) \\ &\quad - L_{\underline{b}} i_{\underline{a}} \eta_\varsigma \Big(Y^{\underline{ab}} dt - \dot\eta^{\underline{a}} Y^{0\underline{b}} dt - \dot\eta^{\underline{b}} Y^{\underline{a}0} dt + \dot\eta^{\underline{a}}\dot\eta^{\underline{b}} Y^{00} dt - (U^{0\underline{b}} - \dot\eta^{\underline{b}} U^{00}) d\dot\eta^{\underline{a}} \Big) \\ &\quad - L_{\underline{a}} \eta_\varsigma(U^{\underline{a}} - \dot\eta^{\underline{a}} U^0 + Y^{0\underline{a}} - \dot\eta^{\underline{a}} Y^{00}) - \frac{1}{2} L_{\underline{a}} \eta_\varsigma \left(\dot\eta^{\underline{a}} \frac{dU^{00}}{dt} + \frac{d}{dt}\left(\dot\eta^{\underline{a}} U^{00}\right) - 2\frac{dU^{\underline{a}0}}{dt} \right) \\ &\quad + i_{\underline{a}} \eta_\varsigma \left(Y^{\underline{a}} dt - \dot\eta^{\underline{a}} Y^0 dt - \frac{dY^{\underline{a}0}}{dt} dt - U^0 d\dot\eta^{\underline{a}} + \frac{d}{dt}\left(\dot\eta^{\underline{a}} Y^{00}\right) dt - Y^{00} d\dot\eta^{\underline{a}} \right) \\ &\quad + \frac{1}{2} i_{\underline{a}} \eta_\varsigma \left(\frac{dU^{00}}{dt} d\dot\eta^{\underline{a}} + \frac{d}{dt}\left(U^{00} d\dot\eta^{\underline{b}}\right) \right) \\ &\quad + \frac{1}{2} \eta_\varsigma \left(\frac{d^2 U^{00}}{dt^2} \right) - \eta_\varsigma \left(\frac{dY^{00}}{dt} \right) - \eta_\varsigma \left(\frac{dU^0}{dt} \right) + \eta_\varsigma(Y^0) + \eta_\varsigma(q). \end{aligned} \tag{8.3.85}$$

To simplify this, recall equation (8.3.21), and add hats back over quantities giving

$$\begin{aligned}\hat{\mathcal{J}} = \frac{1}{2}\hat{L}_{\underline{\hat{a}}}\hat{L}_{\underline{\hat{b}}}\eta_{\varsigma}\left(\hat{U}^{\underline{\hat{a}}\underline{\hat{b}}} - \dot{\hat{\eta}}^{\underline{\hat{b}}}\hat{U}^{\underline{\hat{a}}\hat{0}} - \dot{\hat{\eta}}^{\underline{\hat{a}}}\hat{U}^{\underline{\hat{b}}\hat{0}} + \dot{\hat{\eta}}^{\underline{\hat{a}}}\dot{\hat{\eta}}^{\underline{\hat{b}}}\hat{U}^{\hat{0}\hat{0}}\right)\\ - \hat{i}_{\underline{\hat{a}}}\hat{L}_{\underline{\hat{b}}}\eta_{\varsigma}\left(\hat{Y}^{\underline{\hat{a}}\underline{\hat{b}}} - \hat{Y}^{\underline{\hat{a}}\hat{0}}\dot{\hat{\eta}}^{\underline{\hat{b}}} - \dot{\hat{\eta}}^{\underline{\hat{a}}}\hat{Y}^{\hat{0}\underline{\hat{b}}} + \dot{\hat{\eta}}^{\underline{\hat{a}}}\dot{\hat{\eta}}^{\underline{\hat{b}}}\hat{Y}^{\hat{0}\hat{0}} + \left(\hat{U}^{\hat{0}\underline{\hat{b}}} - \dot{\hat{\eta}}^{\underline{b}}\hat{U}^{\hat{0}\hat{0}}\right)d\dot{\hat{\eta}}^{\underline{a}}\right)\\ - \hat{L}_{\underline{\hat{a}}}\eta_{\varsigma}\left(\hat{U}^{\underline{\hat{a}}} - \hat{U}^{\hat{0}}\dot{\hat{\eta}}^{\underline{\hat{a}}} + \frac{1}{2}\frac{d}{d\hat{t}}\left(\dot{\hat{\eta}}^{\underline{\hat{a}}}\hat{U}^{\hat{0}\hat{0}}\right) - \hat{Y}^{\underline{\hat{a}}\hat{0}}\right)\\ + \hat{i}_{\underline{\hat{a}}}\eta_{\varsigma}\left(\hat{Y}^{\underline{\hat{a}}}dt - d\left(\dot{\hat{\eta}}^{\underline{\hat{a}}}\hat{U}^{\hat{0}}\right) - d\hat{Y}^{\underline{\hat{a}}\hat{0}} + \frac{1}{2}\frac{d^2}{d\hat{t}^2}\left(\dot{\hat{\eta}}^{\underline{\hat{a}}}\hat{U}^{\hat{0}\hat{0}}\right)dt\right) + \eta_{\varsigma}(q). \quad (8.3.86)\end{aligned}$$

Inserting equation (4.4.7) into this and transforming the $\dot{\hat{\eta}}^{\underline{a}}$ terms back into $\dot{\eta}^{\underline{a}}$ using equation (4.4.3) gives equations (4.4.22), (4.4.23), (4.4.26), and (4.4.27), as required. □

These coordinate transformations are the same as those found through the Ellis representation.

8.4 Reconstructing the current 3-form

8.4.1 The reconstruction method

Rather than reconstructing a function using model densities, one can instead reconstruct a function using model forms. Similarly to using densities, this avoids any issues with choosing the correct measure in the choice of model form. For the projection method, using the language of differential geometry provides a clearer geometric approach to the problem, which may be considered clearer to understand compared to the Ellis representation projection, where it is less clear why components of $\mathcal{J}^a$ vanish when integrated over the fibres.

Recall J (equation (8.2.55)), the current 6-form associated with a given $\mathfrak{f}$. In this approach, the current 6-form is the quantity that is reconstructed using model differential forms. Let $J_\Sigma = \Sigma^*(J)$ be the current 6-form at a timeslice t.

$$a_{\mathbf{I}} = \int_\Sigma (\xi - \eta)^{\mathbf{I}} J_\Sigma. \quad (8.4.1)$$

These moments are equivalent to those found by integrating $\mathfrak{f}$.

Proof. To calculate the pullback $\Sigma^*(J)$, consider equation (8.2.55), and note that $\Sigma^*(dt) = 0$, and $\Sigma^*(d\xi^{\underline{a}}) = d\xi^{\underline{a}}$, so

$$\Sigma^*(J) = \Sigma^*(\mathfrak{f} W^a i_a d^7\xi) = \mathfrak{f} W^0 i_0 d^7\xi. \tag{8.4.2}$$

Since $W^0 = 1$,

$$\Sigma^*(J) = \mathfrak{f}\, d^3x\, d^3u \tag{8.4.3}$$

and thus the moments taken in equation (8.4.1) are equivalent to those taken with $\mathfrak{f}$. □

The reconstructed 6-form, $\hat{J}_\Sigma$, is given by

$$\hat{J}_\Sigma = \sum_{\mathbf{K}} c_{\mathbf{K}} \psi_{\mathbf{K}} \tag{8.4.4}$$

where $\psi_{\mathbf{K}} \in \Gamma\Lambda^6\Sigma$ are model 6-forms. Similarly to working with densities, the reconstructed form has the same moments,

$$\begin{aligned} a_{\mathbf{I}} &= \int_\Sigma (\xi - \eta)^{\mathbf{I}} \hat{J}_\Sigma && (8.4.5)\\ &= \sum_{\mathbf{K}} \int_\Sigma (\xi - \eta)^{\mathbf{I}} c_{\mathbf{K}} \psi_{\mathbf{K}} && (8.4.6)\\ &= \sum_{\mathbf{K}} c_{\mathbf{K}} \int_\Sigma (\xi - \eta)^{\mathbf{I}} \psi_{\mathbf{K}} && (8.4.7)\\ &= \sum_{\mathbf{K}} c_{\mathbf{K}} B_{\mathbf{IK}} && (8.4.8) \end{aligned}$$

where

$$B_{\mathbf{IK}} = \int_\Sigma (\xi - \eta)^{\mathbf{I}} \psi_{\mathbf{K}}. \tag{8.4.9}$$

By solving the linear system of equations, the model forms can be found.

In this case, the equivalent model 6-form to give the same result as using model densities would be

$$\psi = \varphi_0 i_0 d^7\xi, \tag{8.4.10}$$

where φ_0 is the model density from section 6.3. This definition follows from equation (2.3.1) and (8.2.53).

The charge can be found by integrating J_Σ over a fibre,

$$\mathfrak{p} = \int_{\mathcal{E}_p} i_1 i_2 i_3 J_\Sigma. \tag{8.4.11}$$

The components of the 4-current scalar field can be found as

$$\mathfrak{T}^{\underline{\mu}} = \int_{\mathcal{E}_p} \frac{u^{\underline{\mu}}}{\gamma} i_1 i_2 i_3 J_\Sigma. \tag{8.4.12}$$

A current 3-form, I, could be found from this, and would be given by

$$I = \mathfrak{p}\, dx^1 \wedge dx^2 \wedge dx^3 + \mathfrak{T}^{\underline{\mu}} i_{\underline{\mu}} \left(dt \wedge dx^1 \wedge dx^2 \wedge dx^3 \right). \tag{8.4.13}$$

In the next subsection a method to directly retrieve the current 3-form from a distribution is presented, using a projection operator.

8.4.2 The projection method

As with the Ellis representation, is it possible to reduce the de Rham representation of 7-current to the 4-current on M. By doing this, the projection method for finding the current from a set of moments can be found using the de Rham representation. Additionally, by using differential geometry to define the projection through a de Rham pushforward, is it clearer to see why the velocity components of the 7-current vanish.

To find the distributional 4-current, a *projection* map, π, is introduced. The projection $\pi : \mathcal{E} \to M$ can be written in terms of coordinates,

$$\pi(t, \underline{x}, \underline{u}) \to (t, \underline{x}). \tag{8.4.14}$$

The pullback of this map, π^*, can be defined in terms of coordinates,

$$\pi^*(t) = t, \quad \pi^*(\underline{x}) = \underline{x}. \tag{8.4.15}$$

The de Rham pushforward of π, $\pi_\varsigma : \Gamma\Lambda^n\mathcal{E} \to \Gamma\Lambda^{n-3}M$ is a map taking an n-form on $\mathcal{E}$ onto an $(n-3)$-form on M. In terms of distributions, the projection π_ς is defined as

$$\pi_\varsigma(\Psi)[\phi] = \Psi[\pi^*(\phi)]. \tag{8.4.16}$$

For regular distributions, it can be shown that the projection can be written as integrals over the fibre, for example

$$\pi_\varsigma(f du^1 \wedge du^2 \wedge du^3) = \int_{\mathcal{E}_p} f du^1 \wedge du^2 \wedge du^3, \tag{8.4.17}$$

$$\pi_\varsigma(f dx^1 \wedge dx^3 \wedge du^1 \wedge du^2 \wedge du^3) = dx^1 \wedge dx^3 \left(\int_{\mathcal{E}_p} f du^1 \wedge du^2 \wedge du^3 \right), \tag{8.4.18}$$

$$\pi_\varsigma(dx^1 \wedge du^2 \wedge du^3) = 0 \tag{8.4.19}$$

i.e. the pushforward integrates a form over the fibre if it contains all the du terms, otherwise it vanishes.

The current 3-form, $I \in \Gamma\Lambda^3 M$, is given by

$$I = \pi_\varsigma(J). \tag{8.4.20}$$

The distributional 4-current, $\mathcal{I}$, can be found equivalently, as

$$\mathcal{I} = \pi_\varsigma(\mathcal{J}). \tag{8.4.21}$$

In terms of coordinates, $\mathcal{I}$ is given by

$$\mathcal{I} = \pi_\varsigma \mathcal{J} = \frac{1}{2} L_{\underline{\mu}} L_{\underline{\nu}} C_\varsigma(V^{\underline{\mu}\underline{\nu}}) - i_{\underline{\mu}} L_{\underline{\nu}} C_\varsigma(X^{\underline{\mu}\underline{\nu}} dt) - L_{\underline{\mu}} C_\varsigma(V^{\underline{\mu}}) + i_{\underline{\mu}} C_\varsigma(X^{\underline{\mu}} dt) + C_\varsigma(q). \tag{8.4.22}$$

Proof. To find $\pi_\varsigma \mathcal{J}$, consider $\pi_* i_a$, where a subscript asterisk represents the pushforward. These pushforwards, for the projection map, are

$$\pi_* i_\mu = i_\mu, \quad \pi_* i_{\mu+3} = 0. \tag{8.4.23}$$

This means that

$$\pi_\varsigma i_{\underline{a}}(\alpha) = \delta^{\underline{\mu}}_{\underline{a}} i_{\underline{\mu}} \pi_\varsigma \alpha. \tag{8.4.24}$$

Using this gives $\pi_\varsigma \mathcal{J}$,

$$\pi_\varsigma \mathcal{J} = \frac{1}{2}\pi_\varsigma L_{\underline{a}} L_{\underline{b}} \eta_\varsigma(V^{\underline{ab}}) - \pi_\varsigma i_{\underline{a}} L_{\underline{b}} \eta_\varsigma(X^{\underline{ab}} dt) \tag{8.4.25}$$

$$- \pi_\varsigma L_{\underline{a}} \eta_\varsigma(V^{\underline{a}}) + \pi_\varsigma i_{\underline{a}} \eta_\varsigma(X^{\underline{a}} dt) + \pi_\varsigma \eta_\varsigma(q)$$

$$= \frac{1}{2} L_{\underline{\mu}} L_{\underline{\nu}} \pi_\varsigma \eta_\varsigma(V^{\underline{\mu\nu}}) - i_{\underline{\mu}} L_{\underline{\nu}} \pi_\varsigma \eta_\varsigma(X^{\underline{\mu\nu}} dt) \tag{8.4.26}$$

$$- L_{\underline{\mu}} \pi_\varsigma \eta_\varsigma(V^{\underline{\mu}}) + i_{\underline{\mu}} \pi_\varsigma \eta_\varsigma(X^{\underline{\mu}} dt) + \pi_\varsigma \eta_\varsigma(q).$$

A sequence of two de Rham pushforwards combine to give

$$\pi_\varsigma \eta_\varsigma(\alpha) = (\eta \circ \pi)_\varsigma(\alpha) = C_\varsigma(\alpha) \tag{8.4.27}$$

where, since η is a prolongation of C, the projection of η gives C. These combine to give equation (8.4.22) as required. □

Hence by using the projection operator, it is clearer to see why the velocity moments, corresponding to terms of the form $V^{\underline{\mu}+3}$ etc., vanish compared to the Ellis representation of the moments.

The de Rham representation of the 4-current found from the projection can be used to find the charge and current through the projection method. Consider $\mathcal{I}$ acting on a test form $\phi \in \Gamma\Lambda^1 M$,

$$\mathcal{I}[\phi] = \frac{1}{2}\int_{\mathbb{R}} V^{\underline{\mu\nu}} C^*(L_{\underline{\mu}} L_{\underline{\nu}} \phi) + \int_{\mathbb{R}} X^{\underline{\mu\nu}} C^*(L_{\underline{\nu}} i_{\underline{\mu}} \phi) dt + \int_{\mathbb{R}} V^{\underline{\mu}} C^*(L_{\underline{\mu}} \phi)$$

$$+ \int_{\mathbb{R}} X^{\underline{\mu}} C^*(i_{\underline{\mu}} \phi) dt + \int_{\mathbb{R}} q C^*(\phi). \tag{8.4.28}$$

Comparing this to the squeezed current 3-form (equation (6.4.20)) gives the same relationship between the components (equation (6.4.15)) as that found through the Ellis representation when integrating over the fibres.

Proof. Writing ϕ as $\phi_\mu dx^\mu$,

$$\mathcal{I}[\phi] = \frac{1}{2}\int_{\mathbb{R}} V^{\underline{\mu\nu}} C^*(L_{\underline{\mu}} L_{\underline{\nu}} \phi_\rho dx^\rho) + \int_{\mathbb{R}} X^{\underline{\mu\nu}} C^*(L_{\underline{\nu}} i_{\underline{\mu}} \phi_\rho dx^\rho) dt + \int_{\mathbb{R}} V^{\underline{\mu}} C^*(L_{\underline{\mu}} \phi_\rho dx^\rho)$$

$$+ \int_{\mathbb{R}} X^{\underline{\mu}} C^*(i_{\underline{\mu}} \phi_\rho dx^\rho) dt + \int_{\mathbb{R}} q C^*(\phi_\rho dx^\rho). \tag{8.4.29}$$

Performing the Lie derivatives and internal contractions,

$$\mathcal{I}[\phi] = \frac{1}{2}\int_{\mathbb{R}} V^{\underline{\mu\nu}} C^*(\partial_{\underline{\mu}}\partial_{\underline{\nu}}\phi_\rho dx^\rho) + \int_{\mathbb{R}} X^{\underline{\mu\nu}} C^*(\partial_{\underline{\nu}}\phi_{\underline{\mu}})dt + \int_{\mathbb{R}} V^{\underline{\mu}} C^*(\partial_{\underline{\mu}}\phi_\rho dx^\rho) + \int_{\mathbb{R}} X^{\underline{\mu}} C^*(\phi_{\underline{\mu}})dt + \int_{\mathbb{R}} qC^*(\phi_\rho dx^\rho). \quad (8.4.30)$$

Noting $C^*(dx^\mu) = \dot{C}^\mu dt$ gives

$$\mathcal{I}[\phi] = \frac{1}{2}\int_{\mathbb{R}} V^{\underline{\mu\nu}} \dot{C}^\rho \partial_{\underline{\mu}}\partial_{\underline{\nu}}\phi_\rho|_C dt + \int_{\mathbb{R}} X^{\underline{\mu\nu}} \partial_{\underline{\nu}}\phi_{\underline{\mu}}|_C dt + \int_{\mathbb{R}} V^{\underline{\mu}} \dot{C}^\rho \partial_{\underline{\mu}}\phi_\rho|_C dt + \int_{\mathbb{R}} X^{\underline{\mu}} \phi_{\underline{\mu}}|_C dt + \int_{\mathbb{R}} q\dot{C}^\mu \phi_\mu|_C dt. \quad (8.4.31)$$

Splitting this into ϕ_0 and $\phi_{\underline{\mu}}$ terms,

$$\mathcal{I}[\phi] = \frac{1}{2}\int_{\mathbb{R}} V^{\underline{\mu\nu}} \dot{C}^0 \partial_{\underline{\mu}}\partial_{\underline{\nu}}\phi_0|_C dt + \frac{1}{2}\int_{\mathbb{R}} V^{\underline{\mu\nu}} \dot{C}^{\underline{\rho}} \partial_{\underline{\mu}}\partial_{\underline{\nu}}\phi_{\underline{\rho}}|_C dt + \int_{\mathbb{R}} X^{\underline{\mu\nu}} \partial_{\underline{\nu}}\phi_{\underline{\mu}}|_C dt + \int_{\mathbb{R}} V^{\underline{\mu}} \dot{C}^0 \partial_{\underline{\mu}}\phi_0|_C dt + \int_{\mathbb{R}} V^{\underline{\mu}} \dot{C}^{\underline{\rho}} \partial_{\underline{\mu}}\phi_{\underline{\rho}}|_C dt + \int_{\mathbb{R}} X^{\underline{\mu}} \phi_{\underline{\mu}}|_C dt + \int_{\mathbb{R}} q\dot{C}^{\underline{\mu}} \phi_{\underline{\mu}}|_C dt + \int_{\mathbb{R}} q\dot{C}^0 \phi_0|_C dt. \quad (8.4.32)$$

Grouping terms together,

$$\mathcal{I}[\phi] = \frac{1}{2}\int_{\mathbb{R}} V^{\underline{\mu\nu}} \dot{C}^0 \partial_{\underline{\mu}}\partial_{\underline{\nu}}\phi_0|_C dt + \frac{1}{2}\int_{\mathbb{R}} V^{\underline{\mu\nu}} \dot{C}^{\underline{\rho}} \partial_{\underline{\mu}}\partial_{\underline{\nu}}\phi_{\underline{\rho}}|_C dt + \int_{\mathbb{R}} \left(X^{\underline{\mu\nu}} + \dot{C}^{\underline{\mu}} V^{\underline{\nu}}\right) \partial_{\underline{\nu}}\phi_{\underline{\mu}}|_C dt + \int_{\mathbb{R}} V^{\underline{\mu}} \dot{C}^0 \partial_{\underline{\mu}}\phi_0|_C dt + \int_{\mathbb{R}} \left(X^{\underline{\mu}} + q\dot{C}^{\underline{\mu}}\right) \phi_{\underline{\mu}}|_C dt + \int_{\mathbb{R}} q\dot{C}^0 \phi_0|_C dt. \quad (8.4.33)$$

Comparing this to equation (6.4.20) gives equations (6.4.15), as with the Ellis representation.

8.5 Future work: modifying the transport equations to add internal structure to a macroparticle

As discussed in section 7.5.2, it may be that charge only needs to be conserved on M, rather than on $\mathcal{E}$. As with the Ellis representation, this means it may be possible to add internal dynamics to the transport equations in the de Rham representation.

If charge is only conserved on M, then the conservation of charge condition becomes

$$d\pi_\varsigma J = 0. \tag{8.5.1}$$

This means that internal structure can be added to the equations as a 7-form $B \in \Gamma\Lambda^7\mathcal{E}$, such that

$$dJ = B, \quad \pi_\varsigma B = 0. \tag{8.5.2}$$

These equations can be applied to distributions, with some distribution $\mathcal{B}$ representing the internal structure of the macroparticle. The modified transport equations, in terms of de Rham currents, become

$$d\mathcal{J} = \mathcal{B}, \quad i_W \mathcal{J} = 0, \quad \pi_\varsigma \mathcal{B} = 0. \tag{8.5.3}$$

□

Chapter 9

Conclusion

This thesis investigated a new type of particle-in-cell code, in which the moments of a macroparticle are used. The dynamics of the moments obeying the Vlasov equation were calculated (equation (4.3.7)). Two different methods to calculate the current from a set of moments were presented. Combining the moment tracking and current construction equations allows a full PIC code using moments to be developed. A potential 1.5D full PIC code implementation, and the algorithms required for this, was discussed.

The dynamics of the moments depend on the Vlasov field and its derivatives. The focus of this thesis was on how the number of moments taken affects the accuracy of the moment tracking. For a full PIC code, the derivatives of the Vlasov field would also be important. If the electromagnetic or gravitational fields quickly vary in space (i.e. the higher order derivatives of the fields are large, as in figure 4.1b), then the moment tracking method will not work well. In this case, there are two possible ways to improve it: use more moments, or use more macroparticles. By using more moments, there are more derivatives to describe the electromagnetic and gravitational fields, so the tracking will be more accurate. By using more macroparticles, the extent each macroparticle represents in phase space will be smaller, so the variation of the fields across this extent will also be smaller. Both

increasing the number of moments and increasing the number of macroparticles will increase the computational load of the model. Future work will need to establish intuition about the correct balance of the number of macroparticles and the maximum order of moments taken.

The moment tracking model is likely to work well in situations where both the distribution of particles represented by a macroparticle can be described by only a small number of moments, and the variation in electromagnetic and gravitational fields across the volume the macroparticle represents is small (figure 4.1a). This corresponds to when the Vlasov field across the extent of the macroparticle can be modelled by just the Vlasov field and a small number of its derivatives at the macroparticle centre. Since numerically calculating the derivatives of the electromagnetic field requires a high density grid, the moment tracking method may also work in cases where a high resolution grid is already needed, such as laser-solid interactions [121, 122]. In such cases, the moment tracking method will be able to model much larger macroparticles, with less particles per cell, even if more cells are needed to compensate for this.

By using the Ellis representation or the de Rham current representation of the moments, coordinate transformations for the moments can be found between frames that mix the space and time coordinates. This is an advantage of using the distributional approach to define moments, as it cannot be done through the standard integral approach.

Both the moment tracking and coordinate transformation results were validated numerically for the case of particles orbiting a black hole. This was done by transporting particles and moments in both Schwarzschild and Kruskal-Szekeres coordinates and comparing results. The numerical results show that a large number of particles can be successfully modelled by a single macroparticle with moments.

This error scales with the order of moments, so for a full PIC code it is likely moments will need to be calculated to an order larger than the quadrupole. The modelling in this simulation was calculated at 10 Schwarzschild radii away from the black hole. This was to model a stable accretion disc. In the development of the theory, there were no assumptions that the macroparticle was far away from the black hole. This means that there is nothing in the theory to stop a macroparticle being close to the singularity. In practice, close to the Schwarzschild radius, the error from only using a finite number of moments will become significant. There are two reasons for this: firstly, the particles being represented by the macroparticle and its moments will begin to undergo spaghettification, and this will cause the higher order moments to become large. Secondly, close to the singularity, the Christoffel symbols in Schwarzschild coordinates become very large, and their derivatives will become even larger. This means the rate of change of the moments will be dominated by the higher order moments which are being neglected in the code. Due to this, the accuracy of the model is yet to be determined in the extreme environments close to the Schwarzschild radius.

In addition to moment tracking, to create a full PIC code, it is necessary to use the moments to find the current distribution, in order to solve Maxwell's equations. Two methods were presented for this. The reconstruction method approximates the original distribution function in position+velocity time-phase space, and then finds the current from this. The projection method uses the Ellis representation of moments to find the charge and current directly. The reconstruction method is more accurate than the projection method, but is more computationally intensive. It is likely that including more moments will improve the accuracy of the projection method.

Lastly, the algorithms needed to create a full 1.5D PIC code were discussed. The main focus of future work will be on testing and evaluating this 1.5D code, to see

if the moment tracking method works at a proof-of-principle level. Initial testing will also be used to develop intuition about the correct balance of the number of macroparticles and the maximum order of moments tracked.

9.1 Wider applications

The main focus of future work was discussed in chapter 7, in developing a full PIC code. Other applications of the moment tracking and coordinate transformations exist, and can also be investigated.

A potential application of the moment tracking method is to model inter-bunch forces within particle accelerators. It is possible to calculate the Liénard-Wiechert fields directly from the moments of a moving quadrupole [46]. By using this method the electromagnetic field, and its derivatives, can be calculated without the need to deposit the charge and current onto a grid. This is particularly useful for modelling coherent synchrotron radiation in particle accelerators, where macroparticles are close together compared to the radius of the beam pipe, such that the effects of boundary conditions on the electromagnetic fields can be ignored.

The applications of the coordinate transformations in astrophysical scenarios are wide. A particularly useful case is the transformation from the global time to the backwards light cone frame. This is particularly useful in cases where black holes are modelled in the fiducial observer (FIDO) frame, where the global time coordinate is significantly different to the time coordinate in the backwards light cone frame. By doing this the difficulty of calculating the backwards light cone through ray tracing only needs to be done once, rather than at each time step. This transformation would allow the moments seen by an observer, at a finite distance away from the black hole, to be calculated.

There are also applications of the coordinate transformation formulae in circular particle accelerators. Results from accelerators are often calculated in Frenet-Serret coordinates, where the parameter is the position along the beamline, rather than time. By finding either the Vlasov equation in Frenet-Serret coordinates, or finding the coordinate transformation between Cartesian and Frenet-Serret coordinate systems for a given beamline, the moment tracking can be applied to circular accelerators. Additionally, by using the spacetime coordinate transformations presented in this article, the coordinate transformation into the frame of an accelerating bunch can be found (figure 1.4b).

Lastly the use of the Vlasov equation to model the dynamics of moments may be extended to modelling stress-energy-momentum quadrupoles as a source for linearised gravity. In [66, 69] it was shown that the dynamics of stress-energy-momentum quadrupoles contain a number of free components, known as *constitutive relations*. In the case of a plasma, these constitutive relations may be determined by the Vlasov equation. In this case, the dynamics will be governed by the divergenceless of the stress-energy-momentum tensor combined, with the Vlasov equation.

Appendix A

Proofs

A.1 Deriving the equations for the field updater at the boundaries

The formula for numerically differentiating a scalar field $f(x)$ across n arbitrarily spaced points, and then evaluating this differential at one of these points is given by [97],

$$\left.\frac{df}{dx}\right|_{x_j} = \sum_{k=0}^{n} f(x_k) \left.\frac{dL_k}{dx}\right|_{x_j} \tag{A.1.1}$$

where L_k is the kth Lagrange polynomial for f at $k = 1 \ldots n$, given by

$$L_k(x) = \prod_{\substack{i=0 \\ i \neq k}}^{n} \frac{(x - x_i)}{(x_k - x_i)}. \tag{A.1.2}$$

To evaluate Maxwell's equations at the grid boundaries, we choose to differentiate over 5 different grid points. This ensures the derivatives are stable. The boundary conditions require that at the cavity walls, certain components of the electromagnetic field vanish. This means that rather than calculating the derivatives over 5 equally spaced points, it is more accurate to calculate over 4 grid points, and half a grid cell to the boundary.

Explicitly calculating the L_1 term to show how these terms are calculated,

$$L_1 = \frac{x-(x_j)}{\left(x_j-\frac{\Delta x}{2}\right)-(x_j)} \times \frac{x-\left(x_j-\frac{3\Delta x}{2}\right)}{\left(x_j-\frac{\Delta x}{2}\right)-\left(x_j-\frac{3\Delta x}{2}\right)} \times \frac{x-\left(x_j-\frac{5\Delta x}{2}\right)}{\left(x_j-\frac{\Delta x}{2}\right)-\left(x_j-\frac{5\Delta x}{2}\right)} \times \frac{x-\left(x_j-\frac{7\Delta x}{2}\right)}{\left(x_j-\frac{\Delta x}{2}\right)-\left(x_j-\frac{7\Delta x}{2}\right)}. \quad \text{(A.1.3)}$$

Simplifying the denominators gives

$$L_1 = \frac{(x-(x_j))}{-\frac{\Delta x}{2}} \times \frac{x-\left(x_j-\frac{3\Delta x}{2}\right)}{\Delta x} \times \frac{x-\left(x_j-\frac{5\Delta x}{2}\right)}{2\Delta x} \times \frac{x-\left(x_j-\frac{7\Delta x}{2}\right)}{3\Delta x}. \quad \text{(A.1.4)}$$

Differentiating this and evaluating at $x = x_j$, noting that only the term where the first term is differentiated will give a non-zero contribution,

$$\left.\frac{dL_1}{dx}\right|_{x=x_j=0} = \frac{1}{\frac{-\Delta x}{2}} \times \frac{\frac{3\Delta x}{2}}{\Delta x} \times \frac{\frac{5\Delta x}{2}}{2\Delta x} \times \frac{\frac{7\Delta x}{2}}{3\Delta x} = -\frac{35}{8\Delta x}. \quad \text{(A.1.5)}$$

Doing this for the remaining terms gives

$$\begin{gathered} \left.\frac{dL_0}{dx}\right|_{x_j} = \frac{352}{105\Delta x}, \quad \left.\frac{dL_1}{dx}\right|_{x_j} = -\frac{35}{8\Delta x}, \quad \left.\frac{dL_2}{dx}\right|_{x_j} = \frac{35}{24\Delta x} \\ \left.\frac{dL_3}{dx}\right|_{x_j} = -\frac{21}{40\Delta x}, \quad \left.\frac{dL_4}{dx}\right|_{x_j} = \frac{5}{56\Delta x}. \end{gathered} \quad \text{(A.1.6)}$$

Inserting these into equation (A.1.1), gives the interpolation polynomial,

$$\left.\frac{df}{dx}\right|_{x_j} = \frac{352}{105\Delta x} f(x_j) - \frac{35}{8\Delta x} f\left(x_j - \frac{\Delta x}{2}\right) + \frac{35}{24\Delta x} f\left(x_j - \frac{3\Delta x}{2}\right) - \frac{21}{40\Delta x} f\left(x_j - \frac{5\Delta x}{2}\right) + \frac{5}{56\Delta x} f\left(x_j - \frac{7\Delta x}{2}\right). \quad \text{(A.1.7)}$$

References

[1] A. Warwick and J. Gratus. *Plasma Phys. Control. Fusion*, 66(1):015014, Dec. 2023.

[2] T. J. M. Boyd. Cambridge, UK ; New York : Cambridge University Press, 2003. ISBN: 978-0-521-45290-8.

[3] W. Crookes. James W. Queen, 1879.

[4] I. Langmuir. *Proc. Natl. Acad. Sci. U. S. A.*, 14(8):627–637, Aug. 1928.

[5] J. Ongena, R. Koch, R. Wolf, and H. Zohm. *Nature Phys*, 12(5):398–410, May 2016.

[6] R. Betti and O. A. Hurricane. *Nature Phys*, 12(5):435–448, May 2016.

[7] T. Tajima and J. M. Dawson. *Phys. Rev. Lett.*, 43(4):267–270, July 1979.

[8] E. Esarey, C. B. Schroeder, and W. P. Leemans. *Rev. Mod. Phys.*, 81(3):1229–1285, Aug. 2009.

[9] E. Esarey, P. Sprangle, J. Krall, and A. Ting. *IEEE Trans. Plasma Sci.*, 24(2):252–288, Apr. 1996.

[10] M. Palmroth et al. *Living Rev. Comput. Astrophys.*, 4(1):1, Aug. 2018.

[11] E. Marsch. *Living Rev. Sol. Phys.*, 3(1):1, July 2006.

[12] U. Samir, K. H. Wright Jr., and N. H. Stone. *Rev. Geophys.*, 21(7):1631–1646, 1983.

[13] D. E. Hastings. *J. Geophys. Res.*, 100(A8):14457–14483, Aug. 1995.

[14] K. Nishikawa, I. Duţan, C. Köhn, and Y. Mizuno. *Living Rev. Comput. Astrophys.*, 7(1):1, July 2021.

[15] K.-D. Weltmann et al. *Plasma Process. Polym.*, 16(1):1800118, 2019.

[16] P. I. John. Tata McGraw-Hill Publishing Company, 2005. ISBN: 978-0-07-058557-7.

[17] T. von Woedtke, S. Reuter, K. Masur, and K.-D. Weltmann. *Physics Reports*, 530(4):291–320, Sept. 2013.

[18] S. Bekeschus et al. *IEEE Trans. Radiat. Plasma Med. Sci.*, 5(3):398–411, May 2021.

[19] A. P. H. Goede. *EPJ Web Conf.*, 189:00010, 2018.

[20] J. E. Foster. *Phys. Plasmas*, 24(5):055501, May 2017.

[21] P. Debye and E. Hückel. *Phys. Z.*, 24:185–206, 1923.

[22] A. Fasoli, S. Brunner, W. A. Cooper, J. P. Graves, P. Ricci, O. Sauter, and L. Villard. *Nature Phys*, 12(5):411–423, May 2016.

[23] D. I. Pontin and E. R. Priest. *Living Rev Sol Phys*, 19(1):1, May 2022.

[24] W. B. Mori and T. Katsouleas. *Phys. Scr.*, T30:127–133, Jan. 1990.

[25] D. A. Burton and A. Noble. *J. Phys. A: Math. Theor.*, 43(7):075502, Feb. 2010.

[26] A. A. Vlasov. *Sov. Phys. Usp.*, 10(6):721, June 1968.

[27] F. L. Hinton and R. D. Hazeltine. *Rev. Mod. Phys.*, 48(2):239–308, Apr. 1976.

[28] J. Büchner. In *Proc. ISSS-7*, pages 23–46, Mar. 2005.

[29] J. Qiang, R. D. Ryne, S. Habib, and V. Decyk. *J. Comput. Phys.*, 163(2):434–451, Sept. 2000.

[30] J. Qiang. *Phys. Rev. Accel. Beams*, 21(5):054201, May 2018.

[31] J. Cai and I. Syratchev. *IEEE Trans. Plasma Sci.*, 47(4):1734–1741, Apr. 2019.

[32] B. Goplen, L. Ludeking, D. Smith, and G. Warren. *Comput. Phys. Commun.*, 87(1):54–86, May 1995.

[33] J. M. Dawson. *Rev. Mod. Phys.*, 55(2):403–447, Apr. 1983.

[34] B. Crinquand. PhD thesis, Université Grenoble Alpes, July 2021.

[35] G. Lapenta. *J. Comput. Phys.*, 334:349–366, Apr. 2017.

[36] T. D. Arber et al. *Plasma Phys. Control. Fusion*, 57(11):113001, Sept. 2015.

[37] J. Derouillat et al. *Comput. Phys. Commun.*, 222:351–373, Jan. 2018.

[38] T. Takizuka and H. Abe. *J. Comput. Phys.*, 25(3):205–219, Nov. 1977.

[39] M. E. Jones, D. S. Lemons, R. J. Mason, V. A. Thomas, and D. Winske. *J. Comput. Phys.*, 123(1):169–181, Jan. 1996.

[40] Y. Sentoku and A. J. Kemp. *J. Comput. Phys.*, 227(14):6846–6861, July 2008.

[41] A. Dymnikov and E. Perelshtein. *Nucl. Instrum. Methods*, 148(3):567–571, Feb. 1978.

[42] P. J. Channell. *IEEE Trans. Nucl. Sci.*, 30(4):2607–2609, Aug. 1983.

[43] P. J. Channell, L. M. Healy, and W. P. Lysenko. *IEEE Trans. Nucl. Sci.*, 32(5):2565–2566, Oct. 1985.

[44] R. B. Appleby, R. J. Barlow, D. Krücker, J. Molson, S. Rowan, S. Tygier, H. Rafique, N. Walker, and A. Wolski. *Comput. Phys. Commun.*, 271:108204, Feb. 2022.

[45] B. Shadwick and J. Wurtele. In *Proc. 1999 Part. Accel. Conf.* Volume 4, 2888–2890 vol.4, Mar. 1999.

[46] J. R. Ellis. *J. Math. Phys.*, 7(7):1185–1197, July 1966.

[47] W. Ackermann and T. Weiland. In *Proc. ICAP 2006*, Chamonix, France, 2006.

[48] R. J. Mason. *J. Comput. Phys.*, 41(2):233–244, June 1981.

[49] A. R. Bell, J. R. Davies, S. Guerin, and H. Ruhl. *Plasma Phys. Control. Fusion*, 39(5):653–659, May 1997.

[50] H. M. Hulburt and S. Katz. *Chem. Eng. Sci.*, 19(8):555–574, Aug. 1964.

[51] H. Grubin, T. Govindan, J. Kreskovsky, and M. Stroscio. *Solid-State Electron.*, 36(12):1697–1709, Dec. 1993.

[52] M. A. Stroscio. *Superlattices Microstruct.*, 2(1):83–87, Jan. 1986.

[53] V. Dyadechko and M. Shashkov. *J. Comput. Phys.*, 227(11):5361–5384, May 2008.

[54] A. B. Langdon. *J. Comput. Phys.*, 6(2):247–267, Oct. 1970.

[55] H. Okuda and C. K. Birdsall. *Phys. Fluids*, 13(8):2123–2134, Aug. 1970.

[56] K. Schwarzschild. *Sitzungsberichte K. Preuss. Akad. Wiss.*:189–196, Jan. 1916.

[57] B. P. Abbott et al. *Phys. Rev. Lett.*, 116(6):061102, Feb. 2016.

[58] O. James, E. von Tunzelmann, P. Franklin, and K. S. Thorne. *Class. Quantum Grav.*, 32(6):065001, Feb. 2015.

[59] B. Cerutti, G. R. Werner, D. A. Uzdensky, and M. C. Begelman. *ApJ*, 770(2):147, June 2013.

[60] B. Crinquand, B. Cerutti, A. Philippov, K. Parfrey, and G. Dubus. *Phys. Rev. Lett.*, 124(14):145101, Apr. 2020.

[61] K. Parfrey, A. Philippov, and B. Cerutti. *Phys. Rev. Lett.*, 122(3):035101, Jan. 2019.

[62] J. Rosenberg and F. Ebrahimi. *Astrophys. J. Lett.*, 920(2):L29, Oct. 2021.

[63] A. A. Philippov and A. Spitkovsky. *Astrophys. J.*, 855(2):94, Mar. 2018.

[64] K. S. Thorne and D. MacDonald. *Mon. Not. R. Astron. Soc.*, 198(2):339–343, Feb. 1982.

[65] I. Y. Dodin and N. J. Fisch. *Phys. Plasmas*, 17(11):112118, Nov. 2010.

[66] J. Gratus and S. Talaganis. *Class. Quantum Grav.*, 40(8):085012, Mar. 2023.

[67] S. L. Ginzburg, V. F. Dyachenko, Y. N. Orlov, N. N. Fimin, and V. M. Chechetkin. *Comput. Math. and Math. Phys.*, 56(9):1611–1619, Sept. 2016.

[68] J. Gratus and T. Banaszek. *Proc. R. Soc. Math. Phys. Eng. Sci.*, 474(2213):20170652, May 2018.

[69] J. Gratus, P. Pinto, and S. Talaganis. *Class. Quantum Grav.*, 38(3):035011, Dec. 2020.

[70] H. Hamburger. *Math. Ann.*, 81(2):235–319, June 1920.

[71] F. Hausdorff. *Math Z*, 16(1):220–248, Dec. 1923.

[72] V. John, I. Angelov, A. A. Öncül, and D. Thévenin. *Chem. Eng. Sci.*, 62(11):2890–2904, June 2007.

[73] L. G. M. de Souza, G. Janiga, V. John, and D. Thévenin. *Chem. Eng. Sci.*, 65(9):2741–2750, May 2010.

[74] H. Cramér. Princeton university press, Princeton, 1946.

[75] G. Talenti. *Inverse Problems*, 3(3):501–517, Aug. 1987.

[76] A. Wolski, M. A. Johnson, M. King, B. L. Militsyn, and P. H. Williams. *Phys. Rev. Accel. Beams*, 25(12):122803, Dec. 2022.

[77] R. Roussel, A. Edelen, C. Mayes, D. Ratner, J. P. Gonzalez-Aguilera, S. Kim, E. Wisniewski, and J. Power. *Phys. Rev. Lett.*, 130(14):145001, Apr. 2023.

[78] M. Pawlak. *IEEE Trans. Inform. Theory*, 38(6):1698–1708, Nov. 1992.

[79] P. Milanfar, W. Karl, and A. Willsky. *IEEE Trans. Image Process.*, 5(3):459–470, Mar. 1996.

[80] L. S. Freedman, V. Fainberg, V. Kipnis, D. Midthune, and R. J. Carroll. *Biometrics*, 60(1):172–181, 2004.

[81] L. S. Freedman, D. Midthune, R. J. Carroll, and V. Kipnis. *Stat. Med.*, 27(25):5195–5216, 2008.

[82] R. McGraw, S. Nemesure, and S. E. Schwartz. *J. Aerosol Sci.*, 29(7):761–772, Aug. 1998.

[83] A. Macchi, A. A. Maradudin, and V. Tognetti. *Phys. Rev. B*, 53(9):5363–5371, Mar. 1996.

[84] S. S. Mizrahi and D. Galetti. *J. Phys. A: Math. Gen.*, 35(15):3535–3546, Apr. 2002.

[85] D. V. Berkov, P. Görnert, N. Buske, C. Gansau, J. Mueller, M. Giersig, W. Neumann, and D. Su. *J. Phys. D: Appl. Phys.*, 33(4):331–337, Feb. 2000.

[86] A. A. Vlasov. *J. Exp. Theor. Phys.*, 8(3):291, 1938.

[87] G. Chen, L. Chacón, and D. C. Barnes. *J. Comput. Phys.*, 230(18):7018–7036, Aug. 2011.

[88] K. Elsässer and S. Popel. *Phys. Plasmas*, 4(7):2348–2356, July 1997.

[89] F. A. Rasio, S. L. Shapiro, and S. A. Teukolsky. *ApJ*, 344:146, Sept. 1989.

[90] R. B. Horne and M. P. Freeman. *J. Comput. Phys.*, 171(1):182–200, July 2001.

[91] J. U. Brackbill and D. W. Forslund. *J. Comput. Phys.*, 46(2):271–308, May 1982.

[92] J. R. Ellis. *Math. Proc. Camb. Philos. Soc.*, 78(1):145–156, July 1975.

[93] W. G. Dixon. *J. Math. Phys.*, 8(8):1591–1605, Aug. 1967.

[94] R. Appleby, G. Burt, J. Clarke, and H. Owen. CRC Press, Dec. 2020. ISBN: 978-1-351-00796-2.

[95] H. Wiedemann. Springer Nature, Jan. 2015. ISBN: 978-3-319-18317-6.

[96] M. Reiser. John Wiley & Sons, Ltd, 2nd edition. ISBN: 978-3-527-62204-7.

[97] R. L. Burden and J. D. Faires. Brooks/Cole, Cengage Learning, Boston, MA, 9th ed edition, 2011. ISBN: 978-0-538-73351-9.

[98] A. Warwick and J. Gratus (2023). "Dataset of moment coordinate transformation", Zenodo. http://dx.doi.org/10.5281/zenodo.8082181.

[99] M. Wright (2016). "Reconstructing functions from moments", Unpublished Lancaster University Master's report.

[100] G. Guennebaud, B. Jacob, et al., 2010.

[101] J. P. Boris. In *Proc. Conf. Numer. Simul. Plasmas 4th*, pages 3–67, Fort Belvoir, VA. Defense Technical Information Center, July 1971.

[102] K. Yee. *IEEE Trans. Antennas Propag.*, 14(3):302–307, May 1966.

[103] Y. Chen, R. Mittra, and P. Harms. *IEEE Trans. Microw. Theory Tech.*, 44(6):832–839, June 1996.

[104] A. J. Kogon and C. D. Sarris. *IEEE Antennas Propag. Mag.*, 64(3):59–70, June 2022.

[105] J.-P. Bérenger. *FERMAT*, 9, 2015.

[106] E. Horowitz. *J. Comput. Phys.*, 68(1):56–65, Jan. 1987.

[107] E. Kaya. *J. Tech. Sci. Technol.*:47–52, 2013.

[108] S. Schnepp, E. Gjonaj, and T. Weiland. In *Proc. EPAC 2006*, 2006.

[109] C. K. Birdsall and A. B. Langdon. McGraw-Hill, 1985. ISBN: 978-0-07-005371-7.

[110] J. Villasenor and O. Buneman. *Comput. Phys. Commun.*, 69(2):306–316, Mar. 1992.

[111] T. Z. Esirkepov. *Comput. Phys. Commun.*, 135(2):144–153, Apr. 2001.

[112] R. Courant, K. Friedrichs, and H. Lewy. *IBM J. Res. Dev.*, 11(2):215–234, Mar. 1967.

[113] R. Hockney. *J. Comput. Phys.*, 8(1):19–44, Aug. 1971.

[114] J. U. Brackbill. *J. Comput. Phys.*, 317:405–427, July 2016.

[115] D. C. Barnes and L. Chacón. *Comput. Phys. Commun.*, 258:107560, Jan. 2021.

[116] A. Leggieri, D. Passi, F. Di Paolo, B. Spataro, and E. Dyunin. *Vacuum*, 122:103–116, Dec. 2015.

[117] S. Zaremba and W. Kleeven. *CERN Yellow Rep. Sch. Proc.*, 1:177–177, June 2017.

[118] D. J. Griffiths. University Press, Cambridge, fifth edition. Edition, 2024. ISBN: 978-1-00-939773-5.

[119] Z. Shen. Springer Dordrecht, 2013. ISBN: 978-94-015-9727-2.

[120] F. Gunneberg and J. Gratus (2024). "The Vlasov equation in a clock-free setting", In preperation.

[121] A. J. Kemp, F. Fiuza, A. Debayle, T. Johzaki, W. B. Mori, P. K. Patel, Y. Sentoku, and L. O. Silva. *Nucl. Fusion*, 54(5):054002, Apr. 2014.

[122] C. Huang et al. *J. Phys.: Conf. Ser.*, 46(1):190, Sept. 2006.